

**SIZE AND SHAPE CONTROLLED SYNTHESIS OF
METAL NANOPARTICLES AND ITS
NANOCOMPOSITES**

AKHILESH RAI

**UNDER THE GUIDANCE OF
DR. MURALI SASTRY**

**PHYSICAL & MATERIALS CHEMISTRY DIVISION
NATIONAL CHEMICAL LABORATORY
PUNE 411 008
INDIA**

FEBRUARY 2007

**SIZE AND SHAPE CONTROLLED SYNTHESIS OF
METAL NANOPARTICLES AND ITS
NANOCOMPOSITES**


THESIS SUBMITTED TO
UNIVERSITY OF PUNE
FOR THE DEGREE OF
DOCTOR OF PHILOSOPHY
IN
BIOTECHNOLOGY

BY

AKHILESH RAI

**PHYSICAL & MATERIALS CHEMISTRY DIVISION
NATIONAL CHEMICAL LABORATORY
PUNE 411 008
INDIA**

FEBRUARY 2007



Dedicated to my
parents and
teachers

DECLARATION

I hereby declare that the thesis entitled “**SIZE AND SHAPE CONTROLLED SYNTHESIS OF METAL NANOPARTICLES AND ITS NANOCOMPOSITES**” submitted for the degree of Doctor of Philosophy in Biotechnology to University of Pune, has been carried out by me at the Physical Chemistry Division of National Chemical Laboratory, Pune under the supervision of Dr. Murali Sastry. Such material as has been obtained by other sources has been duly acknowledged in this thesis. The work is original and has not been submitted in part or full by me for any other degree or diploma to other University.

Date:

Place: Pune

AKHILESH RAI

(Research Student)

Acknowledgement

*I extend my sincere gratitude and appreciation to many people who made this PhD thesis possible. First and foremost, I would like to express my sincere thanks to my supervisor and mentor **Dr. Murali Sastry** for his dedicated help, encouragement, constant support and valuable advice throughout my PhD. I am most indebted to him for exposing me to such an exciting and interesting research area. His tireless enthusiasm and hard work are my source of motivation and always inspire me to work hard throughout my life. It is very rare to find some person, who always inspires to strive and excel in life and I am fortunate that I have found Dr. Sastry. It has been my great pleasure for being a member of his team and to work with such a close association under him.*

My sincere thanks to Dr. B.L.V. Prasad, Dr. Asmita Prabhune and Ms. Suguna Adyantaya for helping me throughout my PhD.

My special thanks to Dr. Absar Ahmad from the Biochemical Sciences Division for his major contributions in plant extract based synthesis of metal nanoparticles.

My special thanks to Renu Pasricha for introducing and giving training of transmission electron microscopy characterization to me and helping me at any odd time. I also like to take this opportunity to thank Dr. Sainkar, Dr. A. B. Mandale, Dr. Ms. Neela Pavasakar, Dr. Patil and Mr. Gaikwad of Center for Material Characterization for their help in different materials characterizations. Without their help completion of the work presented in this thesis was unimaginable.

I thank Drs. Ashavani, Debabrata, Sumant, Saikat, Anita, Kannan, Shankar and Senthil, who readily extended their support to me as senior and fellow group members by helping me in all possible ways. I thank them for extending their friendly gesture and providing me their great company at all times of need to make me feel very comfortable in this group.

My special thanks to fellow labmates, Hrushikesh, Ambarish, Tanushree, Amit, Atul, Vipul, Sourabh, Deepti, Prathap, Sanjay, Minakshi, Manasi, Anil, Imran, Prinyanka, Umesh for always standing by my side and sharing a great relationship as compassionate friends. I will always cherish the warmth shown by them. I sincerely thank them for

putting their efforts in correcting this thesis, many a times by keeping their own work aside. I especially thank Vipul, Amit, Deepti and Mansi for their valuable contribution in this regard.

My heartfelt thanks to Shankar, Amit and Dr. Ankamwar who were involved together with me in some important experiments. Their constant help and valuable contributions are greatly acknowledged.

I express my sincere thanks to the project students, who have helped me in some or other way in the day to day research work.

A special mention of thanks to my friends in NCL, Ambrish, Vinod, Sachin, Atul, Girish, Balachandra, Shekhar and Kamendra for their constant support and cooperation during my stay. Their timely help and friendship shall always be remembered.

My heartfelt thanks to Seena, Ratnesh, Ruchi, Rasesh and Azeet for their constant support.

My special thanks to Director, Dr. S. Sivaram and to Head of the Physical and Materials Chemistry Division Dr. S. Pal, for giving me an opportunity to work in this laboratory and making all facilities available for the pursued research.

I acknowledge the HRDG CSIR for providing me with the necessary funding and fellowship to continue research in NCL.

My special regards to many teachers because of whose teaching at different stages of education has made it possible for me to see this day. My special thanks to my school day teachers, because of their kindness I feel, was able to reach a stage where I could write this thesis.

As always it is impossible to mention everybody who had an impact to this work however there are those whose spiritual support is even more important. I feel a deep sense of gratitude for my mother and father who formed part of my vision and taught me good things that really matter in life. I am also very much grateful to all my family members for their constant inspiration and encouragement.

Finally, I am thankful to library staff and administrative staff of NCL for cooperation.

Akhilesh Rai

Table of Contents

Chapter 1: Introduction

1.1	Introduction	1
1.2	Needs for interdisciplinary field	1
1.3	Different approaches in nanotechnology	3
1.4	Emergence of nanotechnology	5
1.5	Different methods for synthesis of nanoparticles	6
1.6	Various methods for synthesis of anisotropic nanoparticles	13
1.7	Synthesis of core-shell nanoparticles	18
1.8	Shape modification of nanoparticles	19
1.9	Outline of thesis	20
1.10	References	24

Chapter 2: Characterization techniques

2.1	Introduction	45
2.2	UV-vis-NIR spectroscopy	45
2.3	Fourier transform infrared spectroscopy	49
2.4	Transmission electron microscopy	50
2.5	Scanning electron microscopy	52
2.6	Atomic force microscopy	54
2.7	X-ray diffraction	56
2.8	X-ray photoelectron spectroscopy	58
2.9	Gel electrophoresis	61
2.10	References	63

Chapter 3: Synthesis of triangular and hexagonal gold nanoparticles using undialyzed and dialyzed lemongrass leaf extract

3.1	Introduction	64
3.2	Synthesis of gold nanotriangles and nanohexagons using lemongrass leaf extract	67
3.3	Size and shape controlled synthesis of gold nanoparticles	72
3.4	Conclusion	92
3.5	References	93

Chapter 4: Synthesis of triangular gold-silver and spherical gold-titania core-shell nanoparticles

4.1	Introduction	99
4.2	Synthesis anisotropic core-shell nanoparticles	101
4.3	Summary	114
4.4	Synthesis of spherical gold-titania core-shell nanoparticles	114
4.5	Summary	123
4.6	Conclusion	123
4.7	References	125

Chapter 5: Morphological transformation of gold nanotriangles using chemical approaches

5.1	Introduction	130
5.2	Effect of halide ions on the morphology of gold nanotriangles during synthesis	132
5.3	Morphological transformation of preformed gold nanotriangles induced by halide ions	138
5.4	Effect of cationic surfactants on the morphology of gold nanotriangles	143
5.5	Effect of gold ions on the morphology of CTAB and CTAC bound gold nanotriangles	152
5.6	Conclusion	157
5.7	References	159

Chapter 6: Photofragmentation of gold nanotriangles by UV light and synthesis of gold nanotriangles at different temperatures

6.1	Introduction	163
6.2	Effect of Keggin ions during synthesis of gold nanotriangles and UV light irradiation of synthesized nanoparticles	165
6.3	Effect of UV light irradiation on the morphology of Keggin ion bound gold nanotriangles	172
6.4	Temperature dependent synthesis of gold nanotriangles	180
6.5	Conclusion	183
6.6	References	185

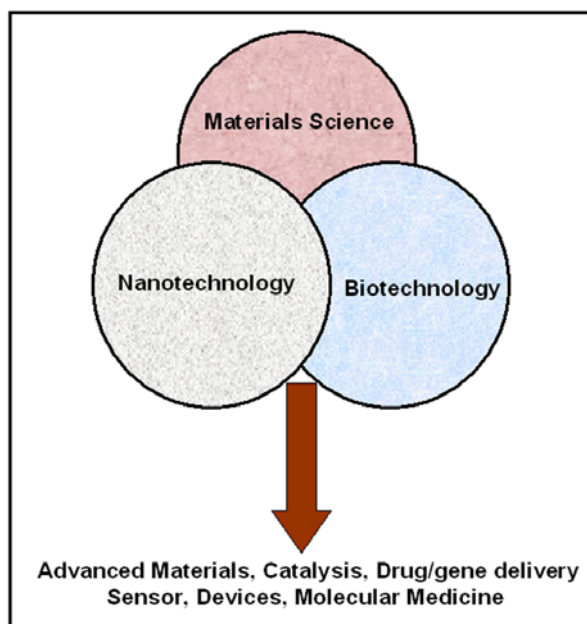
Chapter 7: Conclusions

7.1	Summary of the work	189
7.2	Scope for future work	192

List of Publications	193
-----------------------------	------------

Chapter I

Introduction



This chapter is an introduction to the thesis and gives a brief overview of the complexity involved in the understanding of nature and therefore, the importance of interdisciplinary research. It also emphasizes the different physical, chemical and biological methods, used for the synthesis of nanomaterials. Further, an emphasis on the biomineralization of metal and inorganic materials using natural biological sources has been given in the chapter. This chapter also discusses the various reported protocols used for the synthesis of anisotropic and core-shell nanoparticles of different compositions. Shape transformation of nanoparticles using chemical and physical means has also been described in the chapter.

1.1 Introduction:

Nature always thrives with an amalgamation of complexity, beauty, specificity and diversity. There is a rich and long history of gaining inspiration from nature for the design of noble materials and systems [1-4]. Noble laureate Jean-Marie Lehn used these words to express outlook on the future and prospective of materials chemistry “The essence of chemical science finds its full expression in the words of that epitome of the artist-scientist Leonardo da Vinci: Where Nature finishes producing its own species, man begins, using natural things and with the help of this nature, to create an infinity of species”. The real attraction and complexity of nature is brought out when one starts studying biology. The human body or for that matter any living organism, can be described as a community of molecules wherein individual molecules scurry about like ants or honeybees, each performing its designated task so as to ensure the well-being of the society as a whole. Some gather food, some build structures in which they all dwell, others seek out and repel foreign invaders. Of course, each of these molecular workers is driven not by some autonomous consciousness but by the principles of physical and chemical sciences [5]. DNA, RNA and protein are nanoscale components important for the execution of the functions of life and are the best natural bionanomaterials [6]. Interaction among these components weaves a complicated, optimized, yet perfect biological world. In spite of the difficulties encountered, the field of science is fascinating and researchers plunge into this field due to pure passion. Prof. Albert Einstein quotes “If we knew what it was we were doing, it would not be called research, would it?”

1.2 Needs for interdisciplinary field:

Earlier, for the purpose of studying and understanding, nature was divided into three branches of basic science. Biology was mostly concerned with studying life, how we evolved from sea, diseases and remediation. Chemistry dealt with synthesizing compounds of various compositions and properties, which have an important application in industrial processes and for the betterment of human beings. Physics was concerned with the deepest mystery of universe-like understanding of what is matter and development of new instruments to understand life, and fabrication of new materials. Science is changing rapidly across the borders and now it pays little regard to the

disciplines into which it had been traditionally divided. Finding solutions in different branches of science requires a collective effort of scientists working in various regimes of the basic sciences.

Starting with discovery of double helix structure of DNA, biology has grown from purely descriptive and phenomenological discipline to molecular science. Recombinant DNA technology brought insights into the basic principles of many biochemical processes, and it has also opened the door to modern biotechnology. In view of such revolutionary developments, it seems particularly challenging to fuse biotechnology with materials science. Merging these disciplines will allow us to take advantage of the improved evolutionary biological components to generate new smart materials and, conversely, to apply today's advanced materials and physicochemical techniques to solve biological problems. Nanotechnology is the manipulation of matter on a nanometer scale in order to engineer new materials and devices with superior chemical, physical, optical, electronic and/or biological properties. This so called area of nanotechnology was first thought of by Prof. Feynman and mentioned in his famous talk at Caltech: "There is plenty of room at the bottom" [7]. Since then, tremendous research and search for application potential for this new state of matter has been observed. The unique properties of nanomaterials and structures on the nanometer scale have caught the attention of materials developers. Traditionally, materials scientists, inspired by biological structures and their functions, focused on emulating or duplicating biosystems using mostly synthetic components and following traditional approaches [8-10].

In this era, human beings require sophisticated instruments and advanced materials for the betterment of society and to combat with newly generated diseases and therefore it is necessary to do interdisciplinary work rather than to involve in the individual branch of science. Nanobiotechnology is one of the interdisciplinary fields wherein contributions from physics (explanation of phenomena, developments of instruments), chemistry (synthesis and fabrication of advanced materials) and biology (drug and gene delivery, molecular biology etc) come together to play a synergetic role for the development of new advanced materials. The motivation behind the nanobiotechnology research came from understanding nature, how it works and generates highly complex living entities. Nanobiotechnologists employ the natural principles and

mimic biological systems to fabricate self assembling, self replicating and self organizing advanced materials. With the advent of nanobiotechnology, which is the bioconjugation of different chemicals/biomolecules onto efficient nano templates has resulted in early detection of diseases, toxic gases, glucose monitoring, food testing and drug loading on the nanoparticles and target specific delivery of drugs and genes etc [11]. Nanobiotechnology has also helped in studying different aspects of design and development of molecular motors [12] and smart materials. Recent developments in the fields of microelectromechanical system (MEMS) and nanoelectromechanical system (NEMS) have revolutionarized different areas such as automobiles, biomedicine and electronics etc. For instance, nanorobots, working on the principle of MEMS, may be used for delivering different drugs inside different parts of human body as well as for the repairing of damaged cells.

1.3 Different approaches in nanotechnology:

Products are made from arrangement of atoms. The properties of these products depend upon how these atoms are arranged. Atom is in nanodimension. 'Nano' derives from the Greek word "nanos", which means dwarf or extremely small.






				
Less than a nanometer	Nanometer	Thousands of nanometers	A million nanometers	Billions of nanometers
Individual atoms are up to a few tenths of a nanometer in diameter	Ten shoulder-to-shoulder hydrogen atoms (blue balls) span 1 nanometer. DNA molecules are about 2.5nm wide	Biological cells, like these red blood cells, have diameters in the range of thousands of nanometers	An ant is millions of nanometers across	A two meter tall male is two billion nanometers tall

Figure 1.1: Figure showing comparison of different things present in world.

A nanosecond is a billionth of a second. A nanoliter is a billionth of a liter and similarly, a nanometer is a billionth of a meter or 10^{-9} m. Nanoparticles are small clusters

of atoms about 1 to 100 nm long. To understand how small is a nanometer, we can compare it with some naturally occurring things in the world (Figure 1.1). The idea of manipulating and positioning individual atoms and molecules is still exciting scientist to fabricate new devices. After the famous talk by Nobel physicist Richard Feynman in 1959, nanotechnology researchers have put great emphasis on the development of bottom-up approach, which concerns the self-assembly of molecules and colloidal building blocks to create materials and functional devices [13].

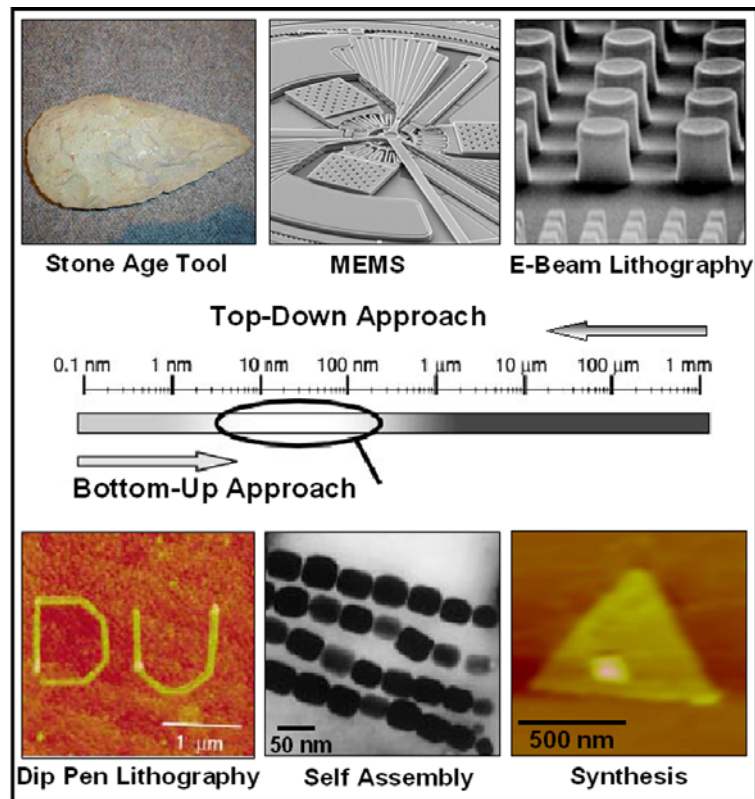


Figure 1.2: Examples that show Top-Down and Bottom-Up approaches for the fabrication of materials. Courtesy: Stone Age tool, MEMS and E-beam lithography images were taken from reference 21 and dip-pen lithography and self-assembly images were taken from reference 11.

Although the bottom-up approach is not new, it plays an important role in the fabrication and processing of nanostructures and nanomaterials. Top-down approach is another way to create smaller devices since old ages. Human beings first learned to fabricate devices such as Stone Age tools from big stones and with course of time, they have perfected in constructing sophisticated devices. Scientists also use existing materials to create smaller and smaller devices at the nano scale (Figure 1.2). These devices

become extremely tiny but they retain their original properties and do not morph into something new. Ball milling or attrition, e-beam lithography and etching are examples of top-down approach [14, 15]. Bottom-up approach promises a better chance to obtain nanomaterials with less defects, more homogeneous chemical composition and better short and long range ordering. On the contrary, top-down approach most likely introduces internal stress, in addition to surface defects and contaminations.

1.4 Emergence of nanotechnology:

Human beings are not the first to create nanomaterials, in fact nature has also provided us with a large number of building blocks in nanodimensions such as amino acids, nucleic acids and lipids. Nature first used the bottom-up approach to construct and fabricate materials. The chemical diversity of these molecules and different ways to assemble or polymerize them together provide an enormous range of nanostructures. Further, advance in biotechnology and chemical synthesis facilitate one to assemble and fabricate building blocks to produce new materials, which have not been made by nature. In attempt to fabricate miniaturized devices, it has been realized that materials in nanodimensions exhibit properties very different from their bulk counterparts. With time, the properties of nanomaterials have been realized, which has led to the potential applications in various fields. The study of biological systems and the engineering of many materials such as colloidal dispersions, metallic quantum dots and catalysts have been in the nanometer regime for centuries. One of the famous and oldest application was the use of gold nanoparticles for staining glasses; for example is lycurgus cup that dates back to 4th century AD [16]. During 17th century AD, colloidal gold nanoparticles gained importance for their curative values [17]. Chinese are also known to use Au nanoparticles as an organic dye to introduce red colour into their ceramic porcelains more than thousand years ago [17]. After a long course, Michael Faraday (1857) had synthesized colloidal gold of ruby red colour by reduction of aqueous chloroaurate ions (AuCl_4^-) using phosphorus dispersed in CS_2 [18]. That time, the gold solution was famous in the name of colloidal solution. The term “colloid” was first coined by Thomas Graham (1861) for suspended smaller particles in liquid medium [19]. During recent developments in this field, the term “colloid” has been replaced by “nanoparticles” to

describe particles with size range from 1 to 100 nm after introduction of the term “Nanotechnology” by Norio Taniguchi [20]. The famous quote of Louis Pasteur “ The role of infinitely small is infinitely large” well suits the current trends of nanotechnology research. After realization of application and importance of nanomaterials in various regimes and in order to explore novel physical properties and phenomena, a number of physical, chemical and biological methods have been developed.

1.5 Different methods for the synthesis of nanoparticles:

Various physical and chemical methods have been reported for the synthesis of inorganic nanoparticles. Spray pyrolysis [22], photoirradiation [23], radiolysis [24], physical vaporization [25], electrochemical [26], ultrasonication [27], solvated metal atom dispersion (SMAD) [28], electrospinning [29], lithography [30], chemical vapor deposition [31], sputtering [32], laser ablation [33] etc. are physical methods, which have been used for synthesis of various compositions of the nanoparticles. Chemical vapor deposition, Electrospinning and lithography methods have been developed preferentially for the synthesis and formation of one dimensional nanostructure materials such as nanowires, nanorods and nanofibres. Similarly, physical vaporization, chemical vapor deposition, electrochemical deposition and sputtering are used for the formation of thin films (two dimensional) on the solid supports. However, chemical routes have received an immense attraction for the synthesis of nanoparticles due to a better control on the size and shape of nanoparticles. Chemical reduction, sol-gel [34], co-precipitation [35], solvothermal [36] and templates based methods [37] are generally employed for the synthesis of various compositions of nanoparticles. Inorganic nanomaterials such as metal, metal oxide and semiconductor nanoparticles can be synthesized by reduction, or oxidation and precipitation of corresponding precursor salts. Although, solvents can vary from water to highly nonpolar media [38], few reports are also available on the synthesis of nanoparticles in ionic liquids [39] and supercritical fluids [40], depending upon the nature of the salts or complexes used for the reaction. The nature of precursor ions also determines the kind of reducing agents to be applied. The chemical reduction method is a very common route for the synthesis of metal nanoparticles of different size and shape. Sol-gel method used for the synthesis and fabrication of oxide nanoparticles especially

ceramics has gained much importance [34]. Recently, size and shape controlled synthesis of metal nanoparticles has lured scientists due to their fine control on the chemical and physical properties with respect to their application as nanodevices. The size, shape and stability of metal nanoparticles can be achieved by incorporating different additives, capping agents and templates. Different templates such as micelles [41], reverse micelles [42], DNA [43], tobacco mosaic virus (TMV) [44], polymeric molecules [45], preformed nanoparticles [46] and mesoporous membranes [47] have been employed in order to attain control over size and shape of the synthesized nanoparticles. Polymer, surfactants and biomolecules are certain examples of capping agents, which have been used for the shape-controlled synthesis of metal nanoparticles [48]. The physical and chemical methods employed for the synthesis of nanoparticles are not environment friendly processes. The nanoparticles synthesized using these methods are toxic to biological cells and therefore an alternative method, which is environmentally benign, is desired for the synthesis and assembly of nanoparticles. Biological sources are a good choice as an environment friendly approach for the synthesis of nanoparticles. Synthesis of core-shell nanoparticles of various compositions has also attracted materials chemists' attention due to a better control on the properties of nanoparticles in comparison to their monometallic form. Recently, another field of interest in nanotechnology has been the shape transformation of nanoparticles using different means. In the following sections of this chapter: 1) biological synthesis of nanoparticles using various sources, 2) various methods used for synthesis of anisotropic nanoparticles, 3) synthesis of different compositions of core-shell nanoparticles and, 4) shape transformation of gold nanotriangles using chemical and physical means have been described.

1.5.1 Biological synthesis of nanoparticles:

How does a complex shape such as spiral shells or spine of sea urchin evolve from a single crystalline material-calcium carbonate? It seems truly extraordinary that nature can assemble, with such exquisite control, a wide variety of functional materials with highly specific morphology, elegant skeletal framework, optical lenses (trilobites) or gravity sensor in the inner ear, from just two kinds of mundane inorganic ions [49]. Biological systems provide many examples of specifically tailored, nanostructured molecules with highly optimized properties and characteristics. These biological

materials can be used in their native form directly extracted from living systems or they can be processed after extraction and modified to their desired form. Many multicellular microorganisms use inorganic materials (calcium carbonates or silica) in combination with organic matrix (proteins, lipid and polysaccharides) to produce hard and functionalized materials such as skeletal, teeth and bones. These organic matrixes have a vital role in controlling the morphology of inorganic compounds [50]. The siliceous structures formed by diatoms and radiolarians [51], calcareous structures [52] and magnetic nanoparticles [53] synthesized by coccoliths and magnetotactic bacteria respectively have been explained on the basis of role of phospholipid membranes and geometric patterning in cells [54]. The compartmentalization and templating afforded by these fundamental cells are found to play a key role in biomineralisation. It was discovered that spherical crystals of magnetite developed when iron oxide was confined inside lipid vesicles, whereas in their absence, another needle shaped goethite structure formed (as in limpet teeth) [55]. Biosilicification by unicellular organisms has been facilitated by polycationic proteins such as silicateins [56] and silaffins [57]. Few more proteins such as frustulins [58] and pleuralins [59] have also been reported for the synthesis of highly complex silica and calcium carbonates structures. Silicateins and silaffins proteins were isolated and purified from the microorganism and were shown to induce the formation of silica by hydrolyzing the dissolved silicic acid [60]. The molecular mechanisms behind the transportation of Ca^{2+} ions and HCO_3^- ions for the synthesis of calcareous structures are not well known. It has been shown that the calcite minerals are coated with polyanions and some acidic polysaccharides [61].

Sastry and coworkers have extensively studied the extracellular synthesis of various polymorphs of calcium carbonates using fungi such as *Fusarium oxysporum* and actinomycetes [62]. They have also shown the synthesis of variable morphology of calcium carbonate nanocrystals [63]. Bioremediation and synthesis of heavy metals such as strontium, lead and cadmium carbonate nanoparticles using the fungus *Fusarium oxysporum* has been reported [64]. In addition to calcium carbonate, synthesis of commercially important oxides, for example, silica, titania, zirconia and barium titanate nanoparticles from respective chemical precursors using fungus *Fusarium oxysporum* has been demonstrated [65]. Further, the extracellular synthesis of silica nanoparticles from

natural source (sand) by bioleaching process and from rice husk using fungus *Fusarium oxysporum* has been reported [66]. Sastry and coworkers have demonstrated that the hydrolyzing protein, which is complex of two proteins of 21 and 24 kDa, are responsible for the hydrolysis of oxide precursors [65a].

Unicellular organisms such as bacteria are well known to produce magnetic nanoparticles either extracellularly or intracellularly; examples include magnetotactic bacteria, which produce magnetite (Fe_3O_4) or greigite (Fe_3S_4) nanoparticles with specific size range (35-120 nm) [67]. Magnetic nanoparticles are also observed in unicellular eukaryotic organisms such as algae [68], dinoflagellates [69], as well as higher organisms like salmon [70], trout [71], carrier pigeons [72], army ants [73] and also in the human brain [74]. The magnetic nanoparticles synthesized inside magnetotactic bacteria are found to be surround by phospholipid membrane and are called magnetosomes. The cubooctahedral, pseudo-hexagonal and bullet shaped magnetic nanoparticles are synthesized intracellularly by these bacteria [67]. Bacterial cells are always exposed to high concentrations of these ions and stressful condition in natural environment and an ability to resist these stresses is essential for their survival. The ability to grow in such conditions might result from specific resistance mechanisms. Such mechanisms include efflux system; alternation of solubility and toxicity by change in the redox state of metal ions; extracellular complexation or precipitation of metals and lack of specific metal transport systems [75]. Recent advances in the understanding of role and applications of microorganisms for bioremediation of toxic metals and radionucleotide contamination has been reported [76]. Natural and genetic engineered bacteria, which are capable of mobilization and immobilization of metal ions, have been used for the bioremediation process [76]. Recently, Sastry's group has shown the extracellular synthesis of magnetite nanoparticles using fungi and bacteria [77].

Microorganisms and metal interaction has gained much attention due to several important applications in the fields of bioremediation, biomineralization, bioleaching and microbial corrosion. Bacterial oxidation of minerals is important in the formation of acid mine drainage and extraction of gold, copper and uranium from ores and has developed growing interest among materials chemists [78]. Recently, the recovery of gold from arsenopyrite-pyrite ores using bioleaching principle has been reported [79]. Beveridge

and co-workers have first demonstrated the synthesis of gold nanoparticles within the cell walls of the bacteria, *Bacillus subtilis* on incubation with Au^{3+} ions [80]. Gold nanoparticles of different geometrical shapes and size in the range from 5 to 25 nm were synthesized inside cells. Fragments of cell walls of bacteria interacted to gold ions (AuCl_3) led to the nucleation and deposition of metal in non-stoichiometric amounts. Tanja Klaus and coworkers have shown the intracellular synthesis of silver nanoparticles using the bacteria, *Pseudomonas stutzeri* AG259 isolated from a silver mine [81]. Silver nanoparticles of well-defined shapes and sizes (100 - 200 nm) were found to synthesize in the periplasmic space of bacteria. The thickness of the periplasm constrains the thickness of crystal but not their width. The bacterial strain takes the advantage of detoxification mechanism to precipitate silver in the periplasm and its reduction to elemental silver. The produced silver was reported to be 5 % of the total bacterial biomass, while in case of mixed culture of *Thiobacillus ferrooxidans* and *Thiobacillus thiooxidans*, silver concentration of upto 25 % of bacterial drymass after leaching of sulphide minerals was reported [82]. Pradeep and coworkers have shown the synthesis of gold, silver and gold-silver alloy nanoparticles of variable morphology using *Lactobacillus* strain from buttermilk. They had observed 35 % accumulation of silver with respect to total bacterial dry biomass [83].

Sastry and coworkers have extensively studied the biosynthesis of nanoparticles of various composition using bacteria and fungi as a living nanofactories. In this attempt, fairly monodisperse gold nanoparticles were synthesized using the extremophilic actinomycete, *Thermomonospora* sp. [84]. *Verticillium* sp. [85] and *Fusarium oxysporum* [86] were used for the synthesis of gold and silver nanoparticles by the bioreduction of their respective precursors. *Verticillium* sp. synthesized nanoparticles intracellularly while *Fusarium oxysporum* synthesized nanoparticles extracellularly and therefore *Fusarium oxysporum* can be used for the large-scale extracellular synthesis of nanoparticles. In another report, gold-silver alloy nanoparticles of varying compositions have also been synthesized using *Fusarium oxysporum* [87]. Furthermore, *Fusarium oxysporum* was used for the synthesis of semiconducting nanoparticles (CdS) by enzymatic reduction of sulfate ions to sulphide ions [88]. Other microorganism such as yeast has also been exploited as an environment friendly source for the synthesis of CdS

[89], ZnS [90] and PbS [91] nanoparticles by various other groups. For example, *Candida glabrata* and *Schizosacchomyces pombe* produce cadmium sulphide nanocrystal by active intracellular uptake of metal followed by its sequestration within small iso-peptides [92].

Although, traditional methods for removal of heavy metals from soils and water have proven to be efficient, but they are expensive, labor intensive and in the case of soils, they produce disturbance in ecosystem. Plants have also been used as an excellent alternative in the extraction of heavy metals from soils and water and the soils can be utilized immediately after treatment application. Aquatic plants such as *Eichhornia crassipes* and *Azolla filiculoids* Lam., which have a high capability to absorb cadmium (Cd), copper (Cu), nickel (Ni) and zinc (Zn), have been used for phytoremediation of polluted water [93]. Several species of *Thalasspi* are well known metallophytes that grow in Cd, Ni, Pb and Zn metalliferous soils [94]. Some plant species are identified as hyper-accumulator of heavy metals in different parts of plants [95]. Agricultural byproducts of *Avena monida* (oat) has been used for the bioreduction of Cr(VI) to Cr(III) [96]. Recently, researchers have realized that plants can also be used for the recovery of highly precious metals such as gold, silver, platinum and palladium, which indicates the wide possibility of phytoremediation technology. Girling and Peterson have shown that *Phacelia sericea* accumulates gold in roots [97]. It has also been shown the Alfalfa plants grown in agar-based media containing gold and silver ions accumulate gold and silver metal in the aerial parts [98]. It is hypothesized that plant secretions especially cyanide may facilitate the uptake of gold ions from soils and it might render gold sufficiently soluble to enable plants to accumulate the metal [99]. These cyanogenic plants produce free cyanide by hydrolysis of cyanogenic glucosides within their tissues [100]. Marcerated tissues of cyanogenic plant have been demonstrated to facilitate the uptake of gold in plants [101]. It has also been shown that plants have more affinity to adsorb gold cyanide salt compared to other salts of gold [100]. Besides metal accumulation in plant cells, plants are also known for the biomineralization of many inorganic materials. For example, calcium oxalate, calcium carbonates and silicon dioxides are found in cactaceae family plants [102]. Silica is present in the form of α -quartz or opal in certain species of cactaceae [103]. Silica is also known to be abundantly present in grasses and rice husks

[104]. Botanical magnetic nanoparticles extracted from grass, which grows in iron rich soils, have been reported [105]. The extracted magnetic nanoparticles from grass are mostly cubooctahedral shaped with a minor population of hexagonal prismatic morphologies. The smallest cubooctahedral nanoparticles were found to be 4 ± 1 nm in size, which is smaller as compared to bacterially synthesized magnetic nanoparticles [105].

Yacaman and coworkers have shown that gold and silver nanoparticles are formed inside different parts of the Alfalfa plant by uptaking corresponding metal ion precursors from the growth media [106]. The intracellular synthesis of metal nanoparticles using plants is not important from the commercial application point of view because of high cost and labor extensive processes for the extraction and purification of metal and therefore, the extracellular synthesis of metal nanoparticles is in high demand due to an easy and cheap source for the same purpose. Keeping this objective in mind, Sastry and coworkers have extensively studied the extracellular synthesis of various compositions of metal nanoparticles using different plant extracts. They have shown that the extract of different parts such as leaves, stems and roots of geranium plant can be used for the extracellular synthesis of different shapes of silver and gold nanoparticles [107]. Neem leaf extract has been used for the rapid synthesis of gold, silver and bimetallic gold core – silver shell nanoparticles [108]. They have also reported the biosynthesis of gold and silver nanoparticles using *Emblica officinalis* fruit extract [109].

All the extracts mentioned above synthesize spherical shape nanoparticles. Anisotropic nanoparticles especially triangular and rod shaped nanoparticles have gained enormous attention because of unique and superior chemical and physical properties as compared to their spherical counterparts. Single crystalline and flat shaped gold nanotriangles have been synthesized using lemongrass and tamarind leaf extract by Sastry's group [110]. They have proposed that smaller spherical nanoparticles sinter and assemble together to form gold nanotriangles at room temperature. Sintering and assembly of nanoparticles is facilitated by aldehydic and ketonic functional groups containing biomolecules present in lemongrass extract [110]. These molecules also preferentially bind to certain lattice planes of initially formed smaller gold nanoparticles and inhibit the growth in that particular direction to promote the formation of triangular

nanoparticles. The edge length of gold nanotriangles and therefore the optical properties could be controlled by merely varying the amount of lemongrass extract in the reaction medium [111]. They have also reported that the rate of reduction of gold ions using lemongrass extract also plays an important role in the synthesis of high yield and large sized gold nanotriangles. Fast reduction rate results in high yield of smaller gold nanoparticles, which are called nuclei, and therefore a small percentage of left gold ions in the solution reduce further on the surface of nuclei to form a low yield of gold nanotriangles [111]. The strong absorption of gold nanotriangles in the NIR region of electromagnetic spectrum could make them a potential candidate in the various applications such as sensors [112], coating of glass window to block NIR light from the solar spectrum [111] and for cancer hyperthermia [113]. In the present study, an attempt has been made to further investigate the size of biomolecules of lemongrass extract, which is responsible for controlling the size and shape of gold nanotriangles.

1.6 Various methods for synthesis of anisotropic nanoparticles:

A number of methods are present in the literature for the size-controlled synthesis of metal nanoparticles. Recently, shape controlled synthesis of metal nanoparticles is being paid much attention because of a fine control over the chemical and physical properties of nanoparticles. Anisotropic nanoparticles such as nanorods/nanowires [114], nanodumbbells [115], nanorattles [116], nanotubes [117], nanocubes [118], nanotriangles [119], nanohexagons [120], nanodiscs [121], starshaped [122], multipods [123], decahedron [124], tetrahedrals [125] and dendritic shaped [126] have been synthesized using various methods. Various methods such as 1) synthesis in the presence of templates, 2) synthesis in the presence of micelles or surfactants, 3) physical process such as lithography, vapor deposition method and 4) synthesis in the presence of capping agents and biological sources, have been employed for the synthesis of anisotropic nanoparticles.

1.6.1 Synthesis in presence of templates:

Template directed synthesis is one of the most exploited methods for the synthesis of anisotropic nanoparticles. In this method, the template serves as a scaffold for the deposition and fabrication of nanoparticles with its shape complementary to the

morphology of used template. Channels in porous materials play an important role in the synthesis of 1D nanostructures. Polymer films containing track-etched channels and anodically etched alumina membrane are mostly used. Synthesis of arrays of gold and silver nanotubes using alumina membrane has been reported [47]. Polycarbonate membranes and mesoporous silica have also been exploited for the synthesis of nanorods and nanowires [47]. Furthermore, pre-synthesized nanoparticles have been used as a template for the synthesis of nanoparticles. Xia *et al.* have used silver nanowires for the formation of Au, Pt, and Pd nanotubes via galvanic displacement reaction [46]. Mirkin's group has used silver nanoprism as sacrificing templates for the fabrication of triangular nanoframes of gold and silver [46d]. Block copolymer and polymer are another examples of templates, which have been employed for the generation of anisotropic nanostructures. These templates have been exploited for the synthesis of Au and Ag nanowires and nanosheets [127]. In a recent study, Schatz and co-workers have observed that Ag nanodisks could be obtained using polystyrene mesospheres as template [128]. DNA is a soft biological material, which has been extensively exploited for the fabrication of nanowires. Cu nanowires, Ag nanorods and Pd nanowires arrays have been fabricated on the solid substrate templated by DNA with direct reduction of metal ions [43]. Wei *et al.* have shown that silver ions bound to DNA networks are reduced using sodium borohydride to generate silver nanoparticles, nanorods and nanowires [129]. The diameter of silver nanoparticles and the aspect ratio of nanorods and nanowires could be controlled by simply varying the concentration of DNA and the reduction time.

1.6.2 Synthesis in presence of micelles/surfactants:

1.6.2.1 Electrochemical method:

Wang and coworkers have demonstrated a method for the synthesis of gold nanorods via electrochemical method by using gold cathode and platinum anode electrode, which are immersed in an electrolyte solution containing a shape inducing surfactant hexadecyltrimethylammonium bromide (CTAB) and rod inducing cosurfactants tetraoctylammonium bromide (TCAB). During growth of gold nanorods, the bulk gold metal is converted from anode to form gold nanoparticles preferentially at the interfacial region of the cathodic surface and within the electrolyte solution [130]. The ratio between surfactants controls the average aspect ratio of gold nanorod. Recently

Mulvaney's group has also proposed the electrochemical mechanism for the growth of nanorods [131]. They have reported that flux of Au(I) bound to cationic micelles to the seed surface is maximum at point of highest curvature, where electrical double layer gradient is highest. Sun *et al.* have shown the synthesis of silver nanotubes using solid electrolytes RbAg_4I_5 under direct current electric field treatment (DCEF) [132].

1.6.2.2 Seed mediated method:

The seed mediated method for the synthesis of gold nanorods/wires is a very popular approach and is established by Murphy's group [133]. The protocol is based on the reduction of metal salt by a weak reducing agent in the presence of preformed metal nanoparticles (seeds) and surfactants. Ascorbic acid is used as a weak reducing agent because it reduces Au^{3+} to Au^0 oxidation state in the presence of CTAB only after addition of gold seeds to prevent any further nucleation. They have also demonstrated the effect of added AgNO_3 in the aspect ratio of gold nanorods [133]. Seed mediated growth under alkaline condition (in presence of NaOH) enables the synthesis of a high yield of gold nanorods. El-Sayed's group has modified these methods resulting in a very high yield of nanorods [134]. It is reported that synthesis of gold nanorods could occur due to the templating action of micelles or preferential binding of surfactant molecules (CTAB) on the $\{110\}$ faces of fcc gold [133f]. Further, Murphy's group has demonstrated that gold nanorods of large aspect ratio can be achieved by using smaller gold nanoparticles as seeds [133b]. They have also shown that Br^- ions as counterions play an important role for the formation of gold nanorods, while Cl^- and I^- ions do not offer similar result [133g]. Recently Mirkin's group has shown the synthesis of gold nanotriangles using seed mediated approach in aqueous solution containing the capping agent (cetyltrimethylammonium bromide (CTAB)), gold ions ($\text{HAuCl}_4 \cdot 3\text{H}_2\text{O}$), reducing agent (ascorbic acid), and NaOH [135]. Chan and coworkers have also demonstrated the large-scale synthesis of silver nanodisk/nanoplates using seed mediated method [136]. Recently Yan's group has shown the synthesis of gold nanorods and bypryramids using cetyltriethylammonium bromide (CTEAB) solution in the presence of silver nitrate [137]. They have observed that a high yield and tunable longitudinal plasmon vibration band from 750 to 1020 nm of gold nanorods could be achieved by simply varying the amount of seeds in the reaction solution.

1.6.2.3 Photochemical method:

Yang's group has demonstrated the synthesis of gold nanorods with highly controllable aspect ratio and a high yield using photochemical method [138]. This method involves the reduction of gold ions using UV light irradiation in the presence of surfactants C₁₆TAB and TC₈AB as well as different amounts of silver ions. Hexadecyltrimethylammonium chloride (HTAC) has also been used for the formation of gold nanorods using photochemical irradiation [139]. The specific concentration of HTAC is responsible for the formation of rod shaped micelles in solution, which promote the synthesis of nanorods instead of spherical nanoparticles. Recently Ahmadi's group has demonstrated the growth of gold nanorods by controlling the intensity of UV light used and time duration for irradiation [140].

1.6.3 Synthesis using physical methods:

Physical methods have been demonstrated for the formation of anisotropic nanoparticles. Nanorods and nanowires have been obtained by vacuum vapor deposition of copper on the carbon film. The rough surfaces of carbon film promote renucleation of copper vapor leading to the linear growth with uniform thickness [141]. Zhou *et al.* have demonstrated the synthesis of silver nanowires by solid-liquid discharge arc. In this method the arc discharge of the silver filaments in NaNO₃ solution leads to the formation of linear structures [142]. Mirkin's group has shown the photoinduced conversion of spherical silver nanoparticles into nanotriangles using a laser light [143]. In recent study, Callegari *et al.* have shown photoinduced conversion of silver nanospheres, wherein the wavelength of light used plays an important role in controlling size and shape of nanoparticles formed [144]. Nanosphere lithography technique has also been used for the synthesizing triangular, cup shaped and crescent shaped nanoparticles. In this method a monolayer of polystyrene spheres is drop-coated on a substrate and then metal is deposited on them by vacuum deposition. On removing the close packed sphere template, highly ordered triangular shaped nanoparticles deposited through the void spaces only remain [145]. Alternatively, the metal layer deposited on the spheres themselves can also be removed by dissolving the polystyrene spheres leading to formation of nanocups [146]. Sastry and coworkers have shown that the physical constrains on the liquid-liquid

and liquid-air interface also promote the synthesis of highly anisotropic nanostructures such as tapes, fractal like structures and plates [147].

1.6.4 Synthesis in presence of capping agents:

Different types of capping agents have been extensively used for the synthesis of triangular, hexagonal and rods shaped nanoparticles. Polyamines [148], lyotropic liquid crystal (LLC) mainly made of poly(ethylene oxide)-poly(propylene oxide)-poly(ethylene oxide) block copolymer and water after adding small amount of capping agents, cetyltrimethylammonium bromide (CTAB) or tetrabutylammonium bromide (TBAB) [149] have been used for the synthesis of gold nanotriangles and hexagons. Poly(N-vinyl-2-pyrrolidone) (PVP) has also been used for the synthesis of triangular and rods shaped nanoparticles of a high yield [150]. PVP molecules interact with the {100} planes as compared to the {111} planes of nanoparticles and promote the growth of anisotropic nanoparticles. Liz-Marzan and coworkers have demonstrated the synthesis of silver nanoprisms by boiling AgNO_3 in N,N-dimethylformamide in presence of poly(vinylpyrrolidone) [151]. Xia's group has reported the synthesis of nanowires of silver and platinum as well as the synthesis of nanocubes and nanotriangles of silver [152]. Other capping agents have also been used for the shape-controlled synthesis of the nanoparticles [153].

1.6.5 Synthesis in presence of biological sources:

Shao *et al.* have demonstrated the synthesis of single crystalline hexagonal and truncated gold nanotriangles using aspartic acid at 25 °C [154]. Similarly starch has been used for the synthesis of triangular nanoparticles in the presence of ultrasonic waves [155]. Small-biomolecules (glycyl glycine) mediated synthesis of silver nanoplates has also been reported by Zhang's group [156]. They have reported that ratio of glycyl glycine to AgNO_3 is key to control the morphology and yield of silver plates. Bacteria [81], silver binding peptides [157] and silver tolerant yeast [91] have been used for fabrication of silver nanoparticles. Chen's group has reported a high yield biological synthesis of gold nanotriangles using extract of *Sargassum* sp. (brown seaweed) [158]. Southam and coworkers have demonstrated the synthesis of gold nanocubes and

octahedral (111) gold plates, when filamentous cyanobacterium (*Plectenoma boryanum* UTEX 485) was exposed to $\text{Au}(\text{S}_2\text{O}_3)_2^{3-}$ ions and AuCl_4^- ion solutions respectively [159].

1.7 Synthesis of core-shell nanoparticles:

In above sections, syntheses of various compositions of monometallic nanoparticles using different physical, chemical and biological methods have been described. Recently, bimetallic nanoparticles have received intense attention owing to their different optical, magnetic, catalytic properties relative to those of individual metals [160]. Since these properties strongly depend upon compositions, sizes and shapes of nanoparticles, extensive research has been carried out in this direction to synthesize core-shell and alloy nanoparticles. The nanoscale coatings not only stabilize colloidal dispersions but also allow modification and tailoring of the nanoparticle properties (optical, catalytic and magnetic) depending on coating compositions [161]. Advance materials derived from core-shell nanoparticles have extensive scientific and technological interest due to their unique properties [162].

Bimetallic nanoparticles can be prepared by the successive reduction of one metal over the nuclei of another to obtain alloy nanoparticles and simultaneous co-reduction of two kinds of metal ions with or without protective agent [163]. Two methods widely used for the surface modification of nanoparticles are of precipitation of shell materials (inorganic) and layer-by-layer deposition of charged species. Preparation and characterization of bimetallic nanoparticles constituting various combinations of noble metals such as Au/Pd [164], Au/Pt [165], Ag/Pd [166], Ag/Pt [167], Ag/Au [168] and Au/Ag [169] has been reported. Synthesis of core-shell nanoparticles of different shapes, for instance rod [169f], rattle [116], dumbbell [115] and triangular [169h], has also been reported. Sastry and coworkers have shown the synthesis of spherical Au/Ag core-shell nanoparticles using Keggin ions as UV switchable reducing agent [169d] and tyrosine as a reducing under alkaline condition agent for the selective reduction of silver ions on the gold nanoparticle surface [169e]. Nanoparticles composed of free electron of metals such as Au and Ag are known to provide strong resonance optical responses when irradiated with light [170], which result in amplification of light induced processes undergone by

molecular localization on their surfaces, such as Raman scattering, giving rise to surface enhanced Raman scattering (SERS) [171].

Apart from metal-metal core-shell nanoparticles, metal-oxide bimetallic nanoparticles have also gained enormous interest because of their application in photodegradation of dyes [172] and organic pollutants in wastewater [173] as well in the development of photochromatic materials [174]. Among inorganic coatings, silica has been used extensively to coat colloid nanoparticles, including metal nanoparticles. Liz-Marzan and coworkers have shown that a vitreophilic metal nanoparticle surface facilitates the formation of uniform silica coatings [175]. Gold nanoparticles were made vitreophilic by using the coupling agent (3-aminopropyl)trimethoxysilane, and silica coatings were obtained by subsequent exposure of the particles to a sodium silicate solution followed by the Stober process [176]. In a recent study, Hardikar and Matijevic have also used the Stober process for silica coating on silver nanoparticles [177]. Recently, Mulvaney *et.al.* reported the encapsulation of metal clusters and semiconductors by silica shells [178]. Titania is another metal oxide that is of interest for coating applications as; it is widely known to be a useful catalyst [179]. Catalytic application demands high surface area to volume ratio and thus significant efforts have been focus on the coating of titania on the high surface area supports such as colloid nanoparticles. Caruso's group has reported the synthesis of gold-titania core-shell nanoparticles by polyelectrolytes complexation with titania precursor [180]. Liz-Marzan and coworkers have shown the one pot synthesis of gold-titania core-shell nanoparticles [181]. In this thesis, an attempt has been made towards the synthesis of triangular Au core - Ag shell nanoparticles and spherical gold core – titania shell nanoparticles.

1.8 Shape modification of nanoparticles:

It remains a major challenge to develop new methods for nanoparticle synthesis to obtain a further variety of more complex nanostructures, for an increasing wide range of applications. One approach is to use preformed nanoparticles for fabrication of new nanostructures, while another approach is to modify the nanoparticle growth reaction *in situ* to favor geometrical and morphological changes in the final nanoparticles. A variety of chemical and physical methods have been developed for the shape transformation of

already formed nanoparticles. Recently, Halas's group has shown the reshaping of metallodielectric nanoparticles upon exposure to CTAB [182]. The metal shell having silica core was observed to undergo morphological change from initial shell structures to that of an elongated or toroid shape nanostructures. Liz-Marzan's group has demonstrated the oxidation of gold nanoparticles in the presence of CTAB using gold ions [183]. They have reported that oxidation preferentially occurs at higher curvature surface of the nanoparticles. Stoeva *et al.* have also shown the reversible transformation of already synthesized gold nanoparticles under reflux condition [184]. Furthermore, physical methods i.e. laser ablation [185] and laser-assisted size reduction [186] have been used to fragment metal nanoparticles into smaller ones through selective heating of parent nanoparticles. Gold nanoparticles of 20 nm size can be selectively transformed into nanonetworks or smaller nanoparticles depending on the proper combination of the fluence of 532 nm laser and the protecting ligand concentration [187]. Shape transformation by laser irradiation has also been observed leading to the formation of Φ shaped nanoparticles from nanorods [188]. In an interesting approach, Roorda *et al.* have demonstrated the formation of gold nanorods by ion beam irradiation of spherical gold-silica core-shell nanoparticles [189]. On the contrary, Mirkin's group has demonstrated the photoinduced transformation of spherical silver nanoparticles into triangular nanoparticles [143]. Similarly, thermally induced transformation of spherical gold clusters to nanocubes has also been demonstrated [190].

1.9 Outline of Thesis:

The work involved in this thesis discusses biological synthesis of gold nanotriangles using lemongrass extract. Different cut-off dialysis bags are used for size selective separation of biomolecules of lemongrass extract. Size and shape controlled synthesis of gold nanotriangles has been achieved by using different cut-off bags. An attempt has also been made to investigate the size of biomolecules, which is responsible for the formation of gold nanotriangles. Synthesis of triangular Au core - Ag shell nanoparticles using ascorbic acid as a reducing agent under alkaline condition has been described in detail. Biological synthesis of spherical gold-titania core-shell nanoparticles using hydrolyzing enzyme from fungus *Fusarium oxysporum* has also been explained.

Shape transformation of gold nanotriangles using different chemical such as halide ions and surfactants has been demonstrated. Furthermore, UV light has been used for the photofragmentation of gold nanotriangles into spherical nanoparticles using Keggin ions (phosphotungstic acid). Temperature dependent synthesis of gold nanoparticles using lemongrass extract as reducing and shape directing agent has been explained. The chapter wise discussion of these studies is as follows:

The second chapter describes the experimental and characterization techniques such as UV-vis-NIR Spectroscopy, Fourier Transform Infrared Spectroscopy (FTIR), Transmission Electron Microscopy (TEM), High-Resolution Transmission Electron Microscopy (HRTEM) Scanning Electron Microscopy (SEM), Atomic Force Microscopy (AFM), Energy Dispersive Analysis of X-ray (EDAX), Isothermal Titration Calorimetry (ITC), X-ray diffraction (XRD) and X-ray Photoemission Spectroscopy (XPS) that are extensively used for the characterization of nanoparticles. The physical principles on which the different techniques are based and their applications to understand various aspects of formation of the nanoparticles have been outlined.

The third chapter describes the size and shape controlled biosynthesis of gold nanoparticles using lemongrass extract. Biological processes for synthesis of metal nanoparticles are economical alternative and challenge for chemical and physical methods available for size controlled synthesis of nanoparticles, which are not environmentally benign. Gold nanotriangles and spherical nanoparticles are obtained by reduction of gold ions using lemongrass extract. The size of gold nanotriangles can be fine tuned by varying the amount of lemongrass extract in reaction solution and thus control the optical properties of gold nanotriangles in NIR region of electromagnetic spectrum. Dialysis is one of the methods for size selective purification of a compound from a crude mixture. The chapter also describes the size and shape controlled synthesis of gold nanotriangles using lemongrass extract during dialysis through different cut-off dialysis bags. We have also attempted to find out the molecular weight of biomolecule(s) in the lemongrass extract, that act as reducing and/or shape directing agents in the synthesis of triangular gold nanotriangles.

The fourth chapter describes the synthesis of triangular Au core-Ag shell nanoparticles. Many protocols have been developed for the synthesis of spherical core-

shell nanoparticles of various compositions but so far only few reports are available for anisotropic core-shell nanoparticles. This chapter describes the synthesis of triangular shape Au-Ag core-shell nanoparticles at room temperature. The chapter emphasizes the thickness control of silver shell on the gold core by varying the pH of reaction solution. The chapter also illustrates the synthesis of spherical shape gold-titania core-shell nanoparticles using a hydrolyzing protein. The hydrolyzing protein has been isolated from the fungus *Fusarium oxysporum*. It is cationic in nature and is a mixture of two protein components. Titania salts are selectively hydrolyzed on the surface by the hydrolyzing protein immobilized on the aspartic acid modified gold nanoparticles leading to gold-titania core-shell nanoparticles.

The fifth chapter illustrates the effect of different halide ions on the morphology of gold nanotriangles during and post synthesis using lemongrass extract. Halide ions have different propensity to adsorb on the different crystallographic faces of gold nanotriangles and modify the morphology of nanoparticles. An attempt has also been made to understand the crystal growth of nanoparticles, which leads to the formation of gold nanotriangles. During the synthesis of gold nanoparticles using lemongrass extract, iodide ions drastically changed the morphology of gold nanoparticles to spherical shape. We have also described the effect of surfactants like Cetyltrimethylammonium bromide (CTAB) and Cetyltrimethylammonium chloride (CTAC) on the morphology of already synthesized gold nanotriangles in the chapter. We have emphasized the effect of different concentration of gold ions on the morphology of gold nanotriangles-surfactants complex.

The sixth chapter discusses the different physical means to control the size and shape of the gold nanotriangles. Temperature is a crucial factor for size-controlled synthesis of nanoparticles. There are several reports on the synthesis of anisotropic nanoparticles at higher temperatures. We have discussed the effect of temperature on the yield and size of the gold nanotriangles in this chapter. The rate of reduction of metal ions governs the shape and size of the synthesized nanoparticles; an attempt has been made to comprehend the nanotriangles growth. At higher temperature, the size and yield of gold nanotriangles synthesized by using lemongrass extract is lower than at room temperature. In this chapter, photo-fragmentation of gold nanotriangles in presence of keggin ions (phosphotungstic acid) by UV light has also been discussed. Keggins ions

are polyoxymetallates and can act as UV-switchable reducing agent. Different concentrations of PTA molecules were added during and post synthesis of gold nanotriangles using lemongrass extract, followed by UV irradiation for 3 hours to break gold nanotriangles into small size gold nanoparticles.

The seventh chapter summarizes the work addressed in the thesis and emphasizes on the possible further research work in this area.

1.10 References:

- [1] Thompson, D. W. *On the Growth and Form* (Cambridge Univ. Press, Cambridge, UK, 1942).
- [2] Stevens, P. S. *Patterns in Nature* (Atlantic Monthly, Boston, 1974).
- [3] Wainwright, S. A.; Biggs, W. D.; Currey, J. D.; Gosline, J. M. *Mechanical Design in Organisms* (Princeton Univ. Press, Princeton, 1976).
- [4] Vogel, S. *Cats' Paws and Catapults* (W. W. Northon & Company, New York, 1998).
- [5] Ball, P. *Designing the Molecular World: Chemistry at the frontier 1994*, Princeton University Press, New Jersey, USA.
- [6] Bao, G. *Single molecule biomechanics: DNA and protein deformation*. In *Mechanics in biology*, Casey, J.; Bao, G. Eds; ASME: New York, 2000; Vol. 242, pp 25-35.
- [7] Mann, S.; Calvet, P. *J. Mater. Sci.* **1998**, 23, 3801.
- [8] Sarikaya, M.; Aksay, I. A. *Biomimetics: Design & Processing of Materials* (American Institute of Physics, New York, 1995).
- [9] Mann, S. *Biomimetic Material Chemistry* (VCH, New York, 1996).
- [10] The classic talk by Richard Feynman entitled "There's plenty of room at the bottom" delivered at the annual meeting of the American Physical Society at the California Institute of Technology in 1959 is possibly the first serious exposition on the problem of manipulating nanoscale objects (the talk is available on the web at <http://www.zyvex.com/nanotech/feynman.html>).
- [11] Niemeyer, C.M. *Angew. Chem. Int. Ed.*, **2001**, 40, 4128.
- [12] A complete issue dedicated to molecular motors: *Acc. Chem. Res.*, **2001**, 34.
- [13] a) Chaudhary, Y. S.; Ghatak, J.; Bhatta, U. M.; Khushalani, D. *J. Mater. Chem.* **2006**, 16, 3619. b) Li, M.; Schnablegger, H.; Mann, S. *Nature*, **1999**, 402, 393. c) Liu, J.; Raveendran, P.; Qin, G.; Ikushima, Y. *Chem. Commun.* **2005**, 2972. d) Wang, C.; Ma, Z.; Su, Z. *Nanotechnology*, **2006**, 17, 1819. e) Stamou, D.; Duschl, C.; Delamarche, E.; Vogel, H. *Angew. Chem. Int. Ed.* **2003**, 42, 5580. f) Liu, B.; Zeng, H. C. *J. Am. Chem. Soc.* **2005**, 127, 18262. g) Correa-Duarte, M. A.; Sobal, N.; Liz-Marzan, L. M.; Giersig, M. *Adv. Mater.* **2004**, 16, 2173. h) Nakao, S.; Torigoe, K.; Kon-No, K.; Yonezawa, T. *J. Phys. Chem. B.* **2002**, 106, 12097. i) Cheng, J. Y.; Zhang, F.; Chuang, V. P.; Mayes, A. M.; Ross, C. A. *Nano Lett.* **2006**, 6, 2099. j)

- Hong, B. H.; Lee, J. Y.; Lee, C.-W.; Kim, J. C.; Bae, S. C.; Kim, K. S. *J. Am. Chem. Soc.* **2001**, *123*, 10748. k) Feldheim, D. L.; Keating, C. D. *Chem. Soc. Rev.* **1998**, *27*, 1. l) Whitesides, G. M.; Grzybowski, B. *Science* **2002**, *295*, 2418.
- [14] a) Bernard F.; Gaffet, E.; Champion, Y.; Budarina, N.; Ustinov A. *J. Phys. IV France*, **2002**, *12*, 6. b) Zhan, Z.; He, Y.; Wang, D.; Gao, W. *Surf. Coat. Technol.* **2006**, *201*, 2684. c) Yilmaz, H.; Isobe, T.; Hotta, Y.; Sato, K.; Watari, K. *J. Chem. Soc. Jap.* **2006**, *114*, 1100. d) Song, M. Y.; Lee, D. S.; mumm, D. R. *Mater. Res. Bull.* **2006**, *41*, 1720. e) Trojanova, Z.; Bosse, M.; Zeigmann, G.; Mielczarek, A.; Ferkel, H. *Key Engin. Mater.* **2006**, *319*, 189. f) Zhang, L. L.; Tu, J. P.; Zhang, h. C.; He, D. N. *Chinese J. Inorg. Chem.* **2006**, *22*, 1591.
- [15] a) Mendes, P. M.; Jacke, S.; Critchley, K.; Plaza, J.; Chen, Y.; Nikitin, K.; Palmer, R. E.; Preece, J. A.; Evans, S. D.; Fitzmaurice, D. *Langmuir* **2004**, *20*, 3766. b) Myers, B. D.; Dravid, V. P. *Nano Lett.* **2006**, *6*, 963. c) Donthu, S.; Pan, Z.; Myers, B.; Shekhawat, G.; Wu, N.; Dravid, V. *Nano Lett.* **2005**, *5*, 1710. d) Murayama, A.; Hirano, H.; Hyomi, K.; Sakuma, M.; Souma, I.; Oka, Y. *J. Luminescence.* **2007**, *122*, 837. e) Mukhopadhyay, R. *Anal. Chem.* **2006**, *78*, 2878. f) Morita, K.; Ohnaka, K. *Ind. Eng. Chem. Res.* **2000**, *39*, 4684. g) Ndoni, S.; Vigild, M. E.; Berg, R. H. *J. Am. Chem. Soc.* **2003**, *125*, 13366. h) Zeng, H. C. *Inorg. Chem.* **1998**, *37*, 1967. i) Hsu, Z. Y.; Zeng, H. C. *J. Phys. Chem. B.* **2000**, *104*, 11891.
- [16] Savage, G. *Glass and Glassware*; Octopus Book: London, 1975. b) Wagner, F. E.; Haslbeck, S.; Stievano, L.; Calogero, S.; Pankhurst, Q. A.; Martinek, K.-P. *Nature* **2000**, *407*, 691. c) Turkevich, J. *Gold Bull.* **1985**, *18*, 86. d) Ayers, A. *Ceramics of the World: From 4000 BC to the Present*, New York, 1992, 284. e) Zhao, H.; Ning, Y. *Gold Bull.* **2000**, *33*, 103.
- [17] a) Antonii, F. *Panacea Aurea-Auro Potabile*; Bibliopolio Frobeniano: Hamburg, **1618**. b) Kunckels, J. *Nuetliche Observationes oder Anmerkungen von Auro und Argento Potabili*; Schutzens: Hamburg, **1676**. c) Helcher, H. H. *Aurum Potabile oder Gold Tinstur*; J. Herbord Klossen: Breslau and Leipzig, **1718**. d) Ostwald, W. *Zur Geschichte des Colloiden Goldes. Kolloid Z.* **1909**, *4*, 5.
- [18] Faraday, M. *Philos. Trans. R. Soc. London* **1857**, *147*, 145.
- [19] Graham, T. *Philos. Trans. R. Soc.* **1861**, *151*, 183.

- [20] Taniguchi, N. 1974. On the Basic Concept of 'Nano-Technology'. In: *Proceedings of the international conference on production engineering. Tokyo, Part II*, Japan Society of Precision Engineering, 1974: 18-23: Tokyo: JSPE.
- [21] a) <http://www.Personal.psu.edu/users/w/x/wxk116/axe/>. b) <http://images.google.co.in/Image?hl=en&q=MEMS&ie=UTF8&oe=UTF.c> c) <http://images.google.co.in/images?hl=en&q=electron%20beam%20lithography&ie=UTF-8&oe=UTF-8&oe>.
- [22] a) Messing, G. L.; Zhang, S. C.; Jayanti, G. V. *J. Am. Ceram. Soc.* **1993**, *76*, 2707. b) Gurav, A.; Kodas, T.; Pluym, T.; Xiong, Y. *Aerosol Sci. Technol.* **1993**, *19*, 411. c) Brennan, J. G.; Seigrist, T.; Carroll, P. J.; Stuczynski, S. M.; brus, L. E.; Steigerwalk, M. L. *J. Am. Chem. Soc.* **1989**, *111*, 4141. d) Osakada, K.; Yamamoto, T. *J. Chem. Soc. Chem. Commun.* **1987**, 1117. e) Steigerwalk, M. L.; Sprinkle, C. R. *J. Am. Chem. Soc.* **1987**, *109*, 7200. f) Kang, Y. C.; Roh, H. S.; Park, S. B. *Adv. Mater.* **2000**, *12*, 451. g) Validzic, I. Lj.; Jokanovic, V.; Uskokovic, D. P.; Nedeljkovic, J. M. *J. Euro. Ceram. Soc.* **2007**, *27*, 927. h) Prathap, P.; Subbaiah, Y. P. V.; Devika, M.; Reddy, K. T. R. *Mater. Chem. Phys.* **2006**, *100*, 375. i) Romero, R.; Leinen, D.; Dalchiele, E. A.; Ramos-Barrado, J. R.; Martin, F. *Thin Solid Films* **2006**, *515*, 1942. j) Ju, S. H.; Kim, D. Y.; Koo, H. Y.; Hong, S. K.; Jo, E. B.; Kang, Y. C. *J. Alloy Comp.* **2006**, 425, 411. k) Krunks, M.; Dedova, T.; Oja-Acik, I. *Thin Solid Films* **2006**, *515*, 1157.
- [23] a) Itakura, T.; Torigoe, K.; Esumi, K. *Langmuir* **1995**, *11*, 4129. b) Ershov, B. G.; Henglein, A. *J. Phys. Chem.* **1993**, *97*, 3434. c) Gutierrez, M.; Henglein, A. *J. Phys. Chem.* **1993**, *97*, 11368. d) Henglein, A.; Mulvaney, P.; Holtzworth, A.; Sosebee, T. E.; Fojitik, A. *Ber. Bunsenges. Phys. Chem.* **1992**, *96*, 754. e) Yonezawa, Y.; Sato, T.; Ohno, M.; Hada, H. *J. Chem. Soc., Faraday Trans. I* **1987**, *83*, 1559. f) Yonezawa, Y.; Sato, T.; Kuroda, S. *J. Chem. Soc. Faraday Trans. I* **1991**, *87*, 1905. g) Torigoe, K.; Esumi, K. *Langmuir* **1993**, *9*, 1964. h) Itakura, T.; Torigoe, K.; Esumi, K. *J. Jpn. Soc. Colour Mater.* **1994**, *67*, 1695. i) Marignier, J. L.; Belloni, J.; Delcourt, M. O.; Chevalier, J. P. *Nature* **1986**, *317*, 344. j) Kurihara, K.; Kizing, J.; Stenius, P.; Fender, J. H. *J. Am. Chem. Soc.* **1983**, *105*, 2574. k) T. Chen, S. Chen, H. Sheu, C. Yeh, *J. Phys. Chem. B* **2002**, *106*, 9717. l) Zhu, J.; Liao, X.; Zhao, X.; Wang, J. *Mater. Lett.* 2001, *47*, 339.

- [24] a) Henglein, A. *Langmuir* **1999**, *15*, 6738. b) A. Henglein, *J. Phys. Chem. B* **2000**, *104*, 1206. c) Joshi, S. S.; Patil, S. F.; Iyer, V.; Mahumuni, S. *Nanostruct. Mater.* **1998**, *10*, 1135. d) Henglein, A.; Meisel, D. *Langmuir* **1998**, *14*, 7392.
- [25] a) El-Shall, M. S. *Appl. Surf. Sci.* 1996, *106*, 347. b) Wegner, K.; Walker, B.; Tsantilis, S.; Pratsinis, S. E. *Chem. Eng. Sci.* 2002, *57*, 1753. c) Vitulli, G.; Bernini, M.; Bertozzi, S.; Pitzalis, E.; Salvadori, P.; Coluccia, S.; Martra, G. *Chem. Mater.* **2002**, *14*, 1183.
- [26] a) Reetz, M. T.; Helbig, W. *J. Am. Chem. Soc.* **1994**, *116*, 7401. b) Reetz, M. T.; Winter, M.; Breinbauer, R.; Thurn-Albrecht, T.; Vogel, W. *Chem. Eur. J.* **2001**, *7*, 1084. c) Reetz, M. T.; Helbig, W.; Quaiser, S. A.; Stimming, U.; Breuer, N.; Vogel, R. *Science* **1995**, *267*, 367. d) Natter, H.; Hempelmann, R. *Electrochim. Acta* **2003**, *49*, 51. e) Rodriguez-Sanchez, L.; Blanco, M. C.; Lopez-Quintela, M. A. *J. Phys. Chem. B* **2000**, *104*, 9683. f) Rodriguez-Sanchez, M. L.; Rodrigues, M. J.; Blanco, M. C.; Rivas, J.; Lopez-Quintela, M. A. *J. Phys. Chem. B* **2005**, *109*, 1183. g) Zhou, M.; Chen, S.; Zhao, S.; Ma, H. *Physica E: Low-Dimensional Systems and Nanostructures* **2006**, *33*, 28. h) Starowicz, M.; Stypuła, B.; Banaś, J. *Electrochem. Commun.* **2006**, *8*, 227. i) Liu, Y.-C., Yu, C.-C. *J. Electrochem. Soc.* **2005**, *585*, 206. j) Liu, Y.-C., Lin, L.-H., Chiu, W.-H. *J. Phys. Chem. B* **2004**, *108*, 19237.
- [27] a) R. A. Salkar, P. Jeevanandam, G. Kataby, S.T. Aruna, Y. Koltypin, O. Palchik, A. Gedanken, *J. Phys. Chem. B* **2000**, *104*, 893. b) Li, C.; Cai, W.; Li, Y.; Hu, J.; Liu, P. *J. Phys. Chem. B* **2006**, *110*, 1546.
- [28] a) Klabunde, K. J.; Timms, P. S.; Skell, P. S.; Ittel, S. *Inorg. Synth.* **1979**, *19*, 59. b) Davis, S. C.; Klabunde, K. J. *Chem. Rev.* **1982**, *82*, 153. c) Kim, J. H.; Germer, T. A.; Mulholland, G. W.; Ehrman, S. H. *Adv. Mater.* **2002**, *14*, 518. d) Klabunde, K. J.; Groshens, T.; Brezinski, M.; Kennelly, W. *J. Am. Chem. Soc.* **1978**, *19*, 59. e) Cardenas-Trivino, G.; Alvial, J. M.; Klabunde, K. J.; Pantoja M. O.; Soto Z. H. *Colloid Polymer Sci.* **1994**, *272*, 310.
- [29] a) Frenot, A.; Chronakis, H. S. *Current opin. Colloid interf. Sci.* **2003**, *8*, 64. b) Reneker, D. H.; Chun, I. *Nanotechnology* **1996**, *7*, 216. c) Fong, H.; Liu, W.; Wang, C. S.; vaia, R. A. *polymer* 2002, *43*, 775. d) Mathews, J. A.; Wnek, G. E.; Simpson,

- D. G.; Bowlin, G. L. *Biomacromolecules* **2002**, *3*, 232. e) Larsen, G.; Vearde-Ortiz, R.; Minchow, K.; Barrero, A.; Loscertales, I. G. *J. Am. Chem. Soc.* **2003**, *125*, 1154. f) Dai, H.; Gong, J.; Kim, H.; Lee, D. *Nanotechnology* **2002**, *13*, 674. g) Li, D.; Xia, Y. *Nano Lett.* **2003**, *3*, 555.
- [30] a) Kunhara, K.; Iwadate, K.; Namatsu, H.; Nagase, M.; Murase, K. *J. Vac. Sci. Technol.* **1995**, *B13*, 2170. b) Liu, H. I.; Beigelsen, D. K.; Ponce, F. A.; Johnson, N. M.; Pease, R. F. *Appl. Phys. Lett.* **1994**, *64*, 1383. c) Xia, Y.; Rogers, J. A.; Paul, K. E.; Whitesides, G. M. *Chem. Rev.* **1999**, *99*, 1823. d) Yin, Y.; Gates, B.; Xia, Y. *Adv. Mater.* **2000**, *12*, 1426. e) Ginger, D. S.; Zhang, H.; Mirkin, C. A. *Angew. Chem. Int. Ed.* **2004**, *43*, 30. f) Lee, S. W.; Oh, B.-H.; Sanedrin, R. G.; Salaita, K.; Fujigaya, T.; Mirkin, C. A. *Adv. Mater.* **2006**, *18*, 1133. g) Wang, L.; Uppuluri, S. M.; Jin, E. X.; Xu, X. *Nano Lett.* **2006**, *6*, 361. h) Choi, Y.-K.; Zhu, J.; Grunes, J.; Bokor, J.; Somorjai, G. A. *J. Phys. Chem. B.* **2003**, *107*, 3340. i) Delamarche, E.; Hoole, A. C. F.; Michel, B.; Wilkes, S.; Despont, M.; Welland, M. E.; Biebuyck, H. *J. Phys. Chem. B.* **1997**, *101*, 9263. j) Kuo, C.-W.; Shiu, J.-Y.; Chen, P. *Chem. Mater.* **2003**, *15*, 2917. k) Wang, W.; Lee, T.; Reed, M. A. *Nano Lett.* **2004**, *4*, 533. l) Bratton, D.; Yang, D.; Dai, J.; Ober, C. K. *Poly. Adv. Technol.* **2006**, *17*, 94.
- [31] a) Jensen, K. F.; Kern, W. *Thin Film Processes II*, Academic Press, San Diego, **1991**. b) Choy, K. L.; *Prog. Mater. Sci.* **2003**, *48*, 57. c) Ser, P.; Kalck, P.; Feurer, R. *Chem. Rev.* **2002**, *102*, 3085. d) Qiu, J.; Li, Q.; Wang, Z.; Sun, Y.; Zhang, H. *Carbon* **2006**, *44*, 2565. e) He, C.; Zhao, N.; Han, Y.; Li, J.; Shi, C.; Du, X. *Mater. Sci. Engin. A* **2006**, *441*, 266. f) Che, G.; Lakshmi, B. B.; Martin, C. R.; Fisher E. R.; Ruoff, R. S. *Chem. Mater.* **1998**, *10*, 260. g) Liao, H.; Hafner, J. H. *J. Phys. Chem. B* **2004**, *108*, 6941. h) Bondi S. N., Lackey, W. J.; Johnson, R. W.; Wang X.; Wang Z. L. *Carbon* **2006**, *44*, 1393.
- [32] a) Wagener, M.; Gunther, B. *J. Magnet. Mag. Mater.* **1999**, *201*, 41. b) Mwabora, J. M.; Lindgren, T.; Avendano, E.; Jaramillo, T. F.; Lu, J.; Lindquist, S.-E.; Granqvist, C.-G. *J. Phys. Chem. B.* **2004**, *108*, 20193. c) Yang, G. H.; Zhang, Y.; Kang, E. T.; Neoh, K. G. *J. Phys. Chem. B.* **2003**, *107*, 2780.
- [33] a) Fojtik, A.; Henglein, A. *Ber. Bunsen-Ges. Phys. Chem.* **1993**, *97*, 252. b) Sibbald, M. S.; Chumanov, G.; Cotton, T. M. *J. Phys. Chem.* **1996**, *100*, 4672. c) Yeh, M.-S.;

- Yang, Y.-S.; Lee, Y.-P.; Lee, H.-F.; Yeh, Y.-H.; Yeh, C.-S. *J. Phys. Chem. B* **1999**, *103*, 6851. d) Mafune, F.; Kohno, J.; Takeda, Y.; Kondow, T.; Sawabe, H. *J. Phys. Chem. B* **2000**, *104*, 8333. e) Mafune, F.; Kohno, J.; Takeda, Y.; Kondow, T.; Sawabe, H. *J. Phys. Chem. B* **2000**, *104*, 9111. f) Mafune, F.; Kohno, J.; Takeda, Y.; Kondow, T.; Sawabe, H. *J. Phys. Chem. B* **2001**, *105*, 5114. g) Brause, R.; Moltgen, H.; Kleinermanns, K. *Appl. Phys. B* **2002**, *75*, 711. h) Liu, C.; Mao, X. L.; Mao, S. S.; Zeng, X.; Greif, R.; Russo, R. E. *Anal. Chem.* **2004**, *76*, 379.
- [34] a) Cannas, C.; Musinu, A.; Peddis, D.; Piccaluga, G. *Chem. Mater.* **2006**, *18*, 3835. b) Cui, H., Zayat, M., Levy, D. *J. Sol-Gel Sci. Technol.* **2005**, *35*, 175. c) Ismail, A. A. *Appl. Catal. B Environ.* **2005**, *58*, 115. c) Liu, C.; Zou, B.; Rondinone, A. J.; Zhang, Z. J. *J. Am. Chem. Soc.* **2001**, *123*, 4344. d) Selvan, S. T.; Hayakawa, T.; Nogami, M.; Kobayashi, Y.; Liz-Marzan, L. M.; Hamanaka, Y.; Nakamura, A. *J. Phys. Chem. B.* **2002**, *106*, 10157. e) Babapour, A.; Akhavan, O.; Moshfegh, A. Z.; Hosseini, A. A. *Thin Solid Film* **2006**, *515*, 771. f) Hyeon-Lee, J.; Beaucage, G.; Pratsinis, S. E. *Chem. Mater.* **1997**, *9*, 2400. g) Lu, Y.; Yin, Y.; Mayers, B. T.; Xia, Y. *Nano Lett.* **2002**, *2*, 183. h) Liu, H.; Yang, W.; Ma, Y.; Cao, Y.; Yao, J.; Zhang, J.; Hu, T. *Langmuir*, 2003, *19*, 3001.
- [35] a) Jayakumar, O. D.; Salunke, H. G.; Kadam, R. M.; Mohapatra, M.; Yaswant, G.; Kulshreshtha, S. K. *Nanotechnology*, **2006**, *17*, 1278. b) Deshpande, V. V.; Patil, M. M.; Navale, S. C.; Ravi, V. *Bull. Mater. Sci.* **2005**, *28*, 2005. c) Yang, H.; Song, X.; Zhang, X.; Ao, W.; Qiu, G. *Mater. Lett.* **2003**, *57*, 3124.
- [36] a) Li, M.; Liu, X.-l.; Cui, D.-l.; Xu, H.-Y.; Jiang, M. -H. *Mater. Res. Bull.* **2006**, *41*, 1259. b) Wei, G.; Nan, C.-W.; Deng, Y.; Lin, Y.-H. *Chem. Mater.* **2003**, *15*, 4436. c) Chaianansutcharit, S.; Mekasuwandumrong, O.; Praserttham, P. *Cryst. Growth Des.* **2006**, *6*, 40. d) Xiong, H.-M.; Shen, W.-Z.; Wang, Z.-D.; Zhang, X.; Xia, Y.-Y. *Chem. Mater.* **2006**, *18*, 3850. e) Sha, G.; Wang, T.; Xiao, J.; Liang, C. *Mater. Res. Bull.* **2004**, *104*, 3893. f) Cushing, B. L.; Kolesnichenko, V. L.; O'Connor, C. J. *Chem. Rev.* **2004**, *104*, 3893. g) Zhang, W.; Yang, Z.; Liu, Y.; Tang, S.; Han, X.; Chen, M. *J. Cryst. Growth* **2004**, *263*, 394.
- [37] a) Qu, L.; Shi, G.; Wu, X.; Fan, B. *Adv. Mater.* **2004**, *16*, 1200. b) Hou, S.; Harrell, C. C.; Trofin, L.; Kohli, P.; Martin, C. R. *J. Am. Chem. Soc.* **2004**, *126*, 5674. c)

- Go1ring, P.; Pippel, E.; Hofmeister, H.; Wehrspohn, R. B.; Steinhart, M.; Go1sele, U. *Nano Lett.* **2004**, *4*, 1121. d) Choi, J.; Sauer, G.; Nielsch, K.; Wehrspohn, R.B.; Go1sele, U. *Chem. Mater.* **2003**, *15*, 776. e) Lahav, M.; Sehayek, T.; Vaskevich, A.; Rubinstein, I. *Angew. Chem. Int. Ed.* **2003**, *42*, 5576. f) Cepak, V. M.; Martin, C. R. *J. Phys. Chem. B* **1998**, *102*, 9985. g) Wu, Y.; Livneh, T.; Zhang, Y. X.; Cheng, G.; Wang, J.; Tang, J.; Moskovits, M.; Stucky, G. D. *Nano Lett.* **2004**, *4*, 2337.
- [38] a) Brust, M.; Walker, M.; Bethell, D.; Schiffrin, D. J.; Whyman, R. J. *J. Chem. Soc., Chem. Commun.* **1994**, 801. b) Brust, M.; Fink, J.; Bethell, D.; Schiffrin, D. J.; Kiely, C. J. *J. Chem. Soc., Chem. Commun.* **1995**, 1655. c) Cardenas-Trivino, G.; Klabunde, K. J.; Dale, E. B. *Langmuir* **1987**, *3*, 986.
- [39] a) Kim, K.-S.; Dembere1nyamba, D.; Lee, H. *Langmuir*, **2004**, *20*, 556. b) Firestone, M. A.; Dietz, M. L.; Seifert, S.; Trasobares, S.; Miller, D. J.; Zaluzec, N. J. *Small*, **2005**, *1*, 754.
- [40] a) Chattopadhyay, P.; Gupta, R. B. *Ind. Eng. Chem. Res.* **2003**, *42*, 465. Ohde, H.; Hunt, F.; Wai, C. M. *Chem. Mater.* **2001**, *13*, 4130. Viswanathan, R.; Lilly, G. D.; Gale, W. F.; Gupta, R. B. *Ind. Eng. Chem. Res.*, **2003**, *42*, 5535.
- [41] a) Capek, I. *Advances in Colloid and Interface Science* **2004**, *110*, 49. b) Meyer, M.; Wallberg, C.; Kurihara, K.; Fendler, J. H. *Chem. Commun.* **1984**, 90. c) Lianos, P.; Thomas, J. K. *Chem. Phys. Lett.* **1986**, *125*, 299. d) Pileni, M. P.; Motte, L.; Petit, C. *Chem. Mater.* **1992**, *4*, 338. e) Petit, C.; Lixon, P.; Pileni, M. P. *J. Phys. Chem.* **1990**, *94*, 1598. f) Petit, C.; Jain, T. K.; Billoudet, F.; Pileni, M. P. *Langmuir* **1994**, *10*, 4446. g) Antonietti, M.; Wenz, E.; Bronstein, L.; Seregina, M. *Adv. Mater.* **1995**, *7*, 1000. T.; Krieger, M.; Boyen, H. G.; Ziemann, P.; Kabius, B. *Langmuir* **2000**, *16*, 407. h) Forster, S.; Antonietti, M. *Adv. Mater.* **1998**, *10*, 195.
- [42] a) Quinlan, F. T.; Kuter, J.; Tremel, W.; Knoll, W.; Risbud, S.; Stroeve, P. *Langmuir* **2000**, *16*, 4049. b) Calandra, P.; Longo, a.; liveri, V. T. *J. Phys. Chem. B* **2003**, *107*, 25. c) Morrison, S. A.; Cahill, C. L.; Carpenter, E. E.; Harris, V. G. *Ind. Eng. Chem. Res.* **2006**, *45*, 1217. d) lisiecki, I. *J. Phys. Chem. B* **2005**, *109*, 12231. e) Koo, H. Y.; Chang, S. T.; Choi, W. S.; Park, J. H.; Kim, D. Y.; Velev, O. D. *Chem. Mater.* **2006**, *18*, 3308. f) Lemyre, J. L.; Ritcey, M.; *Chem. Mater.* **2005**, *17*, 3040. g) Vestal, C. R.; Zhang, Z. J. *Nano Lett.* **2003**, *3*, 1739. h) Tartaj, P.; Tartaj, J. *Chem.*

- Mater.* **2002**, *14*, 536. i) Kitchens, C. L.; Mcleod, M. C.; Roberts, C. B. *J. Phys. Chem. B* **2003**, *107*, 11331. j) Cason, J. P.; Roberts, C. B.; *J. Phys. Chem. B* **2000**, *104*, 1217. k) Hirai, T.; Bando, Y.; Komasaawa, I. *J. Phys. Chem. B* **2002**, *106*, 8976. l) Li, M.; Mann, S. *Langmuir*, **2000**, *16*, 7088. m) Wu, M. L.; Chen, D. H.; Huang, T. C.; *Langmuir*, **2001**, *17*, 3877. n) Doolittle, J. W. Jr.; Dutta, P. K. *Langmuir* **2006**, *22*, 4825. o) Sugimoto, T.; Kimijima, K. *J. Phys. Chem. B* **2003**, *107*, 10753. p) Sangregorio, C.; Galeotti, M.; Bardi, U.; Baglioni, P. *Langmuir*, **1996**, *12*, 5800. q) Bagwe, R. P.; Khilar, K. C. *Langmuir* **2000**, *16*, 905.
- [43] a) Braun, E.; Eichen, Y.; Sivan, U.; Ben-Yoseph, G. *Nature* **1998**, *391*, 775. b) Richter, J.; Seidel, R.; Kirsch, R.; Mertig, M.; Pompe, W.; Plaschke, J.; Schackert, H. K. *Adv. Mater.* **2000**, *12*, 507. c) Patolsky, F.; Weizmann, Y.; Lioubashevski, O.; Willner, I. *Angew. Chem. Int. Ed.* **2002**, *41*, 2323. d) Keren, K.; Gilad, K.R.; Yoseph, G. B.; Sivan, U.; Braun, E. *Science* **2002**, *297*, 72. e) Ford, W. E.; Harnack, O.; Yasuda, A.; Wessels, J. M. *Adv. Mater.* **2001**, *13*, 1793. f) Deng, Z.; Mao, C. *Nano Lett.* **2003**, *3*, 1545.
- [44] a) Shenton, W.; Douglas, T.; Young, M.; Stubbs, G.; Mann, S. *Adv. Mater.* **1999**, *11*, 253. b) Fowler, C. E.; Shenton, W.; Stubbs, G.; Mann, S. *Adv. Mater.* **2001**, *13*, 126. c) Dujardin, E.; Peet, C.; Stubbs, G.; Culver, J. N.; Mann, S. *Nano Lett.* **2003**, *3*, 413. d) Ongaro, A.; Griffin, F.; Beecher, P.; Nagle, L.; Iacopino, D.; Quinn, A.; Redmond, G.; Fitzmaurice, D. *Chem. Mater.* **2005**, *17*, 1959. e) Mao, C.; Solis, D. J. Reiss, B. D.; Kottmann, S. T.; Sweeney, R. Y.; Hayhurst, A.; Georgiou, G.; Iverson, B.; Belcher A. M. *Science* **2004**, *303*, 213. f) Mao, C.; Flynn, C. E.; Hayhurst, A.; Sweeney, R.; Qi, J.; Georgiou, G.; Iverson, B.; Belcher, A. M. *Proc. Nat. Am. Soc.* **2003**, *100*, 6946.
- [45] a) Zhang, M.; Drechsler, M.; Muller, A. H. E. *Chem. Mater.* **2004**, *16*, 537. b) Crooks, R. M.; Lemon, B. I., III; Sun, L.; Yeung, L. K.; Zhao, M. *Top. Curr. Chem.* **2001**, *212*, 81. c) Minko, S.; Kiriy, A.; Gorodyska, G.; Stamm, M. *J. Am. Chem. Soc.* **2002**, *124*, 10192. d) Zhang, D.; Qi, L.; Ma, J.; Cheng, H. *Chem. Mater.* **2001**, *13*, 2753. e) Cornelissen, J. J. L. M.; Heerbeek, R. V.; Kamer, P. C. J.; Reek, J. N. H.; Sommerdijk, N. A. J. M.; Nolte, R. J. M. *Adv. Mater.* **2002**, *14*, 489. f) Kim, U. K.; Cha, S. H.; Shin, K.; Jho, J. Y.; Lee, J. C. *Adv. Mater.* **2004**, *16*, 459. g) Djalali,

- R.; Li, S. Y.; Schmidt, M. *Macromolecules* **2002**, *35*, 4282. h) Hao, E.; Kelly, K. L.; Hupp, J. T.; Schatz, G. C. *J. Am. Chem. Soc.* **2002**, *124*, 15182.
- [46] a) Wiesner, J.; Wokaun, A. *Chem. Phys. Lett.* **1989**, *57*, 569. b) Sun, Y.; Mayers, B. T.; Xia, Y. *Nano Lett.* **2002**, *2*, 481. c) Sun, Y.; Xia, Y. *J. Am. Chem. Soc.* **2004**, *126*, 3892. d) Me'traux, G. S.; Cao, Y. C.; Jin, R.; Mirkin, C. A. *Nano Lett.* **2003**, *3*, 519. e) Song, J. H.; Wu, Y.; Messer, B.; Kind, H.; Yang, P. *J. Am. Chem. Soc.* **2001**, *123*, 10397.
- [47] a) Qu, L.; Shi, G.; Wu, X.; Fan, B. *Adv. Mater.* **2004**, *16*, 1200. b) Hou, S.; Harrell, C. C.; Trofin, L.; Kohli, P.; Martin, C. R. *J. Am. Chem. Soc.* **2004**, *126*, 5674. c) Go1ring, P.; Pippel, E.; Hofmeister, H.; Wehrspohn, R. B.; Steinhart, M.; Go1sele, U. *Nano Lett.* **2004**, *4*, 1121. d) Choi, J.; Sauer, G.; Nielsch, K.; Wehrspohn, R. B.; Go'sele, U. *Chem. Mater.* **2003**, *15*, 776. e) Lahav, M.; Sehayek, T.; Vaskevich, A.; Rubinstein, I. *Angew. Chem. Int. Ed.* **2003**, *42*, 5576. f) Cepak, V. M.; Martin, C. R. *J. Phys. Chem. B* **1998**, *102*, 9985.
- [48] a) Tan, Y.; Dai, X.; Y. Li, ; Zhu, D. *J. Mater. Chem.* **2003**, *13*, 1069. b) Toshima, N.; Wang, Y. *Adv. Mater.* **1994**, *6*, 245. c) Toshima, N.; Harada, M.; Yonezawa, T.; Kushihashi, K.; Asakura, K. *J. Phys. Chem.* **1991**, *95*, 7448. 11 d) Bradley, J. S.; Hill, E. W.; Behal, S.; Klein, C. *Chem. Mater.* **1992**, *4*, 1234; e) Bradley, J. S.; Millar, J. M.; Hill, E. W.; Behal, S.; Chaudret, B.; Duteil, A. *Faraday Discuss.* **1991**, *92*, 255. f) Poulin, J. C.; Kagan, H. B.; Vargaftik, M. N.; Stolarov, I. P.; Moiseev, I. I. *J. Mol. Catal.* **1995**, *95*, 109. g) Amiens, C.; de Caro, D.; Chaudret, B.; Bradley, J. S.; Mazel, R.; Roucau, C. *J. Am. Chem. Soc.* **1993**, *115*, 11638. h) Jiang, X.; Xie, Y.; Lu, J.; Zhu, L.; He, W.; Qian, Y. *Langmuir*, **2001**, *17*, 3795. i) Naka, K.; Yaguchi, M.; Chujo, Y. *Chem. Mater.* **1999**, *11*, 849. j) Warner, M. G.; Reed, S. M.; Hutchison, J. E. *Chem. Mater.* **2000**, *12*, 3316.
- [49] Mann, S. *Biomineralization Principle and Concept in Bioinorganic Materials Chemistry*, Oxford University Press, Oxford, **2001**.
- [50] Klaus-Joerger, T.; Joerger, R.; Olsson, E.; Granqvist, C-G. *Trends Biotech.* **2001**, *19*, 15.
- [51] a) Mann, S., *Nature*, **1993**, *365*, 499. b) Oliver, S., Kupermann, A., Coombs, N., Lough, A.; Ozin, G. A., *Nature*, 1995, *378*, 47. b) Kroger, N., Deutzmann, R.;

- Sumper, M., *Science*, 1999, 286, 1129. c) Parkinson, J.; Gordon, R. *Trends Biotech.* **1999**, 17, 190.
- [52] Young, J. R.; Davis, S. A.; Bown, P. R.; Mann, S. *J. Struct. Biol.* **1999**, 126, 195.
- [53] a) Lovley, D. R., Stolz, J. F., Nord, G. L. and Phillips, E. J. P., *Nature*, **1987**, 330, 252. b) Spring, H. and Schleifer, K. H., *Sys. Appl. Microbiol.* **1995**, 18, 147. c) Dickson, D. P. E., *J. Magn. Magn. Mater.*, **1999**, 203, 46.
- [54] Mann, S. *Angew. Chem. Int. Ed.* **2000**, 39, 3392.
- [55] Mann, S.; Hannington, J. P.; Williams, R. J. P. *Nature* **1986**, 324, 565.
- [56] a) Shimizu, K.; Cha, J.; Stucky, G. D.; Morse, D. E. *Proc. Natl. Acad. Sci. USA* **1998**, 95, 6234. b) Cha, J.; Shimizu, K.; Zhou, Y.; Christiansen, S. C.; Chmelka, B. F.; Stucky, G. D.; Morse, D. E. *Proc. Natl. Acad. Sci. USA* **1999**, 96, 361.
- [57] a) Kroger, N.; Deuzmann, R.; Sumper, M. *Science* **1999**, 286, 1129. b) Kroger, N.; Lorenz, S.; Brunner, E.; Sumper, M. *Science* **1999**, 286, 1129. c) Kroger, N.; Deuzmann, R.; Sumper, M. *J. Biol. Chem.* **2001**, 276, 26066. d) Kroger, N.; Deuzmann, R.; Bergsdorf, C.; Sumper, M. *Proc. Natl. Acad. Sci. USA* **2000**, 97, 14133.
- [58] Kroger, N.; Bergsdorf, C.; Sumper, M. *Eur. J. Biochem.* **1996**, 239, 259.
- [59] a) Kroger, N.; Wetherbee, R. *Protist* **2000**, 151, 263. b) Kroger, N.; Lehmann, G.; Rachel, R.; Sumper, M. *Eur. J. Biochem.* **1997**, 250, 99.
- [60] a) Hecky, R. E.; Mopper, K.; Kilham, P.; Degans, E. T. *Mar. Biol.* **1973**, 19, 323. b) Nakajima, T.; Volcani, B. E. *Science* **1969**, 164, 1400. c) Swift, D.; Wheeler, A. *J. Phycol.* **1992**, 28, 202.
- [61] Bauerlein, E. *Angew. Chem. Int. Ed.* **2003**, 42, 614.
- [62] a) Rautaray, D.; Ahmad, A.; Sastry, M. *J. Mater. Chem.* **2004**, 14, 2333. b) Rautaray, D.; Ahmad, A.; Sastry, M. *J. Am. Chem. Soc.* **2003**, 125, 14656.
- [63] Ahmad, A.; Rautaray, D.; Sastry, M. *Adv. Funct. Mater.* **2004**, 14, 1075.
- [64] a) Sanyal, A.; Rautaray, D.; Bansal, V.; Ahmad, A.; Sastry, M. *Langmuir* **2005**, 21, 7220. b) Rautaray, D.; Sanyal, A.; Adyanthaya, S. D.; Ahmad, A.; Sastry, M. *Langmuir* **2004**, 20, 6827.
- [65] a) Bansal, V.; Rautaray, D.; Bharde, A.; Ahire, K.; Sanyal, A.; Ahmad, A.; Sastry, M. *J. Mater. Chem.* **2005**, 15, 2583. b) Bansal, V.; Rautaray, D.; Ahmad, A.; Sastry,

- M. J. Mater. Chem. **2004**, *14*, 3303. c) Bansal, V., Poddar, P., Ahmad, A., Sastry, M. J. Am. Chem. Soc. **2006**, *128*, 11958.
- [66] a) Bansal, V.; Sanyal, A.; Rautaray, D.; Ahmad, A.; Sastry, M. *Adv. Mater.* **2005**, *17*, 889. b) Bansal, V., Ahmad, A., Sastry, M. J. Am. Chem. Soc. **2006**, *128*, 14059.
- [67] a) Devouard, B.; Posfai, M.; Hua, X.; Bazylnski, D. A.; Frankel, R. B.; Busek, P. R. *Am. Mineral.* **1998**, *83*, 1387, b) Pósfai M.; Cziner K.; Márton E.; Márton P.; Buseck P. R.; Frankel R. R. B.; Bazylnski D. A. *Eur. J. Mineral.* **2001**, *13*, 691. c) Spring, S.; Schleifer, K. H. *Appl. Microbiol.* **1995**, *18*, 147. d) Schueler, D.; Frankel, R. B. *Appl. Microbiol. Biotechnol.* **1999**, *52*, 464.
- [68] Torres de Araujo, F. F.; Pires, M. A.; Frankel, R. B.; Bicudo, C. E. M. *Biophys. J.* **1986**, *50*, 375.
- [69] Bazylnski, D. A.; Frankel, R. B. *Biomineralization* (Ed.: E. Baeuerlein), Wiley-VCH, Weinheim **2000**, p. 41-43.
- [70] Mann, S.; Sparks, N. H.; Walker, M. M.; Kirschvink, J. L. *J. Exp. Biol.* **1988**, *140*, 35.
- [71] a) Walker, M. M.; Diebel, C. E.; Haugh, C. V.; Pankhurst, P. M.; Montgomery, J. C.; Green, C. R. *Nature* **1997**, *390*, 371. b) Diebel, C. E.; Proksch, R.; Green, C. R.; Neilson, P.; Walker, M. M. *Nature* **2000**, *406*, 299.
- [72] Hanzlik, M.; Heunemann, C.; Holtkamp-Rötzler, E.; Winklhofer, M.; Petersen, N.; Fleissner, G. *Biometal*, **2000**, *13*, 325.
- [73] Acosta-Avalos, D.; Wajnberg, E.; Oliveira, P. S.; Leal, I.; Farina, M.; Esquivel, D. *M. J. Exp. Biol.* **1999**, *202*, 2687.
- [74] a) Kirschvink, J. L.; Kobayashi-Kirschvink, A.; Woodford, B. J. *Proc. Natl. Acad. Sci USA* **1992**, *89*, 7683; b) Dobson, J.; Grassi, P. P. *Brain Res. Bull.* **1996**, *39*, 255. c) Schultheiss-Grassi, P. P.; Wessiken, R.; Dobson, J. *Biochem. Biophys. Acta* **1999**, *1426*, 212. d) Schultheiss-Grassi, P. P.; Dobson, J. *BioMetals* **1999**, *12*, 67.
- [75] a) Beveridge, J. T.; Hughes, M. N.; Lee, H.; Leung, K. T.; Poole, R. K.; Savvaides, I.; Silver, S.; Trevors, J. T. *Adv. Microb. Physiol.* **1997**, *38*, 178 b) Silver, S. *Gene* **1996**, *179*, 9. c) Rouch, D. A. Lee, B. T.; Morby, A. T. *J. Ind. Micro.* **1995**, *14*, 132.
- [76] Stephen, J. R.; Macnaughton, S. J. *Curr. Opin. Biotechnol.* **1999**, *10*, 230.

- [77] a) Bharde, A., Rautaray, D., Bansal, V., Ahmad, A., Sarkar, I., Yusuf, S. M., Sanyal, M., Sastry, M. *Small* **2006**, *2*, 135. b) Bharde, A., Wani, A., Shouche, Y., Joy, P. A., Prasad, B. L. V., Sastry, M. *J. Am. Chem. Soc.* **2005**, *127*, 9326.
- [78] a) Lundgren, D. G.; Silver, M. *Annu. Rev. Microbiol.* **1980**, *34*, 263. b) Dopson, M.; Lindstrom, E. B. *Appl. Environ. Microbiol.* **1999**, *65*, 36.
- [79] Harvey, P.I. and Crundwell, F.K. *Appl. Environ. Microbiol.* **1997**, *63*, 2586.
- [80] a) Southam, G.; Beveridge, T. J., *Geochim. Cosmochim. Acta*, **1996**, *60*, 4369. b) Beveridge, T. J.; Murray, R. G. E., *J. Bacteriol.*, **1980**, *141*, 876. c) Fortin, D. Beveridge, T. J. *Biomining: From Biology to Biotechnology and Medical Applications* (ed. Baeuerien, E.), Wiley-VCH, Weinheim, **2000**, p. 7.
- [81] Klaus, T.; Joerger, R.; Olsson, E.; Granqvist, C. G.; *Proc. Natl. Acad. Sci. USA*, **1999**, *96*, 13611.
- [82] Pooley, F.D. *Nature* **1982**, *296*, 642.
- [83] Nair, B.; Pradeep, T. *Cryst. Growth Des.* **2002**, *2*, 293.
- [84] Ahmad, A.; Senapati, S.; Khan, M. I.; Kumar, R.; Sastry, M. *Langmuir* **2003**, *19*, 3550.
- [85] a) Mukherjee, P.; Ahmad, A.; Mandal, D.; Senapati, S.; Sainkar, S.R.; Khan, M.I.; Ramani, R.; Parischa, R.; Ajayakumar, P. V.; Alam, M.; Sastry, M.; Kumar, R. *Angew. Chem. Int. Ed.* **2001**, *40*, 3585. b) Mukherjee, P.; Ahmad, A.; Mandal, D.; Senapati, S.; Sainkar, S. R.; Khan, M. I.; Parischa, R.; Ajayakumar, P. V.; Alam, M.; Kumar, R.; Sastry, M.; *Nano Lett.* **2001**, *1*, 515.
- [86] a) Mukherjee, P.; Senapati, S.; Mandal, D.; Ahmad, A.; Khan, M.I.; Kumar, R.; Sastry, M. *ChemBioChem* **2002**, *3*, 461. b) Ahmad, A.; Mukherjee, P.; Senapati, S.; Mandal, D.; Khan, M.I.; Kumar, R.; Sastry, M. *Colloids Surf. B* **2003**, *28*, 313.
- [87] Senapati, S.; Ahmad, A.; Khan, M. I.; Sastry, M.; Kumar, R. *Small* **2005**, *1*, 517.
- [88] Ahmad, A.; Mukherjee, P.; Mandal, D.; Senapati, S.; Khan, M.I.; Kumar, R.; Sastry, M.; *J. Am. Chem. Soc.* **2002**, *124*, 12 108.
- [89] a) C Cunningham, D. P.; Lundie, L. L. *Appl. Environ. Microbiol.* **1993**, *59*, 7. b) Smith, P. R.; Holmes, J. D.; Richardson, D. J.; Russell, D. A.; Sodeau, J. R., *J. Chem. Soc., Faraday Trans.* **1998**, *94*, 1235.

- [90] Labrenz, M.; Druschel, G. K.; Thomsen-Ebert, T.; Gilbert, B.; Welch, S. A.; Kemner, K. M.; Logan, G. A.; Summons, R. E.; De Stasio, G.; Bond, P. L.; Lai, B.; Kelly, S. D.; Banfield, J. F. *Science*, **2000**, *290*, 252.
- [91] Kowshik, M.; Vogel, W.; Urban, J.; Kulkarni, S. K.; Paknikar, K. M. *Adv. Mater.* **2002**, *14*, 815.
- [92] a) Williams, P.; Keshavarz-Moore, E.; Dunnill P. *J. Biotech.* **1996**, *48*, 259. b) Dameron, C. T.; Reese, R. N.; Mehra, R. K.; Kortan, A. R.; Carroll, P. J.; Steigerwald, M. L.; Brus, L. E.; Winge D. R. *Nature* **1989**, *338*, 596.
- [93] a) Sela, M.; Garty, J.; Tel-Or, E. *New Phytol.* **1989**, *112*, 7. b) Stratford, H. K.; Haller, W. T.; Garrard, L. A. *Aquat. Toxicol.* **1984**, *5*, 117.
- [94] a) Reeves, R. D.; Schwartz, C.; Morel, J. L.; Edmondson, J. *Int. J. Phytorem.* **2001**, *3*, 145. b) Koch, M.; Mummenhoff, K.; Hurka, H. *Biochem. Syst. Ecol.* **1998**, *26*, 823.
- [95] a) Tang, S.; Huang, C.; Zhu, Z. *Pedosphere* **1997**, *7*, 207. b) Rosa, G. De. La.; Peralta-Videa, J. R.; Montes, M.; Parsons, J. G.; Gardea-Torresdey, J. L. *Chemosphere* **2004**, *55*, 1159. c) Asensi, A.; Bennett, F.; Brooks, R.; Robinson, B.; Stewart, R. *Commun. Soil Sci. Plant Anal.* **1999**, *30*, 1615. d) Riddle, S. G.; Tran, H. H.; Dewitt, J. G.; Andrews, J. C. *Environ. Sci. Technol.* **2002**, *36*, 1965.
- [96] Gardea-Torresdey, J. L.; Tiemann, K. J.; Armendariz, V.; Bess-Oberto, L.; Chianelli, R. R.; Rios, J.; Parsons, J. G.; Gamez, G. *J. Hazard. Mater. B* **2000**, *80*, 175.
- [97] Girling, C. A.; Peterson, P. J. *Trace Subst. Environ. Health* **1978**, *12*, 105.
- [98] Gomez, E. A. The nanoparticle formation and uptake of precious metals by alfalfa plants, MS thesis, Department of Chemistry, University of Texas at El Paso, El Paso, TX, July 2002, 81 pp.
- [99] Lungwitz, E. E. *Min. J. London.* **1900**, *17*, 318.
- [100] Conn, E. E. *J. Agric. Food. Chem.* **1969**, *17*, 519.
- [101] Shacklette, H. T.; Lakin, H. W.; Hubert, A. E.; Curtin, G. C. *U. S. Geol. Surv. Bull.* **1970**, *1*.
- [102] a) Arnott, H.J., 1982. *Three systems of biomineralization in plants with comments on the associated organic matrix*. In (Ed.: Nancollas, G. H.), *Biological Mineralization and Demineralization*. Springer Verlag, Berlin, pp. 199–218. b)

- Monje, P.V., Baran, E.J., 2004a. *Plant biomineralization*. In (Ed.: Hemantaranjan, H.), *Advances in Plant Physiology*, vol. 7. Scientific Publishers, Jodhpur, pp. 403–419.
- [103] Monje, P.V., Baran, E.J., *J. Plant Physiol.* **2000**, *157*, 457.
- [104] a) Harrison, C. C. *Phytochemistry* **1996**, *41*, 37. b) Liou, T-H. *Mater. Sci. Engin. A* **2004**, *364*, 313.
- [105] Gajdardziska-Josifovska M.; McClean R.G.; Schofield M.A.; Sommer C.V.; Kean W.F. *Eur. J. Mineral.* **2001**, *13*, 863.
- [106] a) J.L. Gardea-Torresdey, J.G. Parsons, E. Gomez, J.R. Peralta-Videa, H.E. Troiani, P. Santiago, M. Jose-Yacaman, *Nano Lett.* **2002**, *2*, 397. b) J.L. Gardea-Torresdey, E. Gomez, J.R. Peralta-Videa, J.G. Parsons, H. Troiani, M. Jose-Yacaman, *Langmuir*. 2003, *19*, 1357.
- [107] a) Shankar, S. S.; Ahmad, A.; Pasricha, R.; Sastry, M. *J. Mater. Chem.* **2003**, *13*, 1822. b) Shankar, S. S.; Ahmad, A.; Sastry, M. *Biotechnol. Prog.*, **2003**, *19*, 1627. c) Shankar, S. S.; Rai, A.; Ahmad, A.; Sastry, M. *Applied Nanoscience* **2004**, *1*, 69.
- [108] Shankar, S. S.; Rai, A.; Ahmad, A.; Sastry, M. *J. Colloid Interface Sci.*, **2004**, *275*, 496.
- [109] Ankamwar, B.; Damle, C.; Ahmad, A.; Sastry, M. *J. Nanosci. Nanotech.* **2005**, *5*, 1665.
- [110] a) Shankar, S. S.; Rai, A.; Ankamwar, B.; Singh, A.; Ahmad, A.; Sastry, M. *Nat. Mater.* **2004**, *3*, 482. b) Ankamwar, B.; Chaudhary, M.; Sastry, M. *Syn. React. Inorg. Metal-Org. Nano-Metal Chem.* **2005**, *35*, 19.
- [111] Shankar, S. S.; Rai, A.; Ahmad, A.; Sastry, M. *Chem. Mater.* **2005**, *17*, 566.
- [112] Singh, A., Chaudhari, M., Sastry, M. *Nanotechnology* **2006**, *17*, 2399.
- [113] a) Loo, C.; Lin, A.; Hirsch, L.; Lee, M. H.; Barton, J.; Halas, N.; West, J.; Drezek, R. *Technology in Cancer Research and Treatment* **2004**, *3*, 33. b) Hirsch, L. R.; Stafford, R. J.; Bankson, J. A.; Sershen, S. R.; Rivera, B.; Price, R. E.; Hazle, J. D.; Halas, N. J.; West, J. L. *Proc. Natl. Acad. Sci. USA*, **2003**, *100*, 13549. c) Nanospectra biosciences, Inc. Huston Texas, www.nanospectra.com.
- [114] Jana, N. R.; Gearheart, L. A.; Murphy, C. J. *Chem. Commun.* **2001**, 617.
- [115] Huang, C. –C.; Yang, Z.; Chang, H. –T. *Langmuir* **2004**, *20*, 6089.

- [116] Sun, Y.; Wiley, B.; Li, Z.-Y.; Xia, Y. *J. Am. Chem. Soc.* **2004**, *126*, 9399.
- [117] Qu, L.; Shi, G.; Wu, X.; Fan, B. *Adv. Mater.* **2004**, *16*, 1200.
- [118] Xiong, Y.; Chen, J.; Wiley, B.; Xia, Y.; Yin, Y.; Li, Z.-Y. *Nano Lett.* **2005**, *5*, 1237.
- [119] Jin, R.; Cao, Y. W.; Mirkin, C. A.; Kelly, K. L.; Schatz, G. C.; Zheng, J. G. *Science* **2001**, *294*, 1901.
- [120] Kuo, C.-H.; Chiang, T.-F.; Chen, L.-J.; Huang, M. H. *Langmuir* **2004**, *20*, 7820.
- [121] Maillard, M.; Giorgio, S.; Pileni, M.-P. *Adv. Mater.* **2002**, *14*, 1084.
- [122] Sau, T. K.; Murphy, C. J. *J. Am. Chem. Soc.* **2004**, *126*, 8648.
- [123] Teng, X.; Yang, H. *Nano Lett.* **2005**, *5*, 885.
- [124] Chen, Y.; Gu, X.; Nie, C.-G.; Jiang, Z.-Y.; Xie, Z.-X.; Lin, C.-J. *Chem. Commun.* **2005**, 4181.
- [125] Ahmadi, T. S.; Wang, Z. L.; Green, T. C.; Henglein, A.; El-Sayed, M. A. *Science* **1996**, *272*, 1924.
- [126] Zhou, Y.; Yu, S. H.; Wang, C. Y.; Li, X. G.; Zhu, Y. R.; Chen, Z. Y. *Adv. Mater.* **1999**, *11*, 850.
- [127] a) Zhang, D.; Qi, L.; Ma, J.; Cheng, H. *Chem. Mater.* **2001**, *13*, 2753. b) Cornelissen, J. J. L. M.; Heerbeek, R. V.; Kamer, P. C. J.; Reek, J. N. H.; Sommerdijk, N. A. J. M.; Nolte, R. J. M. *Adv. Mater.* **2002**, *14*, 489. c) Kim, U. K.; Cha, S. H.; Shin, K.; Jho, J. Y.; Lee, J. C. *Adv. Mater.* **2004**, *16*, 459. d) Djalali, R.; Li, S.Y.; Schmidt, M. *Macromolecules* **2002**, *35*, 4282.
- [128] Hao, E.; Kelly, K. L.; Hupp, J. T.; Schatz, G. C. *J. Am. Chem. Soc.* **2002**, *124*, 15182.
- [129] Wei, G.; Zhou, H.; Liu, Z.; Song, Y.; Wang, L.; Sun, L.; Li, Z. *J. Phys. Chem. B.* **2005**, *109*, 8738.
- [130] a) Chang, S. S.; Shih, C. W.; Chen, C. D.; Lai, W. C.; Wang, C. R. C. *Langmuir* **1999**, *15*, 701. b) Yu, Y. Y.; Chang, S. S.; Lee, C. L.; Wang, C. R. C. *J. Phys. Chem. B* **1997**, *101*, 6661.
- [131] Perez-Juste, J.; Liz-Marzan, L. M.; Carnie, S.; Chan, D. Y. C.; Mulvaney, P. *Adv. Funct. Mater.* **2004**, *14*, 571.

- [132] Sun, J.; Zhang, J.; Liu, W.; Liu, S.; Sun, H.; Jiang, K.; Li, Q.; Guo, J. *Nanotechnology*, **2005**, *16*, 2412.
- [133] a) Sau, T. K.; Murphy, C. J. *Langmuir* **2004**, *20*, 6414. b) Busbee, B. D.; Obare, S. O.; Murphy, C. J. *Adv. Mater.* **2003**, *15*, 414. c) Murphy, C. J.; Jana, N. R. *Adv. Mater.* **2002**, *14*, 80. d) Jana, N.R.; Gearheart, L.; Murphy, C. J. *Adv. Mater.* **2001**, *13*, 1389. e) Gao, J.; Bender, C. M.; Murphy, C. J. *Langmuir* **2003**, *19*, 9065. f) Gole, A.; Murphy, C. J. *Chem. Mater.* **2004**, *16*, 3633. g) Murphy, C. J.; Sau, T. K.; Gole, A. M. Orendorff, C. J. Gao, J.; Gou, L.; Hunyadi, S. E. Li, T. *J. Phys. Chem. B* **2005**, *109*, 13857. h) Murphy, C. J.; Sau, T. K.; Gole, A. M. Orendorff, C. *MRS Bull.* **2005**, *30*, 349. i) Johnson, C. J.; Dujardin, E.; Davis, S. A.; Murphy, C. J.; Mann, S. *J. Mater. Chem.* **2002**, *12*, 1765-1770. j) Jana, N. R.; Gearheart, L.; Murphy, C. J. *J. Phys. Chem. B* **2001**, *105*, 4065-4067.
- [134] Nikoobakht, B.; El-Sayed, M. A. *Chem. Mater.* **2003**, *15*, 1957.
- [135] Millstone, J. E.; Park, S.; Shuford, K. L.; Qin, L.; Schatz, G. C.; Mirkin, C. A. *J. Am. Chem. Soc.* **2005**, *127*, 5312.
- [136] a) Chen, S.; Carroll, D. L. *Nano Lett.* **2002**, *2*, 1003. b) Chen, S.; Fan, Z.; Carroll, D. L. *J. Phys. Chem. B* **2002**, *106*, 10777. (c) Chen, S.; Carroll, D. L. *J. Phys. Chem. B* **2004**, *108*, 5500.
- [137] Kou, X.; Zhang, S.; Tsung, C-K.; Yeung, M. H.; Shi, Q.; Stucky, G. D.; Sun, L.; Wang, J.; Yan, C. *J. Phys. Chem. B* **2006**, *110*, 16377.
- [138] Kim, F.; Song, J. H.; Yang, P. J. *Am. Chem. Soc.* **2002**, *124*, 14316.
- [139] Esumi, K.; Matsuhisa, K.; Torigoe, K. *Langmuir*; **1995**; *11*, 3285.
- [140] Miranda, O. R.; Ahmadi, T. S. *J. Phys. Chem. B* **2005**, *109*, 15724.
- [141] Liu, Z.; Bando, Y. *Adv. Mater.* **2003**, *15*, 303.
- [142] Zhou, Y.; Yu, S. H.; Cui, X. P.; Wang, C. Y.; Chen, Z. Y. *Chem. Mater.* **1999**, *11*, 545.
- [143] a) Jin, R.; Cao, Y. W.; Mirkin, C. A.; Kelly, K. L.; Schatz, G.C.; Zheng, J. G. *Science* **2001**, *294*, 1901. (b) Jin, R.; Cao, Y. C.; Hao, E.; Metraux, G. S.; Schatz, G. C.; Mirkin, C. A. *Nature* **2003**, *425*, 487.
- [144] Callegari, A.; Tonti, D.; Chergui, M. *Nano Lett.* **2003**, *3*, 1565.

- [145] Haes, A. J.; Zhao, J.; Zou, S.; Own, C. S.; Marks, L. D.; Schatz, G. C.; Van Duyne, R. P. *J. Phys. Chem. B* **2005**, *109*, 11158.
- [146] a) Charnay, C.; Lee, A.; Man, S.-Q.; Moran, C. E.; Radloff, C.; Bradley, R. K.; Halas, N. J. *J. Phys. Chem. B* **2003**, *107*, 7327. b) Love, J. C.; Gates, B. D.; Wolfe, D. B.; Paul, K. E.; Whitesides, G. M.; *Nano Lett.* **2002**, *2*, 891.
- [147] a) Sanyal, A.; Sastry, M.; *Chem. Commun.* **2003** 1236. b) Swami, A.; Kumar, A.; Selvakannan, P. R.; Mandal, S.; Pasricha, R.; Sastry, M. *Chem. Mater.* **2003**, *15*, 17. c) Swami, A.; Kumar, A.; D`Costa, M.; Sastry, M. *J. Mater. Chem.* **2004**, *14*, 2696. d) Swami, A.; Kasture, M.; Pasricha, R.; Sastry, M. *J. Mater. Chem.* **2004**, *14*, 709. e) Sastry, M.; Swami, A.; Mandal, S.; Selvakannan, P. R. *J. Mater. Chem.* **2005**, *15*, 3161.
- [148] Sun, X.; Dong, S.; Wang, E. *Langmuir* **2005**, *21*, 4710.
- [149] Wang, L.; Chen, X.; Zhan, J.; Chai, Y.; Yang, C.; Xu, L.; Zhuang, W.; Jing, B. *J. Phys. Chem. B* **2005**, *109*, 3189.
- [150] a) Zhou, M.; Chen, S.; Zhao, S.; May, H. *Chem. Lett.* **2005**, *34*, 1670. b) Deivaraj, T. C.; Lala, N. L.; Lee, J. Y. *J. Colloid Interface Sci.* **2005**, *289*, 402.
- [151] Pastoriza-Santos, I.; Liz-Marzan, L. M. *Nano Lett.* **2002**, *2*, 903.
- [152] a) Sun, Y.; Xia, Y. *Adv. Mater.* **2003**, *15*, 695. b) Chen, J.; Herricks, T.; Geissler, M.; Xia, Y. *J. Am. Chem. Soc.* **2004**, *126*, 10854. c) Sun, Y.; Xia, Y. *Adv. Mater.* **2002**, *298*, 2176.
- [153] Sun, X.; Dong, S.; Wang, E. *Angew. Chem. Int. Ed.* **2004**, *43*, 6360.
- [154] Shao, Y.; Jin, Y.; Dong, S. *Chem. Commun.* **2004**, 1104.
- [155] Sarma, T. K.; Chattopadhyay, A. *Langmuir* **2004**, *20*, 3520.
- [156] Yang, J.; Lu, L.; Wang, H.; Shi, W.; Zhang, H. *Cryst. Growth Des.* **2006**, *6*, 2155.
- [157] Naik, R. R.; Stringer, S. J.; Agarwal, G.; Jones, S. E.; Stone, M. O. *Nature Mater.* **2002**, *1*, 169.
- [158] Liu, B.; Xie, J.; Lee, J. Y.; Ting, Y. P.; Chen, J. P. *J. Phys. Chem. B* **2005**, *109*, 15256.
- [159] Lengke, M. F.; Fleet, M. E.; Southam, G. *Langmuir* **2006**, *22*, 2780.
- [160] a) Turkevich, J.; Kim, G. *Science* **1970**, *169*, 873. b) Schmid, G.; West, H.; Malm, J. O.; Bovin, J. O.; Grenthe, C. *Chem. Eur. J.* **1996**, *2*, 1099. c) Toshima, N.;

- Harada, M.; Yamazaki, Y.; Asakura, K. *J. Phys. Chem.* **1992**, *96*, 9927. d) Toshima, N.; Hirakawa, K. *Polym. J.* **1999**, *31*, 1127. e) Han, W. S.; Kim, Y.; Kim, K. *J. Colloid Interface Sci.* **1998**, *208*, 272. f) Lee, I.; Han, S. W.; Kim, K. *Chem. Commun.* **2001**, 1782. g) Cottancin, E.; Lerme, J.; Gaudry, M.; Pellarin, M.; Vialle, J. L.; Broyer, M.; Prevel, B.; Treilleux, M.; Melinon, P. *Phys. Rev. B* **2000**, *62*, 5179. h) Treguer, M.; de Cointet, C.; Remita, H.; Khatouri, J.; Mostafavi, M.; Amblard, J.; Belloni, J. *J. Phys. Chem. B* **1998**, *102*, 4310. i) Lu, P.; Dong, J.; Toshima, N. *Langmuir* **1999**, *15*, 7980.
- [161] a) Caruso, F. *Adv. Mater.* **2001**, *13*, 11. b) Oldfield, G.; Ung, T.; Mulvaney, P. *Adv. Mater.* **2000**, *12*, 1519. c) Hall, S. R.; Davis, S. A.; Mann, S. *Langmuir* **2000**, *16*, 1454. d) Matijevic, E. *Langmuir* **1994**, *10*, 8.
- [162] a) Caruso, F.; Spasova, M.; Salgueirino-Macera, V. *Adv. Mater.* **2001**, *13*, 1090. b) Giersig, M.; Ung, T.; Mulvaney, P. *Adv. Mater.* **1997**, *9*, 570. c) Giersig, M.; Liz-Marzan, L. M.; Ung, T.; Su, D. S. Mulvaney, P. *Ber. Bunsen-Ges. Phys. Chem.* **1997**, *191*, 11617. d) Caruso, F.; Lichtenfeld, H.; Mõhwald, H. *J. Am. Chem. Soc.* **1998**, *120*, 8523. e) Caruso, F.; Caruso, R.; Mõhwald, H. *Science* **1998**, *282*, 1111. f) Walsh, D.; Mann, S. *Nature* **1995**, *377*, 320. g) Correa-Duarte, L. M.; Giersig, M.; Liz-Marzan, L. M. *Chem. Phys. Lett.* **1998**, *286*, 497.
- [163] Schmid, G. *Clusters and Colloids; VCH: Weinheim, 1994.*
- [164] a) Yonezawa, T.; Toshima, N. *J. Chem. Soc., Faraday Trans.* **1995**, *91*, 4111. b) Seregina, M. V.; Bronstein, L. M.; Platonova, O. A.; Chernyshov, D. M.; Valetsky, P. M.; Hartmann, J.; Wenz, E.; Antonietti, M. *Chem. Matter.* **1997**, *9*, 923. c) Lee, A. F.; Baddeley, C. J.; Hardacre, C.; Ormerod, R. M.; Lambert, R. M. *J. Phys. Chem.* **1995**, *99*, 6096. d) Mizukoshi, Y.; Okitsu, K.; Maeda, Y.; Zamamoto, T. A.; Oshima, R.; Nagata, Y. *J. Phys. Chem. B* **1997**, *101*, 7033. e) Schmid, G.; Lehnert, A.; Malm, J. O.; Bovin, J. O. *Angew. Chem., Int. Ed. Engl.* **1991**, *30*, 874. f) Kan, C.; Cai, Y.; Li, C.; Zhang, L.; Hofmeister, H.; *J. Phys. D: Appl. Phys.* **2003**, *36*, 1609.
- [165] a) Liz-Marzan, L. M.; Philipse, A. P. *J. Phys. Chem.* **1995**, *99*, 15120. b) Yonezawa, T.; Toshima, N. *J. Mol. Catal.* **1993**, *83*, 167. c) Schmid, G.; West, H.; Mehles, H.; Lehnert, A. *Inorg. Chem.* **1997**, *36*, 891.

- [166] a) Michaelis, M.; Henglein, A.; Mulvaney, P. *J. Phys. Chem.* **1994**, *98*, 6212. b) Esumi, K.; Wakabayashi, M.; Torigoe, K. *Colloids Surf. A* **1996**, *109*, 55. c) Silvert, P.-Y.; Vijayakrishnan, V.; Vibert, P.; Herrera- Urbina, R.; Elhsissen, K. T. *Nanostruct. Mater.* **1996**, *7*, 611. (d) Torigoe, K.; Esumi, K. *Langmuir* **1993**, *9*, 1664.
- [167] Torigoe, K.; Nakajima, Y.; Esumi, K. *J. Phys. Chem.* **1993**, *97*, 8304.
- [168] a) Aihara, N.; Torigoe, K.; Esumi, K. *Langmuir* **1998**, *14*, 4945. b) Itakura, T.; Torigoe, K.; Esumi, K. *Langmuir* **1995**, *11*, 4129. c) Teo, B. K.; Keating, K.; Kao, Y. H. *J. Am. Chem. Soc.* **1987**, *109*, 3494. d) Shi, H. Z.; Zhang, L. D.; Cai, W. P. *J. Appl. Phys.* **2000**, *87*, 1572. e) Hostetler, M. J.; Zhong, C. J.; Yen, B. K. H.; Anderegg, J.; Gross, S. M.; Evans, N. D.; Porter, M.; Murray, R. W. *J. Am. Chem. Soc.* **1998**, *120*, 9396. f) Han, W. S.; Kim, Y.; Kim, K. *J. Colloid Interface Sci.* **1998**, *208*, 272. (g) Papavassiliou, G. C. *J. Phys. F: Metal Phys.* **1976**, *6*, L103. h) Lee, I.; Han, S. W.; Kim, K. *Chem. Commun.* **2001**, 1782. i) Cottancin, E.; Lerme, J.; Gaudry, M.; Pellarin, M.; Vialle, J. L.; Broyer, M.; Prevel, B.; Treilleux, M.; Melinon, P. *Phys. Rev. B* **2000**, *62*, 5179. j) Chen, Y. H.; Yeh, C. S. *Chem. Commun.* **2001**, 371. k) Sato, G.; Kuroda, S.; Takami, A.; Yonezawa, Y.; Hada, H. *Appl. Organomet. Chem.* **1991**, *5*, 261. l) Link, S.; Wang, Z. L.; El-Sayed, M. A. *J. Phys. Chem. B* **1999**, *103*, 3529. m) Freeman, R. G.; Hommer, M. B.; Grabar, K. C.; Jackson, M. A.; Natan, M. J. *J. Phys. Chem.* **1996**, *100*, 718. n) Morriss, R. H.; Collins, L. F. *J. Chem. Phys.* **1964**, *41*, 3357. o) Mulvaney, P.; Giersig, M.; Henglein, A. *J. Phys. Chem.* **1993**, *97*, 1. p) Lu, P.; Dong, J.; Toshima, N. *Langmuir* **1999**, *15*, 7980. q) Takenaka, T.; Eda, K. *J. Colloid Interface Sci.* **1985**, *105*, 342. r) Sinzig, J.; Quinten, M. *Appl. Phys. A* **1994**, *58*, 157. s) Rivas, L.; Sanchez-Cortes, S.; Garcý'a-Ramos, J. V.; Morcillo, G. *Langmuir* **2000**, *16*, 9722. t) Shibata, T.; Bunker, B. A.; Zhang, Z.; Meisel, D.; Vardeman, C. F., II; Gezelter, J. D. *J. Am. Chem. Soc.* **2002**, *124*, 11989. u) Mallik, K.; Mandal, M.; Pradhan, N.; Pal, T. *Nano Lett.* **2001**, *1*, 319.
- [169] Shankar, S. S.; Rai, A.; Ahmad, A.; Sastry, M. *J. Colloid Interface Sci.* **2004**, *275*, 496. b) Lu, L.; Wang, H.; Zhou, Y.; Xi, S.; Zhang, S.; Hu, J.; Zhao, B. *Chem. Commun.* **2002**, *14*. c) Zhu, J.; Wang, Y.; Huang, L.; Lu, Y. *Phys. Lett. A* **2004**,

- 323, 425. d) Mandal, S.; Selvakannan, PR.; Pasricha, R.; Sastry, M. *J. Am. Chem. Soc.* **2003**, *125*, 8441. e) Selvakannan, PR.; Swami, A.; Srisathiyanarayanan, D.; Shirude, P. S.; Pasricha, R.; Mandale, A. B.; Sasty, M. *Langmuir* **2004**, *20*, 7825. f) Liu, M.; Guyot-Sionnest, P.; *J. Phys. Chem. B* **2004**, *108*, 5882. g) Ah, C. S.; Hong, S. D.; Jang, D-J. *J. Phys. Chem. B* **2001**, *105*, 7871. h) Senedrin, R. G.; Georganopoulou, D. G.; Park, S.; Mirkin, C. A. *Adv. Mater.* **2005**, *17*, 1027. i) Huang, C-C.; Yang, Z.; Chang, H-T. *Langmuir* **2004**, *20*, 6092.
- [170] Bohren, C. F.; Huffman, D. R. *Absorption and Scattering of Light by Small Particles*; Wiley: New York, **1983**.
- [171] Moskovits, M. *Rev. Mod. Phys.* **1985**, *57*, 783.
- [172] a) Su, C.; Liao, C-H.; Wang, J-D.; Chiu, C-M.; Chen B-J. *Cata. Today* **2004**, *97*, 71. b) Andersson, M.; Osterlund, L.; Ljungstrom S.; Palmqvist, A. *J. Phys. Chem. B*, **2002**, *106*, 10674. c) Sung-Suh, H. M.; Choi, J. R.; Hah, H. J.; Koo, S. M.; Bae, Y. C. *J. Photocata. Photobio. A* **2004**, *163*, 37.
- [173] Miao, S.; Liu, Z.; Han, B.; Zhang, J.; Yu, X.; Du J.; Sun, Z. *J. Mater. Chem.* **2006**, *16*, 579.
- [174] Naoi, K.; Ohko, Y.; Tatsuma, T. *J. Am. Chem. Soc.* **2004**, *126*, 3664.
- [175] Liz-Marzan, L. M.; Giersig, M.; Mulvaney, P. *Langmuir* **1996**, *12*, 4329.
- [176] Stober, W.; Fink, A.; Bohn, E. *J. Colloid Interface Sci.* **1968**, *26*, 62.
- [177] Hardikar, V. V.; Matijevic, E. *J. Colloid Interface Sci.* **2000**, *221*, 133.
- [178] Mulvaney, P.; Liz-Marzan, L. M.; Giersig, M.; Ung, T. *J. Mater. Chem.* **2000**, *10*, 1259.
- [179] a) Kamat P. V. *Nanoparticles and Nanostructured Films*; J. H. Fendler, Ed.; Wiley-VCH: Weinheim, **1998**, Chapter 9, and references therein. b) Stafford, U.; Gray, K. A.; Kamat, P. V. *J. Phys. Chem.* **1994**, *98*, 6343. c) Ciambelli, P.; Bagnasco, G.; Lisi, L. *Appl. Catal. B* **1992**, *1*, 61.
- [180] Mayya, K. S.; Gittins D. I.; Caruso, F. *Chem. Mater.* **2001**, *13*, 3833.
- [181] Pastoriza-Santos, I.; Koktysh, D. S.; Mamedov, A. A.; Giersig, M.; Kotov, N. A.; Liz-Marzan, L. M. *Langmuir* **2000**, *16*, 2731.
- [182] Aguirre, C. M.; Kaspar, T. R.; Radloff, C.; Halas, N. J. *Nano Lett.* **2003**, *3*, 1707.

- [183] Rodríguez-Fernández, J.; Pérez-Juste, J.; Mulvaney, P.; Liz-Marzán, L. M. *J. Phys. Chem. B* **2005**, *109*, 14257.
- [184] Stoeva, S. I.; Zaikovski, V.; Prasad, B. L. V.; Stoimenov, Peter, K.; Sorensen, C. M.; Klabunde, K. J. *Langmuir* **2005** *21*, 10280.
- [185] a) Fojtik, A.; Henglein, A. *Ber. Bunsen-Ges. Phys. Chem.* **1993**, *97*, 252. b) Sibbald, M. S.; Chumanov, G.; Cotton, T. M. *J. Phys. Chem.* **1996**, *100*, 4672. c) Yeh, M.-S.; Yang, Y.-S.; Lee, Y.-P.; Lee, H.-F.; Yeh, Y.-H.; Yeh, C.-S. *J. Phys. Chem. B* **1999**, *103*, 6851. d) Mafune, F.; Kohno, J.; Takeda, Y.; Kondow, T.; Sawabe, H. *J. Phys. Chem. B* **2000**, *104*, 8333. e) Mafune, F.; Kohno, J.; Takeda, Y.; Kondow, T.; Sawabe, H. *J. Phys. Chem. B* **2000**, *104*, 9111. f) Mafune, F.; Kohno, J.; Takeda, Y.; Kondow, T.; Sawabe, H. *J. Phys. Chem. B* **2001**, *105*, 5114. g) Brause, R.; Möltgen, H.; Kleinermanns, K. *Appl. Phys. B* **2002**, *75*, 711.
- [186] a) Kurita, H.; Takami, A.; Koda, S. *Appl. Phys. Lett.* **1998**, *72*, 789. b) Takami, A.; Kurita, H.; Koda, S. *J. Phys. Chem. B* **1999**, *103*, 1226. c) Mafune, F.; Kohno, J.; Takeda, Y.; Kondow, T. *J. Phys. Chem. B* **2001**, *105*, 9050. d) Mafune, F.; Kohno, J.; Takeda, Y.; Kondow, T. *J. Phys. Chem. B* **2002**, *106*, 7575. e) Mafune, F.; Kohno, J.; Takeda, Y.; Kondow, T. *J. Phys. Chem. B* **2002**, *106*, 8555.
- [187] Mafune, F.; Kohno, J.; Takeda, Y.; Kondow, T. *J. Phys. Chem. B* **2003**, *107*, 12589.
- [188] Link, S.; Burda, C.; Nikoobakht El-Sayed, M. A. *J. Phys. Chem. B* **2000**, *104*, 6152.
- [189] Roorda, S.; van Dillen, T.; Polman, A.; Graf, C.; van Blaafereen, A.; Kooi, B. J. *Adv. Mater.* **2004**, *16*, 235.
- [190] Jin, R.; Egusa, S.; Scherer, N. F. *J. Am. Chem. Soc.* **2004**, *126*, 9900.

Chapter II

Characterization Techniques

The different experimental techniques used during the course of present work are discussed in this chapter.

2.1 Introduction:

The main emphasis of this thesis is as follows: 1) The size and shape controlled synthesis of triangular gold nanoparticles through environmentally benign approach using undialyzed and dialyzed plant extract (lemongrass extract). 2) Synthesis of anisotropic Au core-Ag shell nanoparticles and spherical gold-titania core-shell nanoparticles. 3) Shape transformation of gold nanotriangles by chemical and physical methods. The synthesized gold nanoparticles has been characterized by various techniques such as UV-vis-NIR Spectroscopy, Fourier Transform Infrared Spectroscopy (FTIR), Transmission Electron Microscopy (TEM), Scanning Electron Microscopy (SEM), Atomic Force Microscopy (AFM), X-ray Diffraction (XRD), X-ray Photoelectron Spectroscopy (XPS) and Gel Electrophoresis. This chapter is devoted in explaining the basic principles and the techniques used for the characterization.

2.2 UV-vis-NIR spectroscopy:

Spherical and anisotropic noble metal nanoparticles are ideal candidates for study with UV-vis-NIR spectroscopy, since they exhibit strong surface plasmon resonance absorption in the visible and NIR region of the electromagnetic spectrum. UV-vis-NIR spectroscopy has been extensively used for monitoring the signatures of spherical and triangular nanoparticles formed in different reaction conditions.

2.2.1 Basic principles:

Recently, absorption spectroscopy in the visible and NIR region has long been an important tool to the scientist [1]. Colour transitions arise due to molecular and structural changes in the compounds being examined, leading to the corresponding changes in the ability to absorb light in the visible region of the electromagnetic spectrum. Appearance of particular color arises from the property of the colored material to absorb selectively within the visible region of the electromagnetic spectrum. Absorption of energy leads to a transition of electron from ground state to excited state. Most of the spectra are very broad, smooth curves and not sharp peaks. This is because of fact any change in the electronic energy is accompanied by a corresponding change in the vibrational and rotational energy levels. The magnitude of these energies increases in the following

order: $E_{\text{elec}} < E_{\text{vib}} < E_{\text{rot}}$. A variety of energy absorption is possible depending upon the nature of the bonds within a molecule. For instance, strong σ bonds, in weaker π - bonds or non-bonding (n) and when energy is absorbed all of these types of electrons can be elevated to excited antibonding states represented as σ^* , π^* . Most σ to σ^* absorptions for individual bonds take place below 200 nm in the vacuum ultraviolet region and compounds containing just σ bonds are transparent in the near UV/vis region. $\pi \rightarrow \pi^*$ and $\sigma \rightarrow \sigma^*$ absorptions occur in the near UV/vis region, and result from the presence in molecules of unsaturated groups known as *chromophores*.

The intensity of light passing through a sample is given by the following equation:

$$I = I_0 \exp(-\alpha k x) \dots\dots (1)$$

Where I = intensity of transmitted light; I_0 = intensity of incident light; α = molar absorption coefficient; k = constant; x = path length.

The combined Beer-Lambert law is used for quantification of exact concentration of "unknown" species in a mixture using UV-vis spectroscopy. This can be done by drawing a graph of intensities of absorption for different concentrations of the sample and comparing with a standard graph [1].

The Beer-Lambert law is:

$$A = \epsilon c l \dots\dots (2)$$

Where ϵ = proportionality constant known as the absorptivity.

UV-vis-NIR spectroscopy is a basic tool for characterization of colloidal particles. In particular, spherical metal nanoparticles exhibit surface plasmon resonance absorption in the visible region [2]. Simultaneously, anisotropic nanoparticles also show characteristic absorption in the visible and near infrared (NIR) region. The light absorption by small metal nanoparticles was described by Mie's theory [3]. Mie's theory explained the absorption by small nanoparticles, which have size below the wavelength of light used and particles are well separated in the solution. The absorption spectrum of particles in a given solvent can be calculated from the optical constants of the bulk metal, although the absorption of the nanoparticles is enormously different from that of the bulk metal itself [3]. The absorption spectrum of spherical nanoparticles of size ranging from 3 to 30 nm does not depend upon the particle size. This is because the particles are below the size at which higher order terms in the Mie formula for the absorption constant

become significant. Thus, one has to regard only the dipole term, which depends only on the total metal concentration in the solution and not on particle size.

The absorption coefficient in $\text{mol}^{-1} \cdot \text{L} \cdot \text{cm}^{-1}$ is calculated from the following relation [2, 4]

$$\alpha = \frac{18\pi}{\ln 10} \frac{10^5}{\lambda} \frac{Mn_0^3}{\rho} \frac{\varepsilon_2}{(\varepsilon_1 + 2n_0^2) + \varepsilon_2^2} \dots (3)$$

where λ is the wavelength of light, M and ρ are the molecular weight and density of the metal, n_0 is the refractive index of the solvent and ε_1 and ε_2 are the real and imaginary parts of the dielectric constant of the metal. When the size of the particles becomes smaller than the mean free path of the electrons, the absorption bands are broadened; this is accounted by using size-corrected values of ε_2 [2, 4].

$$\varepsilon_2 = \varepsilon_{2(\text{bulk})} + \left(\frac{\omega_p^2}{\omega^3} \right) (V_F/R) \dots (4)$$

where ω is the frequency of light, ω_p the plasmon frequency, V_F the electron velocity at the Fermi level and R the particle radius (R/V_F , mean time of the free movement of the electrons). Gold and silver particles with diameters of the nanometer scale exhibit very bright colors. The bright colors of noble metal nanoparticles are due to the resonant excitation of a collective oscillation of the conduction band electrons in the particles termed surface plasmon resonance. Conduction electrons (-) and ionic cores (+) in a metal form a plasma state. The movement of electron under the influence of the electric field vector of incoming light leads to a dipole excitation across the spherical particles, the positive polarization charge acting as a restoring force, which makes the electrons oscillates (Figure 2.1). Therefore, electron density within surface layer, thickness of which is about equal to the screening length of a few angstroms, oscillates, whereas the density in the interior of particles remains constant (surface plasmon). Resonance with the incident light is reached at the wavelength where the negative value of ε_1 of metal is equal to twice the dielectric constant of medium (equation 3). Therefore, any changes in the electron density of this surface layer will lead to changes in the plasmon absorption [5]. This surface sensitivity of colloidal nanoparticles has been used to study adsorption/chemisorption of thiols, biomolecules and halide ions [6].

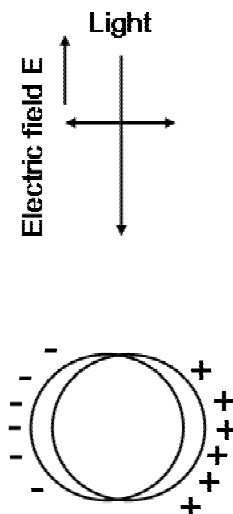


Figure 2.1: Schematic representation of polarization of a spherical metal particle by the electrical field vector of the incoming light.

For larger particles, light cannot polarize the metal nanoparticles homogeneously and therefore, retardation effect leads to the excitation of higher modes. Higher modes in Mie's equation become more dominant with particle size, leading the red shift of absorption band and resulting in bandwidth. Within the size range of 25 nm the nanoparticles can be treated with dipolar approximation and is independent of the particle size [5]. For anisotropic and spheroid nanoparticles, Gans extended Mie's theory for spherical nanoparticles within dipole approximation [7]. The surface plasmon band for nanorods can be split into two bands. The higher wavelength band (low energy band) is caused by the oscillation of the electrons along the major axis of the nanorods and is known as the longitudinal surface plasmon absorption. While the lower wavelength band (high energy band) is caused by oscillation of the electron perpendicular to the major axis of nanorods and is called as the transverse surface plasmon band [5].

In case of gold nanotriangles, electrons oscillation occurs in the plane and out of plane of nanoparticles, leading to the development of a strong band in the NIR region (longitudinal band) and a weak band in the visible region (transverse band). The longitudinal band is also called in the plane plasmon vibration band that appeared to be sensitive to the edge length of gold nanotriangles. The transverse band is assigned to the out of plane dipole vibration band. In certain cases even a weak band intermediate to

these two regions is observed and is assigned to the in plane quadrupole mode of plasmon resonance [8].

UV-vis-NIR spectroscopy was used to monitor the synthesis of gold nanotriangles using undialyzed lemongrass extract and dialyzed lemongrass extract. The formation of triangular Au core-Ag shell nanoparticles and spherical gold-titania core-shell nanoparticles was analysed by using UV-vis-NIR spectroscopy. UV-vis-NIR spectroscopy was also used to monitor the morphological transformation of triangular gold nanoparticles using chemical and physical means. These measurements were done on a JASCO V570 UV/VIS/NIR spectrophotometer operated at a resolution of 1 nm.

2.3 Fourier Transform Infrared Spectroscopy (FTIR):

FTIR is a powerful tool to investigate the presence of functional groups in a given compound. Biomolecules of lemongrass extract bound on the surface of gold nanoparticles give signatures in the infrared region of electromagnetic spectrum. For instance, ketonic group present in lemongrass extract shows band at 1700 cm^{-1} . CTAB and CTAC used for morphology transformation of gold nanotriangles can also be easily detected in the FTIR spectra. The hydrolysing protein used for the synthesis of gold-titania core-shell nanoparticles gives rise to well know FTIR signatures. The position of the amide I (the C=O band in amide linkage at ca. 1650 cm^{-1}), amide II band (the N-H stretch mode of vibration in the polypeptide linkage at ca. 1546 cm^{-1}) and the amide III (the C-N band in the polypeptide chain at ca. 1240 cm^{-1}) bands in the FTIR spectra of proteins is a sensitive indicator of conformational changes in the protein secondary structure [9].

2.3.1 Basic Principle:

The atoms in a molecule do not remain in a fixed relative position and vibrate about some mean position. Due to this vibrational motion if there is a periodic alternation in the dipole moment then such mode of vibration is infrared (IR) active. The IR region of the electromagnetic spectrum is $100\text{ }\mu\text{m} - 1\text{ }\mu\text{m}$ wavelength. The vibrating molecule absorbs energy only from radiation with which it can coherently interact, i.e. the radiation of its own oscillation frequency. The principles of IR can be explained by classical as well as quantum theories [6]. The classical model considers a simple ball and spring

model wherein diatomic molecule with two masses m_1 and m_2 are connected by a spring. According to Hooke's law when spring is displaced,

$$F = -kx \dots (5)$$

Where F = opposing restoring force; k = force constant; x = displacement from equilibrium position. This is simple harmonic equation wherein the frequency of vibration is given by the relation:

$$\nu = \frac{1}{2\pi} \sqrt{\frac{k}{\mu}} \dots (6)$$

Where μ is the reduced mass. Using simple laws of mechanics, a system of masses joined by springs has a number of fundamental modes of vibration each of which has a particular natural frequency.

Silicon is the most commonly used substrate for IR measurements, for variety of reasons. It is chemically very stable and generally not very reactive even at high temperatures. It is excellent for optical studies of deposited films in the visible region using reflection techniques. It does not have strong lattice absorption bands in the useful regions of the infrared and thus can be used for transmission studies in this region. To correct for the lattice absorption bands in silicon, a reference silicon sample is used as a reference.

Gold nanoparticles synthesized using various methods in this thesis have been drop coated on the Si(111) substrate. All FTIR spectra have been carried out on Perkin Elmer Spectrum One FTIR spectrometer operated in the diffuse reflectance mode at a resolution of 4 cm^{-1} .

2.4 Transmission Electron Microscopy (TEM):

TEM is a method to produce images of a sample by illuminating sample with electronic radiation and detecting the electrons that are transmitted through the sample. This technique requires that the thickness of the films under study will be less than 300 \AA ; however, direct observation of one monolayer is not possible because of lack of contrast. The electron energy in TEM is very high (100 keV) and the resolution ranges from 1000 \AA to a few tens of Angstroms. Sample for TEM measurement was prepared by drop coating the carbon-coated Cu grid with liquid sample, allowing the grid to stand for

2 minutes following which extra solution was removed carefully by blotting paper. TEM analysis was performed on a JEOL model 1200EX instrument operated at an accelerating voltage at 120 kV.

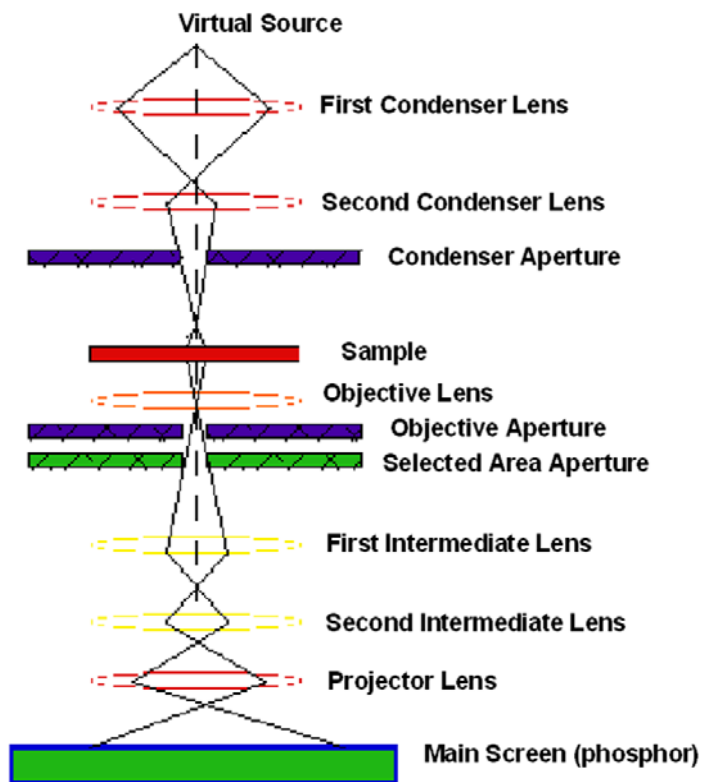


Figure 2.2: Diagram showing the various elements of the TEM instrument.

In TEM instruments, the electron gun usually consists of a tungsten wire filament, which is bent into a hairpin ("V") shape and surrounded by a shield with a circular aperture (1-3 mm diameter) centered just below the filament tip. Electrons in the gun are accelerated across a potential difference of the order of 100,000 volts between the cathode (at high negative potential) and anode (at ground potential). The function of the condenser lens is to focus the electron beam emerging from the electron gun onto the specimen to permit optimal illuminating conditions for visualizing and recording the image. The optical enlarging system of an electron microscope consists of an objective lens followed by one or more projector lenses. The objective lens determines resolution and contrast in the image, and all subsequent lenses bring the final image to a convenient magnification for observation and recording. The objective lens is most critical lens since

it determines the resolving power of the instrument and performs the first stage of imaging. The specimen image generated by the objective lens is subsequently magnified in one or two more magnification stages by the intermediate and projector lens and projected onto a fluorescent screen or photographic plate (Figure 2.2). The darker areas of the image represent those areas of the sample that fewer electrons were transmitted through (they are thicker or denser). The lighter areas of the image represent those areas of the sample that transmit more electrons (they are thinner or less dense).

In present study, TEM has been used to analyze the shape and size of nanoparticles formed by using lemongrass extract. TEM measurements were also carried out to observe the morphology of gold nanoparticles formed using dialyzed extract from different cut-off (3, 12.5 and 30 kDa) bags and also formed during the dialysis of lemongrass extract against HAuCl_4 . The synthesis of core-shell nanoparticles and morphological transformation of gold nanotriangles was also investigated using TEM. High-resolution transmission electron microscopy (HRTEM) of the gold nanotriangle and core-shell nanoparticle samples prepared on carbon coated grids were carried on a JEOL model 3010 operated at an accelerating voltage of 300 kV and FEI G² super Twin 300 kV FEG machine having resolution of 0.1 nm.

2.5 Scanning Electron Microscopy (SEM):

Scanning Electron Microscopy is a powerful tool for direct observation of surfaces because they provide better resolution and depth of field than optical microscope. By scanning with an electron beam that has been generated and focused by the operation of the microscope, an image is formed in much the same way as a television. SEM measurements were performed on a Leica Stereoscan-440 scanning electron microscope instrument equipped with a Phoenix EDAX attachment. SEM was used for analysis of the morphology of gold nanoparticles formed using lemongrass extract.

2.5.1 Basic Principle:

The instrument can be simplified into three major sections: a) electron-optical 'column'; b) vacuum system and c) electronics and display system [10]. A tungsten filament is heated to 2700 K, which produces electrons that are accelerated towards the anode disc. Electrostatic shaping of the electron beam under vacuum gives a beam

diameter of about 50 μm . The ultimate performance of the SEM is mainly limited by the diameter of the beam and hence two lenses and condensers demagnify the beam to around 5 nm. The scanning coils deflect this beam and sweep it over the specimen surface. A cathode-ray display tube is scanned synchronously with the electron beam. The brightness of the display tube is modulated by the signal, which arises from the interaction of the beam with the surface element, which is probed. The strength of this signal is translated into image contrast. Secondary electrons, which the beam probe liberates from the specimen surface, are collected and used as the contrast signal. The yield of collected electrons depends on the nature of the specimen surface and on its inclination with respect to the probing beam. Consequently, one obtains pictures with a high perspective appearance [10]

2.5.2 Specimen- Beam Interaction:

There are different types of interaction of electron beam with the samples as shown in Figure 2.3 [10]. One can have unscattered electron, wherein electron beam (energy in the range of 20 - 30 keV) just passes through the thin sample ($< 1 \mu\text{m}$) and does not contain any information about the sample. Most of electrons are scattered at large angles (0 to 180°) when they interact with positively charged nucleus. These elastically scattered electrons called “backscattered electron” are used for SEM imaging. Some electrons scatter inelastically due to the loss in kinetic energy upon their interaction with orbital shell electrons. Due to electron bombardment, phonons are set up in the specimen resulting considerable heating of the specimen. Incident electrons may knock off loosely bound conduction electrons out of the sample. These are secondary electrons and along with backscattered electrons are widely used for SEM topographical imaging. If the electron beam knocks off an inner shell electron, the atom rearranges by dropping an outer shell electron to an inner one. This excited or ionised atom emits an electron commonly known as the Auger electron. Recently Auger electron spectroscopy (AES) is useful to provide compositional information. Instead of excited atom releasing Auger electron, it can release a photon of electromagnetic radiation. If the amount of energy released is high, the photon will be an X-ray photon. These electrons are characteristic of the sample and can be used for analysis. This type of analysis is known as Energy

Dispersive analysis of X-rays (EDAX). We have used this for spot profile analysis to determine the presence of gold in nanotriangles formed by using lemongrass extract.

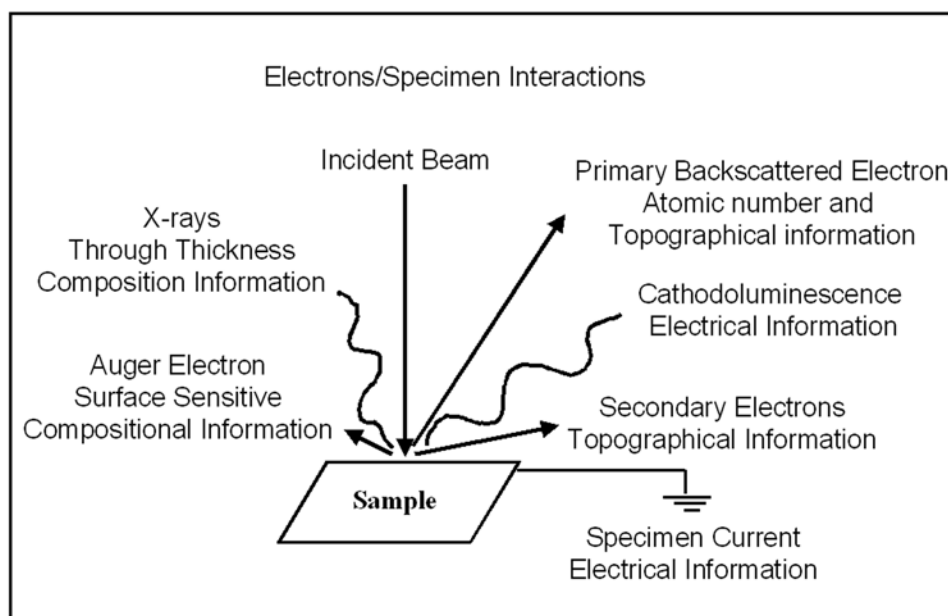


Figure 2.3: Schematic showing the interaction between electron and specimen.

2.6. Atomic Force Microscopy (AFM):

The atomic force microscope (AFM) is a high-resolution type of scanning probe microscope, with demonstrated resolution of fractions of an Angstrom, more than 1000 times better than the optical diffraction limit. The AFM was invented by Binnig, Quate and Gerber in 1986, and is one of the foremost tools for imaging, measuring and manipulating matter at the nanoscale.

2.6.1 Basic Principle:

The AFM consists of a microscale cantilever with a sharp tip (probe) at its end that is used to scan the specimen surface. The cantilever is typically silicon or silicon nitride with a tip radius of curvature on the order of nanometers. When the tip is brought in the proximity of a sample surface, forces between the tip and the sample lead to a deflection of the cantilever according to Hooke's law. Depending on the situation, forces that are measured in AFM include mechanical contact force, Van der Waals forces, capillary forces, chemical bonding, electrostatic forces, magnetic forces (Magnetic force

microscope (MFM)), Casimir forces, solvation forces etc. Typically, the deflection is measured using a laser spot reflected from the top of the cantilever into an array of photodiodes. Other methods that are used include optical interferometry, capacitive sensing or piezoresistive AFM probes. These probes are fabricated with piezoresistive elements that act as a strain gage. Using a Wheatstone bridge, strain in the AFM probe due to deflection can be measured, but this method is not as sensitive as laser deflection or interferometry.

If the tip is scanned at a constant height, there would be a risk that the tip would collide with the surface, causing damage. Hence, in most cases a feedback mechanism is employed to adjust the tip-to-sample distance to maintain a constant force between the tip and the sample.

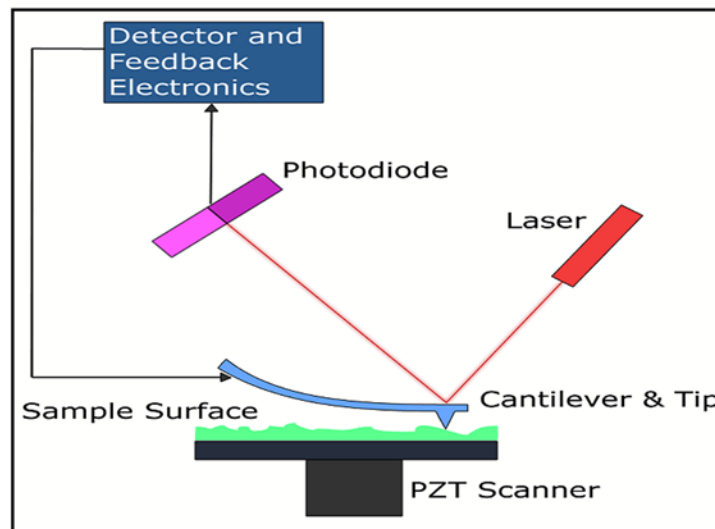


Figure 2.4: Schematic showing various elements of the AFM instrument. (Ref: http://en.wikipedia.org/wiki/Atomic_force_microscope)

Traditionally, the sample is mounted on a piezoelectric tube, that can move the sample in the z direction for maintaining a constant force, and the x and y directions for scanning the sample. Alternately a 'tripod' configuration of three piezo crystals may be employed, with each responsible for scanning in the x , y and z directions. This eliminates some of the distortion effects seen with a tube scanner. The resulting map of the area $s = f(x,y)$ represents the topography of the sample. The AFM can be operated in number of modes, depending on the application. In general, possible imaging modes are divided into

static (also called Contact) modes and a variety of dynamic modes. The AFM images presented in this thesis were taken in the contact mode on the Veeco Nanoscope IV instrument.

2.7 X-ray Diffraction (XRD):

In 1895 after discovering X-ray by Rontgen, Von Laue demonstrated that X-ray could be diffracted by crystal in 1912. In 1935 Le Galley first constructed X-ray powder diffractometer. Largely metallurgists and mineralogists use powder diffraction primarily to study structural imperfections. X-ray are electromagnetic radiation with wavelength of the order of 10^{-10} m. They are typically generated by bombarding a metal with high-energy electrons. The high-energy electron must penetrate through the outer electron shells and interact with the inner-shell (or core) electrons. If more than a critical amount of energy is transferred to an inner-shell electron, that electron is ejected; i.e. it escapes the attractive field of the nucleus, leaving a hole in the inner shell and generates ionized atom (Figure 2.5). The ionized atom can return almost to its lowest energy (ground state) by filling in the missing electron with one from the outer shells. It is this transition which is accompanied either by the emission of an X-ray or an Auger electron. In 1913, Sir W.H. Bragg and his son Sir W.L. Bragg gave the famous Bragg's Law to explain why the cleavage faces of crystals appear to reflect X-ray beams at certain angles of incidence (θ).

$$\text{Bragg's Law ... } n\lambda = 2d \sin\theta \text{ (7)}$$

The variable d is the distance between atomic layers in a crystal, the variable λ is the wavelength of the incident X-ray beam and n is an integer. This observation is an example of X-ray wave interference commonly known as X-ray diffraction (XRD), and was direct evidence for the periodic atomic structure of crystals postulated for several centuries [11]. Although Bragg's law was used to explain the interference pattern of X-rays scattered by crystals, diffraction has been developed to study the structure of all states of matter with any beam, e.g., ions, electrons, neutrons, and protons, with a wavelength similar to the distance between the atomic or molecular structures of interest.

A crystal may be defined as a collection of atoms arranged in a pattern that is periodic in 3D. Crystals are necessarily solids, but not all solids are crystalline. In a perfect single crystal all atoms in the crystal are related either through translational

symmetry or point symmetry. Polycrystalline materials are made up of a great number of tiny single crystals.

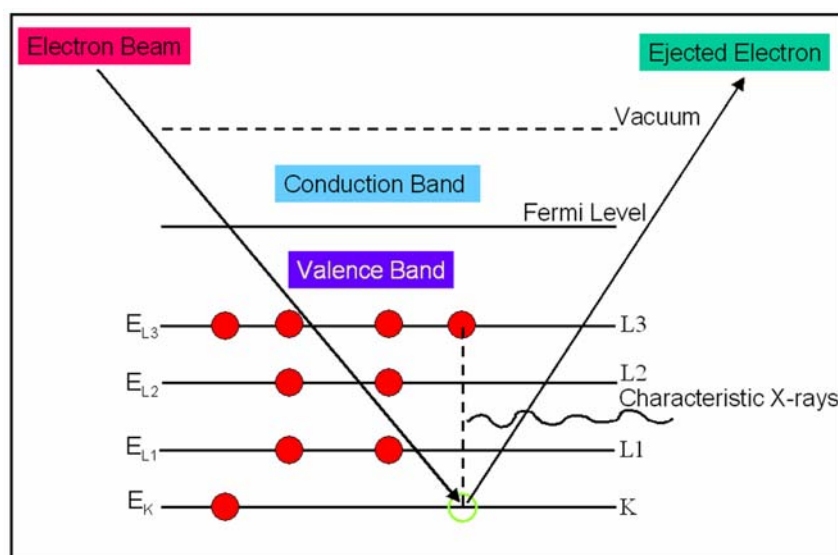


Figure 2.5: Schematic shows the processes that contribute to the generation of X-rays.

In powder diffraction method we can get the information from peak positions, crystal system, space group symmetry, translational symmetry, unit cell dimension, qualitative phase identification, from peak intensities unit cell contents, point symmetry and from peak shapes and widths crystalline size, non-uniform microstrain, extended defects [11]. Deviations from ideal crystallinity, such as finite crystallite size and strain lead to broadening of the diffraction lines. By analyzing this broadening it is possible to extract information about the microstructure of a material. A perfect crystal would extend in all directions to infinity, so we can say that no crystal is perfect due to its finite size. This deviation from perfect crystallinity leads to a broadening of the diffraction peaks. However above a certain size ($\sim 0.1-1 \mu\text{m}$) this type of broadening is negligible. Crystallite size is a measure of the size of a coherently diffraction domain. Due to presence of polycrystalline aggregates crystallite size is not generally the same thing as particle size. In 1918 Scherrer first observed that small crystallite size could give rise to line broadening. He derived a well-known equation for relating the crystallite size to the broadening, which is called the “Scherrer formula”.

$$D_v = K \lambda / (\beta \cos\theta) \dots (8)$$

where, D_v = volume weighted crystallite size, k = Scherrer constant, somewhat arbitrary value that falls in the range 0.87-1, λ = wavelength of the X-ray radiation, β = integral breadth of a reflection (in radians 2θ) located at 2θ .

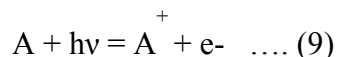
XRD patterns of gold-titania core-shell nanoparticles and different concentrations of Keggin ions bound gold nanotriangles drop coated on glass substrates were recorded on a Phillips PW 1830 instrument operating at a voltage of 40 kV and a current of 30 mA with Cu-K α radiation.

2.8 X-ray Photoemission Spectroscopy (XPS):

X-ray Photoelectron Spectroscopy known as XPS has been developed by Professor K. Siegbahn for which he was awarded the Physics Nobel Prize in 1981. XPS is surface science technique used to study the composition and electronic state of the surface region of a sample. Since, the technique provides a quantitative analysis of the surface composition is sometimes known by the alternative acronym, ESCA (Electron Spectroscopy for Chemical Analysis).

2.8.1 Basic Principle:

XPS is based on well-known photoelectric effect (a single photon in/electron out process) first explained by Einstein in 1905. Photoelectron spectroscopy uses monochromatic sources of radiation (i.e. photons of fixed energy given by relation, $E = h\nu$). In XPS the photon is absorbed by an atom in a molecule or solid, leading to ionization and the emission of a core (inner shell) electron. The kinetic energy distribution of the emitted photoelectrons (i.e. the number of emitted photoelectrons as a function of their kinetic energy) can be measured using any appropriate electron energy analyser and a photoelectron spectrum can thus be recorded. The one way to look at the overall process of photoionization is follows:



Conservation of energy then requires that:

$$E(A) + h\nu = E(A^+) + E(e^-) \dots (10)$$

Since the electron's energy is present solely as kinetic energy (KE) this can be rearranged to give the following expression for the KE of the photoelectron:

$$KE = h\nu - (E(A^+) - E(A)) \dots (11)$$

The final term in brackets, representing the difference in energy between the ionized and neutral atoms, is generally called the binding energy (BE) of the electron - this then leads to the following commonly quoted equation:

$$KE = h\nu - BE \dots (12)$$

the binding energies (BEs) of energy levels in solids are conventionally measured with respect to the Fermi-level of the solid, rather than the vacuum level (Figure 2.6). This involves a small correction to the equation given above in order to account for the work function (ϕ) of the solid,

$$KE = h\nu - BE - \phi \dots (13)$$

Employing photons with fixed energy $h\nu$, it is obvious that if kinetic energy KE and work function ϕ of the sample is measured, it is possible to measure binding energy of electron in solid.

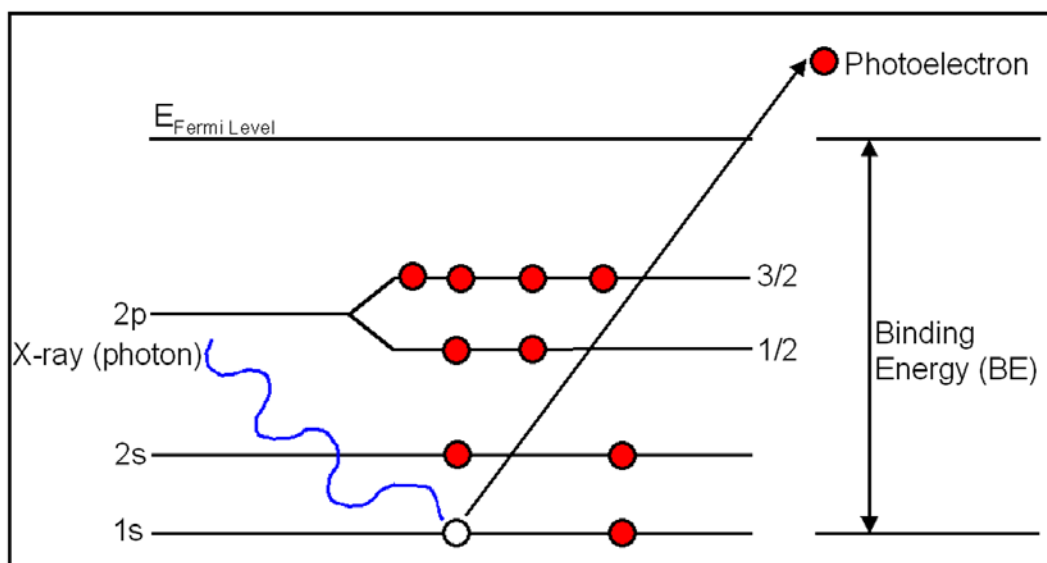


Figure 2.6: Schematic showing photoemission of electron in XPS.

Binding energies being characteristic of atoms, different elements present in the sample under investigation are identified. Electrons traveling through a material have a relatively high probability of experiencing inelastic collisions with locally bound electrons as a result of which they suffer energy loss and contribute to the background of

the spectrum rather than a specific peak. Due to inelastic scattering process, the flux of photoelectrons emerging from the sample is much attenuated. The soft X-rays employed in XPS penetrate a substantial distance into the sample ($\sim \mu\text{m}$). Thus this method of excitation imparts no surface sensitivity at the required atomic scale. However the photoelectrons can escape from only a very short distance beneath the surface ($< 100 \text{ \AA}$). The surface sensitivity thus arises from the emission and detection of the photoemitted electrons.

2.8.2 Chemical Shift:

The exact binding energy of an electron depends not only upon the level from which photoemission is occurring, but also upon:

- (1) the formal oxidation state of the atom
- (2) the local chemical and physical environment

changes in either (1) or (2) give rise to small shifts in the peak positions in the spectrum - so-called chemical shifts. Atoms of a higher positive oxidation state exhibit a higher binding energy due to the extra coulombic interaction between the photo-emitted electron and the ion core. This ability to discriminate between different oxidation states and chemical environments is one of the major strengths of the XPS technique.

The basic requirements for a XPS experiment are:

- (1) X-ray source of fixed-energy radiation (usually Mg $K\alpha$ with $h\nu = 1253.6 \text{ eV}$ or Al $K\alpha$ with $h\nu = 1486.6 \text{ eV}$)
- (2) Concentric hemispherical analyser (CHA), which uses an electric field between two hemispherical surfaces to disperse the electrons according to their kinetic energy, and thereby measure the flux of emitted electrons of a particular energy.
- (3) A high vacuum environment (to enable the emitted photoelectrons to be analysed without interference from gas phase collisions)

For the work described in this thesis, the XPS spectra of C 1s, Au 4f, Ag 3d, Br 3d, Cl 2p, Ti 2p and N 1s core levels were recorded from different samples such as gold nanotriangles, halide ions and surfactants modified gold nanotriangles as well as core-shell nanoparticles deposited on Si(111) wafers. XPS measurement were carried out on a VG Microtech ESCA 3000 instrument at a base pressure better than 1×10^{-9} Torr with un-monochromatized Mg $K\alpha$ radiation (1253.6 eV energy). The measurements were

made in the constant analyzer energy (CAE) mode at pass energy of 50 eV and electron takeoff angle (angle between electron emission direction and surface plane) of 60°. This leads to an overall resolution of ~ 1 eV in the measurements. The chemically distinct components in the core level spectra were resolved by a non-linear least squares fitting algorithm after background removal by the Shirley algorithm [12].

2.9 Gel electrophoresis:

The term electrophoresis describes the migration of a charged particle under the influence of an electric field [13]. Many important biological molecules, such as amino acids, peptides, proteins, nucleotides and nucleic acids, possess ionizable groups and, therefore, at any given pH, exist in solution as electrically charged species either as cations (+) or anions (-). Under the influence of an electric field these charged particles will migrate either to the cathode or to the anode, depending on the nature of their net charge [13]. The equipment required for electrophoresis consists basically of two items, a power pack and an electrophoresis unit (Figure 2.7). Electrophoresis units are available for running either vertical or horizontal gel systems.

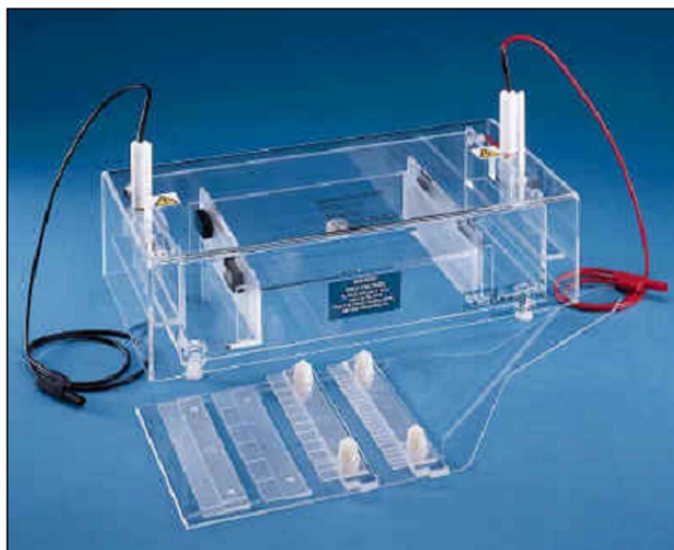


Figure 2.7: Representative horizontal gel electrophoresis system. (Ref: <http://images.google.co.in/images?hl=en&q=Agarose%20gel%20electrophoresis>.)

In this thesis, we have used horizontal gel system to investigate charge on the surface of gold nanotriangles synthesized during dialysis of lemongrass extract against

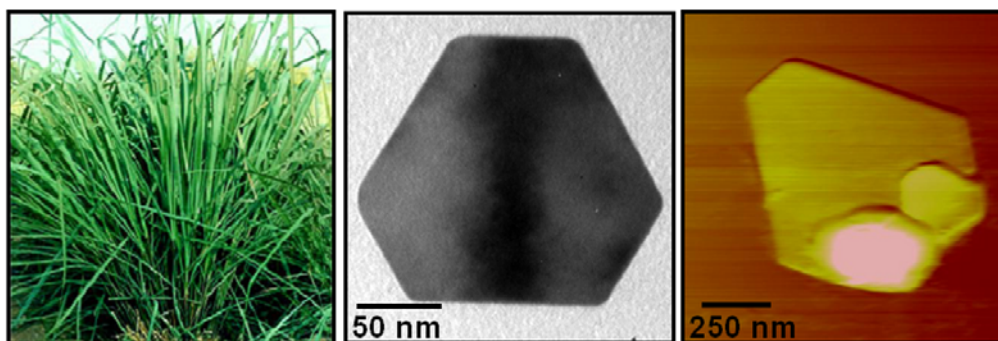
H₂O₂. Horizontal slab gel units are commercially available and routinely used to separate DNA and RNA in agarose gels. Gel dimension is typically 6 cm x 5 cm with thickness of ca. 0.5 mm to 1 mm. A plastic comb is placed in melted agarose gel solution and comb is removed after solidification of gel to get wells for loading samples. The electrophoresis is carried out in the phosphate buffer of pH 7.4.

2.10 References:

- [1] Denney, R.C; Sinclair, R. Visible and Ultraviolet Spectroscopy. Analytical Chemistry by openlearning series, John Wiley and Sons, USA.
- [2] Malvaney, P. *Langmuir* **1996**, *12*, 788.
- [3] Mie, G. *Ann. Phys.* **1908**, *25*, 377.
- [4] Henglein, A. *J. Phys. B.* **1993**, *97*, 5457.
- [5] Burda, C.; Chen, X.; Narayanan, R.; El-Sayed, M. A. *Chem. Rev.* **2005**, *105*, 1025.
- [6] a) Brust, M.; Walker, M.; Bethell, D.; Schiffrin, D.J.; Whyman, R. *J. C. S. Chem Commun.* **1994**, 801. b) Malinsky, M. D.; Kelly, K. L.; Schatz, G. C.; VanDuyne, R. *J. Am. Chem. Soc.* **2001**, *123*, 1471. c) Templeton, A. C.; Wvelfing, W. P.; Murray, R. W. *Acc. Chem. Res.* **2000**, *33*, 27. d) Keating, C. D.; Kovaleski, K. M.; Natan, M. J. *J. Phys. Chem. B* **1998**, *102*, 9404. e) Xu, H.; Bjerneld, E. J.; Kall, M.; Borjesson, L. *Phy. Rev. Lett.* **1999**, *83*, 4357. f) Crumbliss, A. L.; Perine, S. C.; Stonehuerner, J.; Tubergen, K. R.; Zhao, J.; O'Daly, J. P. *Biotech.Bioeng.* **1992**, *40*, 483. g) Gole, A.; Dash, C.; Ramakrishnan, V.; Sainkar, S. R.; Mandale, A. B.; Rao, M.; Sastry, M. *Langmuir* **2001**, *17*, 1674.
- [7] Gans, R. *Ann. Phys.* **1915**, *47*, 270.
- [8] Millstone, J. E.; Park, S.; Shuford, K. L.; Qin, L.; Schatz, G. C.; Mirkin, C. A. *J. Am. Chem. Soc.* **2005**, *127*, 5312.
- [9] a) Dong, A.; Huang, P.; Caughey, W.S. *Biochemistry* **1992**, *31*, 182. b) Kumar, C. V.; McLendon, G. L. *Chem. Mater.* **1997**, *9*, 863. c) Templeton, A. C.; Chen, S.; Gross, S. M.; Murray, R.W. *Langmuir* **1999**, *15*, 66. d) Caruso, F.; Furlong, D. N.; Ariga, Katsuhiko.; Ichinose, I.; Kunitake, T. *Langmuir* **1998**, *14*, 4559.
- [10] Lawes, G. Scanning electron microscopy and X-ray microanalysis: Analytical chemistry by open learning, John Wiley & sons, **1987**.
- [11] Cullity, B. D. "Elements of X-ray diffraction" Addison-Wesley publishing company, Inc. **1959**.
- [12] Shirley, D. A. *Phys. Rev. B* **1972**, *5*, 4709.
- [13] Wilson, K.; Walker, J. "Practical Biochemistry" (5th Edition) Cambridge University Press.

Chapter III

Synthesis of Triangular and Hexagonal Gold Nanoparticles using Undialyzed and Dialyzed Lemongrass Leaf Extract



Lemongrass Leaves

Hexagonal Gold Nanoparticles

*In this chapter, room temperature synthesis of highly anisotropic gold nanoparticles (triangular and hexagonal) using lemongrass (*Cymbopogon flexuosus*) leaf extract has been discussed. Dialysis is used as a novel method to control the size and yield of triangular and hexagonal nanoparticles. 3, 12.5 and 30 kDa cut-off dialysis bags were used for the synthesis of gold nanotriangles during dialysis of lemongrass extract against 10^{-3} M HAuCl_4 solutions. The extract dialyzed using different cut-off bags were also used for the synthesis of gold nanotriangles. The anisotropic nanoparticles display an intense absorption in the NIR region of the electromagnetic spectrum, which can be controlled by varying the amount of lemongrass extract in the reaction medium using different cut-off dialysis bags. The chapter also discusses the size of biomolecules present in lemongrass extract, which play an important role as reducing and shape directing agents for the nanotriangle synthesis.*

3.1 Introduction:

Biology has always fascinated materials scientists due to their precise regulation of the morphology of crystals. Inspired by biomineralization, nanotechnologists have paid much attention towards the synthesis of materials of particular size and shape using biomolecules or organisms as reducing or templating agents. Magnetic nanoparticles present inside magnetotactic bacteria [1], siliceous structures in diatoms [2] and calcareous nanostructures in various organisms [3] etc are motivating factors for scientists to synthesize materials in nanodimensions using biological means. Metal nanoparticles are always attractive candidates because of their unique properties that are different from their bulk counterparts that endow them with numerous applications in opto-electronics [4], catalysis [5], magnetic devices [6], biosensing [7], biodetection [8], and drug/gene delivery [9]. Nowadays, colloid chemistry is challenged to control not only the size of metal nanoparticles but also the shape and morphologies. Shape control is an alternative tool to modulate the optical and catalytic properties of nanomaterials. Much effort has been devoted to the synthesis of various shapes of nanoparticles like nanocubes [10], nanorods/nanowires [11], nanodisks [12], nanotetrapods/nanoarrows/nano-tear drops [13], nanobelts/nanoribbons [14] and nanodumbbells [15] by chemical and physical methods. Recently, synthesis of metal nanoprisms has received enormous attention mainly due to their unusual optical and catalytic properties with potential application in various fields. There are several reports on the synthesis of silver nanotriangles [16] but fewer efforts have been made to synthesize gold nanoprisms [17]. The synthesis of these anisotropic nanoparticles is achieved by chemical and physical means, which are often hazardous to the environment. Thus, there are growing demands for the synthesis of nanoparticles through clean, nontoxic and environment friendly (green chemistry) procedures. Therefore, biological processes that lead to formation of nanomaterials appear to be a promising endeavor as environmentally benign nanofactories.

Beveridge and coworkers first demonstrated the deposition of gold nanoparticles within bacterial cells [18]. Reduction of Ag^+ ions and formation of silver nanoparticles within the periplasmic space of the bacterium *Pseudomonas stutzeri* AG259 was shown by Klaus-Joerger and coworkers [19]. Sastry and coworkers have shown earlier that intra and extracellular synthesis of nanoparticles of various compositions and size could be

achieved by using bacteria and fungi [20]. Brown *et al.* have investigated the polypeptide directed synthesis of gold nanocrystals and found that polypeptides could control the morphology and orientation of nanocrystals [21]. Apart from the microorganisms used for synthesis, biomolecules like starch [22, 17d], aspartic acid [23] and phospholipids [24] have also been used as reducing and stabilizing agents for the synthesis of gold and silver nanostructures. Though microorganisms are utilized for synthesis of various compositions of nanoparticles, the use of plants or plant extracts for synthesis of nanoparticles is an under-exploited area. Plants have been used as phyto-remediation sources for removal of contaminations from soils and water for a long time [25]. Plants are also used for hyper-accumulation of heavy metals in different parts either through reduction of metals ions to lower oxidation state or complexation of biomolecules to metals in its native oxidation state [26]. Jose-Yacaman's group has shown that live Alfalfa plants reduced Au^{3+} ions to Au^0 oxidation state to form metal nanoparticles inside the plants [27]. They have also demonstrated the synthesis of silver nanoparticles inside Alfalfa plant shoots by supplying the Ag^+ ions in the plant growth media [28]. In another report, oat, wheat biomass, geranium and neem plant extracts have been used as reducing agents to synthesize gold nanoparticles of various size and shape [29]. As far as commercial production of metal nanoparticles is concerned, the metal nanoparticles synthesized inside plants and micro-organisms (intracellular) suffer primarily from product harvesting and recovery that are cumbersome and expensive. Therefore, the extracellular synthesis plays a pivotal role in the synthesis of various compositions of nanoparticles in the large scale.

In this chapter, an attempt has been made to synthesize triangular gold nanoparticles using a plant extract. We discuss a single step and room temperature process for synthesis of triangular and hexagonal gold nanoparticles using lemongrass extract as the reducing and shape-directing agent. The yield of the gold nanotriangles by this method is better than other reported chemical and photo-induced methods. As compared to spherical counterparts, triangular and hexagonal gold nanoparticles show two surface plasmon resonance bands; one in the visible region at 520 nm and another in the NIR region of the electromagnetic spectrum [16, 17]. The intense absorption of the triangular nanoparticles in the NIR region could make these nanoparticles potential

candidates for cancer hyperthermia [30] and architectural application in optical coating for blocking the NIR light from the solar spectrum [31]. The absorption by triangular nanoparticles in NIR region depends on their edge length and could be controlled by varying the concentration of lemongrass extract in the reaction medium [31]. Dialysis is a method used particularly in biology to purify a single compound from a mixture of compounds. Dialysis is the process of separating molecules in the solution by difference in their rate of diffusion through a semipermeable membrane (dialysis bag). The purification of a compound using dialysis depends upon the rate of diffusion of molecules through pores of the bag due to concentration gradients across the dialysis bag. A concentration gradient is due to the difference in concentration of solutions separated by the membrane and it determines the rate of diffusion.

Fick's law governs the diffusion of molecules across the dialysis bag. Fick's first law is applied in steady state diffusion i.e., when the concentration within the diffusion volume does not change with respect to time.

$$J = -D \frac{\partial \phi}{\partial x}$$

where

J is the diffusion flux, D is diffusion coefficient

$\frac{\partial \phi}{\partial x}$ is concentration gradient

The size of the pores in the bag and that of the constituents of the mixture is also an important factor for the size selective purification of a compound. Molecules (salts, water or small molecules), small enough to pass through the semipermeable membrane, tend to move into or out of the dialysis bag in the direction of decreasing concentration. Larger molecules, which have dimension significantly greater than the pore diameter, are retained inside the dialysis bag. In this chapter, dialysis is used as a tool to regulate the green chemistry approach of synthesis of nanoparticles of controlled size and shape using lemongrass extract and hence to fine-tune their optical properties. Dialysis has been used for the size selective separation of biomolecules from several sizes of biomolecules of lemongrass extract. Biomolecules of lemongrass extract, which have size below the pore size of corresponding dialysis bags, diffuse from inside the bags to external solutions

(lower concentration), while larger biomolecules remain inside the bags and therefore the concentrations and compositions of extract both inside and outside the dialysis bags are different. The different concentrations of extract both inside and outside the dialysis bags facilitate synthesis of varying yield and size of gold nanotriangles due to the different rate of reduction of gold ions in the solution. In this chapter, we have also strived to investigate the size of biomolecules of lemongrass extract that is responsible for nanotriangle formation using different cut-off *viz*; 3, 12.5 and 30 kDa dialysis bags.

3.2 Synthesis of gold nanotriangles and nanohexagons using lemongrass leaf extract:

3.2.1 Experimental Details:

Lemongrass leaf extract was prepared by boiling 100 g of thoroughly washed and finely cut lemongrass leaves (*Cymbopogon flexuosus*) in 500 mL sterile distilled water. In a typical experiment, 10 mL of this lemongrass extract was added to 90 mL of 10^{-3} M aqueous HAuCl_4 solution. The reduction of AuCl_4^- ions was monitored by recording the UV-vis-NIR absorption spectra as a function of time of reaction of this mixture. The percentage of gold nanotriangles in solution was enhanced up to 98% by centrifuging the nanotriangle solution three times at 1000 rpm for 15 minutes followed by redispersion in water. The UV-vis-NIR spectrum of the purified gold nanotriangles was recorded from a drop-coated film on the quartz slide. Gold nanotriangles synthesized by lemongrass extract were characterized by Transmission electron microscopy (TEM) and Scanning electron microscopy (SEM). Atomic force microscopy (AFM) analysis in the contact mode was done to find out the thickness of the gold nanotriangles.

3.2.2 UV-vis-NIR spectroscopy Analysis:

UV-vis-NIR spectra were recorded as a function of time of reaction for undialyzed lemongrass extract with 10^{-3} M HAuCl_4 solution at room temperature. Curve 1 in Figure 3.1 shows the surface plasmon resonance band (SPR) at ca. 580 nm after 1 h of reaction. With time, the surface plasmon band at 580 nm is gradually shifted to 540 nm with increase in intensity. This change is also accompanied by appearance of a new band in the NIR region of the electromagnetic spectrum. The UV-vis-NIR spectrum of gold

nanoparticles synthesized after 2 h of reaction (curve 2 of Figure 3.1) reveals two SPR bands: one at lower wavelength at 540 nm and another at ca. 1108 nm in the NIR region of the electromagnetic spectrum [32]. The UV-vis-NIR spectra of gold nanoparticles synthesized after 3, 5 and 6 h of reactions (curves 3 to 5 respectively) show an increase in the intensity of SPR band at 540 and 1250 nm and a red shift of the band in the NIR region as compared to curve 2. The red shift in the NIR band reflects an increase in edge length of gold nanotriangles during the growth process [31-33]. Time dependent growth of the NIR band observed in the absorption spectra is a characteristic feature of either formation of aggregated nanoparticles [7a, 34] or the synthesis of anisotropic gold nanoparticles whose aspect ratio increase with time of reaction [12, 35].

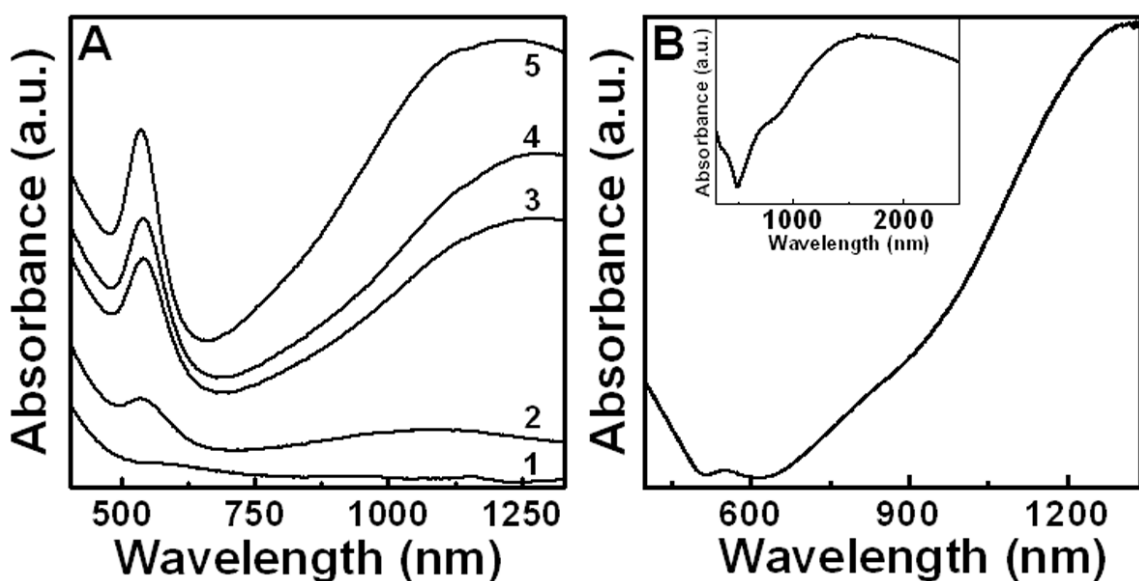


Figure 3.1: **A)** UV-vis-NIR spectra recorded as a function of time of reaction of lemongrass extract with 10^{-3} M HAuCl₄. Curves 1-5 correspond for spectra recorded after 1, 2, 3, 5 and 6 h of reaction respectively. **B)** UV-vis-NIR spectra were recorded from the purified gold nanotriangles after three times centrifugation of solution and in the form of film cast on the quartz substrate (inset of Figure B).

After complete saturation of the reaction, the NIR band does not show an increase in intensity even after a month in the reaction solution, which indicates no further growth of the gold nanotriangles. The TEM image (Figure 3.2) of gold nanoparticles synthesized using lemongrass extract shows a large percentage of gold nanotriangles and spherical nanoparticles with no aggregation of the gold nanoparticles, which have been discussed

below in the text. Thus, from these results, it can be stated that the large absorption in the NIR region of electromagnetic spectra is due to the presence of anisotropic gold nanoparticles like gold nanotriangles and hexagons in the reaction solution. The absorption band observed at 540 nm is due to the combined effect of dipole plasmon band of spherical particles and transverse component of SPR band (out of plane plasmon vibration) of the gold nanotriangles and hexagons while the absorption band observed in the NIR region is due to the longitudinal component of SPR band (in-plane plasmon vibration) [32a, b, d, 36]. Figure 3.1B represents the UV-vis-NIR spectrum of purified gold nanotriangles (after three times centrifugation), which shows high intensity longitudinal SPR band along with a significant loss in the transverse SPR band at 550 nm. The loss in the intensity of the transverse component clearly indicates removal of spherical particles from solution containing gold nanotriangles by the repeated centrifugation process. Interestingly, the in-plane quadrupole plasmon mode of SPR is also observed at ca. 815 nm for the purified gold nanotriangles (Figure 3.1B), which has been reported earlier by Mirkin's group [37]. The inset of Figure 3.1B shows the UV-vis-NIR spectrum of a purified gold nanotriangle film on a quartz substrate, prepared by drop coating and solvent evaporation of the gold nanotriangle solution onto the substrate. The UV-vis-NIR spectrum of gold nanotriangles film shows a shoulder at ca. 720 nm along with an intense longitudinal band at 1660 nm in the NIR region. The observed shoulder at 720 nm in the UV-vis-NIR spectrum for gold nanotriangle film is similar to the transverse absorption band at 550 nm of purified gold nanotriangles, measured in solution form. The observed large red shift of transverse band in spectrum may be due to change in the dielectric environment of nanotriangles during film formation on the quartz substrate [32a, 37]. The extremely large NIR absorption is a result of the in-plane plasmon vibrations or the longitudinal surface plasmon band of gold nanotriangles and hexagons.

3.2.3 Electron microscopy analysis of the gold nanotriangles:

The gold nanoparticles synthesized using lemongrass extract after 6 h of reaction were analyzed by transmission electron microscopy (TEM). The TEM image (Figure 3.2) shows a large population of triangular and hexagonal nanoparticles along with spherical nanoparticles. The edge-to-edge length and yield of nanotriangles is 0.05-2 μm and 45%

respectively. Many nanoprisms have regular edge sides with an angle of 120° (for hexagonal nanoparticles) or 60° (for triangles) between adjacent sides. The yield of gold nanotriangles formed by this method is higher than previous methods reported by other groups [16, 17]. The edges and tips of the gold nanotriangles are smooth and very sharp as observed in the TEM image (Figure 3.2A). Scanning electron microscopy (SEM) image (Figure 3.2B) also shows a large population of anisotropic nanoparticles like gold nanotriangles and nanohexagons. Some of the nanotriangles have truncated vertices, which were also observed previously for silver and gold nanotriangles synthesized using photochemical and thermal methods [16c,d, 17k].

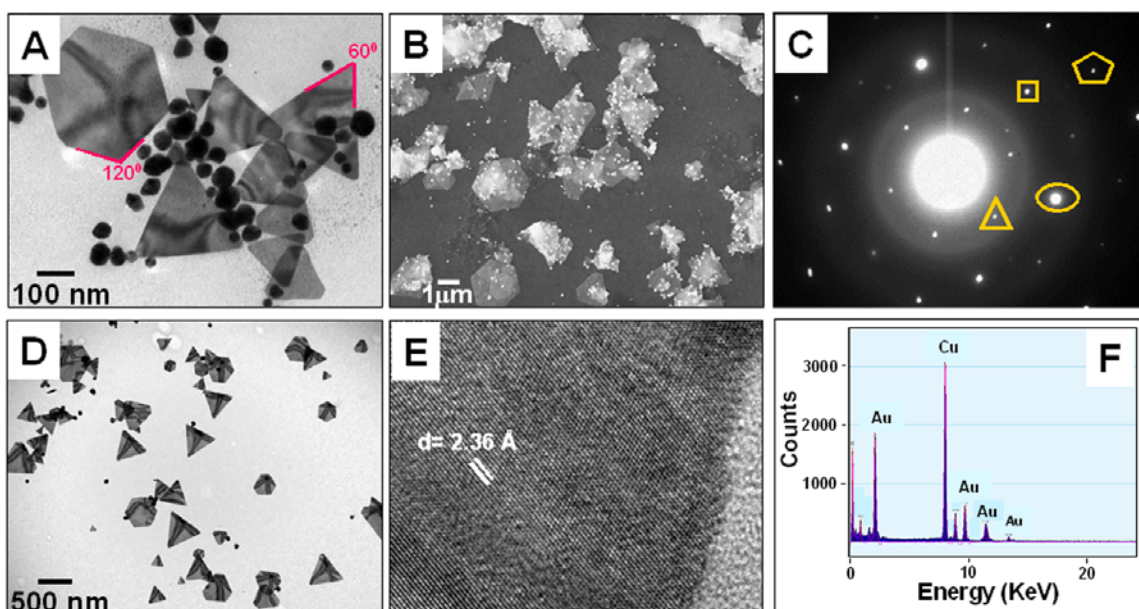


Figure 3.2: A) TEM image of triangular, hexagonal and spherical gold nanoparticles synthesized using lemongrass extract before centrifugation. B) SEM image of lemongrass reduced gold nanotriangles and spherical nanoparticles. C) Selected area electron diffraction (SAED) pattern of gold nanotriangles. Triangle, circular, square and pentagonal boxes in image represent $1/3\{422\}$, $\{220\}$, $\{311\}$ and $\{422\}$ fcc gold lattice planes. D) TEM image of purified gold nanotriangles after three times centrifugation at 1000 rpm. E) High resolution TEM (HRTEM) image of a gold nanotriangle. F) EDAX result for a single gold nanotriangle on copper grid.

Most of the gold nanotriangles in the TEM image show dark lines and bands i.e., fringes with different contrast within particles, which arise due to stresses in particles due to buckling or warping of atomic planes with respect to the electron beam in thin gold nanotriangles [36b, 38]. The contrast present in nanotriangles due to such phenomenon is called bending contours. Liz-Marzan's group has claimed that the origin of bending

contours might be simply due to stress in the crystalline lattice of nanotriangles, which can arise due to the presence of stacking faults in the crystal structures or due to the presence of hexagonal-like monolayer on nanoprism faces, which would slightly distort the (111) plane of the pure fcc cubic structure [39]. At close inspection of the nanotriangles in the TEM image, we can observe spherical nanoparticles below the nanotriangles that indicate the thin nature of triangular gold nanoparticles. Figure 3.2C shows the selected area electron diffraction (SAED) pattern of a single gold nanotriangle, which clearly indicates that it is single crystalline in nature. The hexagonal nature of diffraction spots in the SAED pattern shows that the nanotriangle is highly [111] oriented with top normal to electron beam. The hexagonal spots could be indexed on the basis of face centered cubic (fcc) structure of gold nanoparticles. The triangular, circular, square and pentagonal boxes made on SAED pattern correspond to the forbidden $1/3\{422\}$ and allowed $\{220\}$ $\{311\}$ and $\{422\}$ Bragg reflections respectively. The forbidden reflection in the electron diffraction pattern may be originated due to the presence of twin planes [16h, 40], or due to the presence of [111] directed stacking faults lying parallel to the (111) plane of the gold nanotriangles and extending across the particles [41]. Thus, it is reasonable that the top and bottom parts of the nanotriangles are bound by atomically flat (111) planes [36d]. The TEM image (Figure 3.2D) of gold nanotriangles purified by centrifuging the solution three times at the speed of 1000 rpm shows 98% population of gold nanotriangles along with hexagonal particles, which is consistent with the UV-vis-NIR spectrum of the purified gold nanotriangles (Figure 3.1B). The high resolution TEM (HRTEM) image taken from the flat part of a gold nanotriangle shows lattice spacing of 2.36 Å that corresponds to the (111) plane from the top surface of the gold nanotriangle (Figure 3.2E). Energy dispersive analysis of X-rays (EDAX) from the nanotriangles confirms the presence of only gold in as prepared triangular nanoparticles (Figure 3.2F). The strong signal of copper in the EDAX spectrum comes from the copper TEM grid.

3.2.4 Atomic Force microscopy (AFM) measurements:

Figure 3.3 shows contact mode AFM images of triangular and hexagonal gold nanoparticles with few spherical gold nanoparticles on the surface of nanoparticles. The edges and tips of nanoparticles are observed to be smooth and sharp as can be seen in the TEM analysis (Figure 3.2A). The line profile plots shown at the bottom of Figure 3.3A

and B demonstrate that nanotriangles and nanohexagons have thickness of ca. 15 and 25 nm respectively. The average thickness of gold nanotriangle after measurement of a large number of particles is found to be 18 nm. The edge-to-edge length of the triangular and hexagonal gold nanoparticles is found to be ca. 400 nm and 800 nm respectively.

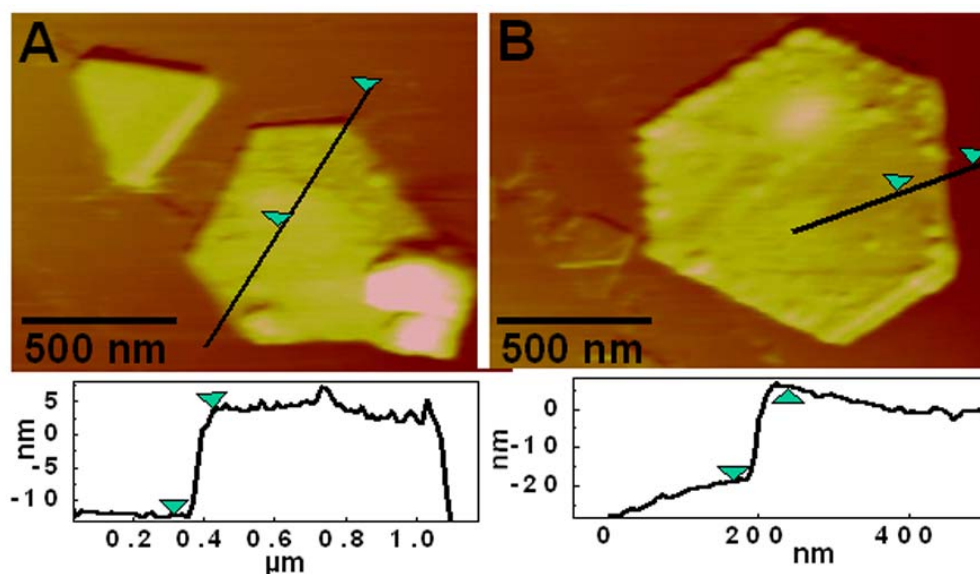


Figure 3.3: **A)** Atomic force microscopy (AFM) image of triangular and hexagonal gold nanoparticles. **B)** Higher magnification AFM image of a hexagonal nanoparticle. The line profile plots at bottom of figures A and B show that triangle and hexagon are of ca. 15 and 25 nm thickness respectively. AFM images were taken in height mode.

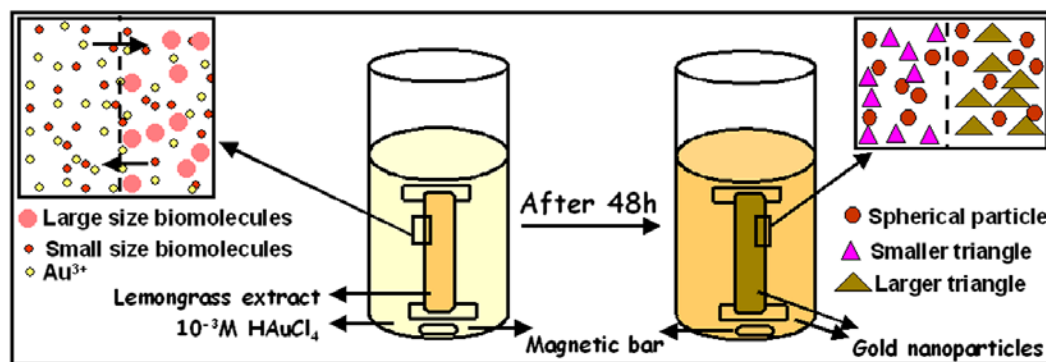
3.3 Size and shape controlled synthesis of gold nanoparticles:

Size and shape controlled synthesis of isotropic or anisotropic metal nanoparticles has been achieved by various methods and this control has allowed these structures to be used in variety of applications such as biodetection [7] and catalysis [42]. Photochemical and thermal methods have been reported to control the dimension of anisotropic nanoparticles through the judicious use of plasmon excitation but these methods are hazardous to the environment [16c,d, i]. Dialysis is one of the methods to control the size and shape and therefore to fine-tune the optical property of nanoparticles through an environmentally benign approach. Different cut-off dialysis bags are used for the controlled diffusion of biomolecules of lemongrass extract to external solution. Diffusions of molecules depend on the concentration gradient across the bag.

3.3.1 Synthesis of gold nanoparticles during dialysis of extract against HAuCl_4 solution:

3.3.1.1 Experimental details:

Before performing the experiments, different cut-off dialysis bags were boiled in Milli-Q water for 10 minutes followed by thorough washing with Milli-Q water to remove contamination from bags. 100 mL of lemongrass extract kept in different cut-off dialysis bags (3, 12.5 and 30 kDa respectively) were dialyzed against 250 mL of 10^{-3} M HAuCl_4 solutions. Scheme 3.1 depicts the dialysis of extract against HAuCl_4 solution and synthesis of gold nanoparticles both inside and outside the dialysis bag. UV-vis-NIR spectroscopy, TEM and FTIR measurements of the gold nanoparticles synthesized inside and outside the dialysis bags were carried out after 48 h dialysis of lemongrass extract in different dialysis bags.



Scheme 3.1: Schematic shows the dialysis of lemongrass extract against HAuCl_4 solution. Insets show diffusion of biomolecules through pores of bag and synthesis of smaller and larger nanotriangles inside and outside the bag respectively.

X-ray photoemission spectroscopy analysis of synthesized gold nanotriangles inside the 12.5 kDa bag, cast as a film on silicon wafer (111), was carried out to know the chemical state of nanoparticles. The charge on the gold nanoparticles synthesized inside different cut-off bags during dialysis of lemongrass extract was determined by gel electrophoresis. 40 mL of 1% ultra pure agarose (high melting agarose) was boiled in water for 10 minutes and the solution was poured in a closed rectangular chamber to form solid gel. The wells were formed by placing a Teflon comb in the gel during the solidification process. The synthesized gold nanoparticles from the different bags were

loaded in the wells and electrophoresis was done in phosphate buffer of pH 7.4 at a constant voltage of 60 volts for 1 h.

3.3.1.2 UV-vis-NIR spectroscopy analysis:

Curves 1-3 in Figure 3.4A shows UV-vis-NIR spectra of gold nanoparticles synthesized inside different dialysis bags (3, 12.5 and 30 kDa bags respectively) during dialysis of lemongrass extract against 10^{-3} M HAuCl_4 solutions. UV-vis-NIR spectra were recorded after 48 h dialysis of extract. On visible inspection, the colour of solution inside the bags turned dark ruby red from initial light brown with the time of reactions. Curves 1 and 2 correspond to gold nanoparticles synthesized inside 3 and 12.5 kDa dialysis bags respectively and show that transverse SPR band centered at 540 nm is accompanied with the longitudinal component as a weak hump at 760 nm.

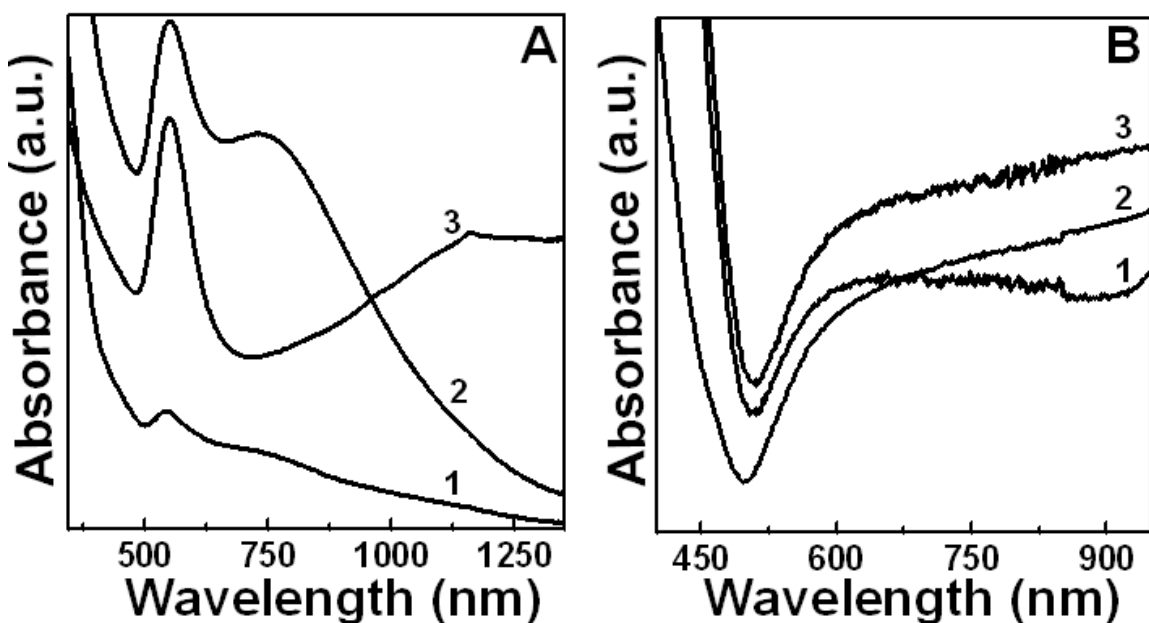


Figure 3.4: A) UV-vis-NIR spectra of the gold nanoparticles synthesized during dialysis of lemongrass extract against 10^{-3} M HAuCl_4 . Curves 1-3 correspond to nanoparticles synthesized inside 3, 12.5 and 30 kDa dialysis bags respectively. B) Curves 1-3 correspond to UV-vis-NIR spectra of gold nanoparticles synthesized outside 3, 12.5 and 30 kDa dialysis bags respectively.

A pronounced change is observed in the absorption spectrum of gold nanoparticles synthesized inside the 30 kDa bag. The UV-vis-NIR spectrum of gold nanoparticles synthesized inside the 30 kDa bag shows transverse SPR band at 540 nm along with the longitudinal SPR band, which appears to go beyond 1250 nm in the NIR

region (curve 3, Figure 3.4A). The intensity of transverse SPR component is higher than longitudinal SPR component in the optical absorption spectra in all cases (curves 1-3). UV-vis-NIR spectra of gold nanoparticles synthesized outside different dialysis bags are shown in Figure 3.4B. The UV-vis-NIR spectrum (curve 1, Figure 3.4B) of gold nanoparticle synthesized outside the 3 kDa bag shows a broad absorption spectrum ranging from 600 to 850 nm. While the absorption spectra of the gold nanoparticles synthesized outside 12.5 and 30 kDa bags appear to be continuously increasing from 600 nm and go beyond 900 nm (curves 2 and 3), which reveal the synthesis of anisotropic nanoparticle such as nanotriangle [17h, 31] as shown in the TEM image (Figure 3.7).

The mechanism for synthesis of gold nanotriangles could be possibly described using following models: (a) Slow rate of reduction of gold ions causes the formation of smaller spherical nanoparticles, which act as nuclei and grow to form flat nanotriangles due to aggregation and rearrangement of these smaller spherical nanoparticles [43]. (b) The initially formed spherical particles act as seed, around which nanotriangle growth occurs in the presence of the shape-directing agent. Such mechanism has also been reported by Mirkin's group during the study of growth of silver nanoprisms by a photo-irradiation method [16c, d]. (c) Fast rate of reduction causes the formation of small-sized gold nanoparticles (nuclei) by consumption of most of gold ions in the solution and hence the small percentage of remaining gold ions further reduce on the surface of nuclei to form smaller gold nanotriangles during the growth process. Therefore, the formation of gold nanotriangles is a kinetically driven process and is facilitated by the oriented growth of smaller nuclei in the (111) plane to form the nanotriangles [44]. (d) The defect in seeds causes oriented growth of the nanoparticles, which leads to the formation of anisotropic nanoparticles [40a]. (e) The "surface wrapping mechanism" in which growth of nanoplates are fast at initial stage of reaction [45]. Once wrapping layer is formed, it promotes the growth of another layer and consequently corrugated edges are formed in nanotriangles. Chen's group has also supported this mechanism for the synthesis of gold nanotriangles [36d].

The colour of the synthesized gold nanoparticle solution after 48 h of dialysis had a golden hue due to the partial reduction of external HAuCl_4 solution by outside diffused extract. It would be worthwhile to mention here that the synthesized gold nanoparticles

settled at the bottom of test tube in form of pellet after 10 h. The gold pellet can again be redispersed in water by ultrasonication. The difference in optical absorption properties of gold nanoparticle synthesized both inside and outside the different cut-off dialysis bags could be due to the variation in size, shape and yield of the gold nanoparticles.

3.3.1.3 TEM analysis:

3.3.1.3.a Inside of the dialysis bags:

TEM micrographs of the gold nanoparticles synthesized inside the different cut-off dialysis bags are shown in Figure 3.5. A large population of spherical nanoparticles along with small-sized gold nanotriangles (Figure 3.5A) are synthesized inside the 3 kDa dialysis bag, which is consistent with the UV-vis-NIR spectrum data (curve 1, Figure 3.4A). The histogram plot shows that the edge-to-edge length of triangular nanoparticles is 145 ± 8 nm (inset of Figure 3.5A). Figure 3.5B shows the high magnification TEM image of truncated gold nanotriangles and hexagonal nanoparticles synthesized inside the 3 kDa bag. It should be realized that biomolecules in the extract are much larger in size compared with Au^{3+} ions and thus the rate of diffusion will be higher for the ions towards inside the bag compared from biomolecules diffusion rate outwards (scheme 3.1). The concentrations of lemongrass extract inside the dialysis bags were in order of 3 kDa > 12.5 kDa > 30 kDa due to difference in the diffusion rate of biomolecules through pores of the dialysis bags and therefore reduction rate of diffused gold ions would also in the same order inside the dialysis bags. The higher concentration of lemongrass extract inside the 3 kDa bag causes fast reduction of diffused gold ions, which lead to the formation of a low yield of (28%) gold nanotriangles (Figure 3.6A). Figure 3.5C and D show the TEM images of a large population of gold nanotriangles and spherical nanoparticles synthesized inside the 12.5 kDa dialysis bag due to the slow rate of reduction of diffused Au^{3+} ions by remaining lemongrass extract present inside the bag. The edge-to-edge length of nanotriangles is 205 ± 20 nm (inset of Figure 3.5C), which is larger than nanotriangle formed inside the 3 kDa bag. The reduction rate of diffused Au^{3+} ions inside the 12.5 kDa dialysis bag was slow in comparison to the 3 kDa dialysis bag and hence formed a large population (54%) of the gold nanotriangles (Figure 3.6A), which is also strongly supported by TEM images (Figure 3.5C and D).

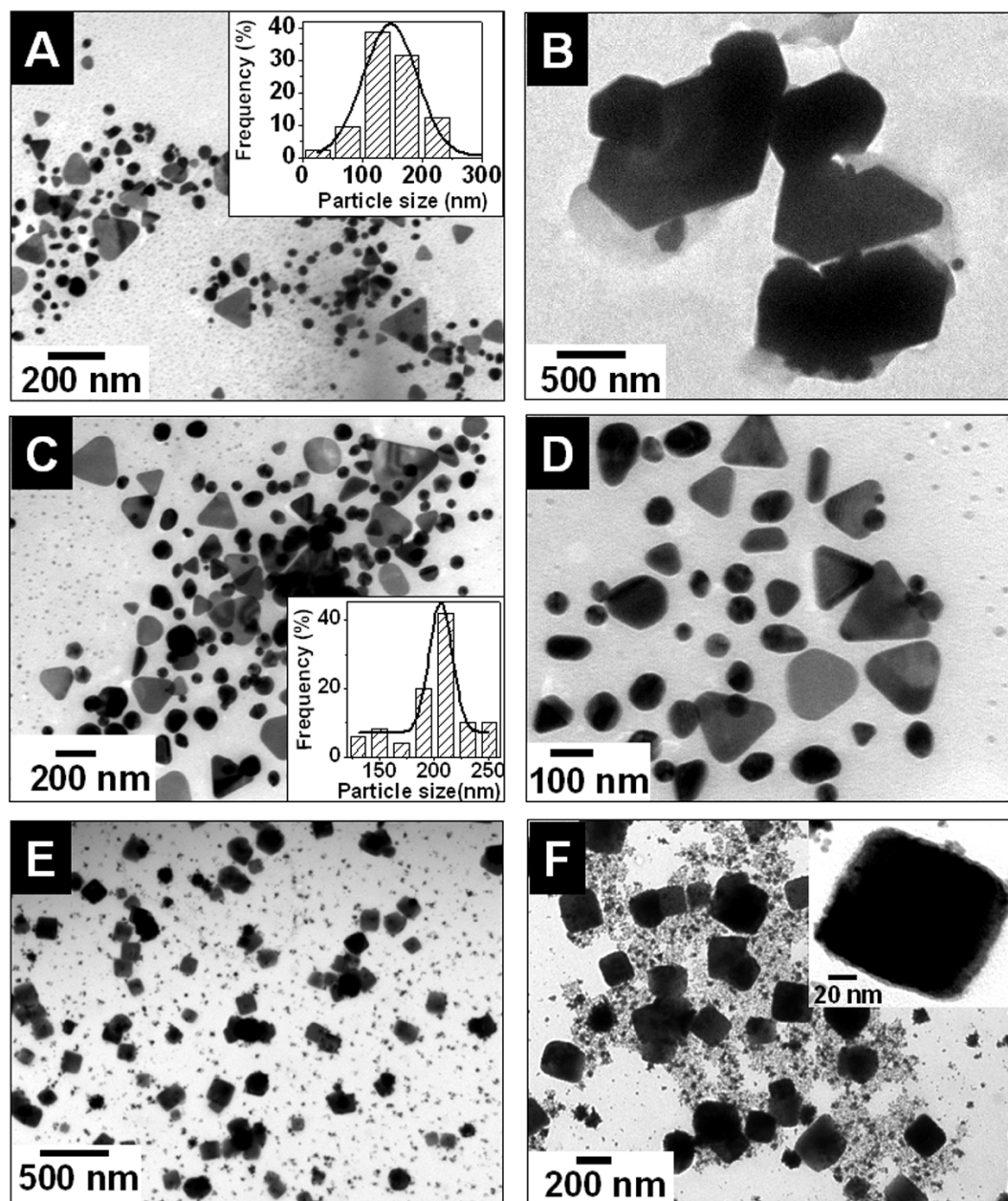


Figure 3.5: Representative TEM images of the gold nanoparticles synthesized inside **A, B**) 3 kDa, **C, D**) 12.5 kDa, **E, F**) 30 kDa dialysis bags. Insets of Figure A and C show histogram analysis of edge-to-edge length of gold nanotriangles synthesized inside 3 and 12.5 kDa dialysis bags respectively while the inset of Figure F shows a high magnification TEM image of a gold nanocube.

A drastic change is observed in the morphology of gold nanoparticles synthesized inside the 30 kDa dialysis bag. TEM images (Figure 3.5E and F) show a huge population of gold nanocubes along with smaller spherical gold nanoparticles, which are synthesized inside the 30 kDa bag. The rate of reduction of diffused Au^{3+} ions inside the 30 kDa bag

was slow due to lower concentration of remaining extract present inside the bag. The composition of extract present inside the 30 kDa bag is also different from 3 and 12.5 kDa extract and thus it promotes the synthesis of gold nanocubes.

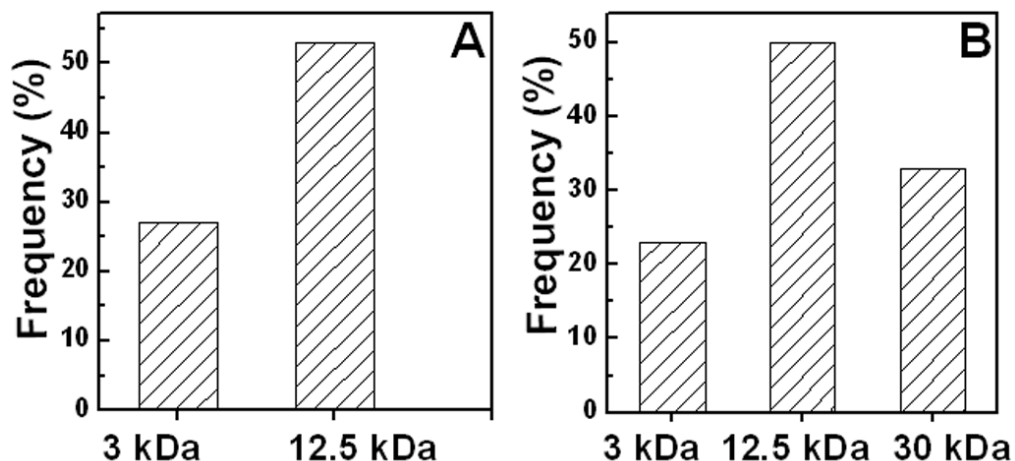


Figure 3.6: Histogram plot A and B show the population of gold nanotriangles formed inside and outside different dialysis bags respectively during the dialysis of extract against HAuCl_4 .

The inset of Figure 3.5F shows a high magnification TEM image of a gold nanocube, which reveals that edges of the gold cube are not very sharp and have less contrast compared with the central part. At close inspection of a high magnification TEM image of the gold nanocube, it can be seen that smaller spherical nanoparticles assemble to form gold nanocube at room temperature. The synthesis of gold nanocubes of various compositions using cumbersome methods has also been reported by many groups [10]. Thus, biomolecules of lemongrass extract, which have size bigger than 30 kDa, do not play any role in nanotriangle formation and form only gold nanocubes. Sastry and coworkers have demonstrated that one of column chromatography fraction of lemongrass extract (W1) is responsible for the synthesis of gold nanocubes [36b]. It should be noticed here that histogram plot (Figure 3.6A) does not show the population of nanotriangles for the 30 kDa bag because nanotriangles were not synthesized inside the bag and nanocubes were observed in the TEM analysis (Figure 3.5E and F).

3.3.1.3.b Outside of the dialysis bags:

The size and shape of gold nanoparticles synthesized outside the dialysis bags was analyzed by TEM measurements.

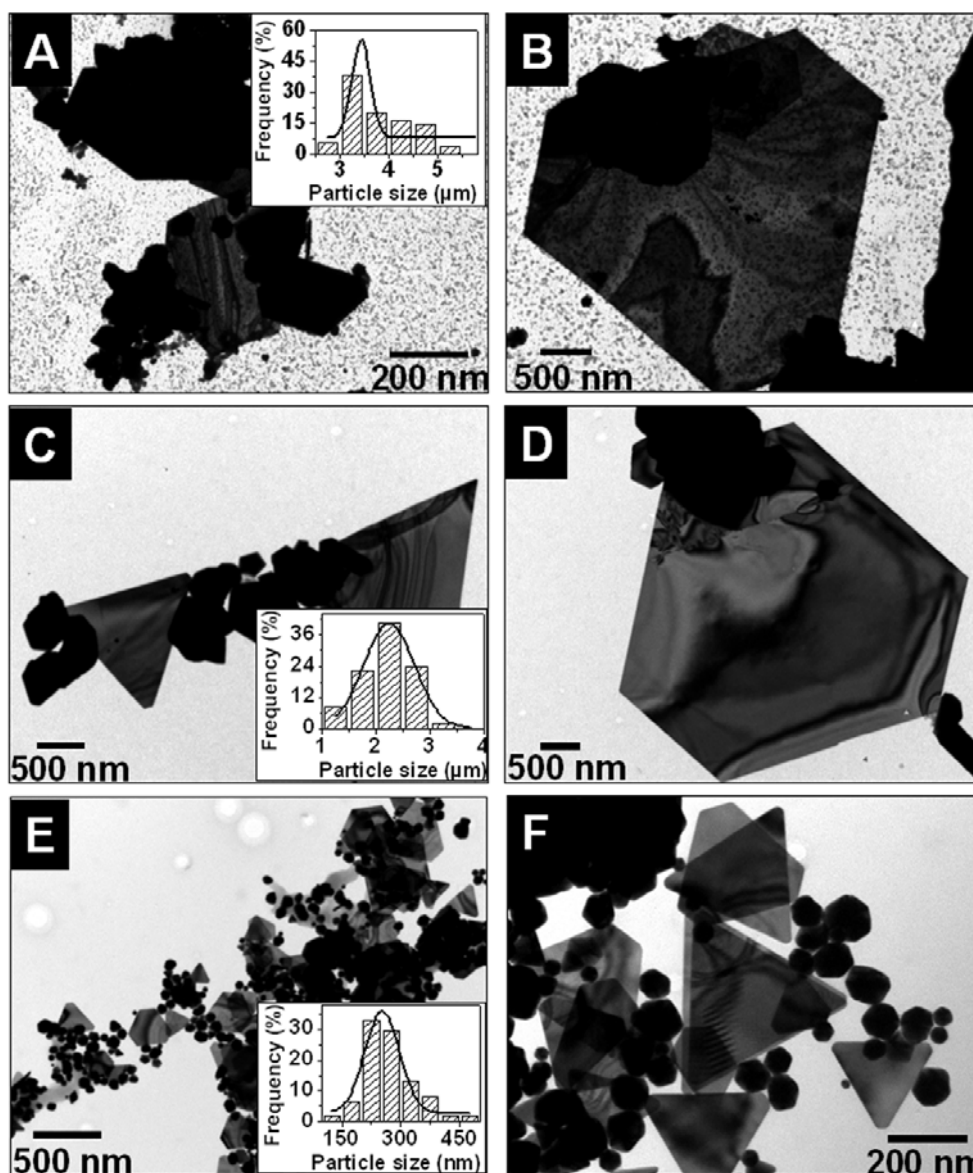


Figure 3.7: Representative TEM images of the gold nanoparticles synthesized outside of **A, B)** 3 kDa, **C, D)** 12.5 kDa and **E, F)** 30 kDa dialysis bags. Insets of Figure A, C and E show histogram analysis of edge-to-edge length of gold nanotriangles synthesized outside the different cut-off bags.

Triangular and hexagonal gold nanoparticles along with spherical nanoparticles are observed in the external solution of 3 kDa dialysis bag experiment (Figure 3.7A). The volume of lemongrass extract that diffuse towards outside bag through the pores of 3 kDa dialysis bag is too low in comparison to volume of external HAuCl_4 solution. Therefore the reduction rate of AuCl_4^- ion solution present outside the 3 kDa bag is very slow, which leads to the formation of large-sized nanotriangles. The obtained nanotriangles and

hexagons are thin and have edge-to-edge length of ca. 3.5 μm (inset of Figure 3.7A). A high magnification TEM image (Figure 3.7B) shows hexagonal gold particle of ca. 4 μm size, which is synthesized outside the 3 kDa dialysis bag. Furthermore, spherical nanoparticles below the thin hexagonal particle can also be seen in the TEM images (Figure 3.7A and B).

The TEM image of nanoparticles synthesized outside the 12.5 kDa dialysis bag shows large-sized gold nanotriangles with spherical nanoparticles (Figure 3.7C). The high magnification TEM image (Figure 3.7D) shows a broad bending contour across the entire truncated nanotriangle. A small concentration of biomolecules that have size below 12.5 kDa diffuse towards outside the bag through pores of the 12.5 kDa bag and reduce the external AuCl_4^- ion solution to form larger gold nanotriangles. The edge-to-edge length of triangular and truncated nanoparticles is $2.3 \pm 1 \mu\text{m}$ (inset of Figure 3.7C). The high concentration of diffused lemongrass extract (size below 30 kDa) outside the 30 kDa bag promote the synthesis of smaller nanotriangles of size $250 \pm 40 \text{ nm}$ (Figure 3.7E and inset of Figure 3.7E) due to the fast reduction of AuCl_4^- ion solution. The TEM image (Figure 3.7F) shows plane-edged gold nanotriangles along with smaller spherical nanoparticles. The population of gold nanotriangles formed outside 12.5 kDa bag is larger (49%) in comparison to gold nanotriangles formed outside 3 kDa (22%) and 30 kDa (34%) dialysis bags due to the different rate of reduction of external AuCl_4^- ion solutions (Figure 3.6B) by diffused lemongrass extracts.

It may be postulated that lemongrass extract has reducing and capping biomolecules. The capping molecules also act like shape-controlling molecule to execute particular shape of the nanoparticles. The reducing molecules in the extract reduce gold ions, while shape-controlling molecules bind on the certain facets of initially formed gold nanoparticles. The growth of facets strongly bound with capping agent is hindered in particular directions whereas the facets weakly attached to the capping molecules grow faster and facilitate the formation of gold nanotriangles [17h, 46]. Therefore, the capping molecules below the 30 kDa size preferentially adsorb on the $\{111\}$ facets of initially formed gold nanoparticles and suppress the growth in the $\langle 111 \rangle$ direction or advance the growth in the $\langle 110 \rangle$ direction to promote the synthesis of nanotriangle [40b, c]. It has been reported in literature that adsorption of chemical species on the surface has dramatic

effect on the surface energies. The {111} plane of gold nanoparticles possesses lowest surface energy and adsorption of suitable species, such as CTAB (cetyltrimethylammonium bromide) [16a, 47], citrate [14, 48] and peptides [49] on this plane further reduce its surface energy and stabilize nanoplates with the {111} plane as a basal plane. From this result, it can be rationalized that biomolecules of lemongrass extract below the 30 kDa size are responsible for the gold nanotriangle formation and act as reducing and capping (shape controlling) agent.

3.3.1.4 FTIR measurement:

FTIR measurements were carried out to identify the biomolecules in lemongrass extract bound on the surface of synthesized gold nanoparticles, which act as reducing and/or capping agent.

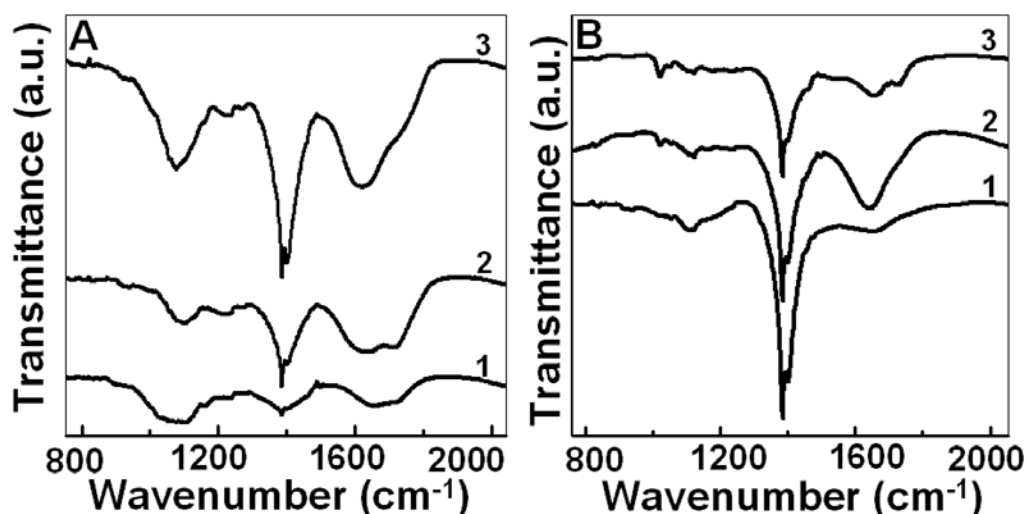


Figure 3.8: Curves 1-3 in Panel A and B correspond to FTIR spectra of the gold nanoparticles synthesized inside and outside 3, 12.5 and 30 kDa dialysis bags respectively.

Curves 1 and 2 of Figure 3.8A represent the FTIR spectra of gold nanoparticles synthesized inside the 3 and 12.5 kDa dialysis bags respectively and show peaks at 1720 (C=O stretching), 1638 (stretching mode of C=C group), 1385 (O-H bending) and 1098 cm^{-1} (from straight chain primary alcohols), which possibly indicate the presence of citral, sugar derivatives and other alcoholic compounds in lemongrass extract [50]. Curve 3 corresponds to gold nanoparticles synthesized inside 30 kDa dialysis bag (Figure 3.8A) and shows that entire peak is similar to curves 1 and 2 except 1720 cm^{-1} peak, which is

absent in the curve 3 indicating the absence of ketonic group on the surface of nanoparticles. The FTIR spectra of the gold nanoparticle synthesized outside the bags show peaks at 1385, 1645 cm^{-1} (curves 1-3, Figure 3.8B) for 3, 12.5 and 30 kDa dialysis bags and a low intensity peak at 1730 cm^{-1} for the nanoparticle synthesized outside the 30 kDa bag (curve 3, Figure 3.8B), which are similar to the FTIR spectra recorded for the nanoparticle synthesized inside the dialysis bags (Figure 3.8A). From the FTIR analysis, we could state that the sugar derivatives and citral molecules would be the main components of biomolecules, which act as reducing and capping agent for the nanotriangle formation.

3.3.1.5 XPS analysis:

A chemical analysis of the gold nanotriangles synthesized inside the 12.5 kDa dialysis bag was investigated by X-ray photoemission spectroscopy (XPS) measurement.

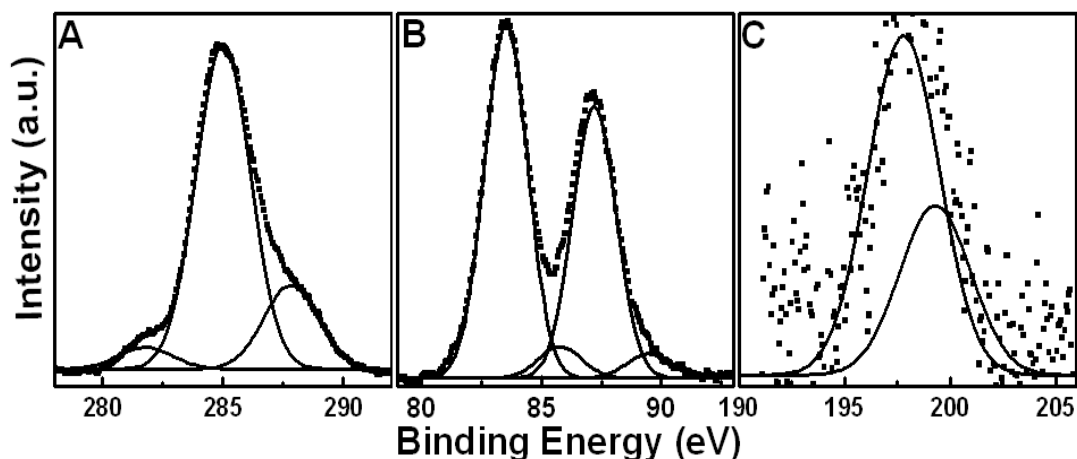


Figure 3.9: XPS spectra of A) C 1s, B) Au 4f and C) Cl 2p core level recorded from the gold nanotriangles synthesized inside 12.5 kDa dialysis bag.

Figure 3.9A, B and C show C 1s, Au 4f and Cl 2p core level spectra respectively for lemongrass reduced gold nanotriangles. C 1s core level spectrum could be decomposed into three chemically distinct components at binding energies of 281.85, 285 and 287.9 eV (Figure 3.9A). The low binding energy peak at 281.85 eV is attributed to aromatic carbon of biomolecules bound on the surface of gold nanotriangles. Apart from the binding energy peak for adventitious carbon at 285 eV, a high binding energy peak at 287.9 eV is attributed to electron emission from the carbon of carbonyl groups (aldehydes

and ketonic carbons) due to induction effect [51]. Induction effects are well known for high binding energy shift of carbon attached to the electron withdrawing groups such as ketonic and carbonyl functional groups [52]. The Au $4f_{7/2}$ core level could be split into two chemically distinct components at 83.5 and 85.8 eV binding energies that correspond to Au(0) and Au(I) oxidation state respectively (Figure 3.9B). The presence of a small amount of Au(I) on the surface of gold nanoparticles is responsible for the high binding energy peak and is caused to stabilize nanoparticles electrostatically against aggregation in solution [53]. It is concluded from these results that the carbonyl compounds present in lemongrass extract interact with Au(I) ions present on the surface of nascent gold nanoparticles and promote the formation of triangular gold nanoparticles. Cl 2p core level could be decomposed into two components centered at 197.8 eV and 199.3 eV for Cl $2p_{3/2}$ and Cl $2p_{1/2}$ respectively (Figure 3.9C). The poor signal of Cl 2p core level observed in a spectrum suggests that a small amount of chloride ions complexed with Au(I) are present on the surface of gold nanotriangles.

3.3.1.6 Identification of charge on the synthesized gold nanoparticles:

The gel electrophoresis is a unique technique to know the charge on the surface of gold nanoparticles.

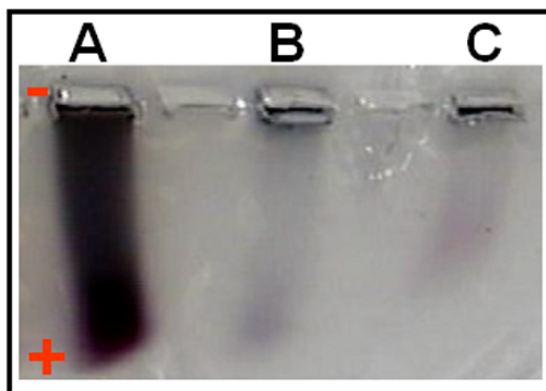


Figure 3.10: Agarose gel electrophoresis image of the gold nanoparticles synthesized inside different dialysis bags. Gold nanoparticles synthesized inside 3, 12.5 and 30 kDa dialysis bags were loaded on A, B and C wells respectively.

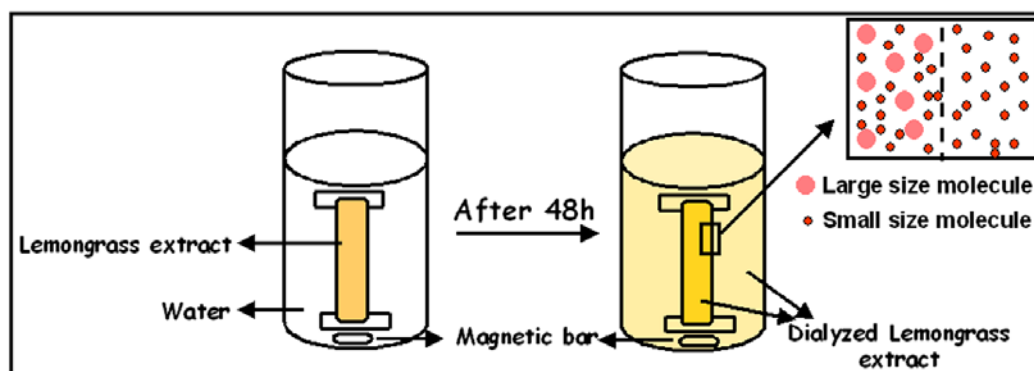
Gold nanoparticles synthesized inside the dialysis bags during dialysis of extract against HAuCl_4 solutions were loaded in the well of 1% agarose gel and were run at a 60 V across the gel for 1 h. The gold nanoparticles moved toward the positive electrode

indicating that they have negative charge due to the presence of biomolecules on the surface of gold nanoparticles (Figure 3.10). The gold nanoparticles synthesized inside the 3 kDa bag are smaller and therefore all nanoparticles enter in the well A and form a continuous smear in the gel. In the case of well B and C, most of the nanoparticles are wedged in the well and some of the smaller nanoparticles enter and form a band in the gel towards the positive electrode.

3.3.2 Synthesis of the gold nanoparticles using dialyzed extract:

3.3.2.1 Experimental Details:

Lemongrass extracts kept in different cut-off dialysis bags (3, 12.5 and 30 kDa) were dialyzed against 250 mL Milli-Q water in three jars for 48 h. Scheme 3.2 shows the dialysis of lemongrass extract against water. After dialysis, the extracts obtained from both inside and outside the dialysis bags were collected. 250 mL of outside dialyzed extract from the bags were rotovapped (Buchi Rotavapor R-205) at 50 °C to obtain 25 mL of concentrated extract solutions.



Scheme 3.2: Schematic shows dialysis of lemongrass extract against water for 48h. Inset shows diffusion of smaller biomolecules through pores of bag against concentration gradient.

1 mL of dialyzed lemongrass extract obtained from inside the dialysis bags was added separately to 10 mL of 10^{-3} M HAuCl_4 solutions as a reducing agent. 1 mL of the concentrated dialyzed extract of outside dialysis bags was also added to 10 mL of 10^{-3} M HAuCl_4 solutions (kept in three test tubes) to synthesize the gold nanoparticles. UV-vis-NIR spectra of all the solutions were recorded after allowing the reaction medium to stand for 48 h when the reduction of Au^{3+} ions in all these reaction solutions had reached

saturation. TEM and FTIR measurements were also carried out to investigate the formation of gold nanotriangles.

Notation used in the following sections:

Dialyzed extract obtained from inside 3 kDa cut-off dialysis bags: 3 in-D extract.

Dialyzed extract obtained from outside 3 kDa cut-off dialysis bags: 3 out-D extract.

Similar notations have also been used for the dialyzed extract obtained from 12.5 and 30 kDa cut-off dialysis bags.

3.3.2.2 UV-vis-NIR spectroscopy and TEM analysis of nanoparticles synthesized using dialyzed extract from the inside bags:

It is also important to investigate the morphology and yield of gold nanoparticles synthesized using dialyzed extract obtained from the different dialysis bags.

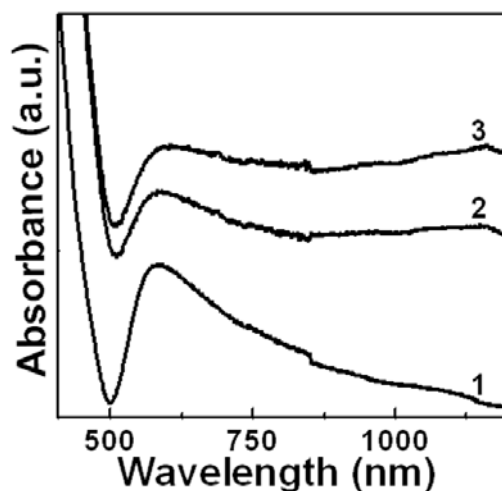


Figure 3.11: Curves 1-3 correspond for UV-vis-NIR spectra of the gold nanoparticles synthesized using 3, 12.5 and 30 in-D extract respectively.

The gold nanoparticles synthesized using dialyzed extracts obtained from the different dialysis bags were monitored by UV-vis-NIR spectroscopy (Figure 3.11). UV-vis-NIR spectra of the synthesized gold nanoparticles were recorded after 48 h of reactions when the reduction of AuCl_4^- ion solution had reached saturation. Curve 1 in Figure 3.11 shows the UV-vis-NIR spectrum of gold nanoparticles synthesized by reduction of AuCl_4^- ion solution using 3 in-D extract. Curve 1 demonstrates a broad

asymmetric absorption spectrum with surface plasmon (SP) band centered at 584 nm. However, the absorption spectra of gold nanoparticles synthesized using 12.5 in-D and 30 in-D extracts (curves 2 and 3 respectively, Figure 3.11) show two bands; one is transverse surface plasmon band centered at ca. 584 nm and another is longitudinal surface plasmon band, which appears to be red shifted beyond 1200 nm.

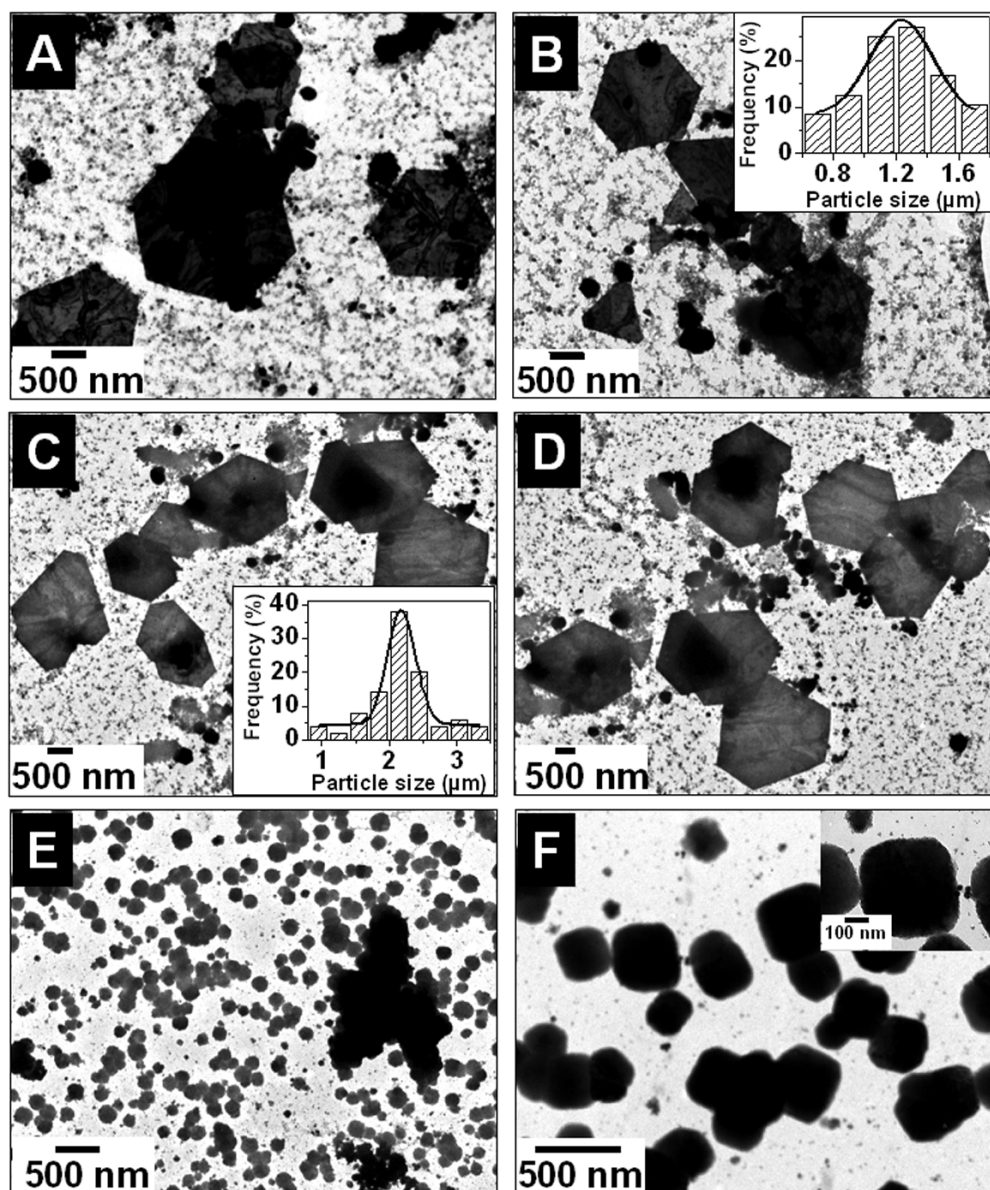


Figure 3.12: Representative TEM images of the gold nanoparticles synthesized using in-D extract obtained from 3 kDa (A, B) 12.5 kDa (C, D) and 30 kDa (E, F) dialysis bags. Insets of Figure B and C show histogram analysis of edge-to-edge length of triangles synthesized using 3 and 12.5 in-D extract respectively. Inset of Figure F shows a high magnification TEM image of gold nanocubes.

A large red shift in longitudinal band indicates the synthesis of triangular nanoparticles with increased edge-to-edge length, which is also confirmed by the TEM analysis. TEM images of gold nanoparticles synthesized using 3 in-D extract show that a large population of spherical and aggregated nanoparticles along with gold nanotriangles of size $1.25 \pm 0.4 \mu\text{m}$ are formed (Figure 3.12A, B and inset of Figure 3.12B). TEM images (Figure 3.12C and D) also show that gold nanotriangles along with spherical nanoparticles are synthesized using 12.5 in-D extract. The edge length of gold nanotriangles is $2.4 \pm 0.4 \mu\text{m}$ (inset of Figure 3.11C) and spherical particles below the thin triangles can easily be distinguished in the TEM image. The population of gold nanotriangles synthesized using 12.5 in-D extract is larger (45%) in comparison to gold nanotriangles formed using 3 in-D extract (30%) as shown in the histogram plot (Figure 3.13A). The gold nanoparticles synthesized using 3 and 12.5 in-D extract also show mostly truncated triangles with a large number of hexagonal particles.

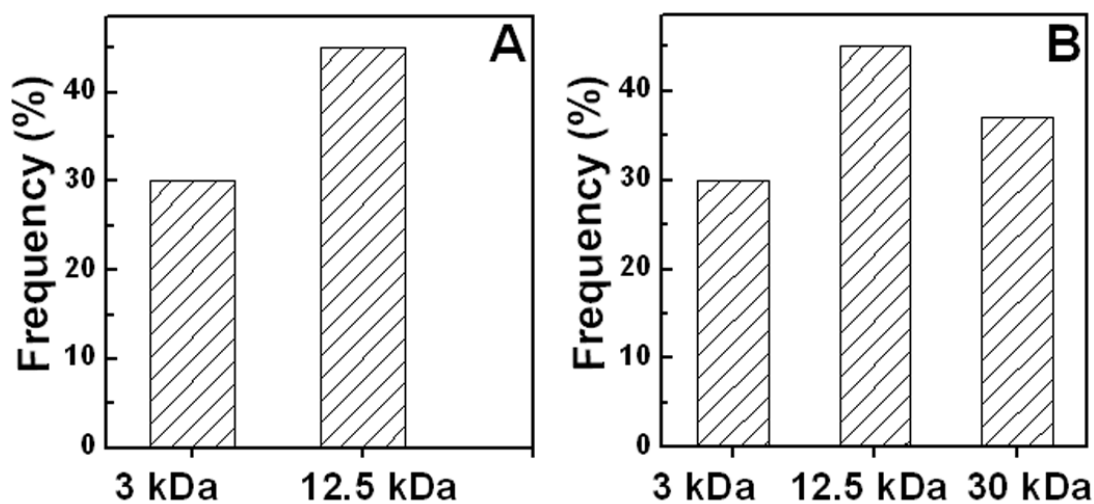


Figure 3.13: Histogram plot A and B show the population of gold nanotriangles synthesis using dialyzed extract obtained from inside and outside different cut-off dialysis bags respectively.

The concentrations of in-D extract obtained from the different dialysis bags were in order of 3 kDa > 12.5 kDa > 30 kDa bags and hence the reduction rate of AuCl_4^- ion solution was fast for the 3 in-D extract in comparison to the other dialyzed extract. Therefore, the population and edge-to-edge length of gold nanotriangles synthesized using 3 in-D extract was less as compared to the 12.5 in-D extract (Figure 3.12 B and C). On the other hand, the gold nanoparticles synthesized using 30 in-D extract have unusual

morphology and mostly gold nanocubes are observed in the TEM images (Figure 3.12E and F). It is observed that the gold nanocubes are made of assembly of smaller spherical gold nanoparticles, which has been described earlier. The inset of Figure 3.12F shows the high magnification TEM image of the gold nanocubes with no sharp edges and corners. These gold nanocubes are similar to the cubes that were obtained by the reduction of gold ions inside 30 kDa dialysis bag during dialysis of extract against HAuCl_4 solution (Figure 3.5E and F). It should be noticed here that the histogram plot does not show the population of gold nanotriangles in the case of nanoparticles synthesized using 30 in-D extract (Figure 3.13A).

3.3.2.3 UV-vis-NIR spectroscopy and TEM analysis of nanoparticles synthesized using dialyzed extract from outside bags:

Figure 3.14 shows UV-vis-NIR spectra of gold nanoparticles synthesized using concentrated out-D extract obtained from the different cut-off dialysis bags.

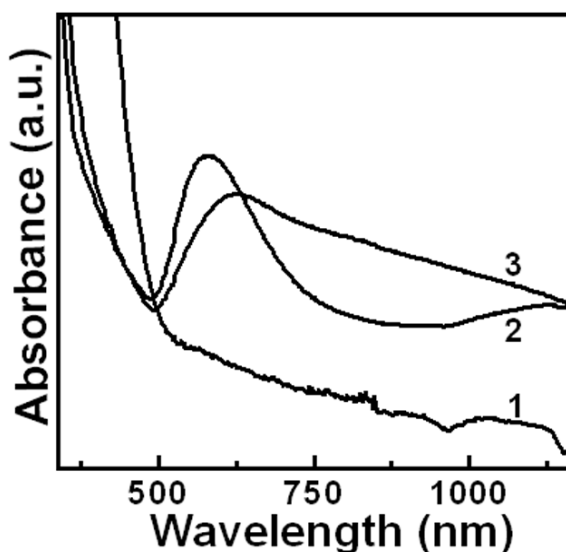


Figure 3.14: Curves 1-3 correspond for UV-vis-NIR spectra of the gold nanoparticles synthesized using 3, 12.5 and 30 out-D extract respectively.

The UV-vis-NIR spectrum of gold nanoparticles synthesized using concentrated 3 out-D extract shows a broad surface plasmon absorption band with a small hump at ca. 557 nm (curve 1, Figure 3.14). The absorption spectrum of the gold nanoparticles synthesized using concentrated 12.5 out-D extract (curve 2, Figure 3.14) shows the transverse surface plasmon band at 576 nm along with the longitudinal surface plasmon

band at ca. 1280 nm. The interesting change is observed in the optical property of gold nanoparticles synthesized using concentrated 30 out-D extract (curve 3, Figure 3.14).

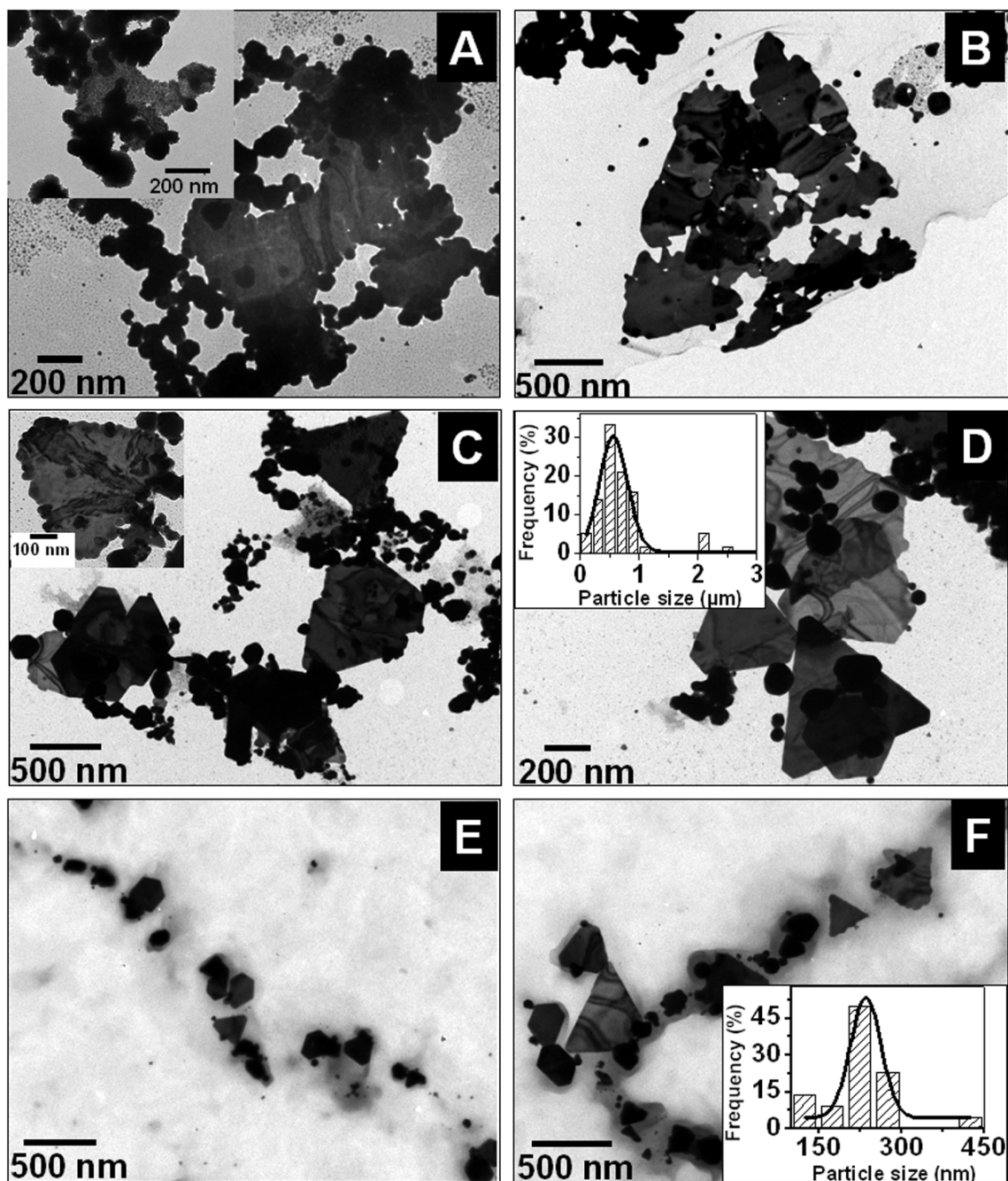


Figure 3.15: Representative TEM images of the gold nanoparticles synthesized using out-D extract obtained from 3 kDa (A, B), 12.5 kDa (C, D) and 30 kDa (E, F) cut-off bags. Insets of Figure A and C show higher magnification TEM image while the insets of D and F show the histogram analysis of edge-to-edge length of gold nanotriangles synthesized using 12.5 and 30 out-D extract respectively.

The UV-vis-NIR spectrum (curve 3, Figure 3.14) shows a very broad absorption band with SPR peak centered at 610 nm, which appears to be red shifted by 40 nm relative to the transverse SPR band of gold nanoparticles synthesized using 3 and 12.5 out-D extracts (curves 1 and 2 respectively, Figure 3.14). The red shift is due to aggregation of nanoparticles in the solution that can be seen in the TEM images (Figure 3.15E and F). The TEM images (Figure 3.15A and B) show that flat anisotropic nanoparticles, deformed nanotriangles and aggregated spherical nanoparticles are synthesized using concentrated 3 out-D extract. The concentrations of out-D extract obtained from the different cut-off dialysis bags were in the reversed order (3 kDa < 12.5 kDa < 30 kDa) to the concentrations of in-D extracts. It is highly likely that low concentration of 3 out-D extract is insufficient to reduce all gold ions present in the solution and thus a small population of deformed and plate like nanostructures are formed. The inset of Figure 3.15A shows the rudimentary stage of gold nanotriangle, wherein smaller spherical nanoparticles are assembled in the form of nanotriangles. It is believed that these nanotriangles are formed due to assembly and sintering of smaller spherical nanoparticles [36b]. The fluidity of spherical nanoparticles required to assemble and form triangular or hexagonal nanoparticles could be provided by ketonic functional groups of biomolecules present in lemongrass extract [36b]. Klabunde's group has also reported the assembly of monodisperse spherical nanoparticle into triangular and hexagonal superlattices in the solution [54]. Few reports are also available on oriented assembly of spherical nanoparticles into triangular nanoparticles [16a, 40c, 55].

TEM images (Figure 3.15C, D and inset of Figure 3.15D) show that spherical nanoparticles along with gold nanotriangles of size 600 ± 5 nm are synthesized using concentrated 12.5 out-D extract. The inset of Figure 3.15C shows the high magnification TEM image of gold nanotriangles with corrugated edges. The gold nanotriangles of small-sized (250 ± 30 nm) along with spherical nanoparticles are synthesized using concentrated 30 out-D extract (Figure 3.15E and F and inset of Figure 3.15F). The high concentration of 30 out-D extract in comparison to the other dialyzed extract caused rapid reduction of the gold ions to synthesize small-sized gold nanotriangles, when compared to the 3 and 12 out-D extract experiments (Figure 3.15 A-D). This result is similar to the TEM image of gold nanotriangles formed outside the 30 kDa dialysis bag during dialysis

of lemongrass extract against 10^{-3} M HAuCl_4 solution (Figure 3.7E and F). Therefore, the initially formed gold nanoparticles (nuclei) during synthesis and biomolecules of extract below 30 kDa play a major role in the formation of gold nanotriangles. The histogram plot shows that the population of gold nanotriangles synthesized using concentrated 12.5 out-D extract is 45% while those synthesized using concentrated 3 and 30 out-D extract are 30% and 42% respectively (Figure 3.13B) due to the different rate of reduction of AuCl_4^- ion solution.

3.3.2.4 FTIR analysis:

Figure 3.16 shows the FTIR spectra of gold nanoparticles synthesized using dialyzed lemongrass extract obtained from different dialysis bags.

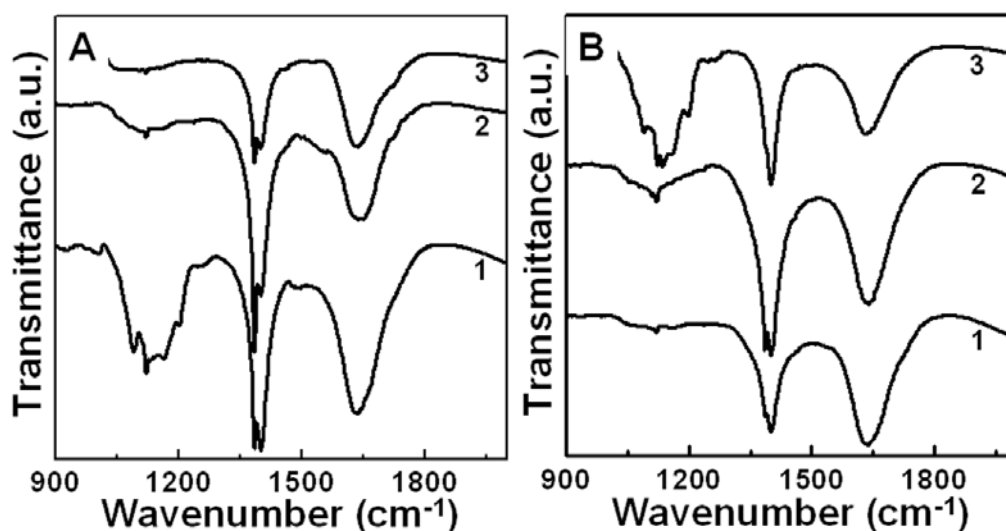


Figure 3.16: Curves 1-3 in Panel A and B correspond for FTIR spectra of the gold nanoparticles synthesized using 3, 12.5 and 30 in-D and out-D extract respectively.

FTIR spectra of gold nanoparticles synthesized using in-D extract obtained from the different dialysis bags show peaks at $1638, 1380 \text{ cm}^{-1}$ (curves 1-3, Figure 3.16A) and peaks at 1119 and 1090 cm^{-1} appeared only for the gold nanoparticles synthesized using 3 in-D extract (curve 1, Figure 3.16A). The gold nanoparticles synthesized using out-D extract from the different dialysis bags show the FTIR peaks (curves 1-3, Figure 3.16B) at the same positions as was seen for the nanoparticles formed by the in-D extract. Furthermore, the FTIR spectrum (curve 1, Figure 3.16A) of gold nanoparticles synthesized using 3 in-D extract is similar to the FTIR spectrum of gold nanoparticles

synthesized using 30 out-D extract (curve 3, Figure 3.16B), which indicates that the compositions of dialyzed extracts are almost same in both cases. The peaks from different spectra are assigned to the functional groups from citral, citronellal and other alcoholic compounds present in lemongrass extract which might act as reducing and shape directing agent for the gold nanotriangle formation.

3.4 Conclusion:

In conclusion, a green chemical approach for the synthesis of triangular and hexagonal gold nanoparticles using natural reducing and shape directing agents has been described. The yield and thickness of the gold nanotriangles are 45% and 18 nm respectively, which are better than other chemical and physical methods reported for the synthesis of triangular gold nanoparticles. Dialysis is used for the size selective separation of biomolecules of lemongrass extract through different cut-off (3, 12.5 and 30 kDa) bags. Biomolecules that have size below the pore size of dialysis bags diffuse from bags and reduce gold ions present outside the dialysis bags to form nanoparticles. Biomolecules of lemongrass extract, which have size below 30 kDa, act as reducing and capping agent to promote the synthesis of gold nanotriangles. Biomolecules selectively bind to the (111) lattice plane of initially formed smaller gold nanoparticles (nuclei) and inhibit the growth in the $\langle 111 \rangle$ direction and therefore advance the growth in the $\langle 110 \rangle$ direction to form gold nanotriangles [40b, c]. The variation in size and yield of gold nanoparticles and consequently change in the optical properties are observed for gold nanoparticles synthesized inside and outside different cut-off dialysis bags. Biomolecules of the extract larger than 30 kDa size are found to form a large percentage of the gold nanocubes at room temperature.

3.5 References:

- [1] a) Lovley, D. R.; Stolz, J. F.; Nord, G. L.; Phillips, E. J. P. *Nature* **1987**, *330*, 252. b) Philse, A. P.; Maas, D. *Langmuir*, **2002**, *18*, 9977.
- [2] a) Mann, S. *Nature* **1993**, *365*, 499. b) Oliver, S.; Kupermann, A.; Coombs, N.; Lough, A.; Ozin, G. A. *Nature* **1995**, *378*, 47.
- [3] Young, J. R.; Davis, S. A.; Bown, P. R.; Mann S. *Journal of Structural Biology* **1999**, *126*, 195.
- [4] (a) Link, S.; El-Sayed, M. A. *J. Phys. Chem. B* **1999**, *103*, 8410. (b) El-Sayed, M. A. *Acc. Chem. Res.* **2001**, *34*, 257.
- [5] Moreno-Manas, M.; Pleixats, R. *Acc. Chem. Res.* **2003**, *36*, 638.
- [6] Liu, C.; Zhang, Z. *J. Chem.Mater.* **2001**, *13*, 2092.
- [7] a) Mirkin, C. A.; Letsinger, R. L.; Mucic, R. C.; Storhoff, J. J. *Nature* **1996**, *382*, 607. b) Han, M., Gao, X., Su, J.Z. & Nie, S. *Nature Biotechnol.* **2001**, *19*, 631. c) Nam, J. M.; Thaxton, C. S.; Mirkin, C. A. *Science* **2003**, *301*, 1884. d) Taton, T. A.; Mirkin, C. A.; Letsinger, R. L. *Science* **2000**, *289*, 1757.
- [8] Nicewarner-Pena, S. R.; Freeman, R. G.; Reiss, B. D.; He, L.; Pena, D.J.; Walton, I. D.; Cromer, R.; Keating, C. D.; Natan, M. J. *Science* **2001**, *294*,137.
- [9] a) Liu, T-Y.; Hu, S-H.; Liu, T-Y.; Liu, D-M.; Chen, S-Y. *Langmuir* **2006**, *22*, 5974. b) Horcajada, P.; Serre, C.; Vallet-Regi, M.; Sebban, M.; Taulelle, F.; Ferey, G. *Angew. Chem. Int. Ed.* **2006**, *45*, 5974. c) Thomas, M.; Klibanov, A. M. *Proc. Natl. Acad. Sci. USA*, **2003**, *100*, 16. d) Xu, X.; Rosi, N. L.; Wang, Y.; Huo, F.; Mirkin, C. A. *J. Am. Chem. Soc.* **2006**, *128*, 9286. e) Sandhu, K. K.; McIntosh, C. M.; Simard, J. M.; Smith, S. W.; Rotello, V. M. *Biocojugate Chem.* **2002**, *13*, 3. f) Han, G.; You, C-C.; Kim, B-j.; Turingan, R. S.; Forbes, N. S.; Martin, C. T.; Rotello V. M. *Angew. Chem. Int. Ed.* **2006**, *45*, 3165.
- [10] a) Sun, Y.; Xia, Y. *Science* **2002**, *298*, 2176. b) Xiong, Y.; Chen, J.; Wiley, B.; Xia, Y.; Yin, Y.; Li, Z. Y. *Nano Lett.* **2005**, *5*, 1237. c) Yu, D.; Yam, V. W-W. *J. Am. Chem. Soc.* **2004**, *126*, 13200. d) Feng, J.; Zeng, H. C. *Chem. Mater.* **2003**, *15*, 2829. e) Gou, L.; Murphy, C. J. *Nano Lett.* **2003**, *3*, 231.
- [11] a) Hutchinson, T. O.; Liu, Y.-P.; Kiely, C.; Kiely, C. J.; Brust M. *Adv.Mater.* **2001**, *13*, 1800. b) Peng, X.; Manna, L.; Yang, W.; Wickham, J.; Scher, E.; Kadavanich,

- A.; Alivisatos A. P. *Nature* **2000**, *404*, 59. c) Busbee, B. D.; Obare, S. O.; Murphy, C. J.; *Adv. Mater.* **2003**, *15*, 414. d) Jana, N.; Gearheart, L.; Murphy, C. J. *Chem. Mater.* **2001**, *13*, 2313. e) Kou, X.; Zhang, S.; Tsung, C-K.; Yeung, M. H.; Shi, Q.; Stucky G. D.; Sun, L.; Wang, J.; Yan, C. *J. Phys. Chem. B* **2006**, *110*, 16377.
- [12] a) Hao, E.; Kelly, K. L.; Hupp, J. T.; Schatz, G. C. *J. Am. Chem. Soc.* **2002**, *124*, 15182. b) Puentes, V. F.; Zanchet, D.; Erdonmez, C. K.; Alivisatos, A. P. *J. Am. Chem. Soc.*; **2002**, *124*, 12874.
- [13] a) Manna, L.; Scher, E. C.; Alivisatos, A. P. *J. Am. Chem. Soc.* **2000**, *122*, 12700. b) Chen, S.; Wang, Z. L.; Ballato, J.; Foulger, S. H.; Carroll, D. L. *J. Am. Chem. Soc.* **2003**, *125*, 16186.
- [14] Sun, Y.; Mayers, B.; Xia, Y. *Nano.Lett.* **2003**, *3*, 675.
- [15] Huang, C.-C.; Yang, Z.; Chang, H.-T. *Langmuir* **2004**, *20*, 6089.
- [16] a) Chen, S.; Carroll, D. L. *Nano.Lett.* **2002**, *2*, 1003. b) Haes, A. J.; Zhao, J.; Zou, S.; Own, C. S.; Marks, L. D.; Schatz, G. C.; Van Duyne, R. P.; *J. Phys. Chem. B.* **2005**, *109*, 11158. c) Jin, R.; Cao, Y.; Mirkin, C. A.; Kelly, K. L.; Schatz, G. C.; Zheng, J. G. *Science* **2001**, *294*, 1901. d) Jin, R.; Cao, Y. C.; Hao, E.; Métraux, G. S.; Schatz, G. C.; Mirkin, C. A. *Nature* **2003**, *425*, 487. e) Callegari, A.; Tonti, D.; Chergui, M. *Nano Lett.* **2003**, *3*, 1565. f) Sun, Y.; Mayers, B.; Xia, Y. *Nano Lett.* **2003**, *3*, 675. g) Sun, Y.; Xia, Y. *Adv. Mater.* **2003**, *15*, 695. h) Chen, S.; Carroll, D. L. *J. Phys. Chem. B* **2004**, *108*, 5500. i) Métraux, G. S.; Mirkin C. A. *Adv. Mater.* **2005**, *17*, 412. j) Bastys, V.; Pastooriza-Santos, I.; Rodriguez-Gonzalez, B.; Vaisnoras, R.; Liz-Marzan, L. M. *Adv. Funct. Mat.* **2006**, *16*, 766.
- [17] a) Milligan, W. O.; Morriss. *J. Am. Chem. Soc.* **1964**, *86*, 3461. b) Chiang, Y. S.; Turkevich, J. *J. Colloid Sci* **1963**, *18*, 772. c) Malikova, N., Pastoriza-Santos, I., Schierhorn, M., Kotov, N.A. & Liz-Marzan, L.M. *Langmuir*, **2002**, *18*, 3694. d) Sarma, T. K.; Chattopadhyay, A.; *Langmuir* **2004**, *20*, 3520. e) Li, Z.; Liu, Z.; Zhang, J.; Han, B.; Du, J.; Gao, Y.; Jiang, T. *J. Phys. Chem. B* **2005**, *109*, 14445. f) Millstone, J. E.; Park, S.; Shuford, K. L.; Qin, L.; Schatz, G. C.; Mirkin, C. A. *J. Am. Chem. Soc.* **2005**, *127*, 5312. g) Kim, F.; Connor, S.; Song, H.; Kuykendall, T.; Yang, P. *Angew. Chem., Int. Ed. Engl.* **2004**, *43*, 3673-3677. h) Wang, L.; Chen, X.; Zhan, J.; Chai, Y.; Yang, C.; Xu, L.; Zhuang, W.; Jing, B. *J. Phys.*

- Chem. B* 2005, 109, 3189. i) Sun, X.; Dong, S.; Wang, E. *Angew. Chem., Int. Ed. Engl.* **2004**, 43, 6360. j) Sun, X.; Dong, S.; Wang, E. *Langmuir* **2005**, 21, 4710. k) Chu, H-C.; Kuo, C-H.; Huang, M. H. *Inorg. Chem.* **2006**, 45, 808.
- [18] a) Southam, G.; Beveridge, T. J. *Geochim. Cosmochim. Acta* **1996**, 60, 4369. b) Beveridge, T. J.; Murray, R. G. E. *J. Bacteriol.* **1980**, 141, 876. c) Fortin, D.; Beveridge, T. J. in *Biomineralization. From Biology to Biotechnology and Medical Applications* (Ed. E. Baeuerien), Wiley-VCH, Weinheim **2000**, 7.
- [19] a) Klaus, T.; Joerger, R.; Olsson, E.; Granqvist, C. G. *Proc. Nat. Acad. Sci.* **1999**, 96, 13611. b) Klaus-Joerger, T.; Joerger, R.; Olsson, E.; Granqvist, C. G. *Trends Biotech.* **2001**, 19, 15. c) Joerger, R.; Klaus, T.; Granqvist, C. G. *Adv. Mater.* **2000**, 12, 407.
- [20] a) Mukherjee, P.; Ahmad, A.; Mandal, D.; Senapati, S.; Sainkar, S. R.; Khan, M. I.; Ramani, R.; Parischa, R.; Ajaykumar, P. V.; Alam, M.; Sastry, M.; Kumar, R. *Angew. Chem. Int. Ed.* **2001**, 40, 3585. b) Mukherjee, P.; Senapati, S.; Mandal, D.; Ahmad, A.; Khan, M. I.; Kumar, R.; Sastry, M. *ChemBioChem* **2002**, 3, 461. c) Mukherjee, P.; Ahmad, A.; Mandal, D.; Senapati, S.; Sainkar, S. R.; Khan, M. I.; Parischa, R.; Ajayakumar, P. V.; Alam, M.; Kumar, R.; Sastry, M. *Nano Lett.* **2001**, 1, 515. d) Ahmad, A.; Mukherjee, P.; Senapati, S.; Mandal, D.; Khan, M. I.; Kumar, R.; Sastry, M. *Coll. Surf. B.* **2003**, 28, 313. e) Ahmad, A.; Mukherjee, P.; Mandal, D.; Senapati, S.; Khan, M. I.; Kumar, R.; Sastry, M. *J. Am. Chem. Soc.* **2002**, 124, 12108. f) Bharde, A.; Wani, A.; Shouche, Y.; Joy, P. A.; Prasad, B. L. V.; Sastry, M. *J. Am. Chem. Soc.* **2005**, 127, 9326. g) Bansal, V.; Poddar, P.; Ahmad, A.; Sastry, M. *J. Am. Chem. Soc.* **2006**, 128, 11958. h) Bansal, V.; Ahmad, A.; Sastry, M. *J. Am. Chem. Soc.* **2006**, 128, 14059. i) Bharde, A.; Rautaray, D.; Bansal, V.; Ahmad, A.; Sarkar, I.; Yusuf, S. M.; Sanyal, M.; Sastry, M. *Small*, **2006**, 2, 135.
- [21] Brown, S.; Sarikaya, M.; Johnson, E. *J. Mol. Biol.* **2000**, 299, 725.
- [22] Raveendran, P.; Fu, J.; Wallen, S. J. *J. Am. Chem. Soc.* **2003**, 125, 13940.
- [23] Shao, Y.; Jin, Y.; Dong, S. *Chem. Commun.* **2004**, 1104.
- [24] Ibano, D.; Yokota, Y.; Tominaga, T. *Chem. Lett.* **2003**, 32, 574.

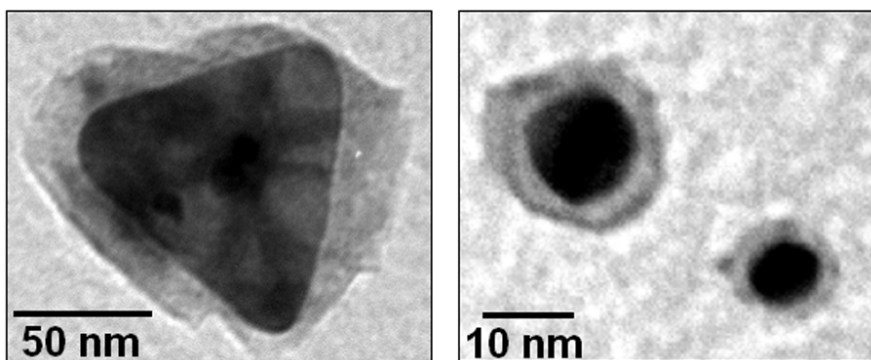
- [25] Gardea-Torresdey, J. L.; Peralta-Videa, J. R.; De La Rosa, G.; Parsons, J. G. *Coord. Chem. Rev.* **2005**, *249*, 1797.
- [26] Anderson, C. W. N.; Brooks, R. R.; Stewart, R. B.; Simcock, R. *Nature*, **1998**, *395*, 553.
- [27] Gardea-Torresdey, J. L.; Parsons, J. G.; Gomez, E.; Peralta-Videa, J.; Troiani, H. E.; Santiago, P.; Jose-Yacaman, M., *Nano Lett.* **2002**, *2*, 397.
- [28] Gardea-Torresdey, J. L.; Gomez, E.; Peralta-Videa, J. R.; Parsons, J. G.; Troiani, H.; Jose-Yacaman, M. *Langmuir* **2003**, *19*, 1357.
- [29] a) Armendariz, V.; Herrera I.; Peralta-Videa, J. R., Jose-Yacaman, M.; Troiani, H.; Santiago, P.; Gardea-Torresdey, J. L. *J. Nanopart. Res.* **2004**, *6*, 377. b) Armendariz, V.; Gardea-Torresdey, J. L.; Jose-Yacaman, M.; Gonzalez, J.; Herrera, I.; Parsons, J. G. *Waste Research Technology Proceeding*, **2002**. c) Shankar, S. S.; Ahmad, A.; Pasricha, R.; Sastry, M. *J. Mater. Chem.* **2003**, *13*, 1822. d) Shankar, S.S.; Ahmad, A.; Sastry, M. *Biotechnol. Prog.*, **2003**, *19*, 1627. e) Shankar, S. S.; Rai, A.; Ahmad, A.; Sastry, M. *Applied Nanoscience* **2004**, *1*, 69. f) Shankar, S. S.; Rai, A.; Ahmad, A.; Sastry, M. *J. Colloid Interface Sci.*, **2004**, *275*, 496.
- [30] a) Loo, C.; Lin, A.; Hirsch, L.; Lee, M. H.; Barton, J.; Halas, N.; West, J.; Drezek, R. *Technology in Cancer Research and Treatment* **2004**, *3*, 33. b) Hirsch, L. R.; Stafford, R. J.; Bankson, J. A.; Sershen, S. R.; Rivera, B.; Price, R. E.; Hazle, J. D.; Halas, N. J.; West, J. L. *Proc. Natl. Acad. Sci. USA*, **2003**, *100*, 13549. c) Nanospectra biosciences, Inc. Huston Texas, www.nanospectra.com.
- [31] Shankar, S. S.; Rai, A.; Ahmad, A.; Sastry, M. *Chem. Mater.* **2005**, *17*, 566.
- [32] a) Mulvaney, P. *Langmuir* **1996**, *12*, 788. b) Linl, S.; El-Sayed, M. *Annu. Rev. Phys. Chem.* **2003**, *54*, 331. c) Sherry, L. J.; Jin, R.; Mirkin, C. A.; Schatz, G. C.; Van Duyne, R. P. *Nano Lett.* **2006**, *6*, 2060. d) Liz-Marzan, L. M. *Langmuir* **2006**, *22*, 32. e) Henglein, A. *J. Phys. Chem. B.* **1993**, *97*, 5457.
- [33] Millstone, J. E.; Métraux, G. S.; Mirkin C. A. *Adv. Func. Mater.* **2006**, *16*, 1209.
- [34] a) Storhoff, J. J.; Lazaides, A. A.; Mucic, R. C.; Mirkin, C. A.; Letsinger, R. L.; Schatz, G. C. *J. Am. Chem. Soc.* **2000**, *122*, 4640. b) Turkevich, J.; Garton, G.; Stevenson P. C. *J. Colloid Interface Sci. Suppl.* **1954**, *9*, 26. c) Mangeney, C.;

- Ferrage, F.; Aujard, I.; Artzner, V. -M.; Jullien, L.; Ouari, O.; Rejai, E. D.; Laschewsky, A.; Vikholm, I.; Sadowski, J. W. *J. Am. Chem. Soc.* **2002**, *124*, 5811.
- [35] a) Landes, C. F.; Link, S.; Mohamed, M. B.; Nikoobakht, B.; El-Sayed, M. A. *Pure Appl. Chem.* **2002**, *74*, 1675. f) Valden, M.; Lai, X.; Goodman, W. *Science* **1998**, *281*, 1647. b) Burda, C.; Chen, X.; Narayanan, R.; El-Sayed, M. A. *Chem. Rev.* **2005**, *105*, 1025.
- [36] a) Kelly, K. L.; Coronado, E.; Zhao, L. L.; Schatz, G. C. *J. Phys. Chem. B* **2003**, *107*, 668-677. b) Shankar, S. S.; Rai, A.; Ankamwar, B.; Singh, A.; Ahmad, A.; Sastry, M. *Nat. Mater.* **2004**, *3*, 482. c) Sosa, I. O.; Noguez, C.; Barrera, R. G. *J. Phys. Chem. B* **2003**, *107*, 6269. d) Liu, B.; Xie, J.; Lee, J. Y.; Ting, Y. P.; Chen, J. P. *J. Phys. Chem. B* **2005**, *109*, 15256.
- [37] a) Ung, T.; Liz-Marza'n, L. M.; Mulvaney, P. *Colloid Sci. A.* **2002**, *202*, 109. b) Kreibig, U.; Vollmer, M. *Optical Properties of Metal Clusters*; Springer Series in Material Science, 25; Springer-Verlag: Berlin, 1995. c) Seker, F.; Malenfant, P. R. L.; Larsen, M.; Alizadeh, A.; Conway, K.; Kulkarni, A.; Goddard, G.; Garaas, R. *Adv. Mater.* **2005**, *17*, 1941.
- [38] Ding, Y.; Wang, Z. L. *J. Phys. Chem. B* **2004**, *108*, 12280.
- [39] Rodriguez-Gonzalez, B.; Pastoriza-Santos, I.; Liz-Marzan, L. M. *J. Phys. Chem. B.* **2006**, *110*, 11796.
- [40] a) Kirkland, A. I.; Edwards, P. P.; Jefferson, D. A.; Duff, D. G. *Annu. Rep. Prog. Chem. Sect. C* **1990**, *87*, 247. b) Lofton, C.; Sigmund, W. *Adv. Funct. Mater.* **2005**, *15*, 1197. c) Li, C.; Cai, W.; Li, Y.; Hu, J.; Liu, P. *J. Phys. Chem. B* **2006**, *110*, 1546. d) Elechiguerra, J. L.; Reyes-Gasga, J.; Yacaman, M. J. *J. Mater. Chem.* **2006**, *16*, 3906.
- [41] Germain, V.; Li, J.; Ingert, D.; Wang, Z. L.; Pileni, M. P. *J. Phys. Chem. B* **2003**, *107*, 8717.
- [42] a) Jana, N. R.; Sau, T. K.; Pal, T. *J. Phys. Chem. B* **1999**, *103*, 115. b) Jana, N. R.; Pal, T. *Langmuir* **1999**, *15*, 3458.
- [43] a) Mullin, J. W. *Crystallization*, Butterworth-Heinemann, Woburn, MA, 1997. b) Turkevich, J.; Stevenson, P. C.; Hillier, J. *J. Phys. Chem.* **1953**, *57*, 670. c) Hu, J. Q.; Chen, Q.; Xie, Z. X.; Han, G. B.; Wang, R. H.; Ren, B.; Zhang, Y.; Yang, Z. L.;

- Tian, Z. Q. *Adv. Funct. Mater.* **2004**, *14*, 183. d) Wiley, B.; Sun, Y.; Xia, Y.; *Langmuir*, **2005**, *21*, 8077. e) Chen, J.; Herricks, T.; Geissler, M.; Xia, Y.; *J. Am. Chem. Soc.* **2004**, *126*, 10854. f) Watzky, M. A.; Finke, R. G. *J. Am. Chem. Soc.*, **1997**, *119*, 10382. g) Murray, C. B.; Norris, D. J.; Bawendi, M. G. *J. Am. Chem. Soc.* **1993**, *115*, 8706. h) Reiss, H. *J. Chem. Phys.* **1951**, *19*, 482. i) Sato, T.; Ruch, R. *Stabilization of Colloidal Dispersions by Polymer Absorption*; Marcel Dekker: New York, 1980; pp 46-51. j) Xia, Y.; Yang, P.; Sun, Y.; Wu, Y.; Mayers, B.; Gates, B.; Yin, Y.; Kim, F.; Yan, H. *Adv. Mater.* **2003**, *15*, 353.
- [44] a) Chiang, Y.-S.; Turkevich, J. *J. Colloid Sci.* **1963**, *18*, 772. b) Engelbrecht, J.; Synman, H. *Gold Bull.* **1983**, *16*, 66. c) Rai, A.; Singh, A.; Ahmad, A.; Sastry, M. *Langmuir* **2006**, *22*, 736.
- [45] Feng, J.; Zeng, H. C. *Chem. Mater.* **2003**, *15*, 2829.
- [46] a) Filankembo, A.; Giorgio, S.; Lisiecki, I.; Pileni, M. P. *J. Phys. Chem. B* **2003**, *107*, 7492. b) Pileni, M. P. *Nat. Mater.* **2003**, *2*, 145.
- [47] Chen, S.; Fan, Z.; Carroll, D. L. *J. Phys. Chem. B* **2002**, *106*, 10777.
- [48] Maillard, M.; Huang, P.; Brus, L. *Nano Lett.* **2003**, *3*, 1611.
- [49] Naik, R. R.; Stringer, S. J.; Argarwal, G.; Jones, S. E.; Stone, M. O. *Nat. Mater.* **2002**, *1*, 169.
- [50] Ciardelli, G.; Chiono, V.; Vozzi, G.; Pracella, M.; Ahluwalia, A.; Barbani, N.; Cristallini, C.; Giusti, P. *Biomacromolecules* **2005**, *6*, 1961.
- [51] Miyama, T.; Yonezawa, Y. *Langmuir* **2004**, *20*, 5918.
- [52] Sastry, M.; Ganguly, P. *J. Phys. Chem. A.* **1998**, *102*, 697.
- [53] Liu, Y. C.; Chuang, T. C. *J. Phys. Chem. B.* **2003**, *107*, 12383.
- [54] a) Stoeva, S.I.; Prasad, B.L.V.; Uma, S.; Stoimenov, P.K.; Zaikovski, V.; Sorensen, C.M.; Klabunde, K.J. *J. Phys. Chem. B* **2003**, *107*, 7441. b) Smetana, A. B.; Klabunde, K. J.; Sorensen C. M. *J. Colloid Interface Sci.* **2005**, *284*, 521.
- [55] a) Deivaraj, T.C.; Lala, N. L.; Lee J. Y. *J. Colloid Interface Sci.* **2005**, *289*, 402. b) Tsuji, T.; Higuchi, T.; Tsuji, M. *Chem. Lett.* **2005**, *34*, 476.

Chapter IV

Synthesis of Triangular Gold-Silver and Spherical Gold-Titania Core-Shell Nanoparticles



In this chapter, we discuss the synthesis of anisotropic Au core-Ag shell nanoparticles using ascorbic acid as a reducing agent under alkaline conditions. The silver ions bind to the surface of negatively charged gold nanotriangles through electrostatic interaction. Ascorbic acid has different reduction ability towards silver ions under varying pH conditions. The bound silver ions on the surface of nanotriangles are reduced by ascorbic acid under alkaline conditions and show a gradual blue shift in the surface plasmon resonance band in the UV-vis-NIR spectra. The thickness of the silver shell around gold nanotriangle is ca. 5 nm that is validated by the AFM and TEM measurements. Biological synthesis of spherical gold-titania core-shell nanoparticles is also described in the chapter. A hydrolyzing enzyme is isolated and purified from the plant pathogenic fungus *Fusarium Oxysporum*. It is cationic in nature and has two protein components of 21 and 24 KDa molecular weight. The hydrolyzing enzyme is capped on the surface of aspartic acid modified gold nanoparticles and after challenging with K_2TiF_6 solution, leads to the formation of spherical gold-titania core-shell nanoparticles. The synthesized titania shells on the surface of gold nanoparticles show brookite and rutile polymorphs of titania.

Part of the work presented in this chapter has been published:

- 1) Rai, A.; Chaudhary, M.; Ahmad, A.; Bhargava, S.; Sastry, M. *Mater. Res. Bull.* **2006**, accepted.

4.1 Introduction:

Bimetallic nanoparticles either in the form of core-shell or alloy structures are being investigated in many fields of science and technology. Core-shell nanoparticles, in particular, have been the subject of extensive research due to their potential applications in many areas such as optoelectronic, catalysis, magnetic and optical devices [1-7]. Various groups have demonstrated that the properties such as surface plasmon resonance (SPR) [8] and Surface Enhanced Raman Scattering (SERS) associated with gold and silver nanoparticles [9] can be tailored by synthesizing these nanoparticles in the core-shell configuration. The deposition of one metal on the preformed monometallic nanoparticle surface of another metal appears to be very effective and is desirable from the application point of view. Bimetallic nanoparticles from the metal salts can be synthesized by two recipes: first is co-reduction of the metal salts to form alloy nanoparticles and second is successive reduction that leads to the formation of core-shell nanostructures. It is postulated that unique physiochemical and catalytic properties of core-shell nanoparticles are improved over their single component counterparts, which are result from the combination of two different metals and their fine structures [10]. These properties strongly depend upon the size, shape and composition of nanoparticles, so extensive research has been carried out on the size, shape and compositions controlled synthesis of core-shell nanoparticles. Various combinations of the core-shell nanoparticles have been fabricated including metal/metal [1], metal/semiconductor [2], semiconductor/semiconductor [3], metal/oxide [4], oxide/metal [5], metal/carbon [6] and metal/magnetic materials [7].

In one report, Sastry and coworkers have shown the phase pure synthesis of spherical Au core-Ag shell nanoparticles using Keggin ions as a reducing agent while in another report, tyrosine was used as a reducing agent under alkaline condition to synthesize Au core-Ag shell nanoparticles [1]. Except for the bulk efforts towards synthesis of spherical core-shell nanoparticles [1], only few attempts have been made towards anisotropic core-shell nanoparticle synthesis, for example, triangular [11], rod [1d, 12], dumbbell [13] and rattle [14] shaped nanoparticle using various chemicals methods. Recently, the synthesis of anisotropic core-shell nanoparticles has attracted immense attention due to significant local field enhancement (lightning rod effect) [15]

and enhanced SERS activity over individual metal nanoparticles and therefore, efforts have been made towards the synthesis of various shape of anisotropic nanoparticles [8-11]. Mirkin's group has demonstrated the synthesis of triangular nanoframe made of gold and silver [16] as well as triangular and corrugated Ag core-Au shell nanoparticles using seed mediated approach [11b].

Except for the synthesis of bimetallic core-shell nanoparticles, coating of inorganic oxides on metals nanoparticles has also evinced keen interest in nanoscience due to numerous applications in catalysis [17], photocatalysis [18], organic waste removal from polluted water [19], biodetection [20] and development of photochromic materials [21]. In the case of oxide nanoparticles, silica is widely used for coating of metals [22], semiconductors [23] and magnetic nanoparticles [24]. Titania is another oxide material, which has strong impact on the industry due to catalytic and photocatalytic property [25]. Several methods such as doping [26], reduction of particle size to nanoscale and synthesis of core-shell configuration [27] are available in the literature for the enhancement of catalytic activity of titania nanoparticles. Kamat's group has shown the photocatalytic activity and surface plasmon modulation of Ag core-TiO₂ shell nanoparticles under UV light [27]. However, unsupported high surface area form of titania is unstable at high temperature for catalytic purpose and therefore many methods have been employed for its coating on the surface of metal [27,28], silica and alumina nanoparticles [29]. Liz Marzan's group has shown a one pot synthesis of Ag core-TiO₂ shell by simultaneous reduction of silver ions and condensation of titanium butoxide [28a]. Caruso's group has also shown the synthesis of Au-TiO₂ core-shell nanoparticles by polyelectrolytes complexation with titania precursor [28b]. Recently, Ag core-TiO₂ shell nanowires with smooth and bristled surfaces were synthesized without using a template [30].

This chapter describes an elegant method for the synthesis of anisotropic triangular Au core-Ag shell nanoparticles at room temperature. Triangular gold nanoparticles are synthesized using lemongrass extract, which has been described in the previous chapter. The cationic silver ions bind to the surface of anionic gold nanotriangles through electrostatic interaction. Ascorbic acid is used as a reducing agent for the reduction of bound silver ions under alkaline condition. The optical properties of

core-shell nanoparticles and thickness of silver shell can be tailored using different concentrations of silver ions and different pH of solutions for the reduction of bound silver ions. A part of this chapter describes the synthesis of spherical gold-titania core-shell nanoparticles using the hydrolyzing enzyme. This method is first of its kind for the synthesis of core-shell nanoparticles using a biological source like protein. The hydrolyzing enzyme was isolated and purified from fungus *Fusarium oxysporum* after challenging with K_2TiF_6 solution. The enzyme was immobilized on gold nanoparticles followed by exposure to K_2TiF_6 , which lead to the formation of spherical gold-titania core shell nanoparticles.

4.2 Synthesis of anisotropic core-shell nanoparticles:

4.2.1 Experimental Details:

The gold nanotriangles used for the synthesis of core-shell nanoparticles were prepared by addition of 8 mL of lemongrass leaf extract in 100 mL of 10^{-3} M aqueous $HAuCl_4$ solution, as discussed in section 3.2 of chapter 3. The UV-vis-NIR spectra were recorded after allowing the reaction medium to stand for 48 h when the reduction of Au^{3+} ions had reached saturation. Using this proportion of lemongrass extract and $HAuCl_4$ solution, the gold nanotriangles exhibiting longitudinal SPR band at 1080 nm could be obtained. The percentage of nanotriangles in the reaction medium could be enhanced by three times centrifugation at 4000 rpm and redispersion of the pellet in water. The pellet of purified nanotriangles was finally diluted to 80 mL in water. Different volumes of 10^{-2} M aqueous $AgNO_3$ solution were added to 9 ml solutions of purified nanotriangles to yield different concentrations of silver ions (5×10^{-5} M, 10^{-5} M, 5×10^{-4} M, 10^{-4} M and 10^{-3} M) in the solutions. The solutions were kept for 24 h to facilitate the binding of Ag^+ ions onto the surface of negative charged gold nanotriangles following which, the gold nanotriangles were separated from the solution by centrifugation at 10000 rpm to get rid of unbound Ag^+ ions present in the reaction medium. The pellet was dissolved in 50 mL Milli-Q water (Millipore Corp., Bedford, MA) following which, the surface bound Ag^+ ions were reduced using ascorbic acid (10^{-3} M) under alkaline conditions with pH varying from 7 to 12. The various stages of reaction for the synthesis of triangular Au core-Ag shell nanoparticles were followed by UV-vis-NIR spectroscopy measurements at room

temperature. Gold nanotriangles and triangular Au core-Ag shell nanoparticles films prepared by solution casting onto highly oriented pyrolytic graphite (HOPG) substrate were analyzed by atomic force microscopy (AFM) in the contact mode.

UV-vis spectroscopy, Transmission electron microscopy (TEM), High-resolution transmission electron microscopy (HRTEM) were carried out to investigate the synthesis of triangular Au core-Ag shell nanoparticles. High-resolution TEM (HRTEM) measurements were carried out on a JEOL-JEM-2010 UHR instrument operated at a lattice image resolution of 0.14 nm. X-ray photoelectron spectroscopy (XPS) analysis of triangular Au core-Ag shell nanoparticle film deposited on Si (111) wafer was also done to confirm the synthesis of core-shell nanoparticles. The core level binding energies (BEs) were aligned according to the adventitious carbon binding energy of 285 eV.

4.2.2 Optimization of silver ions for shell formation:

The ideal concentration of silver ions (AgNO_3) to get a perfect shell on the gold nanoparticles surface was followed by UV-vis-NIR spectroscopy analysis of different concentrations of silver ions added to the lemongrass reduced gold nanotriangles solutions. Curve 1 of Figure 4.1A shows the UV-vis-NIR spectrum of the gold nanoparticles solution containing triangular and spherical nanoparticles, which is synthesized by using lemongrass extract. Curve 1 exhibits two surface plasmon bands; one at 543 nm due to the excitation of dipole surface plasmon resonance of spherical nanoparticles and the transverse component (out of plane vibrations) of SPR band of triangular nanoparticles while another at 1080 nm due to the longitudinal component of SPR band (in-plane vibrations) [11b, 15, 33]. The optical absorption in the NIR region of electromagnetic spectrum is due to the presence of triangular nanoparticles in solution, which is confirmed by the TEM measurement [33a, b]. The TEM measurement (Figure 4.1B) also shows a large population of gold nanotriangles along with few spherical nanoparticles. Some of the gold nanotriangles have truncated vertices, which can be seen in the TEM image. The higher magnification TEM image (Figure 4.1C) shows a single gold nanotriangle, which has sharp tips and smooth edges. The contrast around gold nanotriangles is uniform, which indicates that no material except gold and biomolecules of lemongrass extract are present on the surface of gold nanotriangles. The histogram analysis shows that edge-to-edge length of the gold nanotriangles is 205 ± 8 nm (Figure

4.1D). The small size of gold nanotriangles causes the presence of a distinct band at 1080 nm in the NIR region, which can be changed by varying the edge lengths of anisotropic gold nanoparticles [33b].

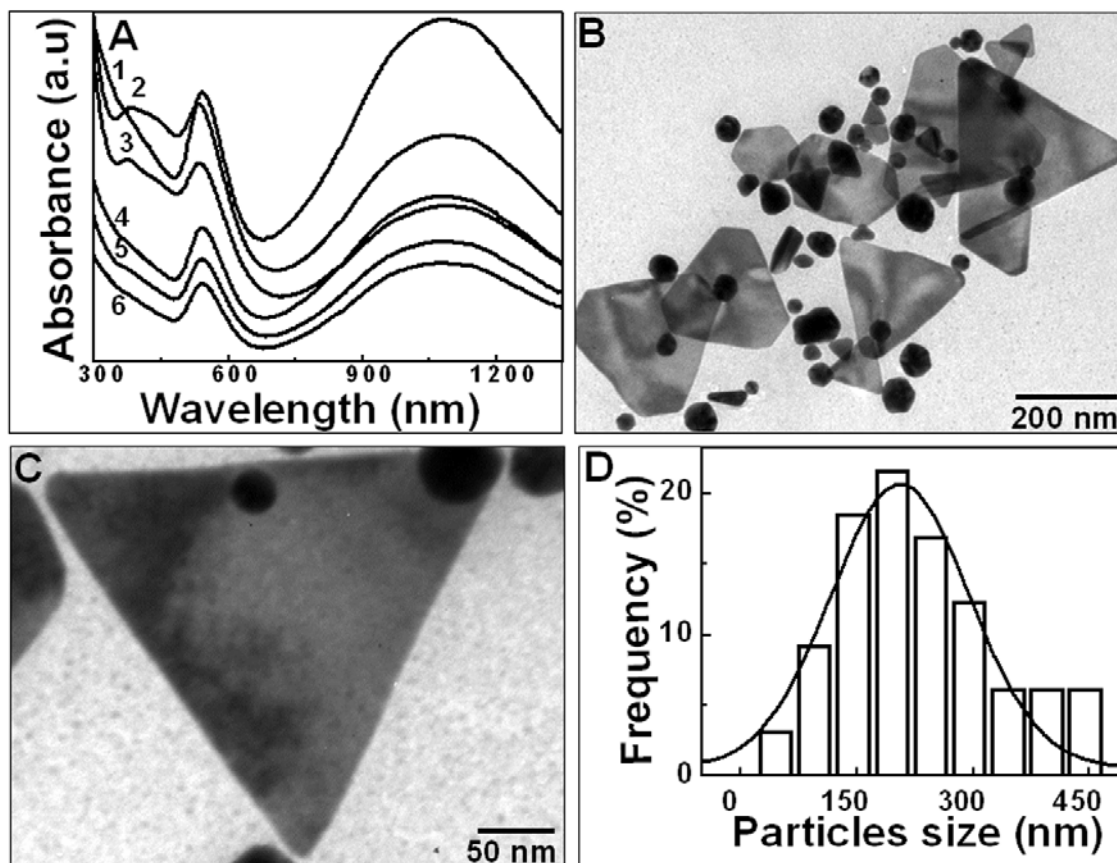


Figure 4.1: **A)** UV-vis-NIR spectra recorded from, curve 1: lemongrass reduced gold nanotriangles solution, curves 2-6: after addition of 10^{-3} , 5×10^{-4} , 10^{-4} , 5×10^{-5} and 10^{-5} M silver ions respectively to the gold nanotriangles. **B)** Lower magnification TEM image of lemongrass reduced gold nanotriangles. **C)** Higher magnification TEM image of a single gold nanotriangle. **D)** The histogram analysis for edge-to-edge length of the gold nanotriangles.

Addition of any additives in the nanotriangles solution could easily be monitored by using UV-vis-NIR spectroscopy due to the change in intensity and the position of surface plasmon (SP) band of the gold nanoparticles. The presence of different concentrations of silver ions in the gold nanotriangles solution change the dielectric environment of gold nanoparticles and hence alter the optical absorption properties of the gold nanoparticles. Curves 2-6 in Figure 4.1A show the UV-vis-NIR spectra of different concentrations (10^{-3} , 5×10^{-4} , 10^{-4} , 5×10^{-5} and 10^{-5} M) of Ag^+ ions bound gold

nanotriangles solutions incubated for 24 h. We believe that positively charged silver ions bind with negatively charged gold nanotriangles through electrostatic interaction. The negative charge on gold nanotriangles is due to the presence of ketonic and aldehydic compounds of lemongrass extract on the surface of particles [34a]. A broad absorption band ranging from 380 to 430 nm and a small hump at 380 nm, which correspond for surface plasmon (SP) band of silver nanoparticles are appeared in curves 2 and 3 respectively due to the partial reduction of Ag^+ ions on the surface of the gold nanotriangles by biomolecules present on the surface of nanotriangles. A blue shift of 10 nm at 543 nm for the gold nanoparticles is also observed in curves 2 and 3. A decrease in the intensity of SP band at 543 and 1080 nm of gold nanoparticles can also be observed (curves 2 and 3), which clearly indicates that silver nanoparticles have been synthesized on the surface of nanotriangles that cause the damping in the absorption band of the gold nanoparticles [15b]. Curves 4-6 also show a decrease in the intensity of SP band of gold nanoparticles along with the absence of SP band of silver nanoparticles at 380 nm. The absence of SP band of silver nanoparticles can be due to the presence of low concentrations of silver ions on the surface of gold nanotriangles. Other groups have also reported that lower concentrations of silver ions do not contribute in the generation of SP band of silver nanoparticles in the absorption spectra of core-shell morphology [34]. From the UV-vis-NIR spectra data, it can be concluded that 10^{-3}M concentration of silver ions are appropriate for the deposition of silver shell around gold nanotriangles.

4.2.3 Time duration for binding of silver ions on triangular Au core nanoparticles:

The ideal time duration for binding of silver ions on the surface of gold nanotriangles is an important factor for the growth of the silver shell. The time duration for binding of 10^{-3}M Ag^+ ions onto the surface of gold nanotriangles was monitored by UV-vis-NIR spectroscopy analysis (Figure 4.2A). The bound Ag^+ ions are eventually reduced by biomolecules of lemongrass extract, which are present on the surface of nanotriangles. Curves 1 and 2 in Figure 4.2A show the SPR band for the gold nanotriangles after 6 and 12 h deposition of Ag^+ ions respectively while curve 3 shows the SPR band at ca. 392 nm for silver nanoparticles as a small shoulder after 18 h deposition along with the absorption band for gold nanotriangles. Curve 4 shows a small hump at 390 nm for the silver nanoparticles and a decrease in the intensity of longitudinal

component of triangular Au core nanoparticles after 24 h deposition of the silver ions. It is concluded that 24 h exposure of Ag^+ ions is important prior to the reduction by ascorbic acid at pH 12. Figure 4.2B and C show TEM micrographs of gold nanoparticles recorded after 6 and 12 h respectively for the binding of silver ions on the nanotriangles surface and subsequent reduction by ascorbic acid.

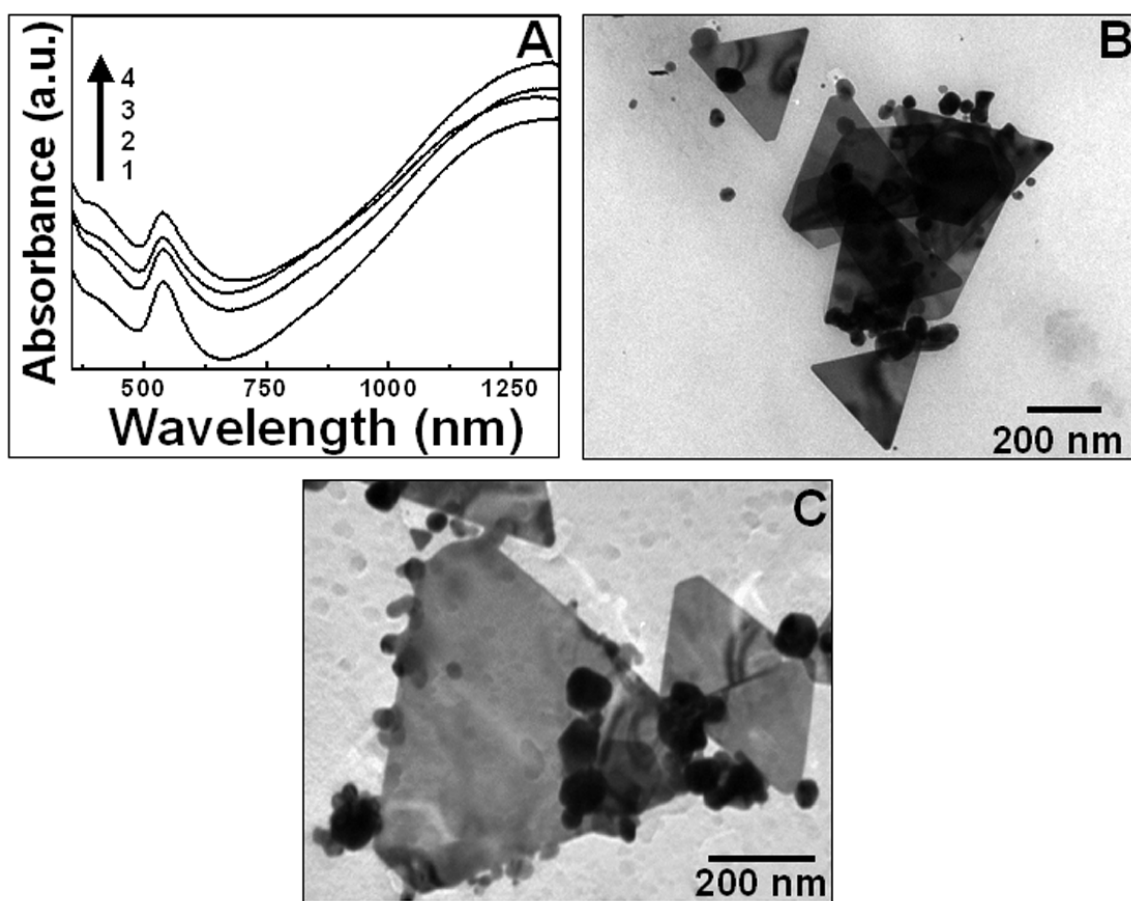


Figure 4.2: **A)** UV-vis-NIR spectra recorded for 6 h (curve 1), 12 h (curve 2), 18 h (curve 3) and 24 h (curve 4) deposition of 10^{-3}M silver ions on the surface of gold nanotriangles. **B and C)** TEM images recorded for the deposited silver ions on gold nanotriangles after 6 h and 12 h respectively and subsequently reduction of bound silver ions by ascorbic acid at pH 12.

Figure 4.2B clearly shows that there is no apparent shell around the nanotriangles and the edges and surfaces of nanotriangles are smooth after binding of Ag^+ ions for 6 h while Figure 4.2C shows small bulb like structures that have grown around the gold nanotriangles after binding of Ag^+ ions for 12 h followed by reduction using ascorbic acid at pH 12. At closer inspection of gold nanotriangles in the TEM image (Figure

4.2C), it seems that the nanotriangles surface is not smooth and it has coarse texture on it, which is not present in the gold nanotriangles after 6 h deposition of Ag^+ ions (Figure 4.2B) as well as control gold nanotriangles (Figure 4.1B and C).

4.2.4 Coating of silver atoms on the surface of nanotriangles:

4.2.4.a UV-vis-NIR spectroscopy analysis:

In order to get complete reduction of silver ions and the formation of silver shell around the surface of gold nanotriangles, ascorbic acid was used as a reducing agent under alkaline condition. Ascorbic acid has two dissociation constants; one at 4.10 ($\text{pK}_{\text{a}1}$) and another at 11.79 ($\text{pK}_{\text{a}2}$) [35]. At low pH, ascorbic acid does not have the ability to reduce silver ions. Ascorbic acid is well known to reduce silver ions under alkaline condition where monoanionic ascorbate ions facilitate the reduction of silver ions. The bound silver ions on the surface of gold nanotriangles were reduced by ascorbic acid under alkaline conditions and thus, we could expect the deposition of reduced silver atoms onto the surface of gold nanotriangles under alkaline pH.

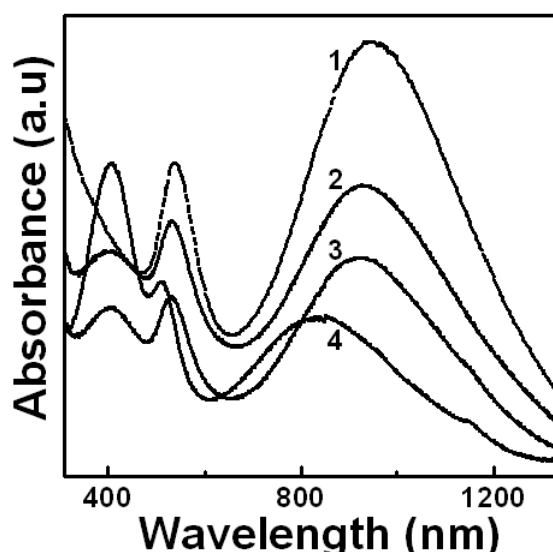


Figure 4.3: UV-vis-NIR spectra recorded for gold nanotriangles (curve 1) and for core-shell nanoparticles synthesized by ascorbic acid at pH 7 (curve 2), pH 10 (curve 3) and pH 12 (curve 4).

Curve 1 in Figure 4.3 shows the UV-vis-NIR spectrum of gold nanotriangles without any addition of silver ions while curves 2 to 4 show the UV-vis-NIR spectra of triangular Au core-Ag shell nanoparticles at pH 7, 10 and 12 respectively. As the pH of

solution increase from 7 to 12, a gradual blue shift in the longitudinal plasmon band of gold nanotriangles and appearance of SP band at 405 nm for silver nanoparticles synthesized on the surface of gold nanotriangles using ascorbic acid can be observed (curves 2-4). A decrease in the intensity of SP peak centered at 528 nm accompanied with a small blue shift of 5 nm can be seen in the UV-vis-NIR spectra of triangular Au core-Ag shell nanoparticles synthesized at pH 7 and 10 respectively (curves 2 and 3). A large blue shift of 20 nm and a decrease in the intensity of SP peak at 511 nm in comparison to the absorption spectrum of gold nanotriangles is observed for silver shell synthesized on the surface of gold nanotriangles at pH 12 (curve 4). It is well known that a blue shift in the surface plasmon (SP) band of gold nanoparticles may be due to the change in dielectric environment (dielectric function of silver is different from gold and varies with thickness of shell), due to an increase of electron density on the metal nanoparticles or due to the formation of Au-Ag interface [1d, 35d, 36]. Therefore, the blue shift and decrease in the intensity of SP band of triangular Au core-Ag shell nanoparticles at different pH could be due to the varying thickness of silver shell around the gold nanotriangles and change in aspect ratio of nanoparticles [1d].

4.2.4.b TEM Analysis:

TEM measurements were performed to observe the morphology of triangular Au core-Ag shell nanoparticles synthesized using ascorbic acid at pH 12. Figure 4.4A shows a low magnification TEM image of core-shell nanoparticles wherein the gold nanotriangles are coated with silver shells. The reduction of silver ions bound to the gold nanotriangles by ascorbate ions results in the formation of silver atoms, which nucleate and grow on the surface of the gold nanotriangle to form silver shell. The TEM micrographs clearly show that the contrast of silver shell is lower than core gold nanotriangles and shell completely covers the gold nanotriangles. The darker contrast observed in the nucleus of core-shell nanoparticles suggests the presence of Au core, because this metal has higher efficiency to scatter electrons. This finding suggests that gold nanoparticles act as seeds for silver deposition, as has also been reported by other groups [13, 35a, 35d, 37]. The inset of Figure 4.4A shows that the surface of nanotriangles has a grainy texture because of the presence of silver nanoparticles on the nanotriangle surface. It can also be seen that small silver nanoparticles assemble on the

surface of gold nanotriangle and then form continuous shell around gold nanotriangle. Figure 4.4B and C show higher magnification TEM images of triangular Au core-Ag shell nanoparticles. It can be observed that some spherical gold nanoparticles present along with nanotriangles are also coated with silver shells.

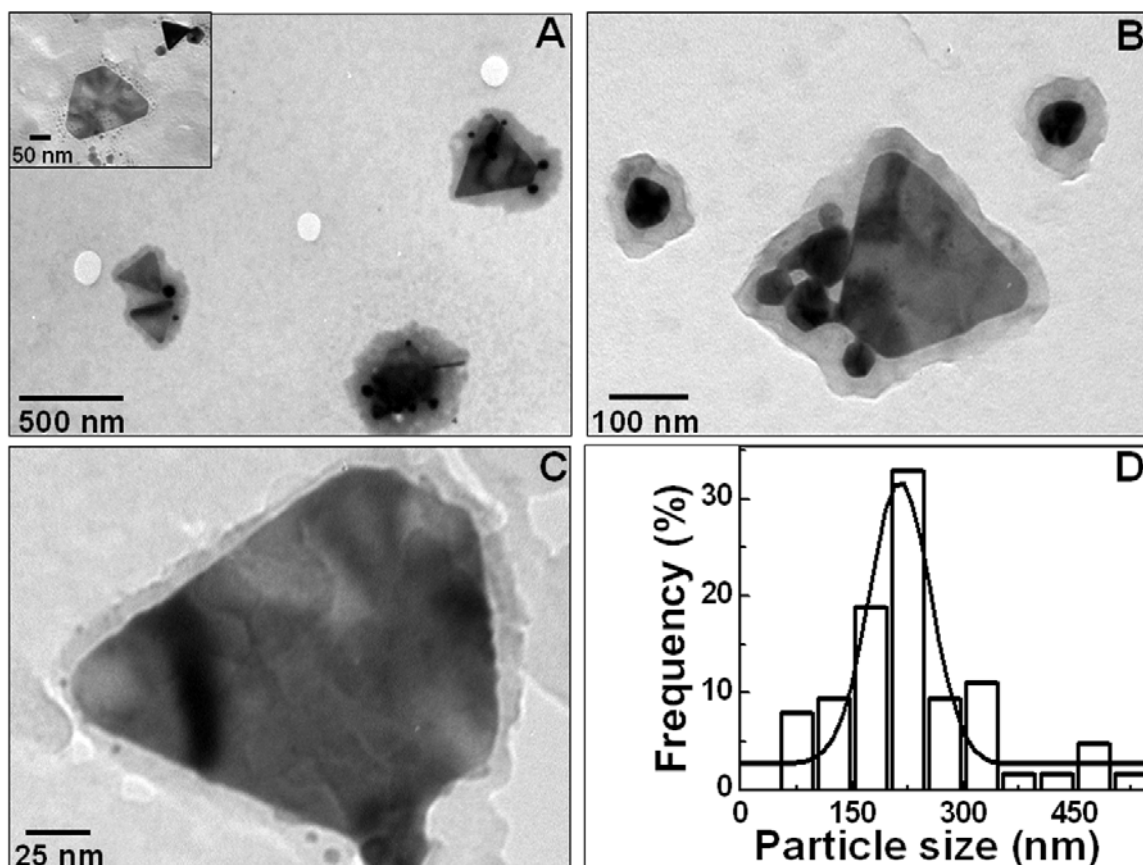
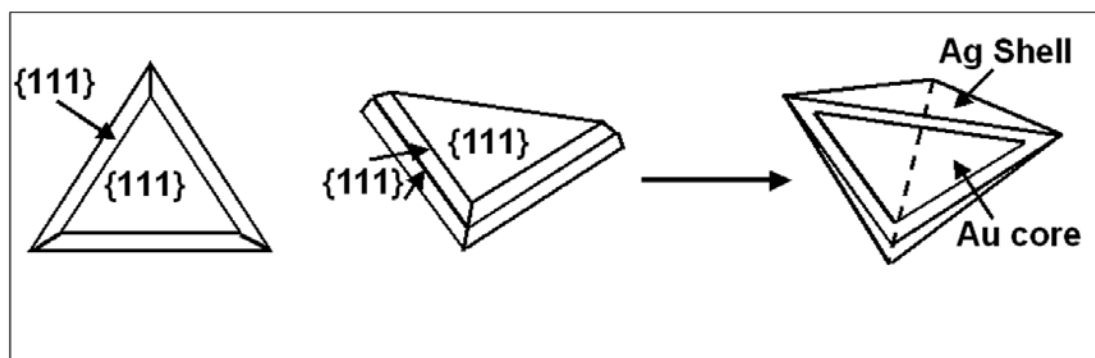


Figure 4.4: **A)** Lower magnification TEM image of triangular Au core-Ag shell nanoparticles synthesized at pH 12. The inset of figure 4.4A shows the silver nanoparticles around gold nanotriangle. **B and C)** Higher magnification TEM images of the core-shell nanoparticles. **D)** Histogram analysis for edge-to-edge length of Au core-Ag shell nanoparticles.

The TEM images clearly indicate that the silver nanoparticles are deposited on (111) lattice plane and edges of gold nanotriangles and the thickness of shell around nanotriangle edges is uniform. The histogram analysis of core-shell nanoparticles shows that edge-to-edge length of triangular Au-Ag core-shell nanoparticles is 214.4 ± 4 nm (Figure 4.4D). By comparing the edge-to-edge length of nanotriangles and core-shell nanoparticles, the thickness of silver shell synthesized around the gold nanotriangle using ascorbic acid is estimated to be ca. 5 nm. The mechanism behind the growth of triangular

core-shell nanoparticles can be explained as follows: the gold nanotriangles consist of two $\{111\}$ facets at top and bottom and six narrow side $\{111\}$ facets (Scheme 4.1). The silver shells having two $\{111\}$ facets on top and bottom and twin pair of 12 alternative $\{100\}$ and $\{111\}$ side facets are grown on these triangular core plates. It may be possible that capping agent selectively binds to the six side twin $\{100\}$ facets and promote the growth of silver shell on the $\{100\}$ facets. Tsuji's group has also reported the synthesis of triangular Au-Ag core-shell nanoparticles using polyol method with a similar mechanism [11a].



Scheme 4.1: Schematic diagram for the gold nanotriangles and triangular Au core-Ag shell nanoparticles.

Figure 4.5 shows a high-resolution TEM (HRTEM) image of a triangular Au core-Ag shell nanoparticle.

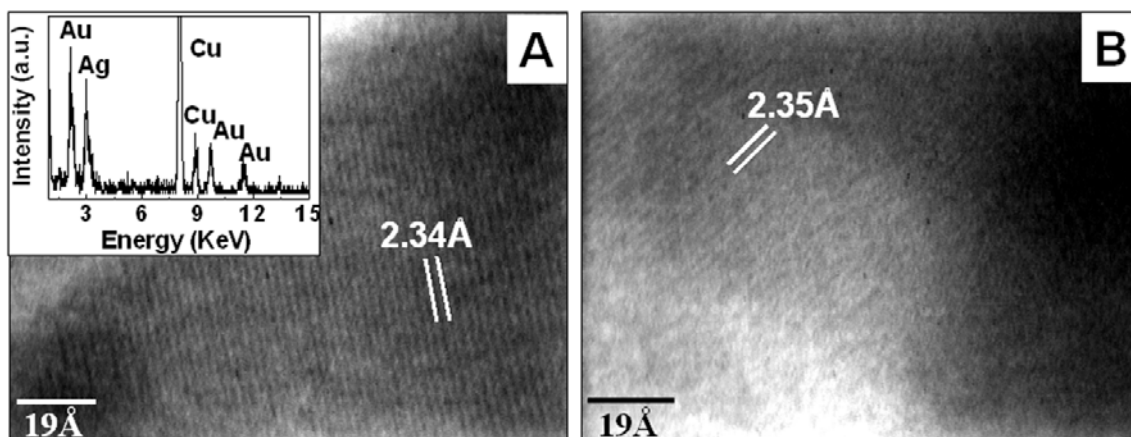


Figure 4.5: **A)** High-resolution TEM (HRTEM) image of core gold nanoparticles. The inset shows energy dispersive analysis of X-rays (EDAX) of triangular core-shell nanoparticles. **B)** HRTEM image of the silver shell of triangular Au core-Ag shell nanoparticles.

A lattice spacing of 2.34\AA is observed from edge of the core gold nanotriangles (Figure 4.5A), which does not match with the already reported lattice spacing of $1/3\{422\}$ -reflection plane of silver nanotriangles [38]. The lattice spacing of 2.34\AA is close to the standard value of 2.36\AA for fcc gold (111) lattice that indicates that the edge of the gold nanotriangle has possibly (111) plane. Figure 4.5B shows a lattice spacing of 2.35\AA for the silver shell around gold nanotriangle, which corresponds to the (111) lattice plane of fcc silver nanoparticles. It would be worth noticing here that though the lattice planes could be imaged at particular instances in general, the lattices of core-shell nanoparticles were very unstable at the boundary under the incident electron beam of the microscope and could not be imaged together. The inset of the Figure 4.5A shows the energy dispersive analysis of X-rays (EDAX) of Au core-Ag shell nanoparticles. EDAX data reveals strong signals of Au and Ag in the sample, which clearly indicates the presence of both in triangular core-shell nanoparticles. There is also a strong signal of Cu in the EDAX data that usually comes from the carbon coated copper TEM grid.

4.2.4.c AFM analysis:

Atomic force microscopy (AFM) measurement was done to analyze the precise thickness of silver shell in the triangular Au core-Ag shell nanoparticles. TEM is able to measure the particle dimension in x-y plane (parallel to TEM grid surface) while AFM can also give accurate height in z direction (perpendicular to the silicon wafer surface). The AFM image of a gold nanotriangle synthesized using lemongrass extract is shown in Figure 4.6A. The truncation of vertices in the gold nanotriangle is clearly evident in the AFM image. These features have repeatedly been seen for a large fraction of the nanotriangles obtained biologically which is also confirmed by the TEM images (Figure 4.1B and C). Indeed, such nanotriangles have also been observed for silver [38, 39] and gold nanoprisms [40] obtained by chemical methods. A 3-dimensional AFM image (Figure 4.6B) of the gold nanotriangle shows that nanotriangle surface is atomically flat which is strongly supported by $1/3\{422\}$ reflection observed in SAED pattern of the gold nanotriangles as shown in Figure 3.2C in chapter three. A topographic height analysis of nanotriangle along the direction indicated by black line in the image is shown in the lower panel of Figure 4.6A, which shows that the gold nanotriangle has an average

thickness of 18 nm. By an analysis of a large number of nanotriangles, the thickness of nanotriangles is found to be 18 ± 2 nm. The AFM image of Au core-Ag shell nanotriangles are shown in Figure 4.6C. It can be observed that the edge of the nanotriangle has more contrast than that of the plane gold nanotriangle (Figure 4.6A), which is due to the reduction of silver ions on the surface and edges of the gold nanotriangles using ascorbic acid at pH 12.

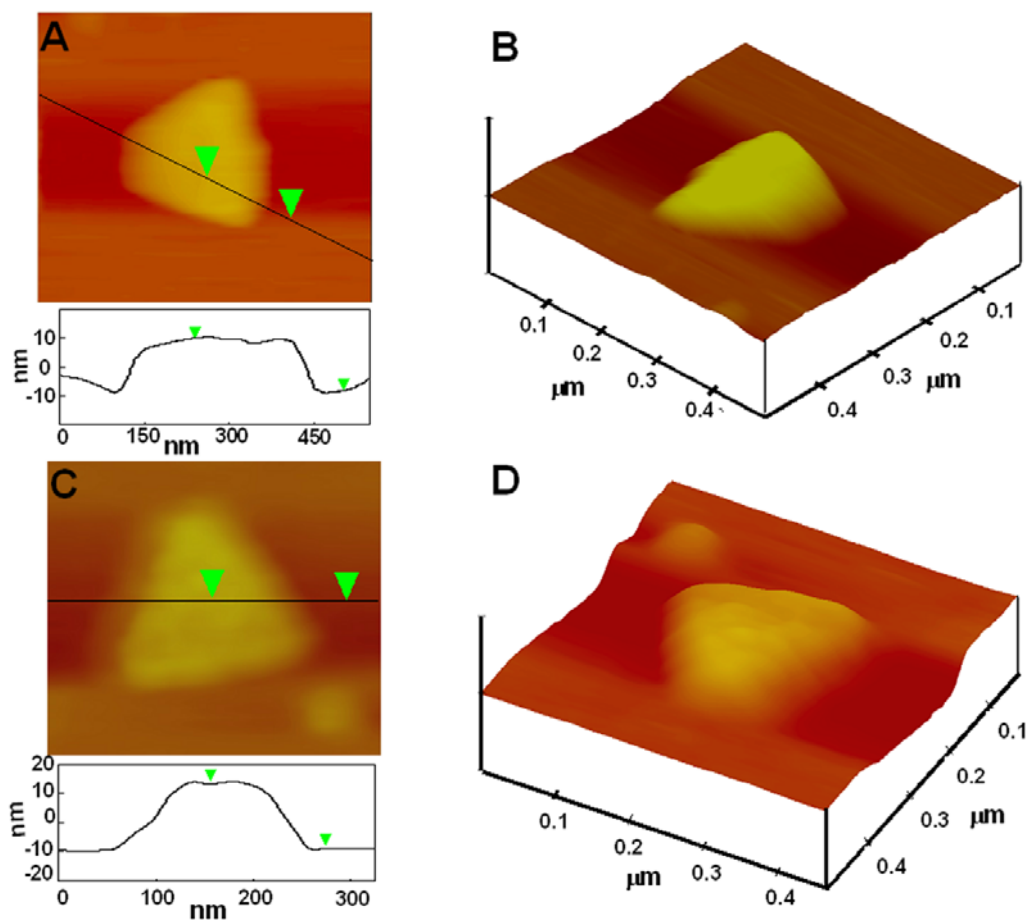


Figure 4.6: **A)** AFM image of triangular gold nanoparticles. **B)** 3D AFM image of the gold nanotriangle. **C)** AFM image of triangular Au core-Ag shell nanoparticles synthesized at pH 12. **D)** 3D AFM image of the core-shell nanoparticles. Bottom parts of Figure 4.6 A and C show the line profile plots of triangles and core-shell nanoparticles respectively.

It can also be seen in 3-dimensional AFM image (Figure 4.6D) that the surface and edges of core-shell nanotriangle are very rough and their morphology is much different from that of the control gold nanotriangles. The line profile analysis of the core-shell nanoparticle along the direction shown in the lower part of Figure 4.6C shows the

thickness to be ca. 23 nm. The thickness of core-shell nanoparticles after measurements of a large number of particles is found to be 23 ± 2 nm. These results clearly indicate the synthesis of triangular core-shell nanostructures with the thickness of the silver shell varying from 2-5 nm that is in good agreement with measurement from the TEM analysis (Figure 4.1B and C).

4.2.4.d Chemical analysis:

It is important to know the fine structure of bimetallic nanoparticles, which can be studied by the XPS measurement. A chemical analysis of triangular Au core-Ag shell nanoparticles synthesized at pH 12, drop coated on Si(111) wafer, was done by X-rays photoemission spectroscopy (XPS).

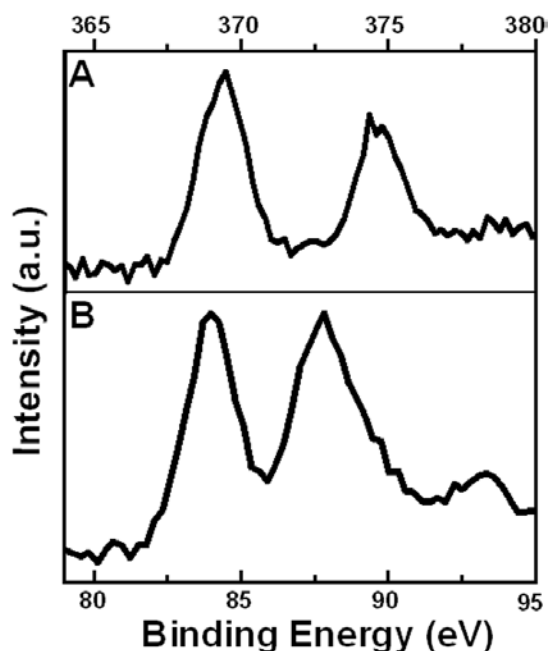


Figure 4.7: XPS spectra of (A) Ag 3d and (B) Au 4f core level of triangular Au core-Ag shell nanoparticles synthesized at pH 12 without background correction.

Figure 4.7A and B show the XPS spectra of Ag 3d and Au 4f core levels respectively without background correction for triangular Au core-Ag shell nanoparticles but accounting for charging of the film (with respect to adventitious C 1s signal of 285 eV BE). A small increase in the background associated with the Au 4f core level in comparison with the Ag 3d core level is observed. The background in the XPS core level spectra arises due to inelastic scattering of electrons during transport within the surface

prior to emission. In the case of Au core-Ag shell nanostructure, the Au 4f electrons stemming from the core are expected to be more effectively scattered by the Ag shell compared to the Ag 3d electrons, thereby giving rise to the difference in the background signals mentioned above. Thus, careful analysis of the background can yield a wealth of information regarding the nature of surfaces and attest the presence of core-shell structures in the sample. The different core levels were then background corrected using the Shirley algorithm [41] prior to curve resolution, and the core levels were aligned with respect to adventitious C 1s binding energy (BE) of 285 eV. C 1s photoemission spectrum is rather complex and could be deconvoluted into three chemically distinct components (Figure 4.8A). In addition to the adventitious C 1s BE peak at 285 eV, peaks at 286.7 and 288.7 eV are also observed. The high BE peak at 288.7 eV is attributed to electron emission from carbons in carbonyl groups (aldehydic or ketonic carbons) [43] while the peak at 286.6 eV is most likely from α carbons to the carbonyl groups. Induction effects are known to influence the BEs of carbons complexed with electron withdrawing functional groups such as carbonyls [43].

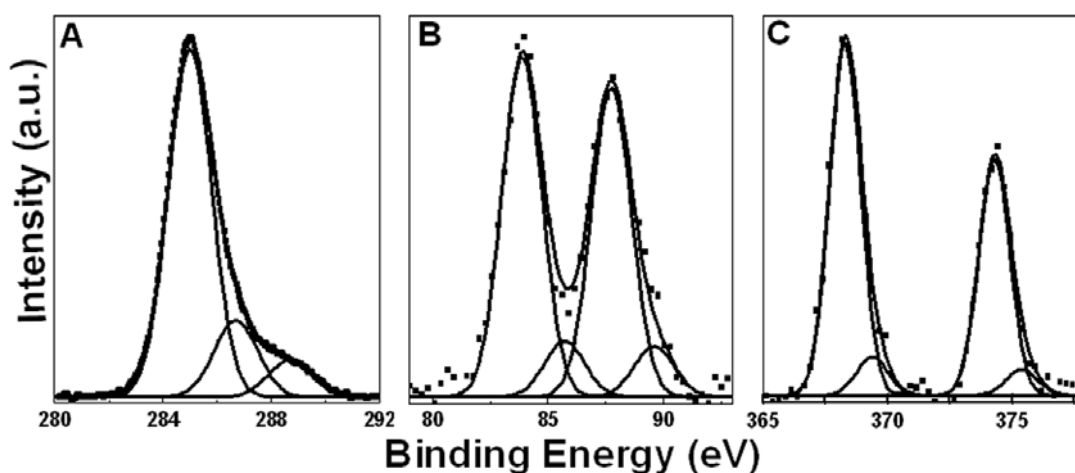


Figure 4.8: XPS spectra of (A) C 1s (B) Au 4f and (C) Ag 3d core level of triangular core-shell nanoparticles after background correction using the Shirley algorithm.

The complex C1s spectrum could be due to carbon coordinated to hydroxyl groups of sugar molecules present in lemongrass extract and bound with the gold nanotriangles. [34a]. The Au 4f_{7/2} core level could be split into two chemically distinct components centered at 83.9 and 85.7 eV BEs that correspond to Au(0) and Au(I)

respectively (Figure 4.8B). The relatively small amount of Au(I) present on the surface of the gold nanoparticles is responsible for the additional peak at high BE and stabilizes the particles electrostatically against aggregation in solution [44]. The Ag 3d spectrum could also be stripped into two chemically distinct spin-orbit pairs. The two chemically distinct Ag 3d_{5/2} components are observed at 368.3 and 369.4 eV BEs (Figure 4.8C). The low BE component is attributed to electron emission from silver nanoparticles (nanoshell) [45] while the high binding energy component arises from silver ions indicating that a small fraction of unreduced Ag⁺ remains bound to the surface of nanoparticles. The XPS signals from Au and Ag in triangular core-shell nanoparticles are strongly evinced by EDAX data (inset of Figure 4.5A).

4.3 Summary:

A facile method for the synthesis of triangular Au core-Ag shell nanoparticles at room temperature has been described in this chapter. The silver ions interact electrostatically with negatively charged gold nanotriangles and bind onto their surface. Ascorbic acid acts as a reducing agent under alkaline conditions for the reduction of bound silver ions on the surface of gold nanotriangles. By varying the pH of solutions, different thickness of silver shells can be coated on the surface of gold nanotriangles.

4.4 Synthesis of spherical gold-titania core-shell nanoparticles:

4.4.1 Experimental Details:

The aqueous gold nanoparticle solution was synthesized by sodium borohydride reduction of chloroauric acid (addition of 0.1 gm NaBH₄ in 100 mL of 10⁻⁴ M of aqueous solution of HAuCl₄) as described in our earlier report [31]. This procedure results in ruby red solution of gold nanoparticles at room temperature. The colloidal gold nanoparticle solution was dialyzed for 24 h in Milli-Q water using a 12.5 kDa cut-off dialysis membrane to remove the excess free borohydride ions and unreduced chloroaurate ions present in the solution. Before dialysis, the bag was boiled in Milli-Q water for 10 minutes followed by repeated washing with water to remove all contamination. The surface functionalization of dialyzed gold nanoparticles was done by the addition of 5 mL of 10⁻³ M aspartic acid in 20 mL of the colloidal gold solution, which was kept for 24 h at room temperature. Then this solution was again dialyzed for 24 h to remove

uncoordinated aspartic acid from the gold nanoparticles. UV-vis spectroscopy analysis was done for the borohydride reduced gold nanoparticles and aspartic acid modified gold nanoparticles. The isolation and purification of hydrolyzing enzyme from fungus *Fusarium Oxysporum* was done by the procedure reported previously [32]. 20 g of thoroughly washed and sterile fungus biomass was suspended in 100 mL of sterile deionized water in 500 mL Erlenmeyer flask under shaking condition (200 rpm) at 25 - 28 °C. The extracellular component (mainly proteins) secreted by the fungus in water after 24 h were collected by filtration and concentrated by lyophilization. The lyophilized extracellular fraction containing a mixture of proteins was dialyzed against deionized water (using a 12.5 kDa cut-off dialysis membrane) and further purified using CM sephadex cation exchange matrix. 100 µL of hydrolyzing enzyme was added in 1 mL aspartic acid modified gold nanoparticles solution and incubated for 24 h at 4 °C. Dialysis was again done against Milli-Q water at 4 °C to remove the unbound protein from solution using 12.5 kDa cut-off dialysis membrane. The low temperature dialysis is important to prevent the denaturation of hydrolyzing protein. 500 µL K_2TiF_6 solution was added in 1 mL of the hydrolyzing enzyme bound gold nanoparticle solution and incubated for 24 h at 4 °C, which led to the formation of spherical gold-titania core-shell nanoparticles. The unreacted K_2TiF_6 was removed from core-shell solution by centrifugation at 15000 rpm for 30 minutes prior to analysis by Transmission electron microscopy (TEM), Fourier transform infrared spectroscopy (FTIR), X ray diffraction (XRD) and X ray photoemission spectroscopy (XPS) analysis.

4.4.2 TEM analysis:

Figure 4.9A shows a low magnification TEM image of borohydride reduced gold nanoparticles. The TEM image clearly shows that the particles are monodisperse and the particles are in close contact after water evaporation during sample preparation in some places in the TEM grid. After surface modification of the gold nanoparticles with anionic aspartic acid, the particles are still spherical with some aggregation, which lead to the formation of elongated nanoparticles as observed in the TEM image (Figure 4.9B). The selected area electron diffraction (SAED) pattern of the borohydride reduced gold nanoparticles (Figure 4.9C) shows that gold nanoparticles are polycrystalline in nature. SAED pattern shows (111), (200), (311) and (220) Bragg's reflections corresponding to

fcc gold with the lattice spacing of 2.35, 2.03, 1.23 and 1.17Å respectively. The hydrolyzing enzyme from fungus *Fusarium oxysporum* was used for the synthesis of gold-titania core-shell nanoparticles [32]. The purified hydrolyzing enzyme is capped on the surface of aspartic acid modified gold nanoparticles. We believe that the cationic hydrolyzing protein interacts with the anionic aspartic acid modified gold nanoparticles and completely cover the surface of gold nanoparticles.

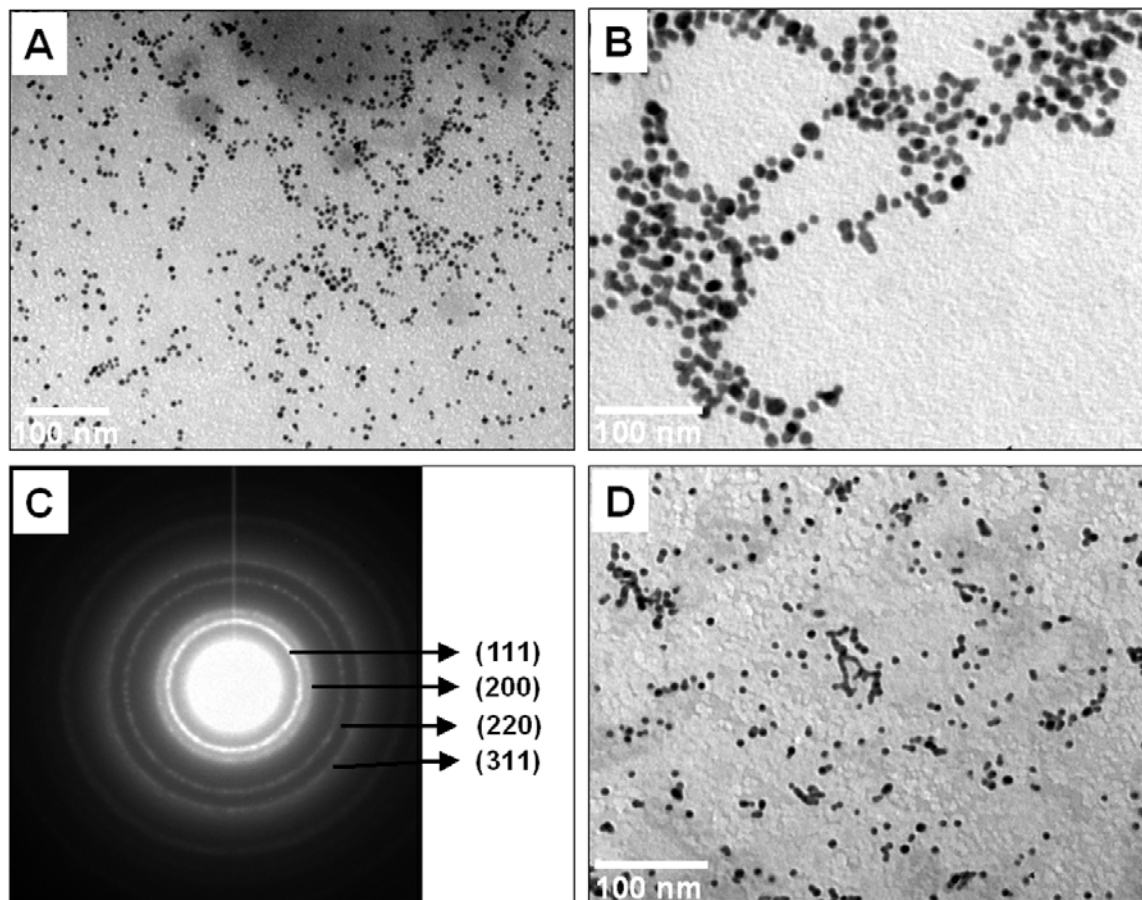


Figure 4.9: Representative TEM images of **A)** Borohydride reduced gold nanoparticles. **B)** Aspartic acid modified gold nanoparticles. **C)** Selected area electron diffraction pattern of the borohydride reduced gold nanoparticles. **D)** The hydrolyzing enzyme-capped aspartic acid modified gold nanoparticles.

The TEM image (Figure 4.9D) of protein capped gold nanoparticles shows that the morphology of particles is spherical and nanowire like few gold nanostructures can also be observed due to assembly or aggregation of spherical gold nanoparticles. After exposing the hydrolyzing protein capped gold nanoparticles with K_2TiF_6 solution at 4 °C,

TiF₆⁻ ions are selectively hydrolyzed on the surface of gold nanoparticles and form gold-titania core-shell nanoparticles. A large population of spherical gold-titania core-shell nanoparticles can be observed in the lower magnification TEM images (Figure 4.10A and B). The contrast of titania shell is different from core gold nanoparticles that can be seen in the higher magnification TEM image (Figure 4.10C). The variation in contrast of core and shell nanoparticles clearly confirms the successful synthesis of core-shell nanoparticles [35]. The higher magnification TEM image (Figure 4.10C) shows that the thickness of titania shell around gold nanoparticles is uniform and envelope gold nanoparticle inside the titania shell.

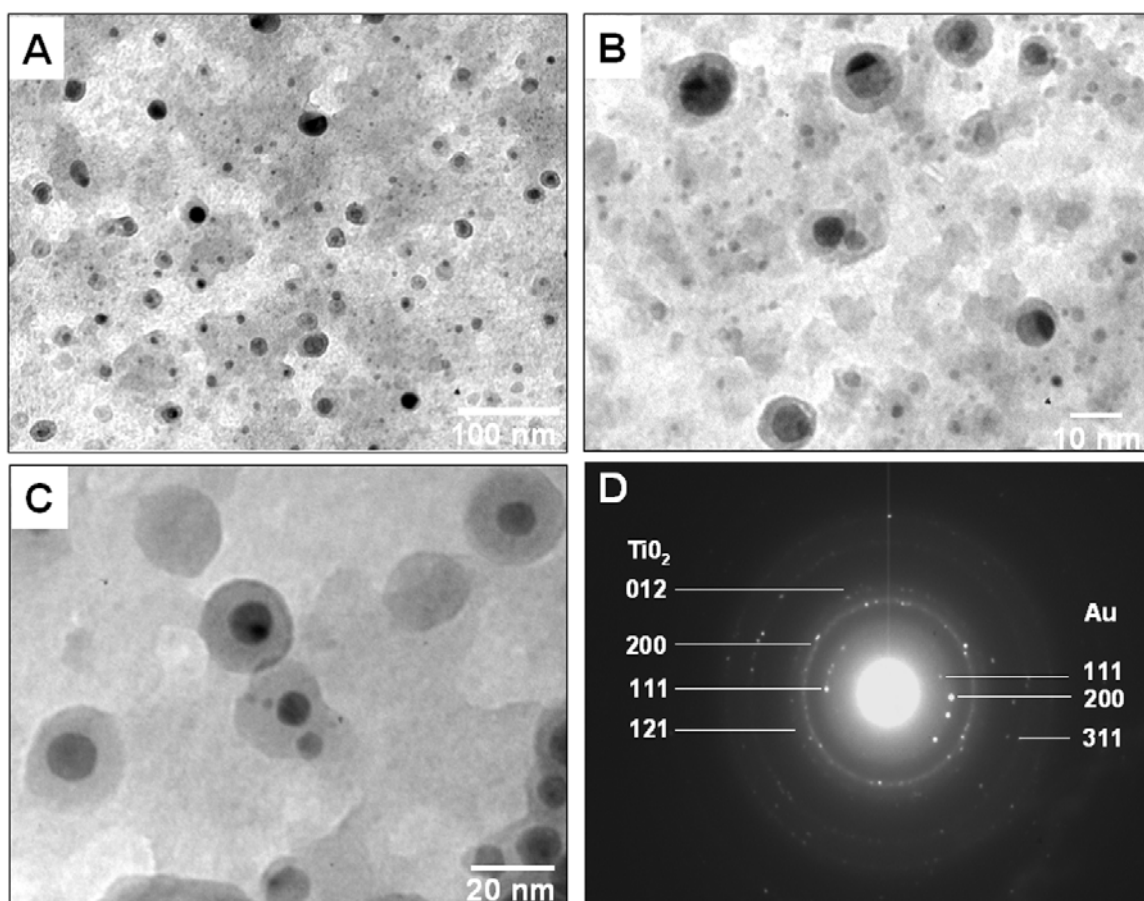


Figure 4.10: A and B) Lower magnification TEM image of the gold-titania core-shell nanoparticles. C) Higher magnification TEM image of core-shell nanoparticles. D) Selected area electron diffraction (SAED) pattern of gold-titania core-shell nanoparticles.

Figure 4.10D shows the selected area electron diffraction (SAED) analysis of gold-titania core-shell nanoparticles that clearly indicates the crystalline nature of gold

core and titania shell in the core-shell nanoparticles. The selected area electron diffraction pattern shows (111), (200) and (311) lattice plane of the core gold nanoparticles that match with Bragg reflection of fcc gold and simultaneously also shows (111), (121), (200), and (012) lattice plane of brookite phase of the titania shell. The diffraction spots are indexed from standard d values of brookite polymorph of TiO_2 [3.47 Å (111), 2.9 Å (121), 2.729 Å (200) and 2.476 Å (012)] [46]. A high-resolution transmission electron microscopy (HRTEM) study was done to identify the lattice planes of core and shell from gold-titania core-shell nanoparticles.

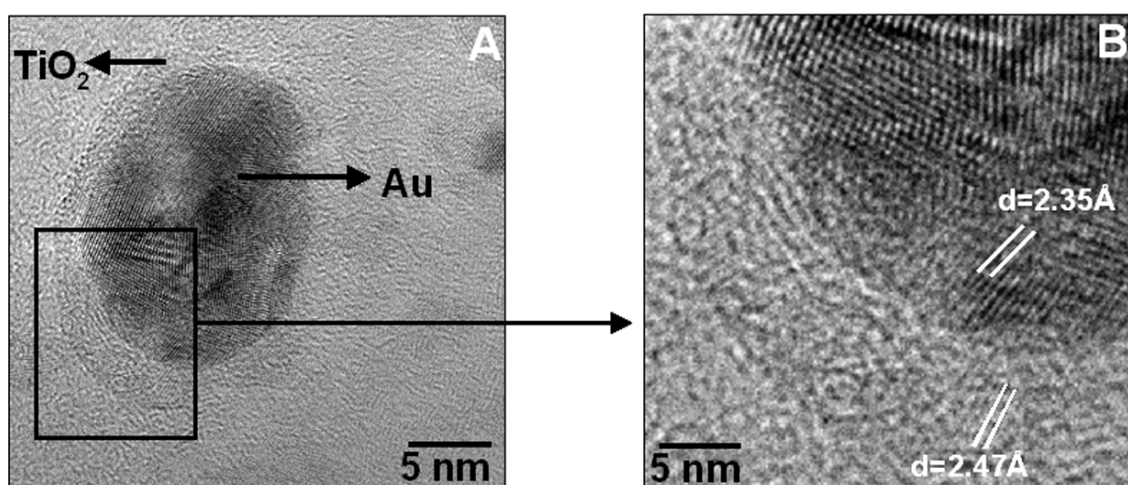


Figure 4.11: A) High-resolution TEM (HRTEM) image of gold-titania core-shell nanoparticle. B) Magnified image of one part of HRTEM image.

Figure 4.11A shows the HRTEM image of core-shell nanoparticles wherein the lattice plane of the core gold nanoparticle is clearly seen. Figure 4.11B shows high magnification of one part of the HRTEM image that reveals the d spacing of 2.35 Å (corresponds to (111) plane of fcc gold) and 2.47 Å (corresponds to (012) lattice plane of brookite phase) values for the gold nanoparticle and titania shell nanoparticles respectively. The HRTEM analysis shows the crystalline nature of titania shell on the surface of gold nanoparticles.

4.4.3 UV-vis Spectroscopy analysis:

The formation of gold-titania core-shell nanoparticles was monitored by UV-vis spectroscopy. Figure 4.12 shows the UV-visible spectra recorded from borohydride

reduced gold nanoparticles, aspartic acid modified gold nanoparticles and gold-titania core-shell nanoparticles. The colour of gold nanoparticles solution synthesized using borohydride reduction method is ruby red. The peak maximum corresponding to plasmon excitation of gold nanoparticles in the aqueous phase occurs at 530 nm (curve 1). The exact position of surface plasmon (SP) peak depends upon particles size and shape and to the electronic and optical properties of medium surrounding the particles [47].

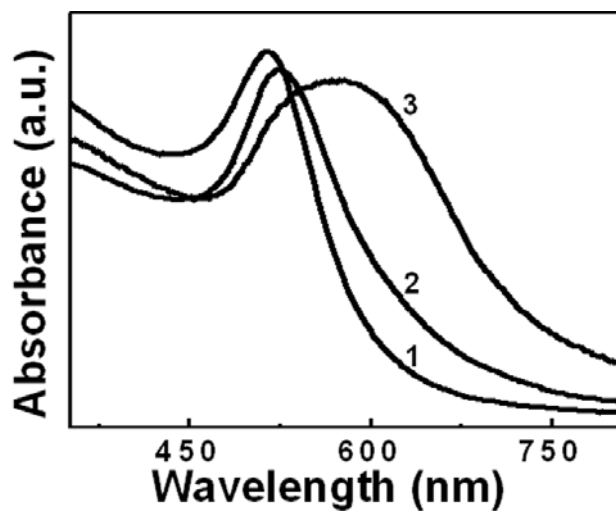


Figure 4.12: UV-vis spectra recorded from borohydride reduced gold nanoparticles (curve 1), aspartic acid modified gold nanoparticles (curve 2) and the hydrolyzing enzyme capped aspartic acid modified gold nanoparticles (curve 3).

After the surface modification with aspartic acid, the UV-vis spectrum (curve 2) shows a red shift and a broadening of surface plasmon (SP) peak, which indicates the complexation of aspartic acid with the surface of gold nanoparticles along with some percentage of aggregation in the solution [48] which is strongly supported by the TEM image (Figure 4.9B). On the visual inspection of solution, the colour of gold nanoparticles turned into slight bluish in nature after the modification that was also authenticated by UV-vis spectroscopy analysis. Anionic aspartic acid was chosen for the surface modification because it imparts negative charge on the gold nanoparticles after surface modification. Curve 3 of Figure 4.12 shows the UV-vis spectrum of gold-titania core-shell nanoparticles and demonstrates a broad absorption surface plasmon band with a large red shift of 50 nm when compared with curve 1. A red shift in SP band of gold nanoparticles could be due to the following reasons; first due to the encapsulation of inorganic layers on the metal nanoparticles surface and second due to an increase in

particles size of the gold nanoparticles [4d, 49]. Titania has a high refractive index of ca. 2.5 which is higher than that of solvent of core-shell nanoparticles [50]. The encapsulation of titania shells on the gold cores causes a change in the dielectric constant of surrounding medium of gold nanoparticles [47] and a red shift in the surface plasmon band of gold-titania core-shell nanoparticles. The UV-vis spectrum of gold-titania core-shell nanoparticles is corroborated with the TEM images (Figure 4.10A-C). An increase in the shell thickness also leads to the broadening of surface plasmon peak. The peak width is related to collision time because metal clusters are more isolated from the nearby nanoparticles due to an increase in the thickness of the oxide shell. Therefore, an increase in the surface plasmon width for smaller particles is related to the confinement of free electrons in the metal core [28d].

4.4.4 Fourier Transform Infrared Spectroscopy (FTIR) analysis:

FTIR measurements were carried out to investigate the presence of hydrolyzing protein and titania shell on the surface of gold nanoparticles.

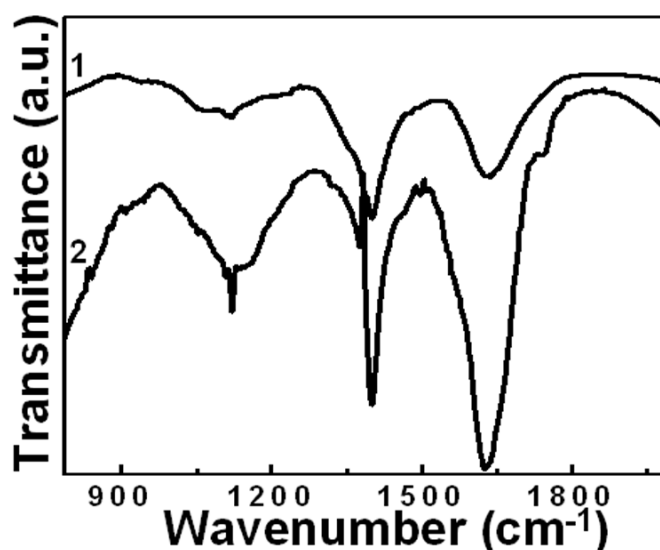


Figure 4.13: The FTIR spectra recorded from the hydrolyzing enzyme (curve 1) and gold-titania core-shell nanoparticles synthesized using the hydrolyzing enzyme (curve 2).

Figure 4.13 shows the FTIR spectra of hydrolyzing protein isolated from fungus (curve 1) and core-shell nanoparticles (curve 2). The peaks at 1632 and 1409 cm^{-1} of curve 1 are attributed to C=O stretching (amide I) and N-H vibration (amide II) respectively, which are characteristic for the presence of protein. The strong FTIR peak at

1109 cm^{-1} in curve 2 is assigned to the excitation of Ti-O-Ti vibration mode while a weak band at 950 cm^{-1} is attributed to the excitation of Ti-O asymmetric stretching of Ti-O-Ti bond [51] in titania shells of the core-shell nanoparticles [52]. Curve 2 also shows the 1632 and 1409 cm^{-1} peaks of amide bands for the presence of hydrolyzing enzyme in the core-shell nanoparticles. The FTIR data clearly shows the presence of titania in the core-shell nanoparticles.

4.4.5 X-ray Diffraction (XRD) analysis:

X-ray diffraction analysis of borohydride reduced gold nanoparticles (curve 1) and gold-titania core-shell nanoparticles (curve 2) were carried out to know the lattice planes of gold nanoparticles and different phases of the synthesized titania shell nanoparticles in the core-shell nanoparticles (Figure 4.14).

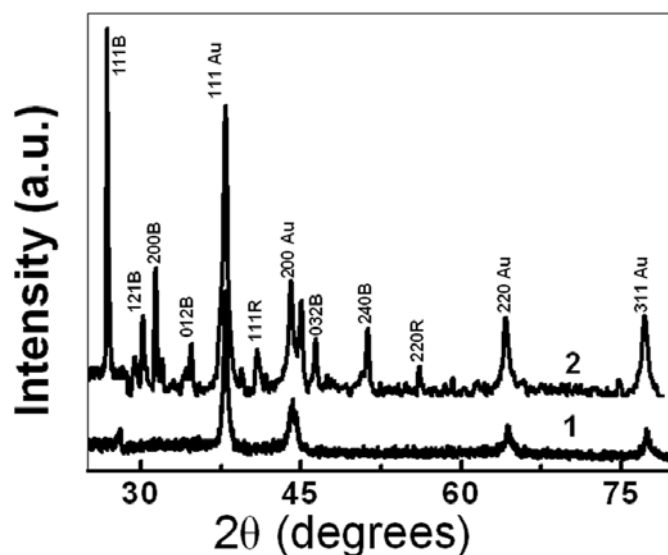


Figure 4.14: XRD diffraction spectra recorded from the borohydride reduced gold nanoparticles (curve 1) and gold-titania core-shell nanoparticles (curve 2).

Curve 1 shows Bragg reflections from (111), (220), (311) and (222) lattice planes of fcc gold nanoparticles. The XRD spectrum of gold-titania core-shell nanoparticles (curve 2) shows the diffraction peaks for (111), (220), (311), (222) lattice planes of the core gold nanoparticles as well as brookite and rutile phase of titania shell nanoparticles [(111), (121), (200), (012), (032) and (240) for brookite and (111) and (220) lattice planes of rutile phase]. The XRD analysis clearly shows that the crystalline and mixed phase of titania shells are formed in core-shell nanoparticles by the hydrolyzing protein which is in

good agreement with the HRTEM result (Figure 4.11). In earlier report from our laboratory, it has been shown that rutile and brookite phase of titania nanoparticles are formed by the hydrolyzing protein from fungus *Fusarium oxysporum* [32]. Bragg reflections of gold core nanoparticles and titania shell nanoparticles from the XRD analysis of core-shell nanoparticles match with the selected area electron diffraction pattern (SAED) (Figure 4.10D) which clearly indicates that the morphology of gold-titania core-shell nanoparticles after drop coating on the glass slide are intact and stable in form of film on the substrate.

4.4.6 X-ray Photoemission Spectroscopy (XPS) analysis:

A chemical analysis of gold-titania core-shell nanoparticles drop coated on Si(111) substrate was carried out by X-ray photoemission spectroscopy (Figure 4.15).

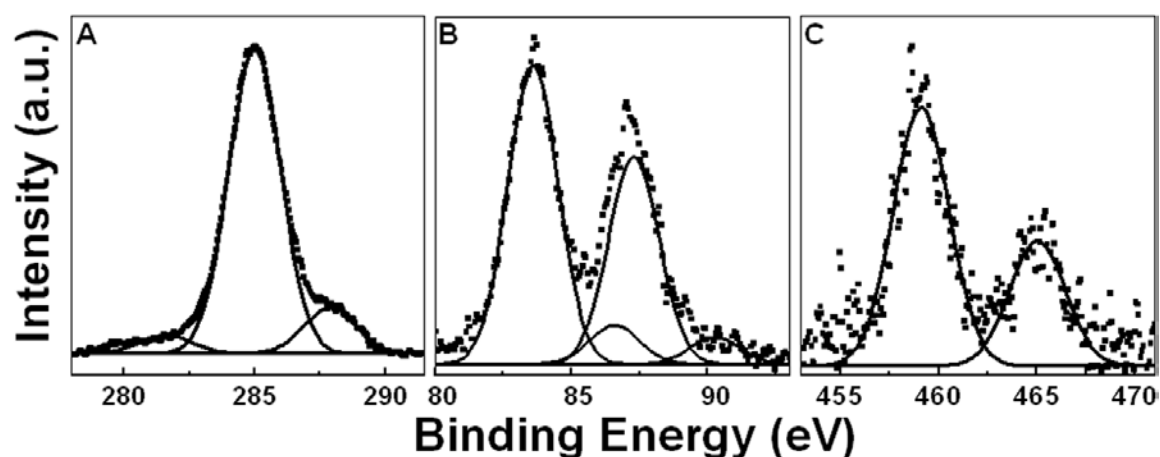


Figure 4.15: XPS spectra recorded from (A) C 1s, (B) Au 4f and (C) Ti 2p core levels of gold-titania core-shell nanoparticles.

Figure 4.15a shows the XPS spectrum for C 1s of gold-titania core-shell nanoparticles. C 1s core level photoemission spectrum is complex and could be stripped into three chemically distinct components. In addition to C 1s peak at 285 eV BE from hydrocarbon chains, peaks at 281.6 and 287.9 eV are also observed. The low BE peak at 281.6 eV is attributed to aromatic carbon from the hydrolyzing protein while the high BE peak at 287.9 eV is assigned to electron emission from carbon present in the carbonyl groups (ketones or carboxylic group of protein) [43]. The Au 4f_{7/2} core level could be decomposed into two distinct components centered at 83.5 and 86.5 eV that correspond

to Au(0) and Au(I) species respectively (Figure 4.15B). The peaks at 83.5 eV can be ascribed to the presence of metallic gold core in core-shell nanoparticles. The Ti 2p core level could also be resolved into the two spin orbit pairs with $2p_{3/2}$ at 459 eV and $2p_{1/2}$ at 465 eV binding energies, which are assigned to the Ti^{4+} oxidation state of TiO_2 (Figure 4.15C) [53]. The spin-orbit splitting between $2p_{3/2}$ and $2p_{1/2}$ core level is 6 eV, which shows the presence of +4 oxidation state of titania in core-shell nanoparticles [54]. The presence of Ti signal in the XPS spectra clearly shows the presence of TiO_2 on the surface of gold nanoparticles.

4.4.7 Summary:

This part of the chapter describes the biological synthesis of gold-titania core-shell nanoparticles using the hydrolyzing protein. The UV-vis spectra and TEM analysis clearly shows the presence of core-shell nanoparticles in the sample. The synthesized core-shell nanoparticles are spherical and rutile and brookite polymorphs of titania are present in shell which are confirmed by the SAED and XRD analyses.

4.5 Conclusion:

Facile protocols for the synthesis of spherical and anisotropic core-shell nanoparticles have been described in this chapter. The triangular Au core-Ag shell nanoparticles are synthesized at room temperature using ascorbic acid as a reducing agent. Ascorbic acid has propensity to reduce silver ions under alkaline conditions, so by varying the pH of gold nanotriangles solutions, different thickness of silver shell could be deposited on the surface of nanoparticles. A large blue shift and a dampening of longitudinal plasmon peak of gold nanotriangles in the UV-vis-NIR spectra is a characteristic feature for the synthesis of triangular core-shell nanoparticles. Owing to highly roughened surface of the core-shell nanoparticles, triangular core-shell nanoparticles might be having potential application in the detection of biomolecules and as a better substrate for Surface Enhance Raman Spectroscopy (SERS) compared to other analogous nanoparticles with smooth surface. The commercially important gold-titania core-shell nanoparticles are also synthesized using hydrolyzing enzyme from fungus *Fusarium oxysporum* at room temperature. The thickness of titania shell is uniform and brookite and rutile phase of titania nanoparticles are synthesized around the surface of

gold core nanoparticles. The spherical gold-titania core-shell nanoparticles can be used as multicolour photochromic material that changes colour reversibly [21] and in photocatalysis under visible and UV light [25].

4.6 References:

- [1] a) Zhou, W. L.; Carpenter, E. E.; Lin, J.; Kumbhar, A.; Slims, J.; O'Connor, C. J. *Eur. Phys. J. D* **2001**, *16*, 289-292. b) Lu, L.; Wang, H.; Zhou, Y.; Xi, S.; Zhang, H.; Hu, J.; Zhao, B. *Chem Commun.* **2002**, *144*. c) Schierhorn, M.; Liz-Marza'n, L. M. *Nano Lett.* **2002**, *2*, 13. d) Liu, M.; Guyot-Sionnest, P. *J. Phys. Chem. B* **2004**, *108*, 5882. e) Selvakannan, PR.; Swami, A.; Srisathiyanarayanan, D.; Shirude, P. S.; Pasricha, R.; Mandale, A. B.; Sastry, M. *Langmuir* **2004**, *20*, 7825. f) Mandal, S.; Selvakannan, PR.; Pasricha, R.; Sastry, M. *J. Am. Chem. Soc.* **2003**, *125*, 8440. g) Damle, C.; Biswas, K.; Sastry, M. *Langmuir* **2001**, *17*, 7156. h) Wu, M-L.; Chen, D-H.; Huang, T-C. *Langmuir* **2001**, *17*, 3877. i) Tan, H.; Li, S.; Fan, W. Y. *J. Phys. Chem. B.* **2006**, *110*, 15812. j) Bala, T.; Arumugam, S.K.; Pasricha, R.; Prasad, B. L. V.; Sastry, M. *J. Mater. Chem.* **2004**, *14*, 1057. k) Bala, T.; Bham, S. D.; Joy, P. A.; Prasad, B. L. V.; Sastry, M. *J. Mater. Chem.* **2004**, *14*, 2941.
- [2] a) Averitt, R. D.; Sarkar, D.; Halas, N. J. *Phys. Rev. Lett.* **1997**, *78*, 4217. b) Yang, Y.; Nogami, M.; Shi, J. L.; Chen, H. R.; Liu, Y.; Qian, S. X. *J. Mater. Chem.* **2003**, *13*, 3026. c) Lei Y.; Chim, W-K. *J. Am. Chem. Soc.* **2005**, *127*, 1487.
- [3] a) Kortan, A. R.; Hull, R.; Opila, R. L.; Bawendi, M. G.; Steigerwald, M. L.; Carroll, P. J.; Brus, L. E. *J. Am. Chem. Soc.* **1990**, *112*, 1327. b) Mews, A.; Kadavanich, A. V.; Banin, U.; Alivisatos, A. P. *Phys. Rev. B* **1996**, *53*, 13242. c) Peng, X. G.; Schlamp, M. C.; Kadavanich, A. V.; Alivisatos, A. P. *J. Am. Chem. Soc.* **1997**, *119*, 7019.
- [4] a) Lu, Y.; Yin, Y. D.; Li, Z. Y.; Xia, Y. N. *Nano Lett.* **2002**, *2*, 785. b) Sakai, H.; Kanda, T.; Shibata, H.; Ohkubo, T.; Abe, M. *J. Am. Chem. Soc.* **2006**, *128*, 4944. c) Eswaranand, V.; Pradeep T. *J. Mater. Chem.* **2002**, *12*, 2421. d) Liz-Marza'n, L. M.; Giersig, M.; Mulvaney, P. *Langmuir* **1996**, *12*, 4329.
- [5] a) Oldenburg, S. J.; Averitt, R. D.; Westcott, S. L.; Halas, N. J. *Chem. Phys. Lett.* **1998**, *288*, 243. b) Graf, C.; Van Blaaderen, A. *Langmuir* **2002**, *18*, 524. c) Hofmeister, H.; Miclea, P-T.; Mrke W. *Part. Part. Syst. Charact.* **2002**, *19*, 359.
- [6] Kim, M.; Sohn, K.; Na, H. B.; Hyeon, T. *Nano Lett.* **2002**, *2*, 1383. b) Nikitenko, S. I.; Koltypin, Y.; Felner, I.; Shames, A. I.; Jiang, J. Z.; Markovich, V.; Gorodetsky, G.;

- Gedanken, A. *J. Phys. Chem. B* **2004**, *108*, 7620. c) Sun, X.; Li Y. *Langmuir* **2005**, *21*, 6019.
- [7] Tang, D.; Yuan, R.; Chai, Y. *J. Phys. Chem. B* **2006**, *110*, 11640.
- [8] Henglein, A. *J. Phys. Chem.* **1993**, *97*, 457.
- [9] a) Srnova-Sloufova, I.; Vickova, B.; Bastl, Z.; Hasslett, T.L. *Langmuir* **2004**, *20*, 3407. b) Bohren, C. F.; Huffman, D. R. *Absorption and Scattering of Light by Small Particles*; Wiley: New York, **1983**.
- [10] a) Caruso, F. *Adv. Mater.* **2001**, *13*, 11. b) Schmid, G. *Chem. Rev.* **1992**, *92*, 1709. c) Aiken, J. D, III.; Finke, R. G. *J. Mol. Catal. A* **1999**, *145*, 1.
- [11] a) Tsuji, M.; Miyamae, N.; Lim, S.; Kimura, K.; Zhang, X.; Hikino, S.; Nishio, M. *Cryst. Growth Des.* **2006**, *6*, 1801. b) Sanedrin, R. G.; Georganopoulou, D. G.; Park, S.; Mirkin, C. A. *Adv. Mater.* **2005**, *17*, 1027.
- [12] Ah, C. S.; Hong, S. D.; Jang, D-J. *J. Phys. Chem. B* **2001**, *105*, 7871.
- [13] Huang, C-C.; Yang, Z.; Chang, H-T. *Langmuir* **2004**, *20*, 6089.
- [14] Sun, Y.; Wiley, B.; Li, Z-Y.; Xia, Y. *J. Am. Chem. Soc.* **2004**, *126*, 9399.
- [15] a) El-Sayed, M. A. *Acc. Chem. Res.* **2001**, *34*, 257. b) Mulvaney P. *Langmuir*, **1996**, *12*, 788.
- [16] Metraux, G.S.; Cao, Y.C.; Jin, R.; Mirkin, C.A. *Nano Lett.* **2003**, *3*, 519.
- [17] a) Kielbassa, S.; Kinne, M.; Behm, R. J. *Langmuir* **2004**, *20*, 6644, b) Ung, T.; Liz-Marza'n, L. M.; Mulvaney P. *J. Phys. Chem. B* **1999**, *103*, 6770. c) Stiehl, J. D., Kim, T. S.; Reeves, C. T.; Meyer, R. J.; Mullins, C. B. *J. Phys. Chem. B* **2004**, *108*, 7917.
- [18] a) Su, C.; Liao, C-H.; Wang, J-D.; Chiu, C-M.; Chen B-J. *Cata. Today* **2004**, *97*, 71. b) Andersson, M.; Osterlund, L.; Ljungstrom S.; Palmqvist, A. *J. Phys. Chem. B*, **2002**, *106*, 10674. c) Sung-Suh, H. M.; Choi, J. R.; Hah, H. J.; Koo, S. M.; Bae, Y. *C. J. Photocata. Photobio. A* **2004**, *163*, 37.
- [19] Miao, S.; Liu, Z.; Han, B.; Zhang, J.; Yu, X.; Du J.; Sun, Z. *J. Mater. Chem.* **2006**, *16*, 579.
- [20] a) Chen, J.; Tang, J.; Yan, F.; Ju, H. *Biomater.* **2006**, *27*, 2313. b) Lin, H-Y.; Chen, C-T.; Chen, Y-C. *Anal. Chem.* **2006**, DOI: 0.1021/ac060833t.
- [21] Naoi, K.; Ohko, Y.; Tatsuma, T. *J. Am. Chem. Soc.* **2004**, *126*, 3664.

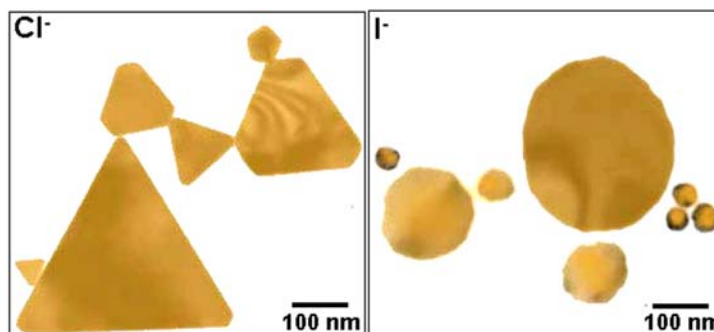
- [22] a) Hall, S. R.; Davis S. A.; Mann, S. *Langmuir* **2000**, *16*, 1454. b) Liz-Marzan, L. M.; Giersig M.; Malvaney, P. *J. Chem. Soc. Chem. Commun.* **1996**, 731. c) Chen, M. M. Yu.; Atz, A. *Langmuir* **2002**, *18*, 8566. d) Poovarodom, S.; Bass, J. D.; Hwang, S-J.; Katz, A. *Langmuir* **2005**, *21*, 12348. e) Nooney, R. I.; Thirunavukkarasu, D.; Chen, Y.; Josephs, R.; Ostafin, A. E. *Langmuir*, **2003**, *19*, 7628. f) Kumar, A.; Pushparaj, V. L.; Murugesan, S.; Viswanathan, G.; Nalamasu, R.; Linhardt, R. J.; Nalamasu, O.; Ajayan, P. M. *Langmuir*, **2006**, *22*, 8631.
- [23] Iawsaki, K.; Torimoto, T.; Shibayama, T.; Takahashi H.; Ohtani, B. *J. Phys. Chem. B* **2004**, *108*, 11946.
- [24] a) Aslam, M.; Fu, L.; Li S.; Dravid, V. P. *J. Colloid. Interface. Sci.* **2005**, *444*, 290. b) Yi, D. K.; Selvan, S. T.; Lee, S. S.; Papaefthymiou, G. C.; Kundaliya D.; Ying, J. *J. Am. Chem. Soc.* **2005**, *127*, 4990.
- [25] a) Kamat, P. V. *Nanoparticles and Nanostructured Films*; J. H. Fendler, Ed.; Wiley-VCH: Weinheim, **1998**; Chapter 9, and references therein. b) Stafford, U.; Gray, K. A.; Kamat, P. V. *J. Phys. Chem.* **1994**, *98*, 6343. c) Ciambelli, P.; Bagnasco, G.; Lisi, L. *Appl. Catal. B* **1992**, *1*, 61. d) Andersson, M.; Osterlund, L.; Ljungstrom, S.; Palmqvist, A. *J. Phys. Chem. B* **2002**, *106*, 10674.
- [26] a) Gao, B.; Ma, Y.; Cao, Y.; Yang, W.; Yao, J. *J. Phys. Chem. B*, **2006**, *110*, 14391. b) Stewart, S. J.; Fernandez-Garcia, M.; Belver, C.; Mun, B. S.; Requejo, F. G. *J. Phys. Chem. B* **2006**, *110*, 16482.
- [27] Hirakawa, T.; Kamat, P. V. *J. Am. Chem. Soc.* **2005**, *127*, 3928.
- [28] a) Sakai, H.; Kanda, T.; Shibata, H.; Ohkubo, T.; Abe, M. *J. Am. Chem. Soc.* **2006**, *128*, 4944. b) Mayya, K. S.; Gittins D. I.; Caruso, F. *Chem. Mater.* **2001**, *13*, 3833. c) Pastoriza-Santos, I.; Koktysh, D. S.; Mamedov, A. A.; Giersig, M.; Kotov, N. A.; Liz-Marzan, L. M. *Langmuir* **2000**, *16*, 2731. d) Tom, R. J.; Nair, A. S.; Singh, N.; Aslam, M.; Nagendra, C. L.; Philip, R.; Vijayamohanan, K.; Pradeep, T. *Langmuir* **2003**, *19*, 3439.
- [29] a) Castillo, P.; Koch, B.; Ruiz, P.; Delmon, B. *J. Mater. Chem.* **1994**, *4*, 903. b) Guo, X. C., Dong, P. *Langmuir* **1999**, *15*, 5535. c) Zhong, Z. Y.; Yin, Y. D.; Gates B.; Xia, Y. N. *Adv. Mater.* **2000**, *12*, 206. d) Holgado, M.; Cintas, A.; Ibisate, M.; Serna, C. J.; Lopez, C.; Meseguer, F. *J. Colloid. Interface. Sci.* **2000**, *229*, 6.

- [30] a) Du, J.; Zhang, J.; Liu, Z.; Han, B.; Jiang T.; Huang, Y. *Langmuir* **2006**, *22*, 1307.
b) Guo, Y-G.; Wan L-J.; Bai, C- L. *J. Phys. Chem. B* **2003**, *107*, 5441.
- [31] Patil, V.; Malvankar, R. B.; Sastry, M. *Langmuir* **1999**, *15*, 8197.
- [32] Bansal, V.; Rautaray, D.; Bharde, A.; Ahire, K.; Sanyal, A.; Ahmad, A. Sastry, M. *J. Mater. Chem.* **2005**, *15*, 2583.
- [33] a) Shankar, S. S.; Rai, A.; Ankamwar, B.; Singh, A.; Ahmad, A.; Sastry, M. *Nature Mater.* **2004**, *3*, 482. b) Shankar, S. S.; Rai, A.; Ahmad, A.; Sastry, M. *Chem. Mater.* **2005**, *17*, 566. c) Shipway, A. N.; Lahav, M.; Gabai, R.; Willner, I. *Langmuir* **2000**, *16*, 8789. d) Kelly, K. L.; Coronado, E.; Zhao, L.; Schatz, G. C. *J. Phys. Chem. B* **2003**, *10*, 668. e) Link, S.; Mohamed, M. B.; El-Sayed, M. A. *J. Phys. Chem. B.* **1999**, *103*, 3073. f) Millstone, J. E.; Park, S.; Shuford, K. L.; Qin, L.; Schatz, G. C.; Mirkin, C. A. *J. Am. Chem. Soc.* **2005**, *127*, 5312. g) Hayens, C. L.; McFarland, A. D.; Zhao, L. L.; Van Duyne, R. P.; Schatz, G. C.; Gunnarsson, L.; Prikulis, J.; Kesemo, B.; Kall, M. *J. Phys. Chem. B* **2003**, *107*, 7337.
- [34] Rivas, L.; Sanchez-Cortes, S.; Garcí'a-Ramos, J. V.; Morcillo, G. *Langmuir* **2000**, *16*, 9722. b) Freeman, R. G.; Hommer, M. B.; Grabar, K. C.; Jackson, M. A.; Natan, M. J. *J. Phys. Chem.* **1996**, *100*, 718.
- [35] a) Kim, F.; Song, J. H.; Yang, P.; *J. Am. Chem. Soc.* **2002**, *124*, 14316. b) Nikoobakht, B.; El-Sayed, M. A. *Chem. Mater.* **2003**, *15*, 1957. c) Pal, T.; De, S.; Jana, N. R.; Pradhan, N.; Mandal, R.; Pal, A.; Beezer, A. E.; Mitchell, J. C. *Langmuir* **1998**, *14*, 4724. d) Hodak, J. H.; Henglein, A.; Giersig, M.; Hartland, G. V.; *J. Phys. Chem. B.* **2000**, *104*, 11708.
- [36] a) Mulvaney, P. *Langmuir* **1996**, *12*, 788. b) Ah, C. S.; Hong, S. D.; Jang, D-J. *J. Phys. Chem. B* **2001**, *105*, 7871.
- [37] Srnova-Sloufova, I.; Lednicky, F.; Gemperle, A.; Gemperlova, J. *Langmuir* **2000**, *16*, 9928.
- [38] a) Jin, R.; Cao, Y.; Mirkin, C. A.; Kelly, K. L.; Schatz, G. C.; Zheng, J. *G. Science* **2001**, *294*, 1901. b) Jin, R.; Cao, Y. C.; Hao, E.; Métraux, G. S.; Schatz, G. C.; Mirkin, C. A. *Nature* **2003**, *425*, 487.
- [39] Germain, V.; Li, J.; Ingert, D.; Wang, Z. L.; Pileni, M. P.; *J. Phys. Chem. B* **2003**, *107*, 8717.

- [40] a) Shao, Y.; Jin, Y.; Dong, S.; *Chem. Commun.* **2004**, 1104. b) Malikova, N.; Pastoriza-Santos, I.; Schierhorn, M.; Kotov, N. A.; Liz-Marzan, L. M. *Langmuir* **2002**, 18, 3694.
- [41] Shirley, D. A. *Phys. Rev. B* **1972**, 5, 4709.
- [42] a) Miyama, T.; Yonezawa, Y. *Langmuir* **2004**, 20, 5918. b) Kumar, A.; Mandal, S.; Selvakannan, P. R.; Pasricha, R.; Mandale, A. B. Sastry, M. *Langmuir* **2003**, 19, 6277.
- [43] Sastry, M.; Ganguly, P. *J. Phys. Chem. A* **1998**, 102, 697.
- [44] Liu, Y. C.; Chuang, T. C. *J. Phys. Chem. B* **2003**, 107, 12383.
- [45] Fadley, C. S.; Shirley, D. A. *J. Res. Nat. Bur. Stand. (U.S.)* **1970**, 74A, 543.
- [46] The XRD patterns were indexed with reference to the crystal structures from ASTM chart: titania (ASTM chart number 3-0380 for brookite).
- [47] Malvaney, P.; Underwood, S. *Langmuir*, **1994**, 10, 3427.
- [48] Joshi, H.; Shirude, P. S.; Bansal, V.; Ganesh K. N.; Sastry, M. *J. Phys. Chem. B* **2004**, 108, 11535.
- [49] a) Link, S.; El-Sayed, M. A. *J. Phys. Chem. B* **1999**, 103, 8410. b) Hearth, J. R.; Knobler, C. M.; Leff, D. V. *J. Phys. Chem. B* **1997**, 101, 189.
- [50] Lide, D. R. *Handbook of Chemistry and Physics*, 81st Edition, **2000**, 4.
- [51] Nakamura, R.; Imanishi, A.; Murakoshi, K.; Nakato, Y. *J. Am. Chem. Soc.* **2003**, 125, 7443.
- [52] a) Shafi, K. V. P. M.; Ulman, A.; Yan, X.; Yang, N. L.; Himmelhaus M.; Grunze, M. *Langmuir*, **2001**, 17, 1726. b) Lee, L. H.; Chen, Y. C. *Chem. Mater.* **2001**, 13, 1137.
- [53] Yang, H. G.; Zeng, H. C. *J. Phys. Chem. B* **2004**, 108, 3492.
- [54] Zhang, Q. L.; Du, L. C.; Weng, Y. X.; Wang, L.; Chen H. Y.; Li, J. Q. *J. Phys. Chem. B* **2004**, 108, 15077.

Chapter V

Morphological Transformation of Gold Nanotriangles Using Chemical Approaches



This chapter describes the morphological transformation of gold nanotriangles using different halide ions (F^- , Cl^- , Br^- , I^-). Halide ions form an incommensurate adlayer on Au (111) lattice planes, in which iodide ions have the highest mismatch with the underlying Au (111) plane in comparison with bromide, chloride and fluoride ions respectively. Iodide ions completely hinder the growth of nanotriangles while bromide ions promote the synthesis of spherical and triangular nanoparticles. Chloride and fluoride ions do not significantly affect the morphology of triangular gold nanoparticles during their synthesis. Halide ions also transform the morphology of already synthesized gold nanotriangles. Iodide and bromide ions transform nanotriangles into circular plate structures and corrugated edged nanotriangles respectively, while chloride and fluoride ions do not impose any transformation on the morphology of nanotriangles. CTAB also has the ability to transform nanotriangles into circular nanoplates, while CTAC does not impart morphological changes in nanotriangles. An attempt has been made to investigate the reversible transformation of circular plate nanoparticles into plane edged gold nanotriangles. Different concentrations of gold ions in the presence of CTAB or CTAC have been used for the modification of gold nanotriangles into highly complex nanostructures, which has also been discussed in this chapter.

Part of the work presented in this chapter has been published:

Rai, A.; Singh, A.; Ahmad, A.; Sastry, M. *Langmuir* **2006**, *22*, 736.

5.1 Introduction:

Morphology controlled synthesis of nanoparticles is a great challenge in materials chemistry because of the strong correlation between the shape and the chemical, physical, optical, electronic, magnetic and catalytic properties of nanoparticles [1]. A wealth of chemical methods have been developed for the synthesis of well-controlled nanoparticle morphologies including prisms [2], rods [3], cubes [4], wires [5], belts [6] and branched multipods [7]. The size and shape controlled synthesis of nanoparticles requires template-based methods (e.g. surfactants [4b,c, f] and anodic porous alumina membranes [8]) and controlled growth condition [9] in the reaction medium.

Though the mechanisms for crystal growth of nanorods have been established by various groups, few attempts have been made to completely understand the growth of triangular nanoparticles. Murphy and coworkers had extensively studied the synthesis of nanorods in the presence of CTAB and attributed the formation of rod-like micelles in solution for the growth of anisotropic nanoparticles. However, they later postulated that CTAB preferentially adsorbs to the long axis crystal faces of nanorods [4c,d, f]. Pileni's group had synthesized copper nanorods in reverse micelles and attributed the shape of nanoparticles to the shape of the micelles [10]. The general strategy to synthesize anisotropic nanoparticles is to induce different relative growth rates of different crystallographic facets. Anisotropic growth of nanoparticles can be achieved by the presence of specific molecules in the growth medium that have preferential binding to different crystallographic facets, while the particles nucleate and grow in solution [2g, 11]. Assembly and sintering of small sized nanoparticles into silver nanotriangles in solution using photo-irradiation approach was proposed by Mirkin's group [2a,b]. Recently, defects and presence of twin planes in silver and gold nanoparticles has been attributed to direct the shape of initially formed nanoparticles into nanotriangles or high aspect ratio platelets [12].

In chapter 3, synthesis of triangular nanoparticles using lemongrass extract was described. It was observed that several ions and molecules are present in the reaction solution, which might be responsible for the growth of gold nanotriangles [2c, d]. Broadly, ketonic and aldehydic functional groups as well as molecules below the size of 30 kDa were claimed to be responsible for the growth of nanotriangles. It is highly

possible that not a single molecule, but many molecules together play a synergistic role and adsorb on certain crystallographic faces of initially formed metal nuclei to promote the growth of triangular morphology. In this chapter, an attempt has been made to understand the role of a single molecule for crystal growth of nanotriangles, in greater detail. In order to study the effect of various halide ions on gold nanoparticle morphology, different salts containing a common cation, but varying halide ions *viz.* KF, KCl, KBr and KI were individually added in the lemongrass-gold ion (AuCl_4^-) growth medium and the effect of these halide ions on the crystal morphology was observed. Iodide and bromide ions are known to be capable of replacing chloride ions from the gold nanotriangles and forming adlayers on the underlying Au (111) lattice planes [13]. Our principal observation is that chloride ions promote the synthesis of nanotriangles while bromide and iodide ions inhibit their growth. Fluoride ions are unable to impose any affect on the crystal growth of nanotriangles. Iodide ions are well known to chemisorb and form an adlayer on the underlying gold, which have largest mismatch with Au (111) lattice plane as compared to other halide ions [14]. The mismatch between gold lattice plane and the iodide ion adlayer creates a strain on the surface of initially formed nanoparticles that inhibits the growth of nanotriangles. Recently, the role of halide ions on crystal growth has gained much attention. Pileni's group has demonstrated that presence of halide ions does not change the morphology of micellar template but drastically change the morphology of copper crystal formed in the solution. They found that NaCl and NaBr promote the synthesis of rod and cubic copper nanocrystals respectively while NaF does not promote any specific shape [13]. Sastry's group has recently shown the effect of halide ions on the morphology of citric acid reduced gold nanotriangles [15]. The effect of chloride ions on the syntheses of silver and copper nanoparticles has also been shown by Xia *et al.* and Roberts *et al.* respectively [16].

An attempt has also been made in this chapter to understand the role of halide ions on the morphology of already formed gold nanotriangles. We observe that iodide ions completely transform the preformed gold nanotriangles into circular plate like structures, while bromide ions induce corrugation at the edges of nanotriangles. In the case of iodide ions, the strain developed on the nanotriangles after adsorption on (111)

lattice planes modifies the nanotriangles into circular disc like nanostructures. Chloride and fluoride ions do not impart any effect on the morphology of gold nanotriangles.

Studies on the morphological change induced by cationic surfactants such as cetyl-trimethylammonium bromide (CTAB) and cetyl-trimethylammonium chloride (CTAC) has also been discussed in this chapter. Though, 10^{-2} M CTAB significantly alters the morphology of triangles to circular plates and corrugated-edged triangles, lower concentrations (10^{-3} M to 10^{-5} M) of CTAB do not have significant affect on the morphology. Halas' group has shown reshaping of metallodielectric nanoparticles upon exposure to CTAB in the aqueous solution [17]. The morphology of gold nanotriangles after treatment with various concentrations of CTAC (10^{-2} M to 10^{-5} M) is intact and similar to lemongrass reduced gold nanotriangles. The reversible transformation of circular nanoplates into triangular nanoparticles using a dialysis method indicates the physical adsorption of surfactants on the surface of gold nanoparticles. Stoeva *et al.* have demonstrated the reversible transformation of gold nanoparticle morphology using alkanethiols and positively charged surfactant didodecyldimethylammonium bromide (DDAB) [18]. It remains a challenge to develop synthesis procedures to achieve complex metal nanostructures because of their wide range of application in catalysis, optical and electronic properties [19]. The addition of different concentrations of gold ions on the CTAB or CTAC bound gold nanotriangles lead to highly complex nanostructures, which is also described in this chapter. The high concentration of gold ions (10^{-2} M) convert CTAB bound gold nanotriangles into highly branched nanostructures while the lower concentration (10^{-5} M) of gold ions oxidize the sharp tips of nanotriangles into circular tips. Gold ions are known to oxidize gold nanoparticles in the presence of CTAB. Nanocoral and nanoflower like structures are obtained after addition of varying concentrations of gold ions in the CTAC bound gold nanotriangles.

5.2 Effect of halide ions on the morphology of gold nanotriangles during synthesis:

5.2.1 Experimental Details:

The effect of different halide ions on the morphology of gold nanoparticles during synthesis was investigated by adding 1 mL of 10^{-2} M respective KX solution (KX=KF,

KCl, KBr and KI) in 9 mL of 10^{-3} M HAuCl₄ solutions containing 0.8 mL of lemongrass extract. The synthesis of gold nanoparticles was investigated using UV-vis-NIR spectroscopy and TEM analysis. The UV-vis-NIR spectra of gold nanoparticles solution containing different halide ions were recorded after 24 h of reactions.

5.2.2 UV-vis-NIR spectroscopy and TEM analysis:

Figure 5.1 shows the UV-vis-NIR spectra of gold nanoparticles synthesized using lemongrass extract in absence (curve 1) and presence of different halide ions (10^{-3} M KF, KCl, KBr and KI) (curves 2-5 respectively). The spectra were recorded after 24 h of reaction. The gold nanotriangle solution without halide ions shows two distinct absorption bands (curve 1) centered at 538 nm (transverse SPR band) and 1035 nm (longitudinal SPR band) [2, 3].

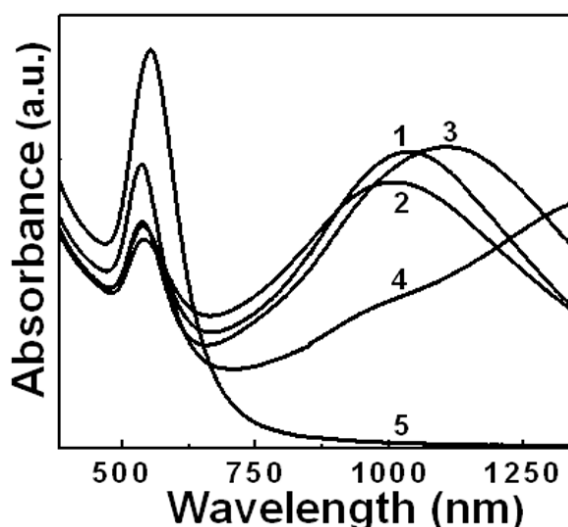


Figure 5.1: UV-vis-NIR spectra recorded from the gold nanotriangles synthesized using lemongrass extract in the absence of halide ions (curves 1) and presence of KF (curve 2), KCl (curve 3), KBr (curve 4) and KI (curve 5).

The TEM image (Figure 5.2A) recorded from this solution indeed shows highly anisotropic flat gold nanotriangles along with spherical nanoparticles. Some of the gold nanotriangles have truncated vertices with edge-to-edge length of ca. 250 nm. The gold nanoparticles synthesized by lemongrass extract possibly have sugar derivative molecules on their surface [4c, d] along with chloride ions contributed from the chloroaurate ions during the reduction process, which has been discussed in the chapter 3. The optical

absorption spectrum of gold nanoparticles synthesized in the presence of KF (curve 2, Figure 5.1) shows a blue shift of 25 nm in the longitudinal SPR band of gold nanotriangles relative to gold nanotriangles synthesized in the absence of halide ions. Along with a blue shift, it is observed that an intensity of both absorption bands has decreased. The size and shape of gold nanotriangles synthesized in the presence of KF are essentially same as compared to nanoparticles synthesized in the absence of halide ions and have well-faceted and truncated morphology (Figure 5.2B). The gold nanoparticles synthesized in the presence of KCl show a large red shift of 80 nm in the longitudinal SPR band (in plane vibration) of gold nanotriangles (curve 3, Figure 5.1).

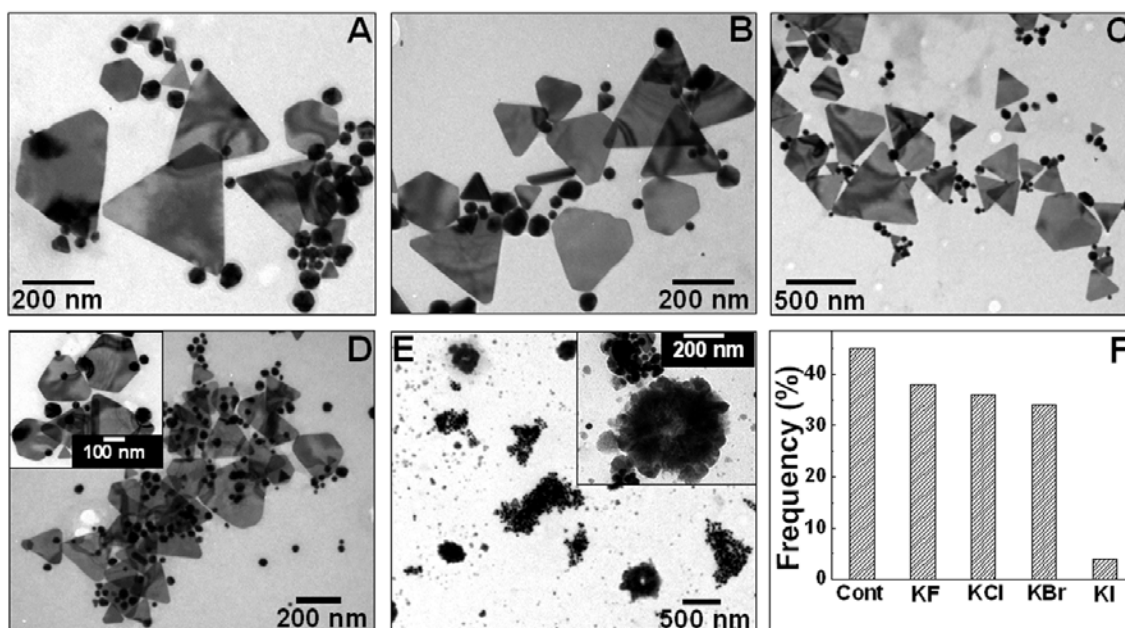


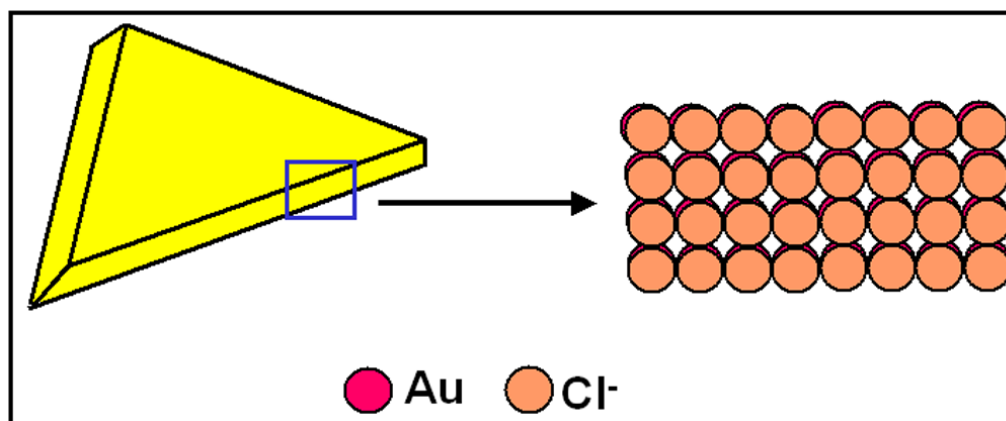
Figure 5.2: TEM images recorded from the gold nanotriangles synthesized in the absence of halide ions (A) and presence of KF (B), KCl (C), KBr (D) and KI (E). The insets of Figure 5.2 D and E show the higher magnification TEM images of gold nanoparticles synthesized in presence of KBr and KI respectively. (F) The histogram analysis of percentage of gold nanotriangles synthesized in the presence of different halide ions.

The TEM image (Figure 5.2C) of gold nanotriangles formed in the presence of KCl shows that the gold nanotriangles are larger in size than control (Figure 5.2A) and have edge length of ca. 320 nm that is in good agreement with the UV-vis-NIR data (curve 1). A pronounced change was observed in the UV-vis-NIR spectrum of gold nanoparticles synthesized in the presence of KBr (curve 4, Figure 5.1). The position of longitudinal SPR band appears to be red shift beyond 1400 nm and is accompanied by an

increase in transverse component of SPR band. The TEM image (Figure 5.2C) shows a large percentage of spherical particles with a marginal increased in edge length of flat gold nanotriangles, which is corroborated with curve 4 of Figure 5.1. The inset of Figure 5.2D shows the higher magnification TEM image of gold nanoparticles synthesized in presence of Br^- ions. It is observed that the smooth-edged gold nanotriangles and hexagons are synthesized in the presence of Br^- ions. A drastic change was observed in the UV-vis-NIR spectrum of gold nanoparticles formed in the presence of KI wherein, an intense SPR band positioned at 554 nm is observed with no evidence of band in the NIR region of the electromagnetic spectrum (curve 5, Figure 5.1). The change in behavior of the UV-vis-NIR spectrum is mirrored in the TEM image of gold nanoparticles (Figure 5.2E). The TEM image of gold nanoparticles synthesized in the presence of I^- ions shows mostly spherical particles with absence of triangular nanoparticles (Figure 5.2E). A small percentage of spherical aggregated nanoparticles can also be seen in the TEM image. I^- ions thus appear to strongly suppress the growth of triangular nanoparticles. The inset of Figure 5.2E shows the higher magnification TEM image of aggregated spherical gold nanoparticles, which is consistent with the corresponding UV-vis-NIR spectrum (curve 5, Figure 5.1), where a single intense absorption band centered at ca. 554 nm is observed. Similar aggregated nanostructures were also observed by Cheng *et al.* in their study of the effect of aqueous KI solution on the morphology of spherical citrate reduced gold nanoparticles, synthesized under boiling conditions [21]. Figure 5.2F shows the relative population of gold nanotriangles when chloroaurate ions were reduced using lemongrass extract in the presence of different halide ions. The population of gold nanotriangles is drastically decreased when different halide ions (KX) were added in the reaction solution during synthesis. Thus, the number of gold nanotriangles is decreased from 45% in control to 4% in the presence of I^- ion, while F^- , Cl^- , and Br^- ions show intermittent population. This result is consistent with the UV-vis-NIR data and TEM results for the corresponding halide ions (Figure 5.1 and 5.2 respectively).

The change in morphology of gold nanoparticles in presence of different halide ions during the synthesis may be rationalized as follows: F^- ions are found not to strongly chemisorb on the surface of gold nanoparticles [22]. Thus, the presence of F^- ions does not significantly alter the size and shape of nanotriangle to any noticeable extent. This is

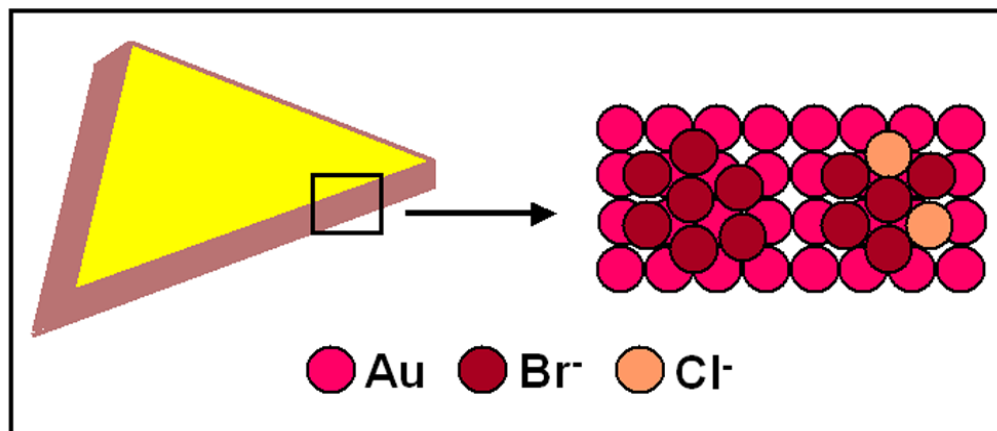
concomitant with the UV-vis-NIR data and TEM images. On the other side, Cl^- , Br^- and I^- ions have the ability to chemisorb on nanoparticle surface and form Au-X bond with force constants in the order of $\text{I}^- > \text{Br}^- > \text{Cl}^-$ [22, 23]. These halide ions have different binding strengths to compete with biomolecules and chloride ions to bind to the nanoparticles surface due to their varying ligating abilities. It is reported that thiols and phosphines, which have better charge transfer ability and polarizability, strongly interact with gold surface in comparison with other functional groups like alcoholic group [24]. The structures of adlayer formed on the surface of gold by Cl^- , Br^- and I^- ions have been well characterized and formation of an incommensurate adlayer of halide ions on gold surface is well established [14, 25].



Scheme 5.1: Schematic showing the adlayer of chloride ions on the Au (111) lattice plane.

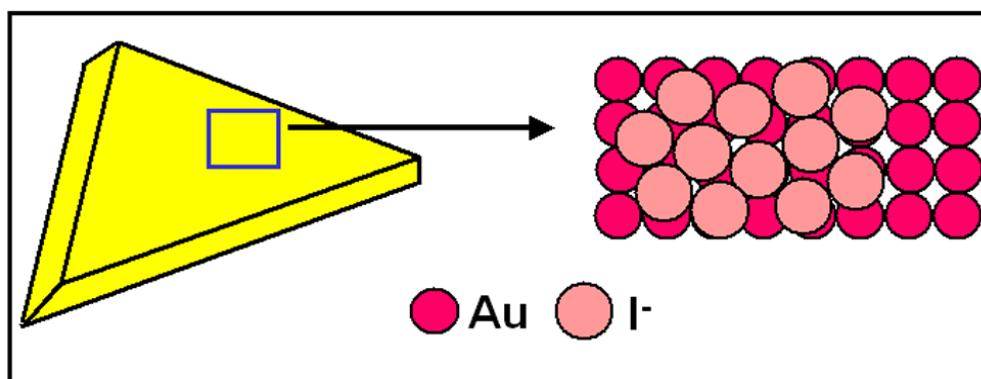
Chloride ions are known to form hexagonal close packed adlayer on Au (111) lattice planes, which is better aligned with the underlying lattice plane of gold. The scheme 5.1 shows the hexagonal packed adlayer of Cl^- ions on the surface of gold nanotriangles. The slight mismatch between the Cl^- ions adlayer and the gold lattice plane causes development of residual strain on the surface of smaller nanoparticles synthesized during initial period of reaction. The strain develops defects like twin planes on the surface, which leads to the oriented growth of smaller nanoparticles into gold nanotriangles. Lofton and Sigmund have also showed that defects in seed nanoparticles play a crucial role in the growth of two-dimensional nanostructures like nanotriangles [12a]. It is also possible that the formation of flat [111] oriented gold nanotriangles or truncated nanotriangles is a result of cooperative effect of Cl^- ions and the biomolecules

present in lemongrass extract. The observed changes in the UV-vis-NIR spectrum could thus be a result of the variation in the relative concentration of competing anions and surface-active biomolecules, which may lead to change in the size and shape of gold nanoparticles.



Scheme 5.2: Schematic showing the adlayer of bromide ions on the edges of gold nanotriangle.

Bromide ions are also known to chemisorb on the surface of gold and form hexagonal packed adlayer with more mismatch with the underlying Au (111) lattice plane relative to chloride ions adlayer on Au (111) plane [25], which is shown in the Scheme 5.2. The mismatch hinders the insignificant growth of gold nanotriangles and promotes the synthesis of spherical nanoparticles, which is in accord with the UV-vis-NIR data and TEM images (Figure 5.1 and 5.2E respectively).



Scheme 5.3: Schematic showing the adlayer of iodide ions on the (111) plane of gold nanotriangle.

The I⁻ ions adlayer has the largest mismatch with Au (111) lattice plane in comparison with other halide ions adlayers (Scheme 5.3) [14], and thus develops interfacial strain, which is not favorable for the formation of gold nanoparticles with extended (111) plane as required for nanotriangle synthesis. We believe that high strain developed on the surface of initially formed nanoparticles prevents two-dimensional growth of nanoparticles and therefore promotes the synthesis of spherical nanoparticles as shown in the TEM image (Figure 5.2E). The aggregation of nanoparticles in the presence of KI could be due to increased covalency of Au-I bond as compared to the other Au-X bonds [21,23].

5.3 Morphological transformation of preformed gold nanotriangles induced by halide ions:

5.3.1 Experimental Details:

Gold nanotriangles were synthesized using the same protocol, which has previously been described in chapter three. The gold nanotriangle solution was purified by repeated centrifugation at 1000 rpm for 15 min (three cycles) followed by redispersion of gold nanotriangles pellet in water. The three times of centrifugation enhanced the percentage of gold nanotriangles relative to spherical nanoparticles from 45 to 95%. To study the effect of halide ions on the morphology of already synthesized and purified gold nanotriangles, 1 mL of 10⁻² M KX (KF, KCl, KBr and KI) solutions were added in 9 mL of purified gold nanotriangle solutions so that the final concentrations of halide ions became 10⁻³ M in 10 mL of solutions and the solutions were further incubated at room temperature for 24 h. UV-vis-NIR spectroscopy, TEM and AFM measurements were done to investigate the change in morphology of gold nanotriangles. AFM measurement was performed in the contact mode to analyze the morphology of nanoparticles. Before doing the XPS measurement, gold nanotriangle solutions treated with halide ions were centrifuged three times to remove the unbound halide ions.

5.3.2 UV-vis-NIR spectroscopy and TEM analysis:

It is interesting to investigate the effect of different halide ions on the morphology of already synthesized lemongrass reduced gold nanotriangles. It is clear that I⁻ ions

among all other halide ions exert most strain on the surface of gold nanoparticles due to largest mismatch with Au (111) plane and therefore they have highest ability to transform the morphology of gold nanoparticles surface [14]. Figure 5.3 shows the UV-vis-NIR spectra of purified gold nanotriangles after treatment with 10^{-3} M concentration of different halide ions (KX) and the spectra were recorded after 24 h of reaction. Curve 1 in Figure 5.3, corresponding to the UV-vis-NIR spectrum of purified gold nanotriangles shows two absorption bands; one at ca. 540 nm as the transverse SPR band and another at ca. 1240 nm as the longitudinal SPR band. A pronounced decrease in the intensity of transverse band in comparison with the corresponding band in the spectrum of as prepared gold nanoparticles (curve 1, Figure 5.1) clearly indicates the removal of maximum population of spherical particles from gold nanotriangle solution.

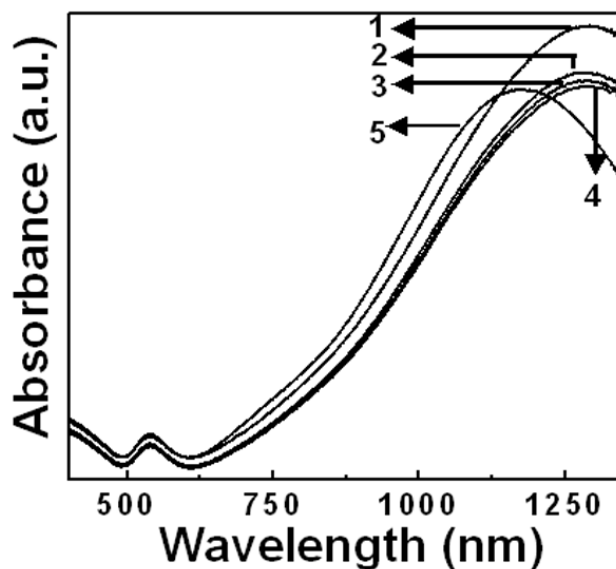


Figure 5.3: UV-vis-NIR spectra recorded for purified gold nanotriangles in the absence of halide ions (curve 1) and after treatment with KF (curve 2), KCl (curve 3), KBr (curve 4) and KI (curve 5).

These purified gold nanotriangles are used for the further experiments. The TEM image (Figure 5.4A) recorded from this solution shows gold nanotriangles with sharp tips as well as with truncated vertices, without the presence of any spherical nanoparticles, which is consistent with the UV-vis-NIR spectrum of purified gold nanotriangles (curve 1, Figure 5.3). The gold nanotriangles have plane and well-defined faceted edges (Figure 5.4A). The UV-vis-NIR spectra of gold nanotriangles treated with 10^{-3} M KF, KCl and

KBr show no shift in the absorption bands as compared to control (curves 2 to 4) and only minor decrease in the intensity of longitudinal band are observed. The addition of KF and KCl did not show any noticeable change in the morphology of gold nanotriangles as observed in the TEM analysis (Figure 5.4B and C), which is in good agreement with the UV-vis-NIR data. Fluoride ions do not have affinity to chemisorb on the surface of gold while Cl⁻ ions preferentially adsorb on surfaces and form adlayer, which is incommensurate with underlying Au (111) plane [22,23]. These ions do not induce interfacial strain and hence change in the morphology of gold nanotriangles is not observed in the TEM images. Though, addition of KBr does not show any change in the UV-vis-NIR data, a small change in the morphology of nanotriangles is observed in the TEM analysis (Figure 5.4D).

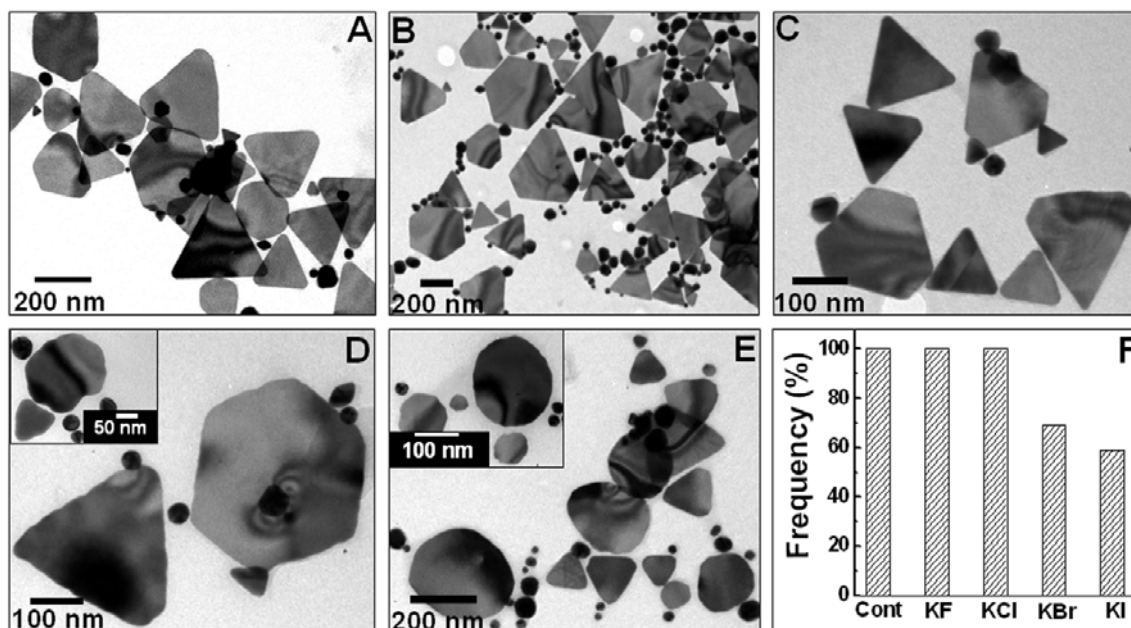


Figure 5.4: TEM images of (A) purified gold nanotriangles in the absence of halide ions and gold nanotriangles treated with (B) KF, (C) KCl, (D) KBr and (E) KI. The insets of Figure 5.4D and E show higher magnification TEM image of nanotriangles treated with KBr and KI respectively. (F) Histogram analysis of percentage of gold nanotriangles after treatment with different halide ions.

It is seen that most of the nanotriangle edges have undergone some changes but the morphology of triangles is still intact in most of the nanoparticles. The edges of nanotriangles are corrugated and have lost the faceted structure after exposure to KBr. The inset of Figure 5.4D shows the higher magnification TEM image of corrugated-

edged gold nanotriangles along with elongated plate like nanostructures after treatment with KBr. Thus, Br^- ions seem to have more inclination to interact with edges of gold nanotriangles as shown in scheme 5.2. It is reported that Br^- ions interact specifically with (110) plane instead of (111) plane [13]. As discussed in earlier chapter, the edges of gold nanotriangles have (110) and (111) planes [26], so Br^- ions chemisorb on the (110) plane of gold nanotriangles as is also evident during nanorod formation [3]. Br^- ions adsorption on the surface is observed to induce reconstruction and hence leads to transformation of plane edged nanotriangles into wavy edged and ill-faceted nanotriangles. No change in the UV-vis-NIR spectrum but a noticeable change in the morphology of nanotriangles in the TEM images clearly reveals that transformation of edges of nanotriangles does not lead to thickening or change in the lateral dimensions of gold nanotriangles. The treatment of gold nanotriangles with KI is observed to have much influence on the morphology and the nanoparticles are transformed into circular and disc like nanostructures (Figure 5.4E). The inset of Figure 5.4 E shows the higher magnification TEM image of circular nanoplates with serrated edges. Iodide ions are reported to have the largest mismatch with underlying Au (111) lattice plane and thus induce more strain on the Au surface, which facilitates the transformation of triangular morphology into circular plate structures to relieve the imposed strain [25]. In fact, I^- ions are known to induce surface reconstruction in case of bulk gold [25c]. Since the nanotriangles are around 20 nm thick, the strain developed on the surface of nanoparticles translates throughout the crystal and completely transforms the triangular structure into circular plate like morphology. It is possible that the strain on surface is relieved via transformation of the morphology. Figure 5.4F shows the histogram analysis of percentage of gold nanotriangles present in solutions after treatment with different halide ions. In case of KF and KCl treated solutions, nanotriangles population are same (100%) as the control while 30% and 40% of nanotriangles are transformed into wavy edged and circular plate like structures in the presence of KBr and KI respectively.

5.3.3 Atomic force microscopy (AFM) analysis:

Figure 5.5 shows the contact mode AFM images of gold nanotriangles treated with KCl, KBr and KI respectively. Figure 5.5A, which corresponds to KCl treated gold

nanotriangles, shows truncated gold nanotriangles. It can clearly be seen from the AFM image that the tips and edges of nanotriangles are sharp and the modification in the morphology of nanotriangles is not observed. In case of KBr treated gold nanotriangles (Figure 5.5B), the tips of the nanotriangles are transformed into circular structures but the overall morphology is still triangular. Conversely, the gold nanotriangles are totally modified into circular plate like nanostructures upon exposure to KI (Figure 5.5C). AFM results of halide ions treated gold nanotriangles are in good agreement with corresponding TEM images (Figure 5.4C-E).

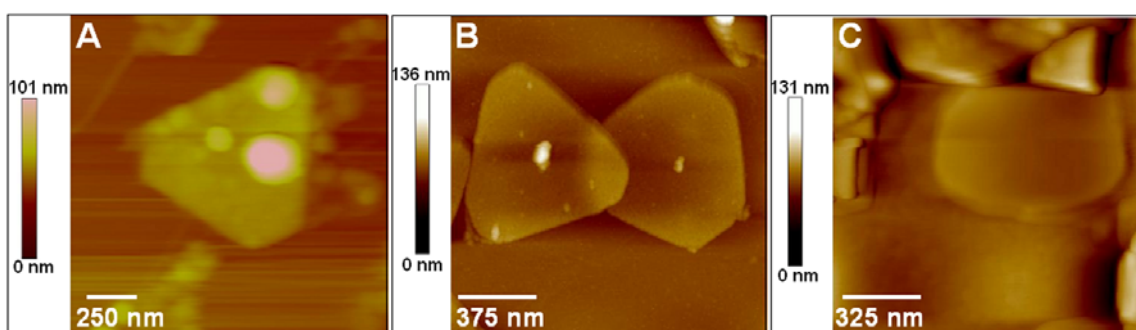


Figure 5.5: Contact mode AFM images of gold nanotriangles after treatment with KCl (A), KBr (B) and KI (C). The AFM images (A, B and C) are height mode image.

5.3.4 X-ray photoemission spectroscopy (XPS) analysis:

The presence or absence of different halide ions on the surface of already synthesized gold nanotriangles after exposure to KF, KCl, KBr and KI were investigated by XPS measurements (Figure 5.6). The gold nanotriangles after treatment with different halide ions were thoroughly washed with water by centrifugation in order to remove unbound halide ions on the surface, prior to casting the thin film on Si (111) substrate for the XPS analysis. In the case of gold nanotriangles exposed to KF, the F 1s core level signal was very poor and below the detection limits of the instrument used (Figure 5.6A). This clearly indicates that F⁻ ions do not play a crucial role in the morphological alternation of gold nanotriangles. Fluoride ions are unable to displace surface bound chloride ions from the surface of nanoparticles that arises as a by-product during the reduction of H₂AuCl₄ using lemongrass extract. The presence of small amount of chloride ions on the surface of gold nanotriangles has been discussed in third chapter. The XPS spectrum of chloride ions treated gold nanotriangles shows detectable signal of Cl 2p

core level due to adsorption of chlorine on the surface (Figure 5.6B). In the case of KBr and KI treated gold nanotriangles, the strong signals of Br 3d and I 3d core levels are obtained, which indicate that these ions strongly bind to the surface of nanoparticles and induce morphological alternation to the gold nanotriangles (Figure 5.6C and D). These results are consistent with the TEM images (Figure 5.4) wherein the morphology alternations are observed after exposure to KBr and KI respectively.

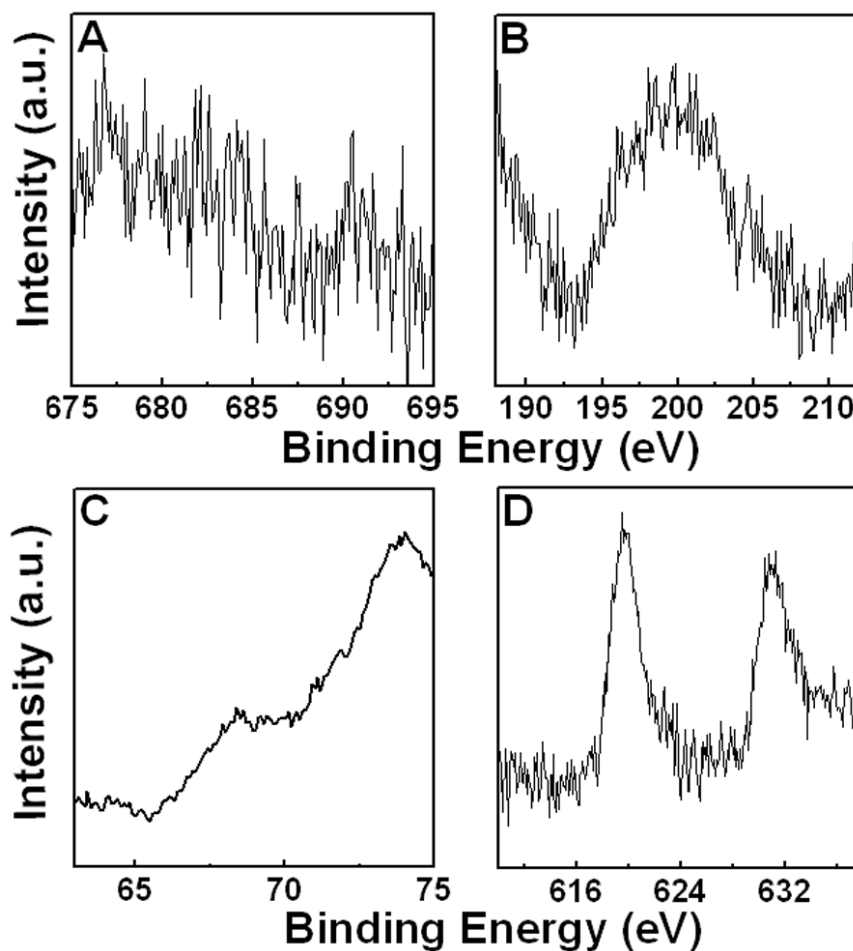


Figure 5.6: XPS spectra recorded for F 1s (A), Cl 2p (B), Br 3d (C) and I 3d (D) core levels, arising from gold nanotriangles treated with KF, KCl, KBr and KI respectively.

5.4 Effect of cationic surfactants on the morphology of gold nanotriangles:

5.4.1 Experimental Details:

To study the effect of different cationic surfactants (CTAB and CTAC) on the morphology of already synthesized gold nanotriangles, different volumes of 10^{-1} M

CTAB and CTAC were added in 9 mL of purified gold nanotriangle solutions to yield different concentrations of surfactants (10^{-2} M, 10^{-3} M, 10^{-4} M and 10^{-5} M respectively) and appropriate amount of water was added in solutions to make up final volume 10 mL. For studying the reversible transformation of nanotriangle morphology, 12.5 kDa dialysis bag (Sigma Chemicals) was preprocessed to remove the impurities as instructed by the manufacture. 10^{-2} M CTAB treated gold nanotriangle solution was dialyzed for 24 h to remove unbound CTAB from the gold nanotriangles solution with frequent change of Milli-Q water. UV-vis-NIR spectroscopy, Fourier transform infrared spectroscopy (FTIR), Transmission electron microscopy (TEM), Atomic force microscopy (AFM) and X-rays photoemission spectroscopy (XPS) were carried out to analyze the change in morphology of gold nanotriangles. The core level spectra were background corrected using the Shirley algorithm [20] and chemically distinct species were resolved using a nonlinear least squares procedure. The core level binding energies (BEs) were aligned with adventitious carbon binding energy of 285 eV. For all the XPS measurements, gold nanoparticle solutions after surfactants treatments were subjected to four cycles of centrifugation and redispersion in deionized water in order to free the nanoparticles from any unbound ions/molecules present in the initial solutions.

5.4.2 UV-vis-NIR and TEM analysis:

Figure 5.7A and B show the UV-vis-NIR spectra of gold nanotriangles treated with different concentrations (10^{-2} M, 10^{-3} M, 10^{-4} M and 10^{-5} M respectively) of cetyl-trimethylammonium bromide (CTAB) and cetyl-trimethylammonium chloride (CTAC) respectively. Curve 1 in Figure 5.7A and B, which corresponds to purified gold nanotriangles, show the transverse component of the surface plasmon (SP) band centered at 540 nm while the longitudinal component appears to go beyond 1400 nm in the NIR region. The optical absorption spectra of gold nanotriangles treated with different concentrations of CTAB and CTAC (curves 2 to 4 of Figure 5.7A and B correspond to 10^{-5} M, 10^{-4} M and 10^{-3} M concentrations of CTAB and CTAC respectively) show the surface plasmon (SP) band similar to purified gold nanotriangles (curve 1). The UV-vis-NIR spectra of gold nanotriangles treated with 10^{-2} M CTAB and CTAC (curve 5 of Figure 5.7A and B) show distinct longitudinal plasmon peak at 1250 nm along with the transverse peak at 540 nm.

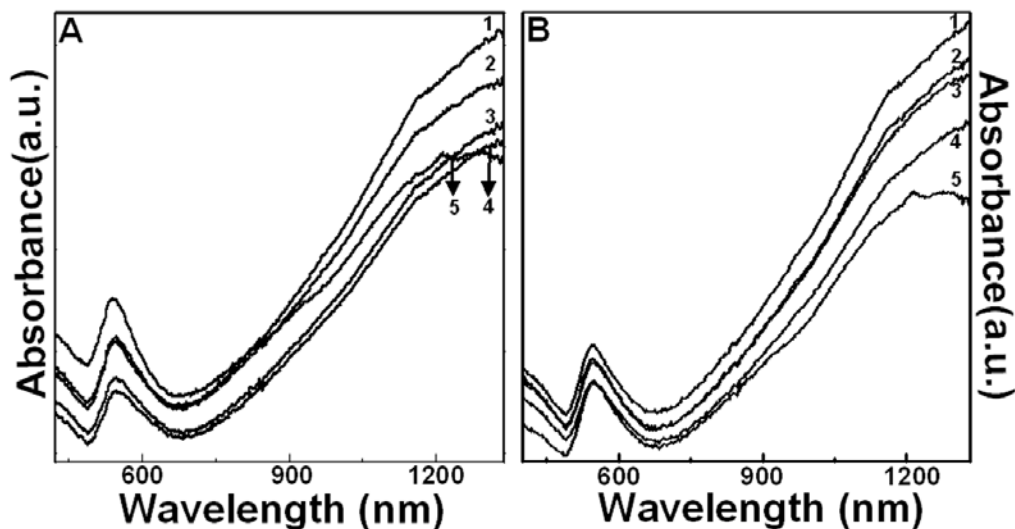


Figure 5.7: A and B) UV-vis-NIR spectra of the purified gold nanotriangles (curve 1) and gold nanotriangles treated with 10^{-5} M (curve 2), 10^{-4} M (curve 3), 10^{-3} M (curve 4) and 10^{-2} M (curve 5) concentration of CTAB (panel A) and CTAC (panel B) respectively.

The change in optical absorption spectra of gold nanotriangles treated with 10^{-2} M concentration of CTAB and CTAC clearly indicates the change in the morphology of gold nanotriangles, which is further confirmed by the TEM analysis (Figure 5.8). Figure 5.8A shows that most of the gold nanotriangles are modified into wavy-edged gold nanotriangles along with circular plate structures after treatment with 10^{-2} M concentration of CTAB. It is observed that the particles still have triangular morphology with corrugated edges, which has also been observed in the case of KBr treated gold nanotriangles (Figure 5.4D). The inset of Figure 5.8A shows truncated nanotriangles and hexagonal nanoparticles with sharp edges without treatment with any surfactant as a control. Figure 5.8B and C show the TEM images of gold nanotriangles after exposure with 10^{-3} M and 10^{-4} M concentrations of CTAB respectively. In this case, few gold nanotriangles are converted into serrated-edged nanotriangles and elongated nanoparticles. The inset of Figure 5.8C shows the higher magnification TEM image of corrugated-edged gold nanotriangles. The curvature at the tips of nanotriangle is not observed in the TEM image (Figure 5.8C). The gold nanoparticles treated with 10^{-5} M concentration of CTAB have plane-edged and sharp tips (Figure 5.8D), which are similar to the control (inset of Figure 5.8A). Therefore, the ideal concentration of CTAB is important to induce morphological change in the gold nanotriangles. The 10^{-3} M – 10^{-5} M

concentrations of CTAB do not have prominent effect on the morphology, while 10^{-2} M concentration of CTAB changes smooth-edged nanotriangles into corrugated-edged nanotriangles, which is strongly supported by the UV-vis-NIR and TEM analysis (Figure 5.7 and 5.8 respectively).

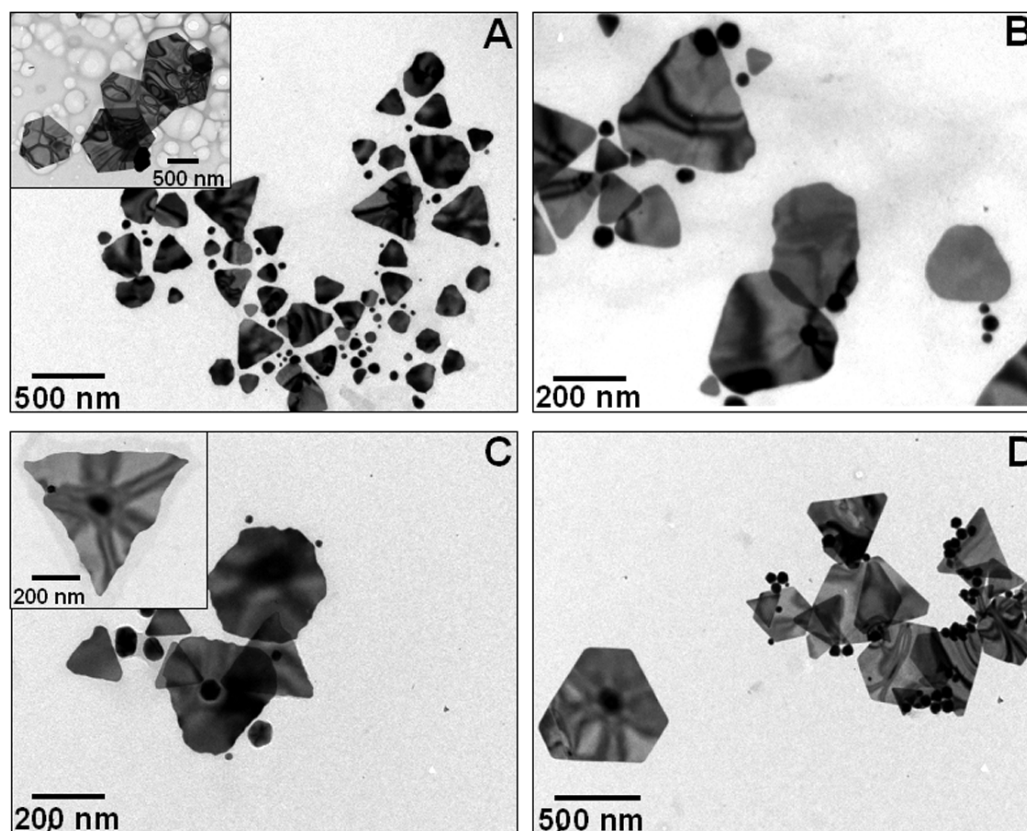


Figure 5.8: Representative TEM images of gold nanotriangles treated with 10^{-2} M (A), 10^{-3} M (B), 10^{-4} M (C) and 10^{-5} M (D) concentrations of CTAB. The inset of Figure 5.8A and C show the TEM images of purified gold nanotriangles and higher magnification TEM image of 10^{-4} M CTAB treated gold nanotriangle respectively.

It has been discussed earlier in this chapter that halide ions have varying ability to chemisorb on the surface of gold nanoparticles. The bromide ions of CTAB also adsorb on the surface of gold nanoparticles and form Au-Br bond with already present gold ions on the surface of nanoparticles [17, 21, 23]. It is reported that adsorption of halide ions on the surface of gold nanoparticles is accompanied by a high mobility of gold surface atoms that causes change in the morphology of nanoparticles [29]. Many reports are also available on chemical specificity of CTAB as well as on the synthesis of gold nanorods in

the presence of CTAB and cosurfactants [4]. These surfactants generally bind to highly unstable (110) facets of nanoparticles and promote the growth in [111] direction to form nanorods. In the case of gold nanotriangles, CTAB could possibly bind to (110) plane of nanotriangles, which is present at edges of nanotriangles, and thus may lead to change in the morphology of nanotriangles. It may be possible that higher concentration of CTAB (10^{-2} M) imparts strain on (110) lattice planes of nanotriangles and thus induces changes in the morphology of nanotriangles into corrugated-edged nanotriangles and circular plate nanostructures (Figure 5.8A).

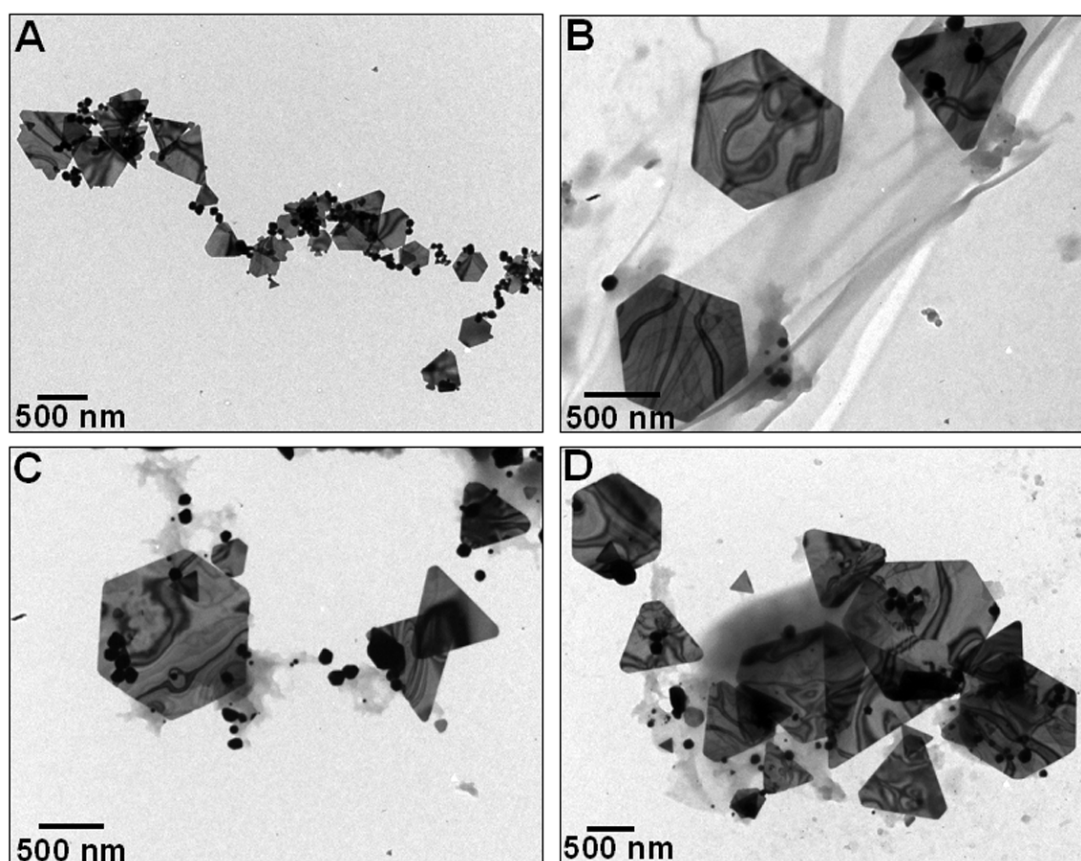


Figure 5.9: Representative TEM images of gold nanotriangles treated with 10^{-2} M (A), 10^{-3} M (B), 10^{-4} M (C) and 10^{-5} M (D) concentrations of CTAC.

However, other concentrations of CTAB (10^{-3} M and 10^{-4} M) do not impart much strain on the surface and only few nanotriangles are converted into corrugated-edged gold nanotriangles, while 10^{-5} M concentration of CTAB is too low to induce changes in the morphology of gold nanotriangles (Figure 5.8B-D). Halas' group has also reported the

reshaping of gold shell of metallodielectric nanoparticles in the presence of CTAB. They have demonstrated that adsorption of bromide ions on this high-energy (110) plane results in unusual strong Raman signal at 174 cm^{-1} for Au-Br bond vibration [17]. Chloride ions of CTAC do not have high affinity to interact with gold in comparison with the bromide ions of CTAB and hence do not impart strain on the surface of nanoparticles. Therefore, change in the morphology of nanotriangles is not observed for varying concentrations (10^{-2} M , 10^{-3} M , 10^{-4} M and 10^{-5} M respectively) of CTAC (Figure 5.9A-D). For all the concentrations of CTAC used (Figure 5.9), the morphology of nanotriangles is intact and edges of nanotriangles are smooth as similar to that of control (inset of Figure 5.8A). It can be rationalized from this analysis that bromide ions and specific concentration of surfactants are important for the shape modification of nanoparticles.

5.4.3 Atomic force microscopy (AFM) analysis:

The contact mode AFM image of gold nanotriangles treated with 10^{-2} M CTAB (Figure 5.10A) shows that the sharp tips of nanotriangles are converted into circular structures but the overall morphology still looks like triangular.

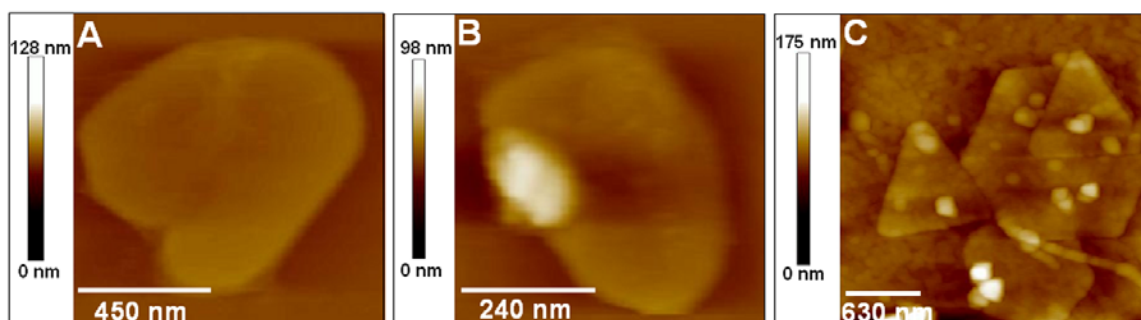


Figure 5.10: Contact mode AFM images of gold nanotriangle treated with 10^{-2} M CTAB (A), 10^{-3} M CTAB (B) and 10^{-2} M CTAC (C). All the AFM images are taken in the height mode.

Figure 5.10B shows elongated gold nanoparticles after exposure to 10^{-3} M CTAB as was observed previously in the TEM image (Figure 5.8B). The AFM image (Figure 5.10C) of 10^{-2} M CTAC treated gold nanotriangles shows that the nanoparticles have plane edges and sharp tips. The curvature at the tip of nanotriangles is not observed in the AFM image, which is in good agreement with the TEM results (Figure 5.9A).

5.4.4 X-ray photoemission spectroscopy (XPS) analysis:

XPS measurements were carried out to investigate the presence of CTAB and CTAC on the surface of gold nanotriangles. In case of CTAB treated gold nanotriangles, a strong Br 3d signal is observed which clearly indicates that bromine ions of CTAB strongly bind to the surface of gold nanotriangles.

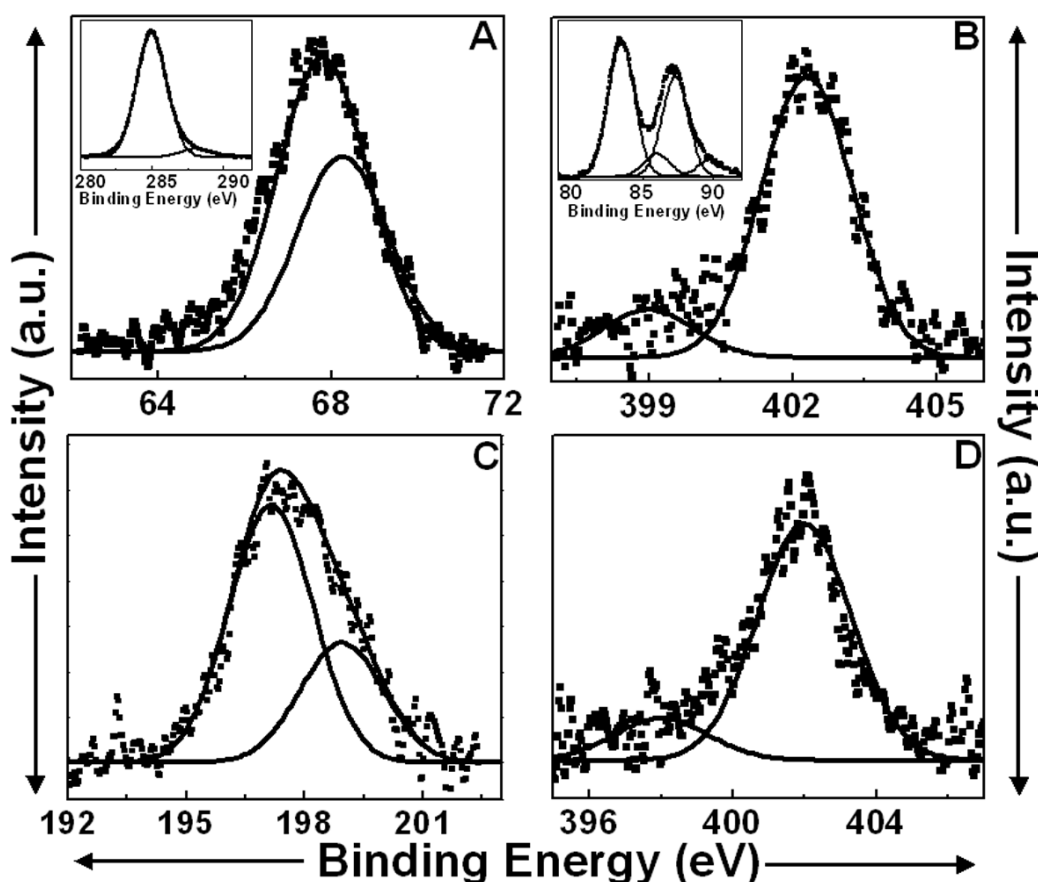


Figure 5.11: XPS spectra of Br 3d (A) and N 1s (B) core levels of CTAB treated gold nanotriangles. The insets of Figure 5.11A and B show C 1s and Au 4f core levels from CTAB treated gold nanotriangles. Figure 5.11C and D show Cl 2p and N 1s core levels of CTAC treated gold nanotriangles.

The Br 3d signal could be stripped into two distinct spin-orbit pairs centered at 67.6 and 68.3 eV binding energies which are attributed to $3d_{5/2}$ and $3d_{3/2}$ core levels of the bromine present in CTAB (Figure 5.11A). The bromine is in form of Br^- ion in a CTAB molecule and is attached to N^+ of long chain hydrocarbon, due to which Br $3d_{5/2}$ core level is shifted towards lower binding energy of 67.6 eV [30]. The N 1s core level could be deconvoluted into two peaks centered at 398.9 and 402.3 eV that could be

assigned to N^0 and N^+ species of nitrogen respectively (Figure 5.11B). The inset of Figure 5.11A shows the XPS spectrum of C 1s core level which could be again deconvoluted into two chemically distinct peaks; one is centered at 285 eV for carbon from hydrocarbon chain of CTAB, while another peak is centered at 288 eV for C-N bond of CTAB. Au 4f core level could be stripped into two peaks centered at 83.6 and 86 eV which is assigned to Au(0) and Au(I) species respectively present in the gold nanotriangles (inset of Figure 5.11B) [2d]. It may be possible that the bromide ions interact with Au(I) and form complex (Au-Br bond) on the surface of nanotriangles.

The photoemission spectrum of Cl 2p core level of CTAC treated gold nanotriangles is shown in Figure 5.11C. Cl 2p core level could be deconvoluted into two chemically distinct peaks at 197.1 and 200 eV for $2p_{3/2}$ and $2p_{1/2}$ respectively. Binding energy of Cl $2p_{3/2}$ is lower than standard core level energy of $2p_{3/2}$ (199 eV) due to the interaction with N^+ species of CTAC. The weak Cl 2p spectrum confirms the poor adsorption of CTAC on the surface of gold nanotriangles. N 1s core level shows two peaks centered at 398 eV for N^0 and 402 eV for N^+ states of CTAC [30]. The poor signal of N 1s core level also indicates that CTAC adsorbs inadequately on the surface of gold nanotriangles. The XPS results strongly support the TEM results (Figure 5.8 and 5.9) that CTAB adsorbs strongly on the surface and alter the morphology of nanotriangles while the poor adsorption of CTAC on the surface of nanotriangle does not affect the nanotriangles' morphology.

5.4.5 FTIR analysis:

FTIR analyses of CTAB and CTAC treated gold nanotriangles were carried out on Si(111) substrate in the form of thin films (Figure 5.12). The FTIR spectra of CTAB and CTAC capped gold nanotriangles show characteristic CH_2 and CH_3 vibration peaks for long chain hydrocarbon of surfactants (curves 3 and 4 respectively), which are similar to CH_2 and CH_3 vibration peaks for free CTAB and CTAC (curves 1 and 2 respectively) [28]. It is well known that the symmetric and anti-symmetric vibration of methylene segments can be used as a sensitive indicator of ordering of alkyl chain and the higher energy of CH_2 vibration corresponds to the frequency of gauche defects in the hydrocarbon chain of surfactant [28]. The symmetric and anti-symmetric vibrations of CH_2 segments of CTAB and CTAC capped gold nanotriangles are located at 2876 and

2945 cm^{-1} respectively and show a little shift to higher frequency in comparison with CH_2 vibration (symmetric and anti-symmetric) of pure CTAB and CTAC which are present at 2848 and 2920 cm^{-1} respectively. The shift of methylene band to higher energy indicates higher surface coverage of CTAB on the gold nanotriangles [27, 31]. In case of CTAC capped gold nanotriangles, the FTIR spectrum (curve 4) shows a weak intensity of CH_2 vibration, which indicates a weak adsorption of CTAC on the surface of gold nanotriangles. In the lower frequency region, free CTAB and CTAC show (curves 3 and 4) bands at 917, 942 and 966 cm^{-1} that correspond to C-N^+ stretching bond.

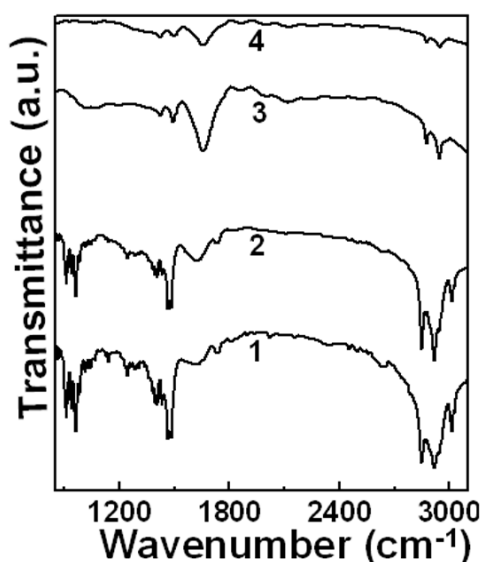


Figure 5.12: FTIR spectra of CTAB (curve 1), CTAC (curve 2), CTAB treated gold nanotriangles (curve 3) and CTAC treated gold nanotriangles (curve 4).

The FTIR spectrum of CTAB treated gold nanotriangles shows peak at 1054 cm^{-1} for stretching mode of C-N^+ to the gold surface [32]. While CTAC treated gold nanotriangles shows a weak band near 1054 cm^{-1} , which clearly indicates that CTAC adsorbs poorly on the surface of gold nanotriangles. This data strongly supports the XPS data of CTAC treated gold nanotriangles (Figure 5.11C and D).

5.4.5 Reversible morphology transformation of CTAB modified gold nanotriangles:

Figure 5.13 shows the reversible transformation of circular nanoplates and wavy-edged gold nanotriangles into plane-edged gold nanotriangles using dialysis method at room temperature. The circular plate nanostructures and wavy-edged gold nanotriangles

(Figure 5.13A), formed after exposure of 10^{-2} M concentration of CTAB to gold nanotriangles, were dialyzed against water using 12.5 kDa dialysis bag for 24 h. The TEM image of dialyzed gold nanoparticles shows plane-edged gold nanotriangles without any curvature at tips and edges of the gold nanotriangles (Figure 5.13B). The reversible transformation of nanotriangular morphology clearly indicates physical association of surfactants on the surface of nanoparticles, which can be removed via a simple dialysis protocol. Conversely, Klabunde's group has reported the reversible transformation of gold nanoparticle morphology using harsh chemical protocol under reflux condition. The morphological transformation was carried out by changing ratio of reactive, competing reagents and more specifically alkylthiols versus tetralkylammonium salts [18].

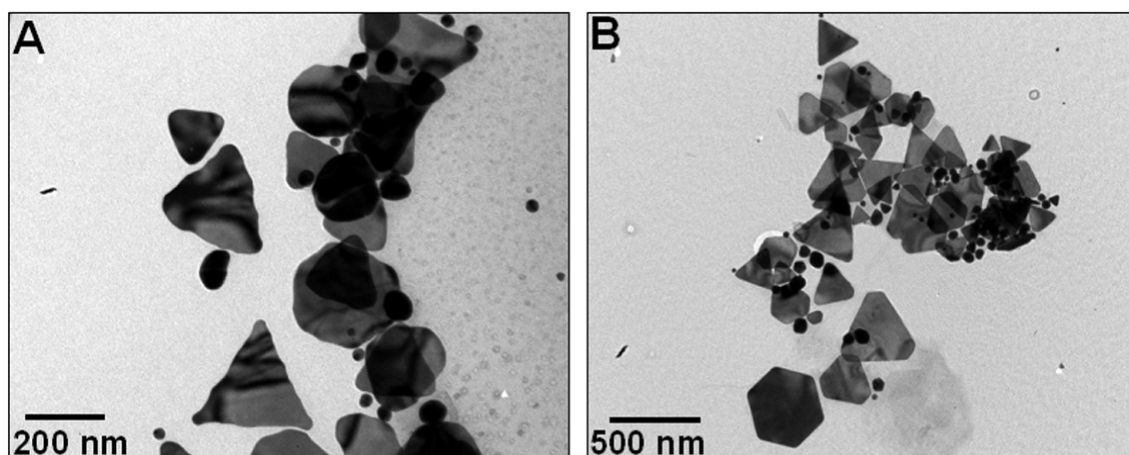


Figure 5.13: Representative TEM images of CTAB modified gold nanotriangles (A) and after dialysis of CTAB modified gold nanotriangles for 24 h (B).

5.5 Effect of gold ions on the morphology of CTAB and CTAC bound gold nanotriangles:

5.5.1 Experimental Details:

To investigate the effect of gold ions (AuCl_4^-) on 10^{-2} M CTAB bound gold nanotriangles or 10^{-2} M CTAC bound gold nanotriangle solutions, different volumes of 10^{-1} M concentration of HAuCl_4 solutions were added to 9 mL of nanotriangles-CTAB or nanotriangles-CTAC solutions so that the final concentrations of gold ions became 10^{-3} M, 5×10^{-4} M, and 10^{-5} M in nanoparticle solutions. All the reaction solutions were kept at room temperature for 24 h, following which they were analyzed by UV-vis-NIR

spectroscopy, TEM and AFM measurements. Prior to performing measurements, these solutions were subjected centrifugation and subsequent washing with water (four times) in order to remove the unreacted gold ions and surfactants.

5.5.2 UV-vis-NIR spectroscopy analysis:

It is also interesting to investigate the effect of gold ions on the morphology of CTAB and CTAC bound gold nanotriangles. Gold ions are known to oxidize gold nanoparticles in the presence of CTAB due to the change in reduction potential of AuCl_4^- upon complexation with CTAB [33]. Figure 5.14A and B correspond to the UV-vis-NIR spectra recorded after addition of varying concentrations (10^{-3} M, 5×10^{-4} M, and 10^{-5} M respectively) of gold ions (AuCl_4^-) in 10^{-2} M CTAB bound gold nanotriangles and 10^{-2} M CTAC bound gold nanotriangles complex respectively. The UV-vis-NIR spectrum of gold nanotriangle solution without treatment with surfactants as a control shows two absorption bands as discussed previously in section 5.4.2 (curve 1 of Figure 5.14A and B). CTAB and CTAC treated gold nanotriangle solutions also show two optical absorption bands at 540 nm (transverse SP band) and 1250 nm (longitudinal SP band) (curve 2 of Figure 5.14A and B). The UV-vis-NIR spectra of CTAB bound gold nanotriangles after the addition of 10^{-3} M and 5×10^{-4} M concentration of AuCl_4^- (curves 3 and 4 respectively) show different absorption spectra in comparison to the control (curve 1). A large blue shift of 70 nm in the transverse surface plasmon (SP) band along with the appearance of new absorption band at 400 nm due to the complexation of Au^{3+} with CTAB is observed in the absorption spectra (curves 3 and 4). The presence of SP peak at 400 nm is due to interband transition with some contribution from light scattering as discussed by Liz-Marzan's group [33]. The longitudinal band of gold nanotriangles is totally diminished after addition of 10^{-3} M and 5×10^{-4} M concentrations of gold ions, as can be seen in the inset of Figure 5.14 (curves 3 and 4). In the case of 10^{-3} M and 5×10^{-4} M concentrations of gold ions treated CTAC bound gold nanotriangle solutions, the UV-vis-NIR spectra (curves 3 and 4 of Figure 5.14B respectively) show a complete disappearance of longitudinal band and simultaneously show the presence of new absorption bands (336 and 324 nm in curve 3 and 4 respectively) in the UV region of electromagnetic spectra.

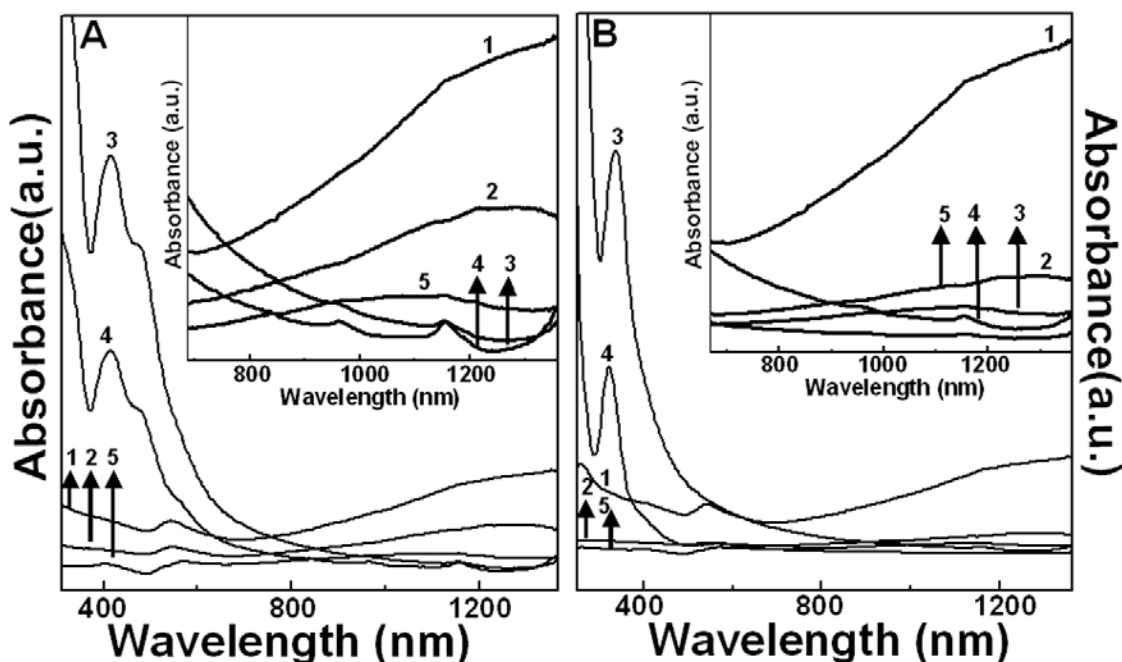


Figure 5.14: A and B represent the effect of different concentrations of Au^{3+} ions on CTAB modified gold nanotriangles and CTAC modified gold nanotriangles respectively. The UV-vis-NIR spectra recorded for gold nanotriangles (curve 1), CTAB modified gold nanotriangles (curve 2 in panel A) and CTAC modified gold nanotriangles (curve 2 in panel B) are shown. Curves 3 to 5 in panel A and B represent the UV-vis-NIR spectra of CTAB and CTAC modified gold nanotriangles after addition of 10^{-3} M, 5×10^{-4} M and 10^{-5} M Au^{3+} ions respectively. The insets in panel A and B show magnified spectra in the NIR region for curves 1 to 5.

The appearance of a new band at 336 and 324 nm in the UV region may be due to the presence of CTAC- Au^{3+} complexes in solution. The presence of new bands and disappearance of longitudinal band in case of gold ions treated CTAB bound gold nanotriangles and CTAC bound gold nanotriangles suggests the generation of new morphology from gold nanotriangles. Lower concentration of gold ions (10^{-5} M) does not show any detectable changes in the optical absorption spectra of CTAB or CTAC treated gold nanotriangles (curve 5 of Figure 5.14A and B).

5.5.3 TEM and AFM analysis:

The evolution of new morphology after the addition of different concentrations of gold ions (AuCl_4^-) to CTAB or CTAC bound gold nanotriangle complex was monitored using TEM and AFM. Figure 5.15A and B correspond to the TEM micrographs after addition of 10^{-3} M concentration of gold ions to the 10^{-2} M CTAB bound gold nanotriangle solution.

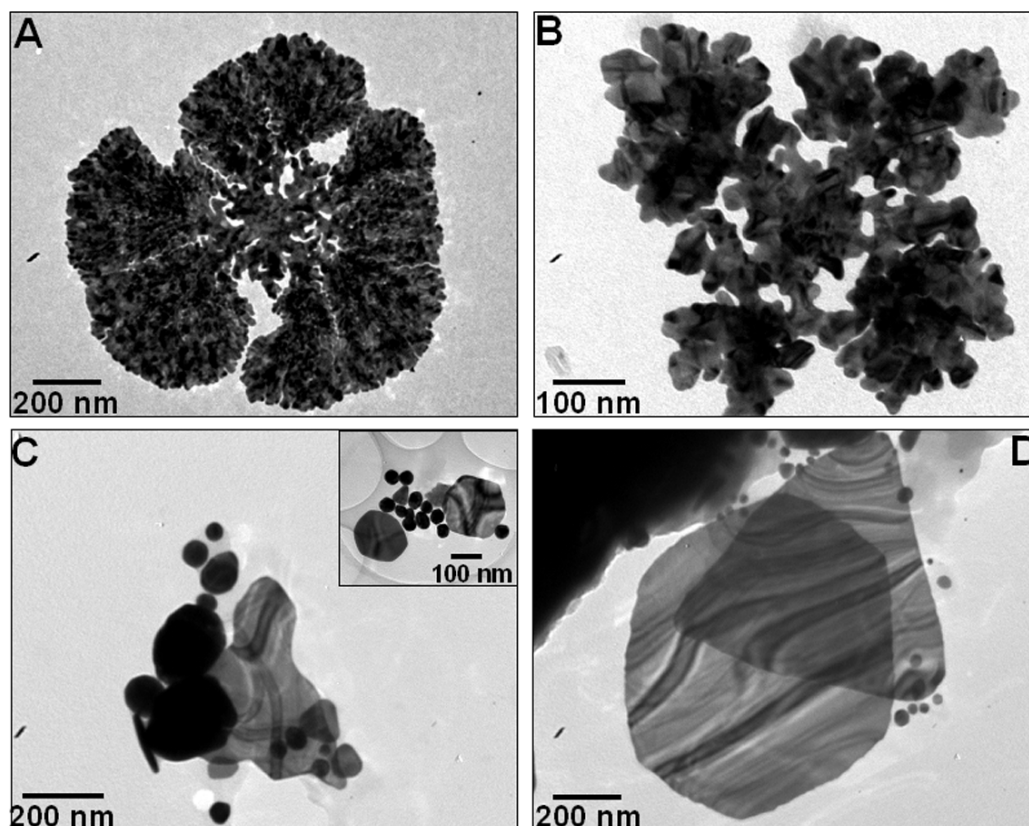


Figure 5.15: Representative TEM images after addition of 10^{-3} M Au^{3+} ions (A, B) and 10^{-5} M Au^{3+} ions (C, D) in CTAB bound gold nanotriangles. The inset of Figure 5.15C shows the TEM image of gold nanotriangles from other part of copper grid.

The TEM images clearly demonstrate a drastic change in the morphology of gold nanotriangles to the highly branched nanostructures. At close inspection of the TEM image, it can be observed that the central part of nanostructure has triangle like morphology and secondary growth occurred from edges and tips of the central region. The already grown secondary structures are highly branched and irregular in the shape. Since, CTAB principally binds to the edges and tips of nanotriangles, it is possible that secondary growth of nanoparticles could have occurred from edges and tips of the gold nanotriangles. CTAB used for this experiment is above critical micelle concentration (cmc) and hence forms micelle. The flux of micelles and added gold ions is more at the tips of nanotriangles [34] and thus gold ions present in the micelles are reduced at the tips to form highly branched nanostructures. The contact mode AFM image also shows branched nanostructures that are formed after assembly of small sized nanoparticles (Figure 5.16A), which is in good agreement with the TEM images. In case of addition of

10^{-5} M concentration of Au^{3+} to the CTAB bound gold nanotriangle solution, the oxidation of tips of nanotriangles and hexagons is observed, which converts sharp tips into circular tips (Figure 5.15C, D and the inset of Figure 5.15C). The oxidation of gold nanorods at higher curvature surface by using the gold ions in the presence of CTAB has been reported by Liz-Marzan's group [33]. Addition of gold ions to CTAC bound gold nanotriangle solution also forms fascinating complex nanostructures, as observed in the TEM images (Figure 5.17).

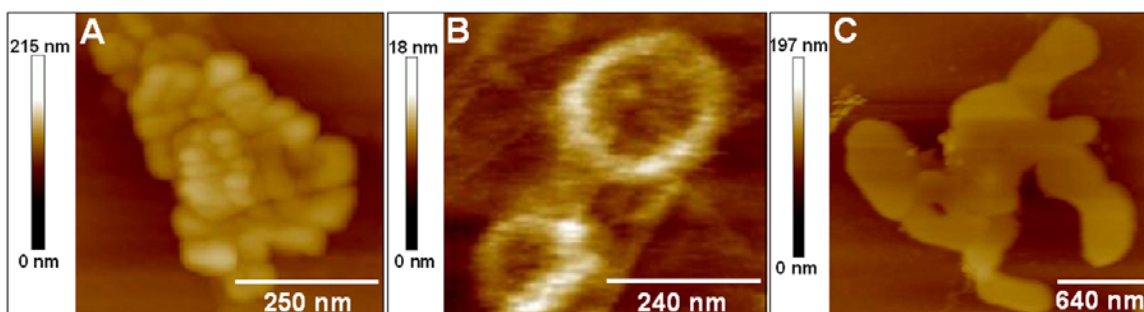


Figure 5.16: (A) Contact mode AFM image after the addition of 10^{-3} M concentration of Au^{3+} ions to the CTAB bound gold nanotriangles. (B and C) AFM images after addition of 10^{-3} M and 10^{-5} M concentrations of Au^{3+} ions to the CTAC bound gold nanotriangles respectively. All the AFM images are taken in height mode.

The TEM images recorded for the addition of 10^{-3} M concentration of AuCl_4^- to the CTAC bound gold nanotriangle solution show coral like nanostructures (Figure 5.17A and B). Aggregated nanostructures can be seen in the central part of the coral nanostructures, which are joined to outer flat type of particles through thread like elongated nanostructures (inset of Figure 5.17A). Figure 5.17B distinctly shows that the periphery of coral particle has flat nanostructures, which is joined to the central part with elongated nanostructures. A careful observation of nanoparticle shows that outer part is made of irregular and flat shaped smaller nanoparticles. The atomic force microscopy (contact mode AFM) image (Figure 5.16B) also shows the ring like nanostructures in which thick gold nanoparticles on the periphery surround the gold nanoparticles present in the central part of rings. Figure 5.17C shows the TEM image of gold nanoparticles after addition of 10^{-5} M concentration of AuCl_4^- to CTAC bound gold nanotriangle solution. The central part of nanostructures is made of branched and aggregated nanostructures, which are surrounded by the flat petal like nanoparticles. The

nanoparticles synthesized in this reaction in fact look like nanoflowers. The higher magnification TEM image shows that petal like particles have random shape and that cover the central part of nanoflowers (Figure 5.17D).

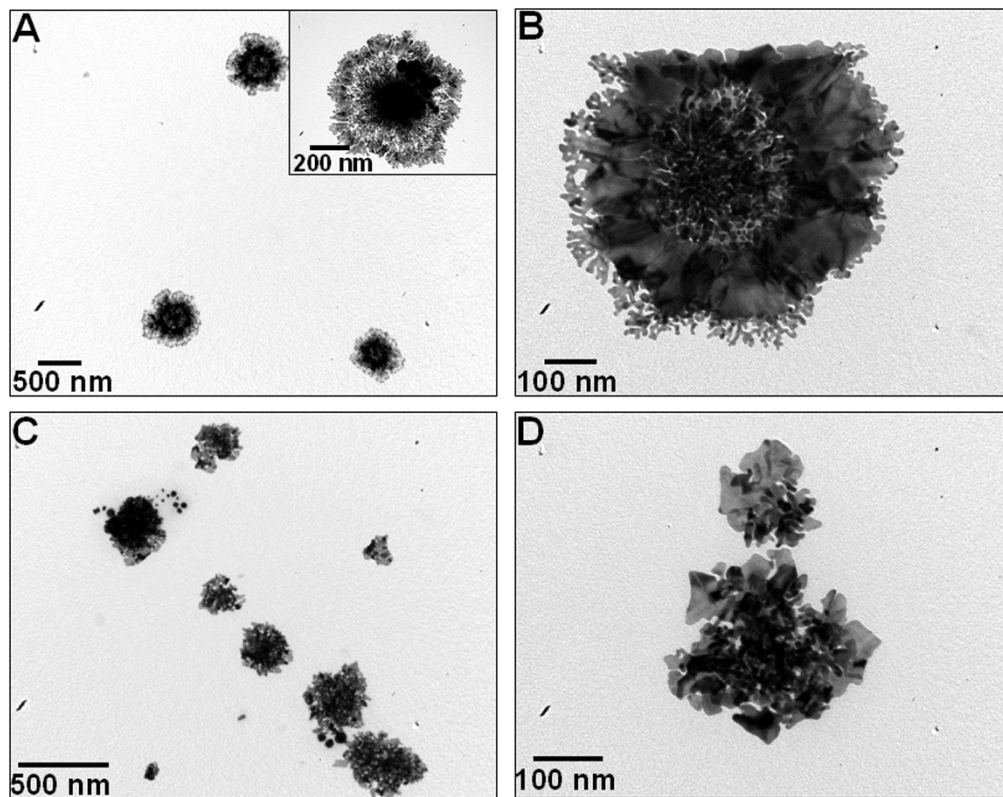


Figure 5.17: Representative TEM images after addition of 10^{-3} M (A, B) and 10^{-5} M (C, D) Au^{3+} ions in CTAC bound gold nanotriangles. The inset of Figure 5.18A shows higher magnification TEM image of gold nanoparticle after addition of 10^{-3} M AuCl_4^- ions in the CTAC bound gold nanotriangles.

Recently, Au-Pt bimetallic nanoflowers fabricated on the polyamidoamine dendrimers modified surface by electrodeposition have been reported [35]. The AFM image (Figure 5.16C) also demonstrates the presence of flat and elongated nanostructures in the gold nanoflower. The flat particles are smaller in size and assemble together to form an elongated nanoparticle.

5.6 Conclusion:

The chapter describes the halide ions mediated shape transformation of the gold nanotriangles. Iodide ions form adlayer on Au (111) plane and have the largest mismatch

with underlying lattice plane of gold (111) in comparison to the adlayers of bromide, chloride and fluoride ions. Moreover, iodide ions have the highest ability to transform nanotriangles into circular plate like nanostructures while the bromide ions form corrugated edge nanotriangles. Chloride and fluoride ions do not change the morphology of gold nanotriangles. During the synthesis of nanoparticles using lemongrass extract, the iodide ions completely hinder the growth of gold nanotriangles and form spherical and aggregated nanoparticles, while the bromide and chloride ions promote the synthesis of nanotriangles. The morphological transformation of gold nanotriangles using various concentrations of cationic surfactants such as CTAB and CTAC show that halide ions are important for the shape modification of nanotriangles. A long chain hydrocarbon of surfactant does not play much role in the shape transformation of gold nanotriangles. 10^{-2} M concentration of CTAB modify plane-edged gold nanotriangles into wavy-edged nanotriangles and circular plate nanoparticles while 10^{-3} M to 10^{-5} M concentrations of CTAB do not significantly affect the morphology of nanotriangles. On the other hand, 10^{-2} M to 10^{-5} M concentrations of CTAC do not play any role in morphological transformation of gold nanotriangles. The reversible transformation of gold nanotriangle morphology using dialysis at room temperature has also been discussed. The reversible transformation strongly signifies the physical association of surfactants on the surface of gold nanoparticles. Gold ions also change the morphology of CTAB or CTAC bound gold nanotriangles. The highly branched nanostructures and nanocoral are synthesized after addition of 10^{-2} M concentration of gold ions to the CTAB bound gold nanotriangles and CTAC bound gold nanotriangles solutions respectively. While 5×10^{-5} M concentration of gold ions oxidize sharp tips of nanotriangles into rounded structure for CTAB bound gold nanotriangles and also form nanoflower with CTAC bound gold nanotriangle solution. The ability to transform morphology and fabricate complex structures *in situ* opens new regime to control the optical and structural properties of the metal nanoparticles.

5.7 References:

- [1] a) Xia, Y.; Yang, P.; Sun, Y.; Wu, Y.; Gate, B.; Yin, Y.; Kim, F.; Yan, H. *Adv. Mater.* **2003**, *15*, 353. b) Wu, Y.; Messer, B.; Yang, P. *Adv. Mater.* **2001**, *13*, 1487. c) Kovtyukhova, N. I.; Mallouk, T. E. *Chem. Eur. J.* **2002**, *8*, 4354. d) Salzemann, C.; Lisiecki, I.; Brioude, A.; Urban, J.; Pileni, M. P. *J. Phys. Chem. B* **2004**, *108*, 13243. e) Jana, N. R.; Gearheart, L.; Obare, S. O.; Murphy, C. J. *Langmuir* **2002**, *18*, 922. f) Ngo, A. T.; Pileni, M. P. *Colloids Surf. A* **2003**, *228*, 107. g) Puentes, V. F.; Krishnan, K. M.; Alivisatos, A. P. *Science* **2001**, *291*, 2115. h) Wang, Z. L.; Ahmad, T. S.; El-Sayed, M. A. *Surf. Sci.* **1997**, *380*, 302. i) Burda, C.; Chen, X.; Narayanan, R.; El-Sayed, M. A. *Chem. Rev.* **2005**, *105*, 1025.
- [2] a) Jin, R.; Cao, Y.; Mirkin, C. A.; Kelley, K. L.; Schatz, G. C.; Zheng, J. G. *Science* **2001**, *294*, 1901. b) Jin, R.; Cao, Y.; Hao, E.; Metraux, G. S.; Schatz, G. C.; Mirkin, C. A. *Nature* **2003**, *425*, 487. c) Shankar, S. S.; Rai, A.; Ankamwar, B.; Singh, A.; Ahmad, A.; Sastry, M. *Nat. Mater.* **2004**, *3*, 482. d) Shankar, S. S.; Rai, A.; Ahmad, A.; Sastry, M. *Chem. Mater.* **2005**, *17*, 566. e) Métraux, G. S.; Mirkin C. A. *Adv. Mater.* **2005**, *17*, 412. f) Sarma, T. K.; Chattopadhyay, A.; *Langmuir* **2004**, *20*, 3520. g) Wang, L.; Chen, X.; Zhan, J.; Chai, Y.; Yang, C.; Xu, L.; Zhuang, W.; Jing, B. *J. Phys. Chem. B* **2005**, *109*, 3189. h) Leng, Y.; Wang, Y.; Li, X.; Liu, T.; Takahashi, S. *Nanotechnology*, **2006**, *17*, 4834. i) Bastys, V.; Pastoriza-Santos, I.; Rodríguez-González, B.; Vaisnoras, R.; Liz-Marzán, L. M. *Adv. Funct. Mater.* **2006**, *16*, 766. j) Lengke, M. F.; Fleet, M. E.; Southam, G. *Langmuir* **2006**, *22*, 2780. k) Li, C.; Cai, W.; Li, Y.; Hu, J.; Liu, P. *J. Phys. Chem. B* **2006**, *110*, 1546. l) Tian, X.; Chen, K.; Cao, G. *Mater. Lett.* **2006**, *60*, 828.
- [3] a) Peng, X.; Manna, L.; Yang, L. L.; Wickham, J.; Scher, E.; Kadavanich, A.; Alivisatos, A. P. *Nature* **2000**, *404*, 59. b) Busbee, B. D.; Obare, S. O.; Murphy, C. J. *Adv. Mater.* **2003**, *15*, 414. c) Jana, N. R.; Gearheart, L.; Murphy, C. J. *J. Phys. Chem. B* **2001**, *105*, 4065. d) Murphy, C. J.; Jana, N. R. *Adv. Mater.* **2002**, *14*, 80. e) Kim, F.; Song, J. H.; Yang, P. *J. Am. Chem. Soc.* **2002**, *124*, 14316. f) Nikoobakht, B.; El-Sayed, M. A. *Chem. Mater.* **2003**, *15*, 1957. g) Pérez-Juste, J.; Liz-Marzán, L. M.; Carnie, S.; Chan, D. Y. C.; Mulvaney, P. *Adv. Funct. Mater.* **2004**, *14*, 571. h) Link, S.; Burda, C.; Nikoobakht, B.; El-Sayed, M. A. *J. Phys. Chem. B* **2000**, *104*,

6152. i) Nikoobakht, B.; El-Sayed, M. A. *J. Phys. Chem. A* **2003**, *107*, 3372. j) Murphy, C. J.; Sau, T. K.; Gole, A.; Orendorff, C. J. *Mater. Res. Bull. Soc.* **2005**, *30*, 349. k) Gulati, A.; Liao, H.; Hafner, J. H. *J. Phys. Chem. B* **2006**, DOI: 10.1021/jp061269t. l) Grzelczak, M.; Pe´rez-Juste, J.; Rodri´guez-Gonza´lez, B.; Liz-Marza´n, L. M. *J. Mater. Chem.* **2006**, *16*, 3946. m) Zijlstra, P.; Bullen, C.; Chon, J. W. M.; Gu, M. *J. Phys. Chem. B* **2006**, *110*, 19315. n) Kou, X.; Zhang, S.; Tsung, C.-K.; Yeung, M. H.; Shi, Q.; Stucky, G. D.; Sun, L.; Wang, J.; Yan, C. *J. Phys. Chem. B* **2006**, *110*, 16377.
- [4] a) Ahmadi, T. S.; Wang, Z. L.; Green, T. C.; Henglein, A.; El-Sayed, M. A. *Science* **1996**, *272*, 1924. b) Sun, Y.; Xia, Y. *Science* **2002**, *298*, 2176. c) Jin, R.; Egusa, S.; Scherer, N. F. *J. Am. Chem. Soc.* **2004**, *126*, 9900. d) Sau, T. K.; Murphy, C. J. *J. Am. Chem. Soc.* **2004**, *126*, 8648. e) Kim, F.; Connor, S.; Song, H.; Kuykendall, T.; Yang, P. *Angew. Chem. Int. Ed.* **2004**, *43*, 3673. f) Yu, D.; Yam, V. W.-W. *J. Am. Chem. Soc.* **2004**, *126*, 13200. g) Chen, J.; McLellan, J. M.; Siekkinen, A.; Xiong, Y.; Li, Z.-Y.; Xia, Y. *J. Am. Chem. Soc.* **2006**, DOI: 10.1021/ja066023g.
- [5] a) Sun, Y.; Mayers, B.; Herricks, T.; Xia, Y. *Nano Lett.* **2003**, *3*, 955. b) Sun, Y.; Yin, Y.; Mayers, B.; Herricks, T.; Xia, Y. *Chem. Mater.* **2002**, *14*, 4736. c) Sun, Y.; Mayers, B.; Xia, Y. *Adv. Mater.* **2003**, *15*, 641. d) Jeong, U.; Camargo, P. H. C.; Lee, Y. H.; Xia, Y. *J. Mater. Chem.* **2006**, *16*, 3893.
- [6] Sun, Y.; Mayers, B.; Xia, Y. *Nano Lett.* **2003**, *5*, 675.
- [7] a) Hao, E.; Bailey, R. C.; Schartz, G. C.; Hupp, J. T.; Li, S. *Nano Lett.* **2004**, *4*, 327. b) Chen, S.; Wang, Z. L.; Ballato, J.; Foulger, S. H.; Carroll, D. L. *J. Am. Chem. Soc.* **2003**, *125*, 16186. c) Milliron, D. J.; Highes, S. M.; Cui, Y.; Manna, L.; Li, J.; Wang, L.; Alivisatos, A. P. *Nature* **2004**, *430*, 190. d) Reculosa, S.; Mingotaud, C.; Bourgeat-Lami, E.; Duguet, E.; Ravaine, S. *Nano Lett.* **2004**, *4*, 1677. e) Shen, G.; Lee, C.-J. *Cryst. Growth Des.* **2005**, *5*, 1085. f) Wu, H.-Y.; Liu, M.; Huang, M. H. *J. Phys. Chem. B* **2006**, *110*, 19291. g) Zhou, G.; Lu, M.; Xiu, Z.; Wang, S.; Zhang, H.; Zhou, Y.; Wang, S. *J. Phys. Chem. B* **2006**, *110*, 6543.
- [8] Chae, W.-S.; Lee, S.-W.; Kim, Y.-R. *Chem. Mater.* **2005**, *17*, 3072.
- [9] Ah, C. S.; Yun, Y. J.; Park, H. J.; Kim, W. J.; Ha, D. H.; Yun, W. S. *Chem. Mater.* **2005**, *17*, 5558.

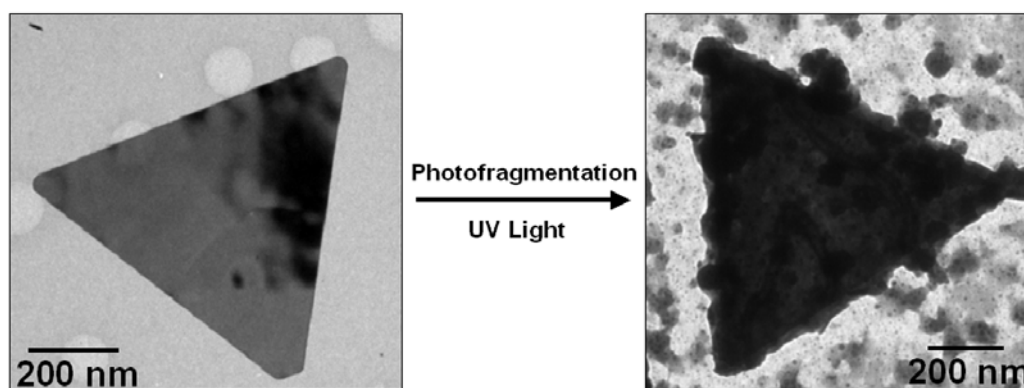
- [10] a) Pileni, M.; Gulik-Krzywicki, T.; Tanori, J.; Filankembo, A.; Dedieu, J. *Langmuir* **1998**, *14*, 7359. b) Tanori, J.; Pileni, M. *Langmuir* **1997**, *13*, 639. c) Filankembo, A.; Pileni, M. *Appl. Surf. Sci.* **2000**, *164*, 260. d) Lisiecki, I.; Billoudet, F.; Pileni, M. *J. Phys. Chem.* **1996**, *100*, 4160. e) Lisiecki, I.; Filankembo, A.; Sack-kongehl, K.; Weiss, K.; Pileni, M. *J. Urban Phys. Rev. B: Condens. Matter Mater. Phys.* **2000**, *61*, 4968.
- [11] Yang, J.; Lu, L.; Wang, H.; Shi, W.; Zhang, H. *Cryst. Growth Des.* **2006**, *6*, 2155.
- [12] a) Lofton, C.; Sigmund, W. *Adv. Funct. Mater.* **2005**, *15*, 1197. b) Elechiguerra, J. L.; Reyes-Gasga, J. Yacaman, M. J. *J. Mater. Chem.* **2006**, *16*, 3906.
- [13] a) Filankembo, A.; Pileni, M.P. *J. Phys. Chem.B* **2000**, *104*, 5865. b) Filankembo, A.; Giorgio, S.; Lisiecki, I.; Pileni, M. P. *J. Phys. Chem. B.* **2003**, *107*, 7492. c) Pileni, M. P. *Nat. Mater.* **2003**, *2*, 145. d) Pileni, M. P. *Langmuir* **2001**, *17*, 7476. e) Pileni, M. P. *C. R. Chimie* **2003**, *6*, 965.
- [14] Ocko, B. M.; Watson, G. M.; Wang, J. *J. Phys. Chem.* **1994**, *98*, 897.
- [15] Shankar, S. S.; Bhargava, S.; Sastry, M. *J. Nanosci. Nanotech.* **2005**, *5*, 1721.
- [16] a) Kitchens, C. L.; McLeod, M. C.; Roberts C. B. *Langmuir* **2005**, *21*, 5166. b) Im, S. H.; Lee, Y. T.; Wiley, B.; Xia, Y. *Angew. Chem. Int. Ed. Engl.* **2005**, *44*, 2154.
- [17] Aguirre, C. M.; Kaspar, T. R.; Radloff, C.; Halas, N. J. *Nano Lett.* **2003**, *3*, 1707.
- [18] Stoeva, S. I.; Zaikovski, V.; Prasad, B. L. V., Stoimenov, Peter, K.; Sorensen, C. M.; Klabunde, K. J. *Langmuir* **2005** *21*, 10280.
- [19] a) Link, S.; El-Sayed, M. A. *J. Phys. Chem. B* **1999**, *103*, 8410. b) El-Sayed, M. A. *Acc. Chem. Res.* **2001**, *34*, 257. c) Moreno-Manas, M.; Pleixats, R. *Acc. Chem. Res.* **2003**, *36*, 638.
- [20] Shirley, D. A. *Phys. Rev. B.* **1972**, *5*, 4709.
- [21] Cheng, W.; Dong, S.; Wang, E. *Angew. Chem. Int. Ed.* **2003**, *42*, 449.
- [22] Gao, P.; Weaver, M. J. *J. Phys. Chem.* **1986**, *90*, 4057.
- [23] Wasileski, S. A.; Weaver, M. J. *J. Phys. Chem. B* **2002**, *106*, 4782.
- [24] a) Prasad, B. L. V.; Stoeva, S. I.; Sorensen, C. M.; Klabunde, K. J. *Chem. Mater.* **2003**, *15*, 935. b) Zhang, P.; Sham, T. K. *Phys. Rev. Lett.* **2003**, *90*, 245502.

- [25] a) Magnussen, O. M.; Ocko, B. M.; Adzic, R. R.; Wang, J. X. *Phys. Rev. B* **1995**, *51*, 5510. b) Magnussen, O. M.; Ocko, B. M.; Wang, J. X.; Adzic, R. R. *J. Phys. Chem.*, **1996**, *100*, 5500. c) Gao, X.; Weaver, M. J. *J. Phys. Chem.* **1993**, *97*, 8685.
- [26] a) Germain, V.; Li, J.; Ingart, D.; Wang Z. L.; Pieni, M. P. *J. Phys. Chem. B* **2003**, *107*, 8717. b) Maillard, M.; Giorgio, S.; Pileni, M. P. *Adv. Mater.* **2002**, *14*, 1084. c) Wang, Z. L. *J. Phys. Chem. B* **2000**, *104*, 1153.
- [27] Cheng, W.; Dong, S.; Wang, E. *Langmuir* **2003**, *19*, 9434.
- [28] a) Hostetler, M. J.; Stokes, J. J.; Murray, R. W. *Langmuir* **1996**, *12*, 2, 3604. b) Badia, A.; Singh, S.; Demers, L.; Cuccia, L.; Brown, G. R.; Lennox, R. B. *Chem. Eur. J.* **1996**, *2*, 359. c) Dubois, L. H.; Nuzzo, R. G. *Annu. Rev. Phys. Chem.* **1992**, *43*, 437. d) Ulman, A. *An Introduction to Ultrathin Organic Films*; Academic: New York, 1991. e) Bain, C. D.; Whitesides, G. M. *Angew. Chem., Int. Ed. Engl.* **1989**, *28*, 506. f) Snyder, R. G.; Maroncelli, M.; Strauss, H. L.; Hallmark, V. M. *J. Phys. Chem.* **1986**, *90*, 5623.
- [29] Zou, S.; Gao, X.; Weaver, M. J. *Surf. Sci.* **2000**.
- [30] Wagner, C. D; Riggs, W. M.; Davis, L. E.; Moulder, J. F.; Muilenberg, G. E. *Handbook of X-ray photoemission spectroscopy*, Perkin Elmer Corp. Publishers, Eden Prairie, MN, **1979**.
- [31] Zhang, L.; Sun, X.; Song, Y.; Jiang, X.; Dong, S.; Wang, E. *Langmuir* **2006**, *22*, 2838.
- [32] Nikoobakht, B.; El-sayed, M. A. *Langmuir* **2001**, *17*, 6368.
- [33] Rodríguez-Fernández, J.; Pérez-Juste, J.; Mulvaney, P.; Liz-Marzán L. M. *J. Phys. Chem. B* **2005**, *109*, 14257.
- [34] Pérez-Juste, J.; Liz-Marzán, L. M.; Carnie, S.; Chan, D. Y. C.; Mulvaney, P. *Adv. Funct. Mater.* **2004**, *14*, 571.
- [35] Qian, L.; Yang, X. *J. Phys. Chem. B.* **2006**, *110*, 16672.

Chapter VI

Photofragmentation of Gold Nanotriangles

Synthesis of Gold Nanotriangles at Different Temperatures



In this chapter, room temperature synthesis of gold nanoparticles using lemongrass extract, in the presence of different concentrations of Keggin ions (phosphotungstate ions) has been described. Higher concentration (10^{-2} M) of Keggin ions inhibits the growth of gold nanotriangles, while lower concentrations (10^{-3} M to 10^{-5} M) of Keggin ions do not significantly affect the synthesis of gold nanotriangles. Keggin ions may bind to certain crystallographic plane(s) of initially formed gold nanoparticles and hinder the growth of nanotriangles. The synthesized gold nanoparticles were irradiated by UV light in the presence of Keggin ions in order to fragment the triangular nanoparticles into spherical nanoparticles. An attempt has been also made to fragment the already synthesized gold nanotriangles into spherical nanoparticles by UV light. Various degree of fragmentation has been achieved by using different concentrations of Keggin ions. The reaction temperature is a crucial factor to control the yield and morphology of nanoparticles formed. Synthesis of gold nanotriangles using lemongrass extract at different temperatures (40-80 °C) has also been discussed in this chapter.

Part of the work presented in this chapter has been published:

Rai, A.; Singh, A.; Ahmad, A.; Sastry, M. *Langmuir* **2006**, *22*, 736.

6.1 Introduction:

Small metal and semiconductor nanoparticles have been used in many different fields including catalysis, microelectronics and nanosensors since they exhibit optical and/or electronic properties different from their bulk counterparts owing to their nanometer-order size [1]. While the particle size is an important factor in controlling different properties of nanoparticles, the shape of nanoparticles also play a crucial role in modulating these properties [2]. In this context, it is significant to develop a low cost and effective method to synthesize nanoparticles with the desired shape. In previous chapter, morphological transformation of gold nanotriangles using various halide ions and surfactants was described. This chapter deals with physical means to control the morphology and yield of nanoparticles formed. Recently, along with chemical means [3], physical means [4] have also received an immense interest to modulate the morphology of preformed nanoparticles. However, once the particles are formed, it is difficult to alter the morphology of nanoparticles *in situ* and therefore numerous methods have been established to modulate the morphology of nanoparticles in solution.

A physical method called “laser ablation” has been used to synthesize metal nanoparticles in solution [5]. The size distribution of nanoparticles tends to be wide because aggregation of ablated atoms and clusters is difficult to control. Recently, laser assisted size reduction method has been developed to shatter metal nanoparticles into smaller nanoparticles through selective heating caused by resonant electronic vibration of the parent nanoparticles [4e, 6]. Several reports are available in the literature on the laser assisted size reduction of metal nanoparticles in solution using different lasers [4a, b]. For instance, gold nanorods can be thermally shattered into spherical nanoparticles by a femtosecond laser or fragmented into smaller nanoparticles by a nanosecond laser irradiation [7]. Conversely, Mirkin’s group has shown the photoinduced conversion of spherical nanoparticles to nanoprisms by a 40 W fluorescent light source [8]. Callegari *et al.* have shown that the particle size and shape can be controlled by using choosing wavelength(s) of light in order to drive photochemical growth [9]. Though most of the reports deal with the synthesis [10] or fragmentation [4-6] of metal nanoparticles using different laser sources, so far only few attempts have been made to synthesize or fragment the nanoparticles using UV light. Sastry and coworkers have shown the

preparation of core-shell nanoparticles of various compositions in the presence of Keggin ions using UV light irradiation [11]. They have also shown the synthesis and assembly of Au, Ag, CdS and CaCO₃ nanoparticles in the presence of Keggin ions by UV light irradiation [12]. Chen's group has shown the shape-controlled synthesis of gold nanoparticles using UV light irradiation [13]. Synthesis of Ag, Au, Pt and Pd nanoparticles using reduced form of polyoxometallates [(PW₁₂O₄₀)³⁻ and (SiW₁₂O₄₀)⁴⁻] have also been reported [14].

Polyoxometallates (POM) have well defined structures and properties with diverse applications in the field of biochemistry, analytical chemistry and solid state devices and have also been used as antiviral and antitumor agents [15]. Keggin ions is a subset of POM and have the general formula (XM₁₂O₄₀)⁽⁸⁻ⁿ⁾⁻, where M corresponds to W or Mo and X corresponds to a hetroatom such as P, Si, Ge, with n being the valency of X [16]. Keggin ions containing cations and other components such as water, are arranged in a well defined secondary three-dimensional structures and the stability of Keggin ion molecules depends on the nature of counter ions and amount of water [17]. Under UV light irradiation, Keggin ions get electrons from secondary alcohols and undergo multielectron redox processes without any appreciable disruption to the original structures [18]. They can be reduced photochemically, electrolytically as well as with reducing agents. The reduced form of Keggin ions has typical dark blue colour due to intervalent charge transfer between tungsten atoms and due to d-d transition [18]. Hence, polyoxometallates are also called hetropoly blues [19].

In this chapter, synthesis of gold nanoparticles using lemongrass extract in the presence of different concentrations of phosphotungstate ions (PTA) has been described. Phosphotungstate ion (PW₁₂O₄₀)³⁻ is a large molecule with a molecular weight of 2880. Higher concentration (10⁻² M) of phosphotungstate ions inhibits the growth of gold nanotriangles, while lower concentrations do not affect the synthesis of nanotriangles. The synthesized gold nanotriangles after exposure to UV light undergo photofragmentation, which leads to the formation of spherical nanoparticles. Different concentrations of PTA molecules have also been used to get varying percentage of fragmentation of already synthesized gold nanotriangles under UV light irradiation. It should be noticed here that phosphotungstate ions (PTA) have been used in all

experiments discussed in this chapter and mentioned as Keggin ions throughout the text. The temperature of reaction medium is another parameter, which governs the yield and morphology of nanoparticles formed. There are various reports on the shape-controlled synthesis of spherical, cubes, and triangular Au nanoparticles as well as Au-Pt bimetallic nanoparticles at higher temperature [20]. In this chapter, an attempt has also been made to synthesize gold nanotriangles using lemongrass extract at different temperatures. The rate of reduction of gold ions plays an important role in determining the synthesis of gold nanotriangles. At higher temperatures, the percentage of gold nanotriangles relative to spherical particles is significantly reduced, while lower reaction temperatures promote nanotriangles formation.

6.2 Effect of Keggin ions during synthesis of gold nanotriangles and UV light irradiation of synthesized nanoparticles:

6.2.1 Experimental Details:

Gold nanotriangles were synthesized using lemongrass extract in the presence of different concentrations of Keggin ions. Different volumes of 10^{-1} M concentration of Keggin ions (phosphotungstic acid ($\text{H}_3\text{PW}_{12}\text{O}_{40}$) purchased from Aldrich Chemicals and used as received) were added in 10 mL of 10^{-3} M HAuCl_4 solutions containing 0.8 mL of lemongrass extract to yield different concentrations of Keggin ions (10^{-2} M, 10^{-3} M and 10^{-4} M). These solutions were kept at room temperature for 24 h to allow the reactions to reach saturation. 1 mL isopropyl alcohol was added in the synthesized gold nanoparticle solutions. Thereafter, these solutions were deaerated with nitrogen gas by purging for 15 minutes to remove free oxygen from the solutions, following which they were irradiated by UV light (pyrex filter > 280 nm, 450 W Hanovia medium pressure lamp) for 3 h. UV-vis-NIR spectroscopy and TEM measurements were carried out to investigate the optical properties and morphology of gold nanoparticles formed.

6.2.2 UV-vis-NIR spectroscopy and TEM analysis:

Figure 6.1A shows the UV-vis-NIR spectra of gold nanoparticles synthesized using lemongrass extract in the presence of different concentrations (10^{-2} M, 10^{-3} M and 10^{-4} M) of Keggin ions. Curve 1 in Figure 6.1A corresponds to the UV-vis-NIR spectrum

of gold nanoparticles synthesized in the absence of Keggin ions, which shows two absorption bands; one at 540 nm due to transverse component of surface plasmon (SP) and another in the NIR region of the electromagnetic spectra (longitudinal component of SP), which extends beyond 1200 nm [21]. Two absorption bands in the spectrum clearly suggest the presence of spherical and triangular nanoparticles in solution as further shown in the TEM image (Figure 6.1B).

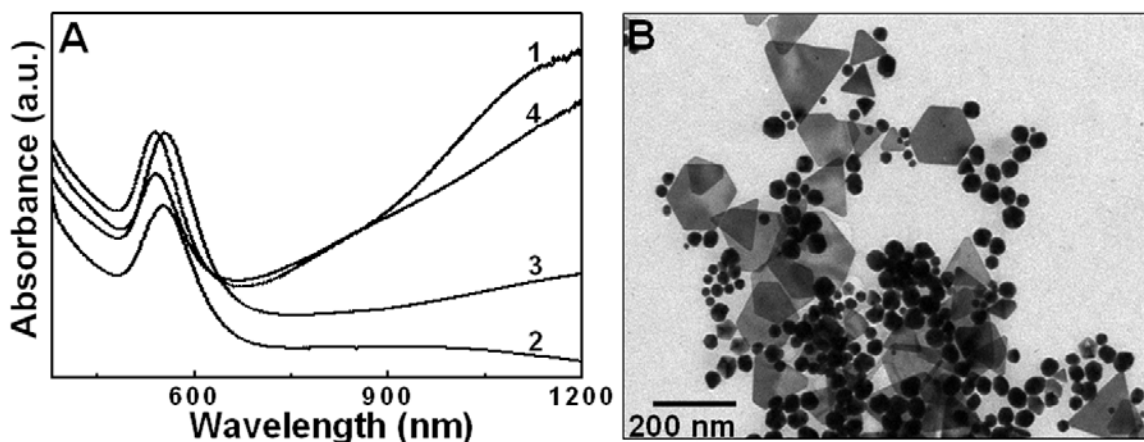


Figure 6.1: A) UV-vis-NIR spectra recorded from lemongrass reduced gold nanoparticles (curve 1) and gold nanoparticles synthesized using lemongrass extract in the presence of 10^{-2} M (curve 2), 10^{-3} M (curve 3) and 10^{-4} M (curve 4) concentrations of Keggin ions. B) Representative TEM image of gold nanoparticles synthesized in the absence of Keggin ions.

The UV-vis-NIR spectrum of gold nanoparticles synthesized in the presence of 10^{-2} M concentration of Keggin ions shows an intense transverse SP band at 552 nm along with a weak and broad longitudinal SP band in range from 770 nm to 1000 nm (curve 2, Figure 6.1A). The TEM image (Figure 6.2A) shows the presence of spherical and triangular nanoparticles in the solution. An intense transverse SP band clearly shows the synthesis of a large population of spherical particles (73%) in comparison to gold nanotriangles (27%) (Figure 6.2B), which indicates that high concentration of Keggin ions hinders the growth of triangular nanoparticles. It is possible that 10^{-2} M concentration of Keggin ions bind to crystallographic facets of initially formed smaller nanoparticles and inhibit the two dimensional growth of gold nanotriangles in the reaction solution. Keggin ion (phosphotungstate ion) is a large complex and may bind to most of initially formed gold nanoparticle lattice planes. Therefore, remaining gold ions in the solution may not be able to access lattice planes of initially formed nanoparticles

and would not contribute to advancing the growth of gold nanoparticles. However, lower concentrations (10^{-3} M and 10^{-4} M) of Keggin ions are not sufficient for binding on the most of lattice plane of smaller nanoparticles and so a high yield of gold nanotriangles are synthesized using lemongrass extract in presence of these concentrations in comparison to 10^{-2} M Keggin ions experiment.

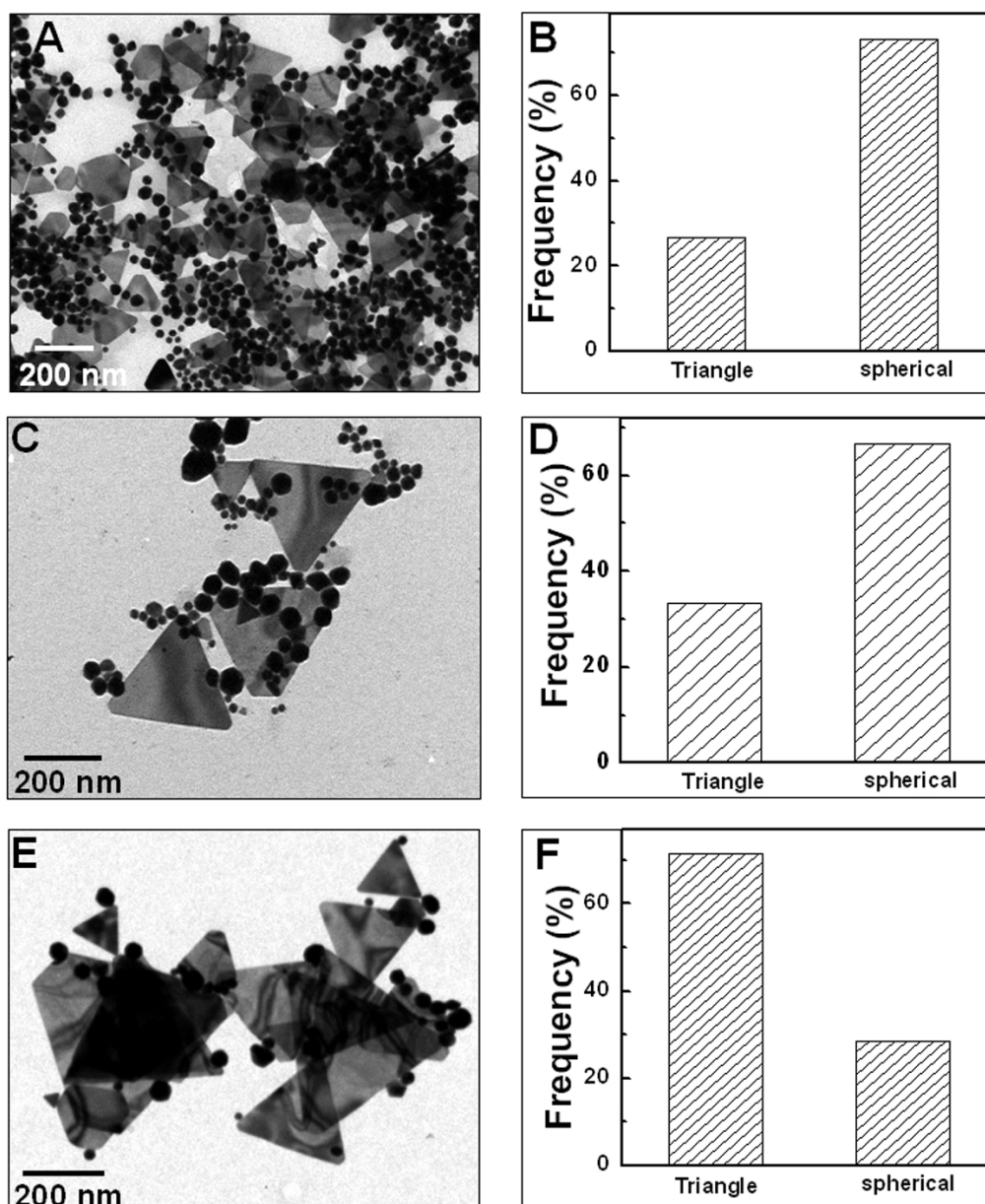


Figure 6.2: Representative TEM images of gold nanoparticles synthesized in the presence of (A) 10^{-2} M, (C) 10^{-3} M and (E) 10^{-4} M concentrations of Keggin ions and corresponding histogram plots are shown in Figure B, D and F respectively.

Curve 3 in Figure 6.1A corresponds to the gold nanoparticles synthesized in the presence of 10^{-3} M concentration of Keggin ions, which shows a strong transverse SP band at 552 nm along with a weak longitudinal SP band that appears to go beyond 1200 nm in the NIR region. The TEM image (Figure 6.2C) shows that spherical and triangular nanoparticles are synthesized in the solution using lemongrass extract in the presence of 10^{-3} M Keggin ions. The histogram plot (Figure 6.2D) shows that a low yield of gold nanotriangles (34%) and a high yield of spherical nanoparticles (66%) are synthesized, which is strongly supported by the UV-vis-NIR data (curve 3, Figure 6.1A). In case of curve 2 and 3, a small red shift of 16 nm is observed in transverse band, which indicates a small aggregation of the gold nanoparticles in the solutions, as also observed in the TEM image (Figure 6.2A and C). The UV-vis-NIR spectrum of gold nanoparticles synthesized in the presence of 10^{-4} M concentration of Keggin ions demonstrates a transverse band at 540 nm along with a high intensity longitudinal SP band, which appears to go beyond 1200 nm in the NIR region. The TEM image (Figure 6.2E) clearly shows the synthesis of gold nanotriangles with smooth edges and sharp tips. The histogram plot (Figure 6.2F) shows that a high yield of gold nanotriangles (72%) in comparison to the spherical nanoparticles is synthesized in the presence of 10^{-4} M concentration of Keggin ions, which is strongly corroborated with the UV-vis-NIR data (curve 4).

6.2.3 UV-vis-NIR spectroscopy and TEM analysis after UV light irradiation:

Figure 6.3A shows the UV-vis-NIR spectra of UV light irradiated gold nanoparticle synthesized in the presence of different concentrations of Keggin ions. Curve 1 shows the UV-vis-NIR spectrum of UV light irradiated gold nanoparticles solution without Keggin ions (control). The spectrum (curve 1) shows two surface plasmon bands centered at 540 nm (transverse SP band) and 1180 nm (longitudinal SP band). The absorption spectrum (curve 1, Figure 6.3A) is similar to the UV-vis-NIR spectrum of gold nanoparticles synthesized in the absence of Keggin ions (curve 1, Figure 6.1A), which indicates that the morphology of nanoparticles was not changed after UV light irradiation. The TEM image (Figure 6.3B) also shows that the morphology of nanoparticles after UV light irradiation is spherical and triangular, which is analogous to the TEM image of gold nanoparticles synthesized in the absence of Keggin ions (Figure 6.1B). Curve 2 shows the UV-vis-NIR spectrum of aqueous 10^{-2} M Keggin ions solution

before irradiation. The spectrum does not show a band in the visible or NIR region due to the colourless solution of Keggin ions. This is due to the charge transfer transition that occurs between the tungsten metal, which has a vacant d-orbital (+6 or d^0 oxidation state) and the donor oxygen ion [19]. Curve 3 corresponds to UV light irradiated gold nanoparticles synthesized in the presence of 10^{-2} M Keggin ions and shows that transverse and longitudinal peak of gold nanotriangles are totally diminished and new peaks at ca. 500 and 760 nm arise after UV light irradiation, which are signatures of the dark blue colour solution. From a dramatic decrease in the absorbance of longitudinal band, we can infer that triangular nanoparticles have been fragmented into spherical nanoparticles.

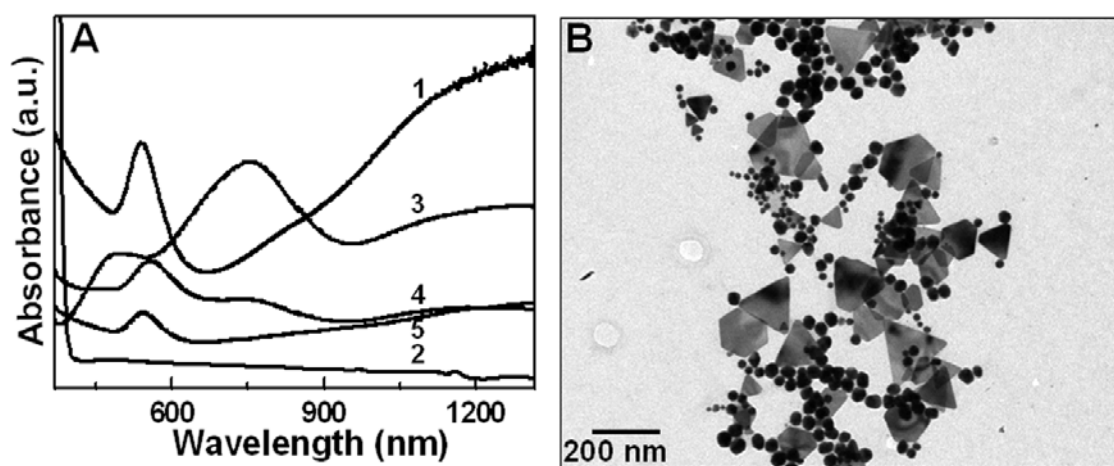


Figure 6.3: A) UV-vis-NIR spectra recorded from UV light irradiated gold nanoparticles, synthesized in absence of Keggin ions (curve 1) and in the presence of 10^{-2} M (curve 3), 10^{-3} M (curve 4) and 10^{-4} M (curve 5) concentrations of Keggin ions. Curve 2 corresponds to UV-vis-NIR spectrum of unreduced 10^{-2} M Keggin ions. B) Representative TEM image of UV light irradiated gold nanoparticles, synthesized in the absence of Keggin ions.

The peak at 760 nm is due to the intervalent metal transition between one tungsten atom (d^1 state) and another tungsten atom (d^0 state) as well as due to the d-d transition [19]. The dark blue solution (reduced state of Keggin ions) is stable only for a few hours, which suggests the aerial oxidation of reduced state to the original ground state. The TEM image (Figure 6.4A) of gold nanoparticles fragmented in the presence of 10^{-2} M Keggin ions shows that a large percentage of spherical nanoparticles have been formed due to the photofragmentation of triangular nanoparticles by using UV light. The

histogram analysis (Figure 6.4B) also shows that only 12% triangular nanoparticles remain in the solution after UV light irradiation in comparison to 27% population of nanotriangles, which are present in the original solution (Figure 6.2B). There are two possible mechanisms for the photofragmentation of gold nanoparticles: (1) thermal explosion [6a] (2) charge induced explosion [22].

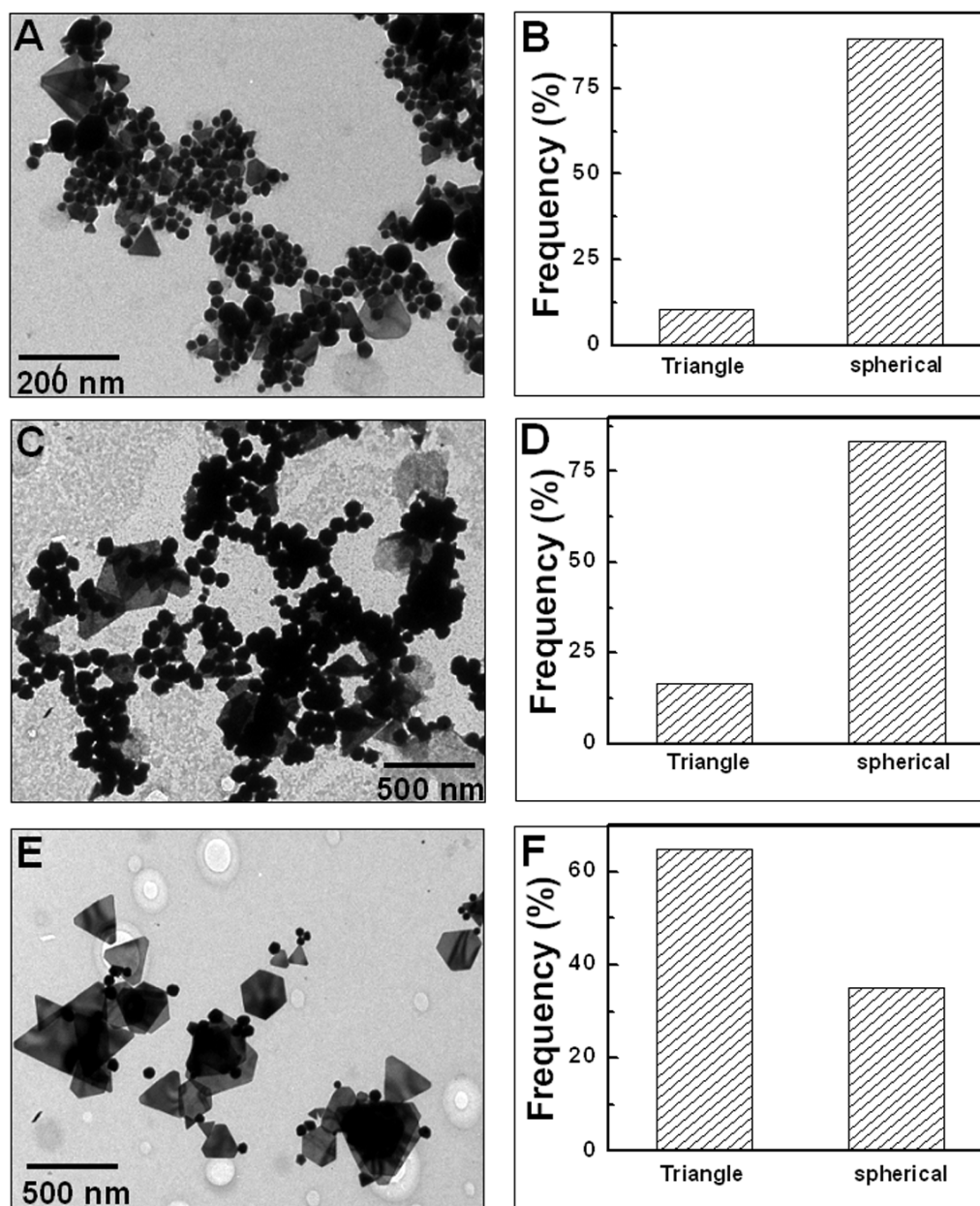


Figure 6.4: Representative TEM images of UV light irradiated gold nanoparticles, which are synthesized in the presence of (A) 10^{-2} M, (C) 10^{-3} M and (E) 10^{-4} M concentrations of Keggin ions and corresponding histogram plots are shown in Figure B, D and F respectively.

Thermal explosion mechanism does not work for the UV light irradiated gold nanotriangles (synthesized in the absence of Keggin ions) experiment and the fragmentation of nanotriangles is also not observed in the TEM image (Figure 6.3B). We had measured the temperature of solution during irradiation and it was found to be 35 °C, which is close to room temperature. Keggin ions are known to reduce in the presence of secondary alcohol (isopropyl alcohol) under UV light at inert condition [19]. During the reduction process under UV light, each Keggin ion molecule gets one electron from secondary alcohol and Keggin ion molecules move to +5 oxidation state from the initial +6 oxidation state [19]. Thus, a single Keggin ion becomes single electron rich after UV light irradiation. Electron density on the surface of gold nanotriangles bound to Keggin ions may be increased after UV light irradiation and gold nanotriangles will be efficiently ionized to cause repulsive explosive [23]. Due to electron-electron charge repulsion on the surface of nanotriangles, gold nanotriangles are believed to shatter into spherical nanoparticles.

In case of UV light irradiated gold nanoparticles synthesized in the presence of 10^{-3} M Keggin ions, the UV-vis-NIR spectrum (curve 4, Figure 6.3A) shows transverse peak at 540 nm and a weaker longitudinal peak at 1180 nm. Curve 4 also shows a weak peak centered at 760 nm due to a small concentration of Keggin ions (10^{-3} M) in solution. The strong absorption peak at around 540 nm clearly indicates that nanotriangles have been fragmented into spherical nanoparticles. The TEM image also demonstrates the presence of spherical and aggregated nanoparticles along with a small percentage (16%) of triangular nanoparticles (Figure 6.4C and D). It has been reported that the released gold atoms during fragmentation have a strong tendency to rapidly aggregate into smaller spherical nanoparticles [24]. Gold atoms or small gold nanoparticles could also diffuse to and aggregate at the surface of triangular nanoparticles [6d], as observed in the TEM image (Figure 6.4C). The histogram plot (Figure 6.4D) shows a large yield of spherical nanoparticles (84%) in comparison to 66% population of spherical nanoparticles in the original solution (Figure 6.2D).

Curve 5 (Figure 6.3A) corresponds to the UV-vis-NIR spectrum of gold nanoparticles synthesized in the presence of 10^{-4} M concentration of Keggin ions. The spectrum shows transverse and longitudinal SP peaks for spherical and triangular gold

nanoparticles along with the absence of peak at 760 nm for reduced state of Keggin ions, which is similar to the control (curve 1, Figure 6.3A). The TEM image recorded from this solution shows a large percentage of triangular nanoparticles (65%) (Figure 6.4E and F). The population of gold nanotriangles is nearly similar to the nanotriangles synthesized in the presence of 10^{-4} M Keggin ions (Figure 6.2F). Gold nanotriangles have well faceted edges and sharp tips, which are similar to the UV light irradiated gold nanotriangles (in the absence of Keggin ions) (Figure 6.3B) and nanotriangles synthesized in the presence of 10^{-4} M Keggin ions (Figure 6.2E). Therefore, a lower concentration of Keggin ions is unable to fragment gold nanotriangles into spherical nanoparticles by UV light irradiation.

6.3 Effect of UV light irradiation on the morphology of Keggin ion bound gold nanotriangles:

6.3.1 Experimental Details:

In a typical experiment, 8 mL of lemongrass extract was added to 100 mL of 10^{-3} M HAuCl_4 and the reaction was kept at room temperature for 24 h to facilitate complete reduction of AuCl_4^- ions. Gold nanotriangles were purified by three times centrifugation at 1000 rpm for 15 minutes [25]. The obtained gold nanotriangle pellet was diluted to 80 mL in Milli-Q water. To observe the effect of different concentrations of Keggin ions on the morphology of already synthesized gold nanotriangles, different volumes of 10^{-1} M Keggin ions were added to 8 mL of purified gold nanotriangle solutions in order to yield different concentrations of Keggin ions (10^{-2} M, 10^{-3} M, 10^{-4} M, 10^{-5} M respectively) and these solutions were allowed to stand at room temperature for 24 h for binding of Keggin ions to the gold nanotriangles. These solutions were subjected to centrifugation (three times) at 1000 rpm for 15 minutes to remove unbound Keggin ions from gold nanotriangle solutions and the obtained pellets were diluted to 10 mL in Milli-Q water. One mL of isopropyl alcohol was added in these solutions and the corresponding solutions were deaerated by nitrogen gas for 15 minutes, following which irradiated for 3 h by UV light. To study the time dependent photofragmentation of gold nanotriangles, 10^{-2} M Keggin ions bound gold nanotriangle solutions were photo-irradiated for different time (30, 60, 90 and 120 minutes respectively). UV-vis-NIR spectroscopy, TEM, FTIR,

XRD and XPS measurements were carried out to investigate the effect of Keggin ions on the morphology of gold nanotriangles.

6.3.2 Concentration dependent fragmentation of nanotriangles:

6.3.2.1 UV-vis-NIR spectroscopy and TEM analysis:

Figure 6.5 shows the UV-vis-NIR spectra of different concentrations of Keggin ions bound gold nanotriangle solutions after photo-irradiation for 3 h. Curve 1 shows UV-vis-NIR spectrum of UV light irradiated gold nanotriangles in the absence of Keggin ions. The absorption spectrum shows two peaks; one peak is centered at 540 nm (transverse SP band), while another peak is centered at 1320 nm (longitudinal SP band). The TEM image (Figure 6.3B), which is discussed earlier in this chapter, indicates that UV light does not fragment gold nanotriangles in the absence of Keggin ions. Curve 2 corresponds to UV-vis-NIR spectrum of 10^{-2} M Keggin ions bound gold nanotriangles after UV light irradiation. A drastic change is observed in curve 2, which shows that the intensity of transverse and longitudinal SP band of gold nanotriangles is decreased and a new broad band at 760 nm is developed in comparison to curve 1.

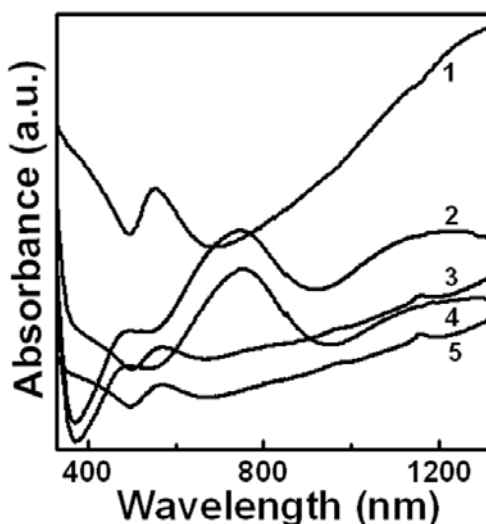


Figure 6.5: UV-vis-NIR spectra recorded from UV light irradiated gold nanotriangles (curve 1) and UV light irradiated gold nanotriangles bound to 10^{-2} M (curve 2), 10^{-3} M (curve 3), 10^{-4} M (curve 4) and 10^{-5} M (curve 5) concentrations of Keggin ions.

The origin of this band is due to forbidden d-d transition and also due to Intervalent Charge Transfer (IVCT) band, which gives the solution a deep blue colour

[19]. The TEM image of this solution shows that gold nanotriangles have fragmented into spherical and aggregated nanoparticles (Figure 6.6A). Large aggregates of gold nanoparticles could be formed due to a rapid aggregation of smaller gold nanoparticles, which are formed during the fragmentation of nanotriangles. Some gold nanotriangles and hexagonal nanoparticles along with the aggregates of small nanoparticles on the surface of these nanoparticles are observed in the TEM image (inset of Figure 6.6A). Curve 3 in Figure 6.5A corresponds to irradiated gold nanotriangles bound to 10^{-3} M Keggin ions and shows a similar absorption spectrum with decrease in the intensity of transverse and longitudinal bands as well as a new 760 nm band in comparison to the curve 1.

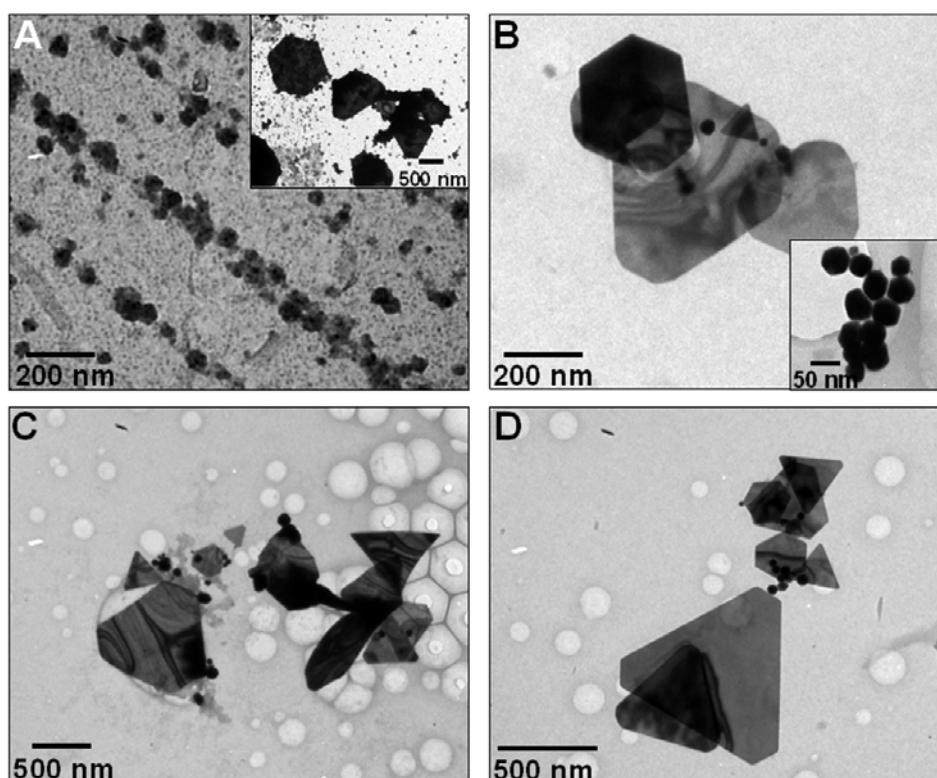


Figure 6.6: Representative TEM images of UV light irradiated gold nanotriangles bound to 10^{-2} M (A and inset of A), 10^{-3} M (B and inset of B), 10^{-4} M (C) and 10^{-5} M (D) concentrations of Keggin ions.

The TEM image recorded from this solution shows well-faceted edged gold nanotriangles along with spherical nanoparticles (Figure 6.6B and inset of B). Large aggregates of gold nanoparticles are not observed in the TEM image. Curves 4 and 5

correspond to the UV-vis-NIR spectra of irradiated gold nanotriangle bound to 10^{-4} M and 10^{-5} M Keggin ions respectively. Curves 4 and 5 show the transverse and longitudinal bands of gold nanotriangles without the presence of a band at 760 nm, which are similar to curve 1. The absence of the band at 760 nm clearly indicates that these concentrations of Keggin ions are not sufficient to fragment the nanotriangles. The TEM images also show that the morphology of nanotriangles is intact and aggregates of smaller nanoparticles are also not observed (Figure 6.6C and D). From these results, it can be rationalized that 10^{-2} M concentration of Keggin ions is sufficient to shatter nanotriangles into spherical nanoparticles.

6.3.3 Time dependent UV light irradiation of nanotriangles:

UV light irradiation of 10^{-2} M Keggin ions bound gold nanotriangles was carried out for different time intervals to identify the initial time of fragmentation of the gold nanotriangles.

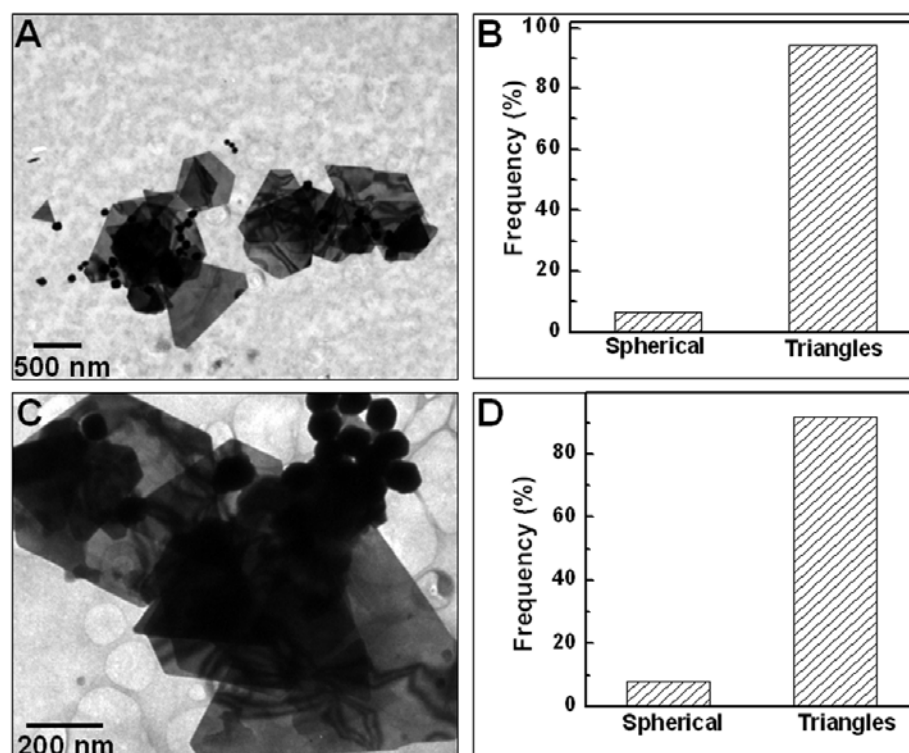


Figure 6.7: Representative TEM images of 10^{-2} M Keggin ions bound gold nanotriangles after UV light irradiation for 30 minutes (A) and 60 minutes (C). Figure B and D show histogram plots of spherical and triangular nanoparticles obtained after 30 and 60 minutes of UV light irradiation respectively.

The TEM image (Figure 6.7A) shows that the morphology of nanotriangle is intact and nanotriangles have smooth edges and tips after irradiation for 30 minutes. The population of gold nanotriangles is 94% after UV light irradiation for 30 minutes (Figure 6.7B). The TEM image of gold nanoparticles after irradiation for 60 minutes shows that the morphology of nanotriangles is not distorted and the population of nanotriangles is 89% in comparison to spherical nanoparticles (Figure 6.7C and D). Spherical nanoparticles and some spherical aggregates can also be observed in the TEM image (Figure 6.7C).

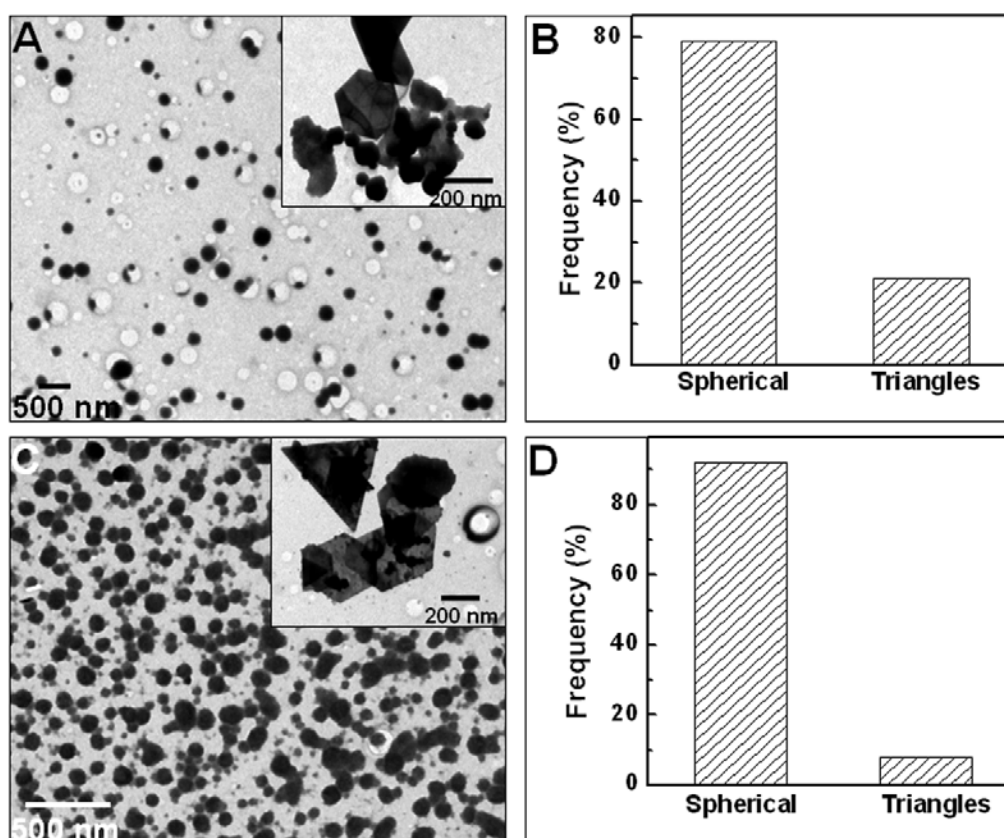


Figure 6.8: Representative TEM images of 10^{-2} M keggin ions bound gold nanotriangles after UV light irradiation for 90 minutes (A) and 120 minutes (C). Figure B and D show histogram plots of spherical and triangular nanoparticles obtained after 90 and 120 minutes of UV light irradiation respectively.

Figure 6.8A and B show a large population (79%) of spherical nanoparticles, which were formed during fragmentation of nanotriangles by UV light for 90 minutes. Gold nanotriangles along with the aggregated spherical nanoparticles are observed in the

TEM image (The inset of Figure 6.8A). Figure 6.8C corresponds to the TEM image of gold nanoparticles formed after irradiation of gold nanotriangles bound to Keggin ions for 120 minutes. The histogram analysis shows a large population of spherical and aggregated nanoparticles (92%) in comparison to gold nanotriangles. At closer inspection of nanotriangles in the TEM image (inset of Figure 6.8D), aggregates of spherical nanoparticles can be seen on the surface of nanotriangles and hexagonal nanoparticles.

6.3.4 FTIR measurement:

Figure 6.9 represents the Fourier transform infrared (FTIR) spectra of pure Keggin ion (curve 1), photo-irradiated gold nanotriangles bound to 10^{-2} M Keggin ions (curve 2) and gold nanoparticles synthesized in the presence of 10^{-2} M Keggin ions (curve 3). Curve 1 shows the W-O asymmetric vibration frequency at 982 cm^{-1} , W-O-W bending vibration at 890 cm^{-1} and P-O asymmetric stretching vibration at 1081 cm^{-1} [26].

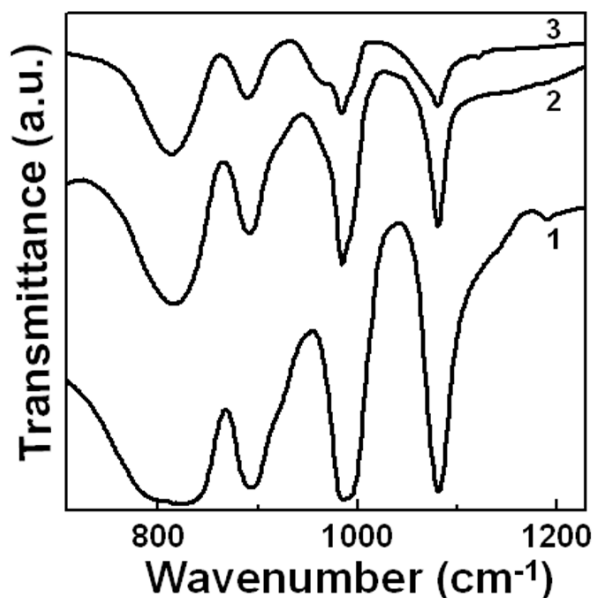


Figure 6.9: FTIR spectra recorded from pure Keggin ions (curve 1), UV light irradiated gold nanoparticles bound to Keggin ions (curve 2) and gold nanoparticles synthesized in the presence of 10^{-2} M Keggin ions (curve 3).

Comparing the curves 2 and 3 with curve 1, it is observed that the FTIR bands occur at same wavenumber as that observed for the curve 1, which clearly indicate that phosphotungstic acid molecules in the photo-irradiated Keggin ions bound gold

nanotriangles and in the gold nanoparticles synthesized in the presence of Keggin ions have not undergone the structural changes.

6.3.5 XPS measurement:

Figure 6.10 represents the XPS spectra of 10^{-2} M Keggin ions bound gold nanotriangles after irradiation, which is recorded from a drop-coated film of the corresponding solution. W 4f and Au 4f core level spectra were background corrected by using the Shirley algorithm [27] and charge correction of core level was done with respect to adventitious C 1s core level binding energy (285 eV). Figure 6.10A shows the W^{6+} core level spectrum, which could be resolved into 2 spin-orbit pairs (splitting ~ 2.18 eV) with a $4f_{7/2}$ binding energy of 36.74 eV, indicating that Keggin ions have W-O binding [26e]. The presence of 2 pairs suggests that W is likely to be present in W^{5+} and W^{6+} oxidation states. The presence W 4f core level spectrum strongly signifies that the surface of gold nanotriangles is bound with Keggin ion molecules. Figure 6.10B represents the Au 4f core level spectrum, which could be stripped into a single spin-orbit pair with $4f_{7/2}$ binding energy of 84 eV. The XPS spectrum does not show the presence of additional component of Au $4f_{7/2}$, which indicates that gold ions (Au^+) present on the gold nanotriangles were reduced by Keggin ions during UV light irradiation.

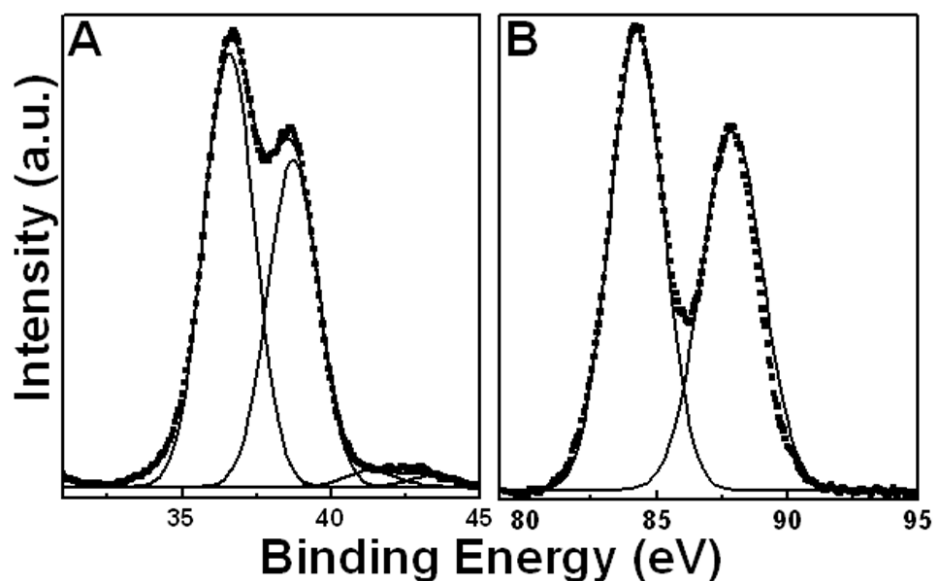


Figure 6.10: XPS spectra of W 4f (A) and Au 4f (B) core level arising from UV light irradiated Keggin ions bound gold nanotriangles together with the spin-orbit pairs.

6.3.6 XRD measurement:

Figure 6.11 shows the X-ray diffraction spectra recorded from the UV light irradiated gold nanotriangles bound to different concentrations of Keggin ions. Curve 1 corresponds to UV light irradiated gold nanotriangles bound to 10^{-2} M Keggin ions.

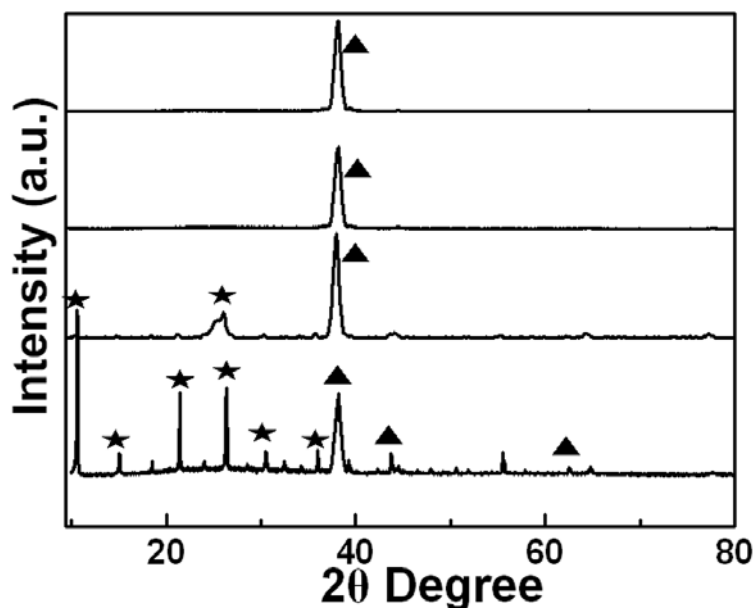


Figure 6.11: XRD spectra recorded from UV light irradiated gold nanotriangles bound to 10^{-2} M (curve 1), 10^{-3} M (curve 2), 10^{-4} M (curve 3) and 10^{-5} M (curve 4) concentrations of Keggin ions.

‘Star’ marks on the curve 1 represent Bragg reflections from Keggin ions bound on the surface of gold nanotriangles, while the ‘triangle’ marks show Bragg reflections from the fcc structure of gold. A large number of Bragg reflections corresponding to (210), (311), (004), (214), (512), (430), (043) and (516) lattice planes can be observed for Keggin ions in the curve 1 [28]. Bragg reflections at 38.35° , 43.75° and 64.85° correspond to the (111), (200) and (220) lattice planes of gold (curve 1) [29]. Curve 2 (UV light irradiated 10^{-3} M Keggin ion bound gold nanotriangles) shows Bragg reflections corresponding to (430) and (111) lattice planes of Keggin ions and gold respectively. Strong Bragg reflections corresponding to Keggin ions are not observed for 10^{-4} M and 10^{-5} M Keggin ions bound gold nanotriangles after photo-irradiation but Bragg reflection (38.35°) for the gold is observed (curves 3 and 4 respectively), which evidently suggest that these concentrations of Keggin ions are not sufficient to photofragment gold nanotriangles, as was also observed during the TEM measurements (Figure 6.6C and D).

6.3.7 Summary:

To summarize, it has been demonstrated that different concentrations of Keggin ions (phosphotungstate ions) can control the yield of gold nanotriangles with respect to spherical nanoparticles during synthesis using lemongrass extract. Gold nanotriangles have been fragmented to spherical and aggregated nanoparticles under UV light in the presence of different concentrations of Keggin ions. The varying percentage of fragmentation can be achieved by using different concentrations of Keggin ions.

6.4 Temperature dependent synthesis of gold nanotriangles:

The temperature of the reaction medium is a critical factor that determines the nature of nanoparticles formed. The yield and morphology of nanotriangles formed is controlled by varying the rate of reduction of gold ions using lemongrass extract at different temperatures.

6.4.1 Experimental Details:

The role of temperature on the morphology of the biologically prepared gold nanoparticles was studied by carrying out the reaction of 0.8 mL of lemongrass leaf extract with 10 mL of 10^{-3} M HAuCl₄ solution at 40, 50, 60, 70 and 80 °C for 5 h. UV-vis-NIR spectroscopy and TEM measurement were carried out after 5 h of reaction for the corresponding solutions.

6.4.2 UV-vis-NIR spectroscopy and TEM measurement:

Figure 6.12A shows the UV-vis-NIR spectra recorded after complete reduction of gold ions using lemongrass extract at different temperatures. Curve 1 corresponds to gold nanoparticles synthesized at room temperature and shows two absorption bands; transverse band (out of plane vibration) centered at 540 nm, while the longitudinal band (in plane vibration) appears to go beyond 1250 nm in the NIR region. Curves 2-6 correspond to gold nanoparticles formed at 40, 50, 60, 70 and 80 °C respectively. Comparing the curves 2-6 with curve 1, it is observed that as the temperature of the reaction medium increases, the longitudinal SP band shifts gradually to lower wavelength from 1200 nm (curve 1) to ca. 800 nm at 80 °C (curve 6) along with an increase in the transverse SP band.

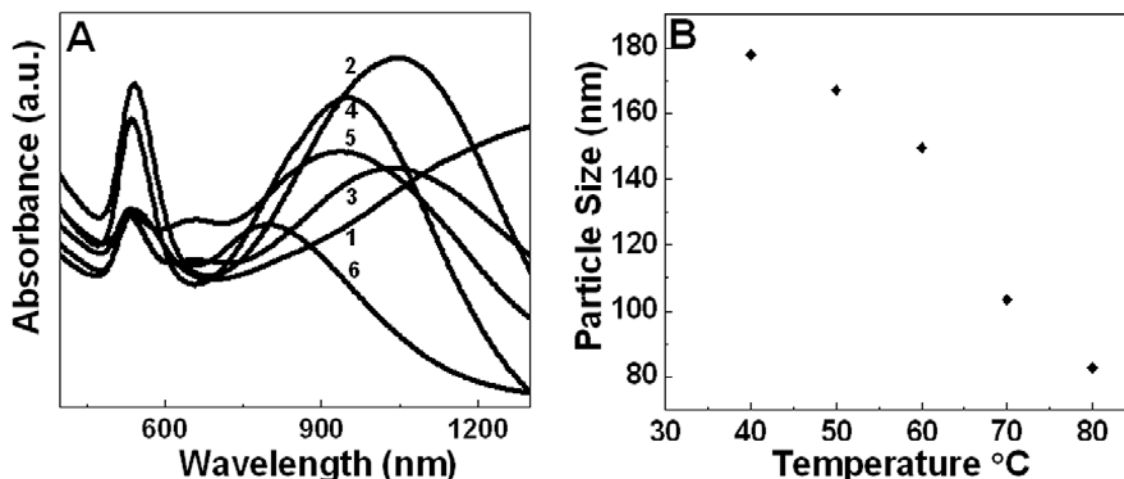


Figure 6.12: A) UV-vis-NIR spectra recorded from gold nanoparticles synthesized at room temperature (curve 1), 40 °C (curve 2), 50 °C (curve 3), 60 °C (curve 4), 70 °C (curve 5) and 80 °C (curve 6). Figure B depicting the average edge length of gold nanotriangles synthesized at different temperatures.

Sastry and coworkers have reported that a shift towards lower wavelength of the longitudinal band is symptomatic of a reduction in the edge length of gold nanotriangles or a decrease in the nanoparticle aspect ratio [25b]. Moreover, an increase in the intensity of transverse SP band indicates the presence of an increasing percentage of spherical nanoparticles in comparison to triangular nanoparticles, as the temperature of reaction medium is increased. Figure 6.13A-E show the TEM images of gold nanoparticles formed at different temperatures (40, 50, 60, 70 and 80 °C respectively). Figure 6.13A and B show that a large population of nanotriangles is synthesized using lemongrass extract at 40 and 50 °C respectively. Figure 6.13C-E show that the population of nanotriangles decreases and concomitantly the population of spherical nanoparticles increases, as the reaction temperature is increased from 60 to 80 °C, which is strongly supported by the UV-vis-NIR spectra (Figure 6.12A). Some percentage of aggregation can also be observed in the Figure 6.13C-E. Figure 6.13F shows the population of spherical and triangular nanoparticles, which is estimated from Figure 6.13A-E and other similar TEM images. The histogram plot (Figure 6.13F) shows that the population of nanotriangles decreases monotonically, accompanied by an increase in the population of spherical nanoparticles from 40 °C reaction to 80 °C reaction, again in good accord with the UV-vis-NIR data (Figure 6.12A).

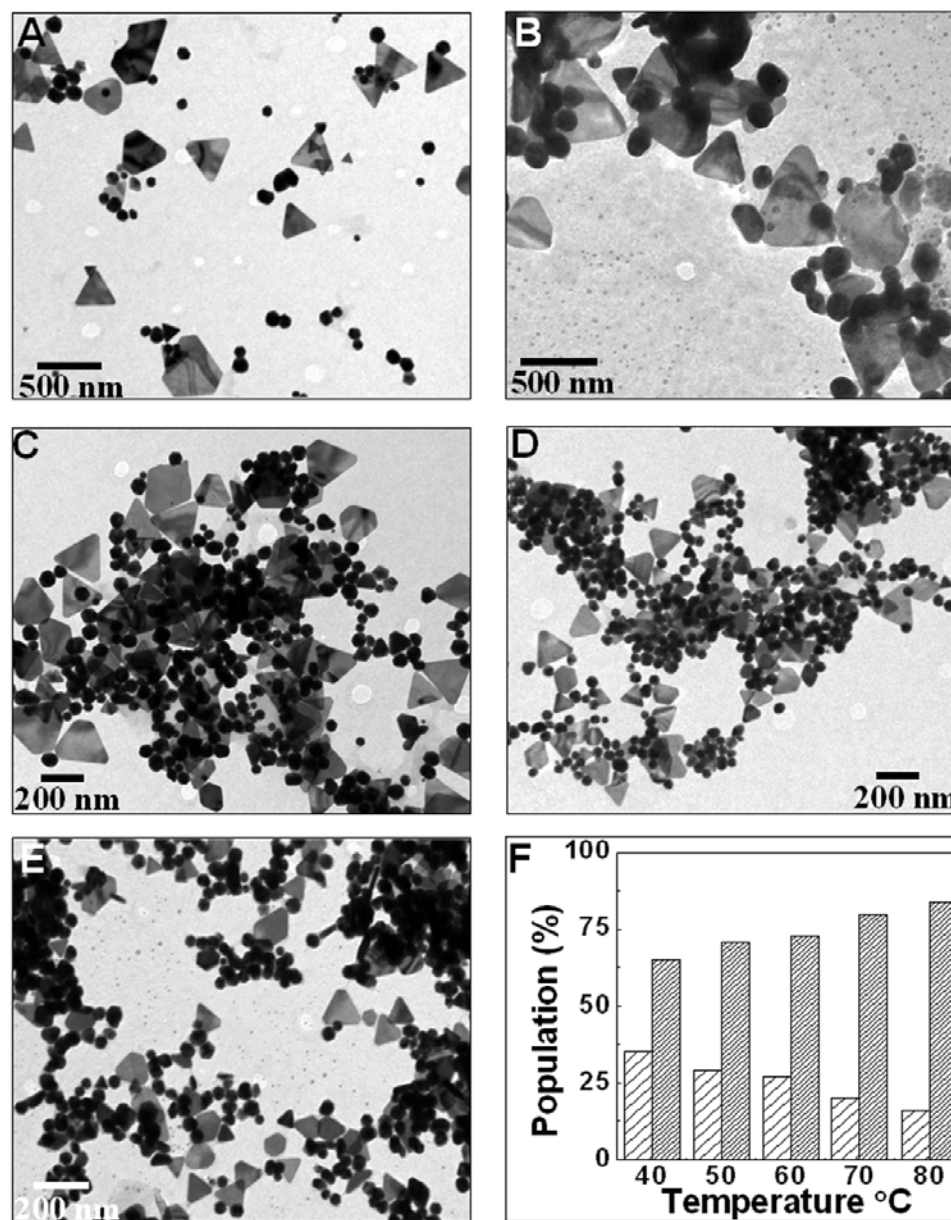


Figure 6.13: Representative TEM images of gold nanoparticles synthesized at 40 °C (A), 50 °C (B), 60 °C (C), 70 °C (D) and 80 °C (E). Figure F shows histogram plot of spherical and triangular gold nanoparticles synthesized at different temperatures. Light hatches line represents gold nanotriangles and dark hatches line represent spherical nanoparticles.

Figure 6.12B shows the average edge length of nanotriangles formed in the different reactions, as the temperature is increased. An analysis of edge length of triangular nanoparticles in the overall population shows that the average edge length of

triangular nanoparticles decreases from ca. 180 nm (40 °C) to ca. 80 nm (80 °C) with increasing temperatures. Increasing the reaction temperature during reduction of HAuCl₄ solution using lemongrass extract has led to an increase in the rate of reduction and thus results in increase in nucleation, which tends to increase the population of spherical nanoparticles. However, due to higher rate of reduction, most of the chloroaurate ions are consumed in the formation of nuclei and thus the growth process onto the surface of the preformed nuclei is stalled. Thus, we get much higher population of spherical nanoparticles as compared to the triangular nanoparticles, when the temperature of the reaction medium is increased (Fig 6.13E). The formation of the gold nanotriangles is a kinetically driven process and is a result of aggregation and rearrangement of smaller nanoparticles, which act as a nuclei for the further growth, leading to anisotropic structures [30]. Hence, a slow rate of reduction of metal ions at lower temperature might possibly facilitate the oriented growth of nuclei and thus should promote the formation of anisotropic nanoparticles [3e]. Thus, simple variation in the temperature of the reaction medium during reduction of gold ions by lemongrass extract enables tailoring of the size of the triangular nanoparticles and thus, their optical properties.

6.4.3 Summary:

The varying yields and edge lengths of gold nanotriangles synthesized using lemongrass extract at different reaction temperatures have been described in this chapter. The reduction rate of reaction is a crucial parameter to control the morphology of nanoparticles formed. As the temperature of the reaction medium increases from 40 °C to 80 °C, the edge length of triangular nanoparticles decreases steadily from ca. 180 nm to ca. 80 nm and thus optical properties can be fine-tuned in the NIR region.

6.5 Conclusion:

In this chapter, we have shown that different concentrations of Keggin ions affect the yield of gold nanotriangles during synthesis using lemongrass extract. Keggin ions bind to certain crystallographic facets of initially formed gold nanoparticles and inhibit two-dimensional growth of nanoparticles, leading to the growth of triangular nanoparticle. After UV light irradiation of Keggin ion bound gold nanotriangles, the photofragmentation of nanotriangles has been observed. Varying percentage of

fragmentation can be achieved by using different concentrations of Keggin ions. The increased charge repulsion on the surface of gold nanotriangles promotes the fragmentation of gold nanotriangles. The photofragmentation of already synthesized gold nanotriangles using different concentrations of Keggin ions under UV light irradiation has also been described in this chapter. 10^{-2} M concentration of Keggin ions fragment gold nanotriangles to spherical and aggregated nanoparticles, while lower concentrations of Keggin ions is not sufficient enough to fragment gold nanotriangles. Keggin ions bound to gold nanoparticles might have important applications as anti-tumor/bacterial/viral drugs [15] and in removal of organic dyes from polluted water [31]. The temperature of reaction medium is another parameter, which controls the particle size and yield of nanoparticles formed. In this chapter, the role of temperature on the yield of nanotriangles synthesized using lemongrass extract has been described. With increasing temperature, the gold nanotriangles become smaller and also of reduced percentage relative to spherical particles. The ability to tailor the size/morphology of gold nanoparticles and thus their optical properties by simple variation in experimental conditions by a fully green chemistry approach could be important in applications such as hyperthermia [32] and architectural optical coatings [25b].

6.6 References:

- [1] a) Kreibig, U.; Vollmer, M. *Optical Properties of Metal Clusters*; Springer: Berlin, 1995. b) Link, S.; El-Sayed, M. A. *J. Phys. Chem. B* **1999**, *103*, 8410. c) El-Sayed, M. A. *Acc. Chem. Res.* **2001**, *34*, 257. d) Moreno-Manas, M.; Pleixats, R. *Acc. Chem. Res.* **2003**, *36*, 638. e) Daniel, M. C.; Astruc, D. *Chem. Rev.* **2004**, *104*, 293. f) Thomas, K. G.; Kamat, P. V. *Acc. Chem. Res.* **2003**, *36*, 888. g) Sastry, M.; Rao, M.; Ganesh, K. N. *Acc. Chem. Res.* **2002**, *35*, 847. h) Crooks, R. M.; Zhao, M.; Sun, L.; Chechik, V.; Yeung, L. K. *Acc. Chem. Res.* **2001**, *34*, 181.
- [2] Narayanan, R.; El-Sayed, M. A. *J. Am. Chem. Soc.* **2004**, *126*, 7194.
- [3] a) Filankembo, A.; Pileni, M. P. *J. Phys. Chem. B* **2000**, *104*, 5865. b) Filankembo, A.; Giorgio, S.; Lisiecki, I.; Pileni, M. P. *J. Phys. Chem. B.* **2003**, *107*, 7492. c) Pileni, M. P. *Nat. Mater.* **2003**, *2*, 145. d) Pileni, M. P. *Langmuir* **2001**, *17*, 7476. e) Pileni, M. P. *C. R. Chimie* **2003**, *6*, 965. e) Shankar, S. S.; Bhargava, S.; Sastry, M. *J. Nanosci. Nanotech.* **2005**, *5*, 1721. (f) Chens, C. L.; McLeod, M. C.; Roberts C. B. *Langmuir* **2005**, *21*, 5166. g) Im, S. H.; Lee, Y. T.; Wiley, B.; Xia, Y. *Angew. Chem. Int. Ed. Engl.* **2005**, *44*, 2154.
- [4] a) El-Sayed, M. A. *Acc. Chem. Res.* **2001**, *34*, 257. b) Kamat, P. V. *J. Phys. Chem. B* **2002**, *106*, 7729. c) Kamat, P. V.; Flumiani, M.; Hartland, G. V. *J. Phys. Chem. B* **1998**, *102*, 3123. d) Takami, A.; Yamada, H.; Nakano, K.; Koda, S. *Jpn. J. Appl. Phys.* **1996**, *35*, L781. e) Kurita, H.; Takami, A.; Koda, S. *Appl. Phys. Lett.* **1998**, *72*, 789.
- [5] a) Fojtik, A.; Henglein, A. *Ber. Bunsen-Ges. Phys. Chem.* **1993**, *97*, 252. b) Sibbald, M. S.; Chumanov, G.; Cotton, T. M. *J. Phys. Chem.* **1996**, *100*, 4672. c) Yeh, M.-S.; Yang, Y.-S.; Lee, Y.-P.; Lee, H.-F.; Yeh, Y.-H.; Yeh, C.-S. *J. Phys. Chem. B* **1999**, *103*, 6851. d) Mafune, F.; Kohno, J.; Takeda, Y.; Kondow, T.; Sawabe, H. *J. Phys. Chem. B* **2000**, *104*, 8333. e) Mafune, F.; Kohno, J.; Takeda, Y.; Kondow, T.; Sawabe, H. *J. Phys. Chem. B* **2000**, *104*, 9111. f) Mafune, F.; Kohno, J.; Takeda, Y.; Kondow, T.; Sawabe, H. *J. Phys. Chem. B* **2001**, *105*, 5114. g) Brause, R.; Moiltgen, H.; Kleinermanns, K. *Appl. Phys. B* **2002**, *75*, 711.
- [6] a) Takami, A.; Kurita, H.; Koda, S. *J. Phys. Chem. B* **1999**, *103*, 1226. b) Mafune, F.; Kohno, J.; Takeda, Y.; Kondow, T. *J. Phys. Chem. B* **2001**, *105*, 9050. c) Mafune, F.;

- Kohno, J.; Takeda, Y.; Kondow, T. *J. Phys. Chem. B* **2002**, *106*, 7575. d) Mafune, F.; Kohno, J.; Takeda, Y.; Kondow, T. *J. Phys. Chem. B* **2002**, *106*, 8555.
- [7] a) Link, S.; Burda, C.; Nikoobakht, B.; El-Sayed, M. A. *J. Phys. Chem. B* **2000**, *104*, 6152. b) Link, S.; Burda, C.; Mohamed, M. B.; Nikoobakht, B.; El-Sayed, M. A. *J. Phys. Chem. A* **1999**, *103*, 1165.
- [8] Jin, R.; Cao, Y.; Mirkin, C. A.; Kelley, K. L.; Schatz, G. C.; Zheng, J. G. *Science* **2001**, *294*, 1901.
- [9] Callegari, A.; Tonti, D.; Chergui, M. *Nano Lett.* **2003**, *3*, 1565.
- [10] a) Rele, M.; Kapoor, S.; Palit, D. K.; Mukherjee, T. *Res. Chem. Inter.* **2004**, *30*, 847. b) Sakamoto, M.; Tachikawa, T.; Fujitsuka, M.; Majima, T. *Langmuir* **2006**, *22*, 6361. c) Zhang, J.; Worley, J.; Dénommée, S.; Kingston, C.; Jakubek, Z. J.; Deslandes, Y.; Post, M.; Simard, B. *J. Phys. Chem. B* **2003**, *107*, 6920. d) Chand, W-S.; Park, J-W.; Rawat, V.; Sands, T.; Lee, G. U. *Nanotechnology* **2006**, *17*, 5131.
- [11] a) Mandal, S.; Selvakannan, P.R.; Pasricha, R.; Sastry, M. *J. Am. Chem. Soc.* **2003**, *125*, 8440. b) Mandal, S.; Mandale, B. A.; Sastry, M. *J. Mater. Chem.* **2004**, *14*, 2868.
- [12] a) Sanyal, A.; Mandal, S.; Sastry, M. *Adv. Func. Mater.* **2005**, *15*, 273. b) Mandal, S.; Rautaray, D.; Sastry, M. *J. Mater. Chem.* **2003**, *13*, 3002. c) Mandal, S.; Rautaray, D.; Sanyal, A.; Sastry, M. *J. Phys. Chem. B* **2004**, *108*, 7126. d) Rautaray, D.; Sainkar, S. R.; Sastry, M. *Langmuir* **2003**, *19*, 10095.
- [13] Zhou, Y.; Wang, C. Y.; Zhu, Y. R.; Chen, Z. Y. *Chem. Mater.* **1999**, *11*, 2310.
- [14] Troupis, A.; Hiskia, A.; Papaconstantinou, E. *Angew. Chem. Int. Ed.* **2002**, *41*, 1911.
- [15] Yamase, T. *J. Mater. Chem.* **2005**, *15*, 4773.
- [16] Huheey, J. E. *Inorganic Chemistry (Third Edition)*, 698.
- [17] Misono, M. *Mater. Chem. Phys.* **1987**, *17*, 103.
- [18] Pope, M. T.; Muller, A. *Angew. Chem. Int. Ed.* **1991**, *30*, 34.
- [19] Papaconstantinou, E. *Chem. Soc. Rev.* **1989**, *18*, 1.

- [20] a) Fleming, D. A.; Williams, M. E. *Langmuir* **2004**, *20*, 3021. b) Jin, R.; Egusa, S.; Scherer, N. F. *J. Am. Chem. Soc.* **2004**, *126*, 9900. c) Chu, H-C.; Kuo, C-H.; Huang M. H. *Inorg. Chem.* **2006**, *45*, 808. d) Metraux, G. S.; Mirkin, C. A. *Adv. Mater.* **2005**, *17*, 412. e) Garcia-Gutierrez, D. I.; Gutierrez-Wing, C. E.; Giovanetti, L.; Ramallo-Lo'pez, J. M.; Requejo, F. G.; Jose-Yacaman, M. *J. Phys. Chem. B* **2005**, *109*, 3813.
- [21] a) Mulvaney, P. *Langmuir* **1996**, *12*, 788. b) Linl, S.; El-Sayed, M. *Annu. Rev. Phys. Chem.* **2003**, *54*, 331. c) Sherry, L. J.; Jin, R.; Mirkin, C. A.; Schatz, G. C.; Van Duyne, R. P. *Nano Lett.* **2006**, *6*, 2060. d) Liz-Marzan, L. M. *Langmuir* **2006**, *22*, 32. e) Henglein, A. *J. Phys. Chem. B.* **1993**, *97*, 5457.
- [22] a) Na'her, U.; Bjornholm, S.; Fraundorf, S.; Garcias, F.; Guet, C. *Phys. Rep.* **1997**, *285*, 245. (b) Last, I.; Schek, I.; Jortner, J. *J. Chem. Phys.* **1997**, *107*, 6685. (c) Last, I.; Jortner, J. *Phys. Rev. Lett.* **2001**, *87*, 033401.
- [23] Kamat, P. V.; Flumiani, M.; Hartland, G. V. *J. Phys. Chem. B* **1998**, *102*, 3123.
- [24] Dawson, A.; Kamat, P. V. *J. Phys. Chem. B* **2001**, *105*, 960.
- [25] a) Shankar, S. S.; Rai, A.; Ankamwar, B.; Singh, A.; Ahmad, A.; Sastry, M. *Nat. Mater.* **2004**, *3*, 482. b) Shankar, S. S.; Rai, A.; Ahmad, A.; Sastry, M. *Chem. Mater.* **2005**, *17*, 566.
- [26] a) Perez-Maqueda, I. A.; Matijevic, E. *Chem. Mater.* **1998**, *10*, 1430. b) Gole, A.; Sastry, M. *Inorg. Chem. Commun.* **2001**, *3*, 568. c) Southward, B. W. L.; Vaughan, J. S.; Connor, C.T. O. *J. Catal.* **1995**, *153*, 293. d) Paze, C.; Bordiga, S.; Zecchina, A. *Langmuir* **2000**, *16*, 8139. e) Medinaa, A.; Solis, J. L.; Rodriguez, J.; Estrada, W. *Solar Energy Materials & Solar Cells* **2003**, *80*, 473.
- [27] Shirley, D. A. *Phys. Rev. B* **1972**, *5*, 4709.
- [28] PCPDF File No. 37-0570.
- [29] PCPDF File No. 04-0784.
- [30] a) Chiang, Y-S.; Turkevich, J. *J. Coll. Sci.* **1963**, *18*, 772. b) Engelbrecht, J.; Synman, H. *Gold Bulletin*, **1983**, *16*, 66.
- [31] Chen, C.; Wang, Q I.; Lie, P.; Song, W.; Ma, W.; Zhao, A. *Environ. Sci. Technol.* **2006**, *40*, 3965.

- [32] a) Loo, C.; Lin, A.; Hirsch, L.; Lee, M. H.; Barton, J.; Halas, N.; West, J.; Drezek, R. *Technology in Cancer Research and Treatment* **2004**, *3*, 30. b) Hirsch, L. R.; Stafford, R. J.; Bankson, J. A.; Sershen, S. R.; Rivera, B.; Price, R. E.; Hazle, J. D.; Halas, N. J.; West, J. L. *Proc. Natl. Acad. Sci. USA*, **2003**, *100*, 135491. c) Nanospectra biosciences, Inc. Huston Texas, www.nanospectra.com, Simpson, C. R.; Kohl, M.; Essenpreis, M.; Cope, M. *Phys. Med. Bio.* **1998**, *43*, 24652478. d) Anderson, R. R.; Parrish, J. A. *J. Invest. Dermatol.* **1981**, *77*, 13.

Chapter VII

Conclusions

This chapter contains concluding remarks on the salient features of the work described in the thesis and future potential developments in the area.

7.1 Summary of the work:

The main emphasis of work presented in this thesis has been to demonstrate the synthesis of gold nanotriangles, core-shell nanoparticles of various compositions and shape modification using different chemical and physical means. The aspects that have been covered in this thesis are: 1) Synthesis of gold nanotriangles using undialyzed and dialyzed lemongrass extract at room temperature. 2) Synthesis of triangular Au core- Ag shell nanoparticles and spherical gold-titania core-shell nanoparticles. 3) Shape transformation of gold nanotriangles using different halide ions and surfactants. 4) Photofragmentation of gold nanotriangles using Keggin ions under UV light irradiation. 5) Effect of temperatures on the synthesis of gold nanotriangles using lemongrass extract.

Room temperature and environmentally benign approach for the synthesis of gold nanotriangles and hexagons using undialyzed lemongrass extract as reducing and shape-directing agents has been demonstrated. The yield of gold nanotriangles synthesized using lemongrass extract is found to be 45%, which is higher than the previously reported chemical and photochemical methods. The AFM analysis showed that thickness of nanotriangle was ca. 18 nm. Different cut-off dialysis bags (3, 12.5 and 30 kDa) were used for dialysis of lemongrass extract against 10^{-3} M HAuCl_4 solution. Biomolecules, which have size below pore size of the dialysis bag used, diffuse from the inside bag to the external gold ion solution in the direction of decreasing concentration and reduce gold ions to synthesize spherical and triangular nanoparticles. The concentrations of extracts inside the different bags were found to be in the following order: 3 kDa > 12 kDa > 30 kDa, while the concentrations of extract outside the bags were in the reverse order. Spherical nanoparticles and a small percentage of gold nanotriangles were synthesized inside 3 kDa bag due to the fast reduction of diffused gold ions inside the bag. A large percentage of triangular and cubic nanoparticles were synthesized inside 12.5 and 30 kDa bags respectively due to the slow reduction of gold ions. A varying yield and size of gold nanotriangles were also found to be synthesized outside the different cut-off bags due to different rate of reduction of gold ions by outside-diffused lemongrass extract. In another experiments, lemongrass extract was dialyzed against water using 3, 12.5 and 30 kDa cut-off bags and dialyzed extract obtained from both inside and outside bags were used for the reduction of 10^{-3} M HAuCl_4 solution. Spherical nanoparticles along with the smaller

nanotriangles were synthesized using dialyzed extract obtained from inside the 3 and 12.5 kDa bags, while the gold nanocubes were observed, when gold ions were reduced using dialyzed extract obtained from inside a 30 kDa bag. Synthesis of different size and yield of gold nanotriangles using dialyzed extract obtained from outside the different dialysis bags have also been demonstrated. FTIR analysis showed that sugar derivatives and citral molecules found in lemongrass extract act as reducing and shape-directing agent for the synthesis of nanotriangles.

Synthesis of triangular Au core-Ag shell nanoparticles using ascorbic acid as a weak reducing agent under alkaline pH has been demonstrated. It was shown that 10^{-3} M concentration of silver ions was perfect to synthesize silver shell around gold core nanoparticles. Positively charged silver ions interact with negatively charged gold nanotriangles through electrostatic interaction. The bound silver ions on the surface of gold nanotriangles were reduced by ascorbic acid under different alkaline pH to achieve varying thickness of silver shell. The thickness of silver shell synthesized at pH 12 was estimated to be ca. 5 nm. Synthesis of spherical gold-titania core-shell nanoparticles using the hydrolyzing enzyme from fungus *Fusarium oxysporum* has also been demonstrated. A hydrolyzing enzyme has ability to hydrolyze TiF_6^- ions to titania nanoparticles. The enzyme was immobilized on the surface of aspartic acid modified spherical gold nanoparticles and subsequently exposed to TiF_6^- ion solution leading to the formation of spherical gold-titania core-shell nanoparticles. XRD analysis showed that brookite and rutile polymorphs of titania were synthesized on the surface of gold nanoparticles.

Shape transformation of already synthesized gold nanotriangles using halide ions and the effect of halide ions on the growth of nanotriangles during synthesis using lemongrass extract have been demonstrated. Fluoride and chloride ions do not affect the morphology of gold nanotriangles, while bromide ions promote corrugation on the edges of nanotriangles. A drastic change in the morphology of nanotriangles after treatment with iodide ions was observed. Iodide ions transform nanotriangles into circular plate like nanostructures. Iodide ions have highest ability to chemisorb on the surface of gold nanotriangles compared to the other halide ions and thus create the highest strain on the underlying Au (111) lattice planes. The shape transformation has been attributed to the

strain developed by the adlayers of Γ ions on the (111) lattice planes of gold nanotriangles. Furthermore, the prominent effects of halide ions on the growth of nanotriangles during synthesis have been demonstrated. It was shown that fluoride ions do not affect the growth of nanotriangles, while chloride ions promote the synthesis of triangular nanoparticles. It was proposed that Cl^- ions having the ability to chemisorb on the (111) lattice of fcc gold with a hexagonal closed packed structure could be responsible for the formation of $\langle 111 \rangle$ oriented gold nanotriangles and nanohexagons. On the contrary, bromide and iodide ions inhibit the growth of nanotriangles due to their higher tendency to chemisorb and produce strains on the surface of initially formed gold nanoparticles. Similarly the effects of cationic surfactants such as CTAB and CTAC have also been studied. 10^{-2} M concentration of CTAB transforms gold nanotriangles into circular plate like structures, while lower concentrations do not have significant effect on the morphology of nanotriangles. On the other hand, CTAC does not affect the morphology of gold nanotriangles due to the presence of chloride ions. Gold ions also transform gold nanotriangles into highly branched nanostructures in the presence of 10^{-2} M concentration of CTAB, while modify them into nanocoral and nanoflowers like structures in the presence of 10^{-2} M concentration of CTAC.

Photofragmentation of gold nanotriangles into spherical and aggregated nanoparticles in the presence of Keggin ions under UV light irradiation has been demonstrated. Different concentrations of Keggin ions (10^{-2} M to 10^{-5} M) were used to achieve the varying percentage of fragmentation of already synthesized gold nanotriangles. Keggin ions get reduce from M^{6+} to M^{5+} oxidation state in the presence of iso-propyl alcohol under the UV light irradiation and therefore show dark blue colour after reduction. The high electron density on the surface of gold nanotriangles bound with Keggin ions after UV light irradiation cause fragmentation of triangles into spherical nanoparticles due to charge repulsion. Gold nanotriangles synthesized in the presence of different concentration of Keggin ions using lemongrass extract have also been demonstrated. It is believed that high concentration (10^{-2} M) of Keggin ions binds to lattice planes of initially formed gold nanoparticles and inhibits the growth of nanoparticles in the $\langle 111 \rangle$ direction. Gold nanotriangles synthesized in the presence of different concentrations of Keggin ions were also UV light irradiated in order to fragment

nanotriangles into spherical nanoparticles. Synthesis of gold nanotriangles at different temperatures using lemongrass extract has been described in the last chapter. Synthesis of nanotriangles is a kinetically driven process and fast reduction at higher temperature facilitates the synthesis of nanotriangles of a low population and smaller size. It has also been shown that the NIR absorption peak of gold nanotriangles could be fine-tuned by merely varying the edge length of gold nanotriangles.

7.2 Scope for future work:

The size-controlled synthesis of gold nanotriangles is an interesting result and might have potential applications in many fields. It would be interesting to use these gold nanoparticles for hyperthermic treatment of cancerous cells due to their high absorbance in the NIR region of the electromagnetic spectrum. Since the human body tissues can sufficiently transmit light in the range from 800 to 1100 nm, irradiation of suitably surface modified gold nanotriangles with cancer cell specific antibody, which are selectively localized near the cancerous tissue, may kill the cells in the local vicinity of gold nanotriangles. Gold nanotriangles could also be used for delivery of drugs or genes. Gold nanoparticles would act as a non-viral vector for the delivery of gene inside the biological cells.

We have already studied the effect of different halide ions and cationic surfactants on the morphology of gold nanoparticles during synthesis so it is worth to studying the effect of different anionic surfactants on the growth of nanoparticles. It has been shown in previous reports that presence of silver ions enhances the population and aspect ratio of gold nanorods. Similar effect can be studied in the case of gold nanoparticles synthesized using biological means. Polyoxometallates are well known for their diverse applications such as degradation of dyes and antiviral as well as antitumor agents. Thus, it would be significant to immobilize polyoxometallates on the surface of metal nanoparticles and investigate their potential applications in biomedical areas and also in removal of waste from polluted water.

List Of Publications

1. Biological Synthesis of triangular gold nanoprisms.
S. Shiv Shankar, **Akhilesh Rai**, Balaprasad Ankamwar, Amit Singh, Absar Ahmad, Murali Sastry *Nature Materials*, **2004**, 3, 482.
2. Rapid synthesis of Au, Ag and bimetallic Au core-Ag shell nanoparticles using Neem (*Azadirachta indica*) leaf broth.
S. Shiv Shankar, **Akhilesh Rai**, Absar Ahmad, Murali Sastry *J. Colloid Interface Science*, **2004**, 275, 496.
3. Biosynthesis of silver and gold nanoparticles from extract of different parts of the geranium plant.
S. Shiv Shankar, **Akhilesh Rai**, Absar Ahmad, Murali Sastry *Applied Nanoscience*, **2004**, 1, 69.
4. Controlling the optical properties of lemongrass extract synthesized gold nanotriangles and potential application in infrared-absorbing optical coatings.
S. Shiv Shankar, **Akhilesh Rai**, Absar Ahmad, Murali Sastry *Chemistry of Materials*, **2005**, 17, 566.
5. Role of halide ions and temperatures on the morphology of biologically synthesized gold nanotriangles.
Akhilesh Rai, Amit Singh, Absar Ahmad, Murali Sastry *Langmuir* **2006**, 22, 773.
6. Synthesis of triangular Au core-Ag shell nanoparticles.
Akhilesh Rai, Minakshi Chaudary, Absar Ahmad, Suresh Bhargava, Murali Sastry *Material Research Bulletin* (accepted).

7. Dialysis as tool for controlling morphology of gold nanoparticles using lemon grass extract.

Akhilesh Rai, Absar Ahmad, Murali Sastry *Langmuir* (communicated).

8. Biological Synthesis of spherical gold-titania core-shell nanoparticles.

Akhilesh Rai, Absar Ahmad, Murali Sastry, Chemistry of Materials (Communicated).

9. Photofragmentation of gold nanotriangles using Keggin ions.

Akhilesh Rai, Murali Sastry, *J. Nanoscience and Nanotechnology* (communicated).

10. The effect of surfactants on the morphology of biologically synthesized gold nanotriangles, reversible transformation of morphology and synthesis of highly complex nanostructures at room temperature using gold ions.

Akhilesh Rai, Murali Sastry, *J. Material Chemistry* (communicated).